IL
NUOVO CIMENTO
ORGANO DELLA SOCIETÀ ITALIANA DI FISICA
SOTTO GLI AUSPICI DEL CONSIGLIO NAZIONALE DELLE RICERCHE

VOL. II, N. 6 *Serie decima* 1° Dicembre 1955

La solution générale des équations d'Einstein

$$g^{\mu\nu}_{+-};_{\varrho} = 0 .$$

S. MAVRIDÈS

Institut Henri Poincaré - Paris

(ricevuto il 25 Luglio 1955)

Summary. — The rigorous calculation of the general solution of Einstein's equations $g^{\mu\nu}_{+-};_{\varrho} = 0$ leads, for the affine connexion, to a simple univocally determinated and completely explicited expression, in function of the contravariant components ($h^{\mu\nu} = g^{\mu\nu}_{--}$ and $f^{\mu\nu} = g^{\mu\nu}_{\vee}$) of the fundamental tensor $g^{\mu\nu}$. The existence conditions of this general solution are also explicited.

Considérons l'équation fondamentale de la théorie d'Einstein

$$g_{\mu\nu;\varrho} = 0 , \tag{I}$$
$$_{+-}$$

Les dérivations + et — sont rapportées, par hypothèse, à une connexion affine que nous supposerons a priori quelconque et que nous désignerons par $\Gamma^{\varrho}_{\mu\nu}$ [1].

On connait [2] la solution générale des équations (I) qui détermine complètement la connexion affine $\Gamma^{\varrho}_{\mu\nu}$ en fonction du tenseur fondamental $g_{\mu\nu}$. Cette solution s'exprime directement au moyen d'une métrique qui — à un in-

[1] Dans la théorie d'Einstein-Schrödinger la connexion $L^{\varrho}_{\mu\nu}$ qui satisfait (1) doit etre telle que

$$L_{\varrho} = L^{\sigma}_{\varrho\sigma} = 0 .$$
$$_{\vee}$$

Pour rester dans le cas général, nous ne poserons pas, a priori, cette condition.

[2] M. A. TONNELAT: *Journ. Phys. Rad.*, **12**, 81 (1951); **16**, 21 (1955).

variant près — coïncide avec les $\gamma_{\mu\nu}$ $(= g_{\mu\nu})$. Or, A. LICHNEROWICZ [3] a donné des arguments pour caractériser la métrique non par les $\gamma_{\mu\nu}$ mais — à un invariant près — par les $h^{\mu\nu}$ $(= g^{\mu\nu})$. Il est donc souhaitable d'exprimer la connexion affine non pas en fonction des $g_{\mu\nu}$, mais en fonction des $g^{\mu\nu}$. Pour cela, on peut évidemment transposer la solution calculée par M. A. TONNELAT en utilisant les relations de correspondance entre les variables $\gamma_{\mu\nu}$, $\varphi_{\mu\nu}$ $(= g_{\mu\nu})$ et $h^{\mu\nu}$, $f^{\mu\nu}$ $(= g^{\mu\nu})$ [4]. Mais pratiquement, il est moins compliqué de reprendre la question à la base et de résoudre les équations

$$\overset{\mu\ \nu}{g^{+\ -}}_{;\varrho} = 0 \,. \tag{II}$$

La méthode de résolution est, bien entendu, analogue à celle de M. A. TONNELAT. Il existe néanmoins des différences importantes que nous allons indiquer.

La possibilité d'obtenir la solution des équations $\overset{\mu\ \nu}{g^{+\ -}}_{;\varrho} = 0$ tient, en grande partie, au choix des notations. Nous avons gardé autant que possible celles d'Einstein, et adapté celles de M. A. Tonnelat au problème posé.

La forme de la solution générale obtenue, ses conditions d'existence sont simples.

1. – Préliminaires mathématiques.

1·1. *Les relations entre les composantes des tenseurs* $g^{\mu\nu}$ *et* $g_{\mu\nu}$. – Ces relations ont été établies et indiquées in extenso par M. A. TONNELAT [4]. Nous adopterons également la convention suivante: *une même lettre désigne toujours les composantes covariantes d'un tenseur, le déterminant formé au moyen de ces composantes et le mineur relatif à chacune d'elles.* Scindons les composantes $g_{\mu\nu}$ et $g^{\mu\nu}$ en parties symétriques et antisymétriques. Nous aurons ainsi $(gg^{\mu\nu} = \text{mineur } g_{\mu\nu})$:

$$g_{\mu\nu} = \gamma_{\mu\nu} + \varphi_{\mu\nu}, \tag{1}$$

$$g^{\mu\nu} = h^{\mu\nu} + f^{\mu\nu}, \tag{2}$$

g, γ, φ, h et f désignent les déterminants formés par les $g_{\mu\nu}$, $\gamma_{\mu\nu}$, $\varphi_{\mu\nu}$, $h_{\mu\nu}$ et $f_{\mu\nu}$; $gg^{\mu\nu}$, $\gamma\gamma^{\mu\nu}$, $\varphi\varphi^{\mu\nu}$, $hh^{\mu\nu}$ et $ff^{\mu\nu}$ les mineurs relatifs à ces mêmes éléments. Par définition

$$g_{\mu\varrho}g^{\mu\sigma} = g^{\sigma\mu}g_{\varrho\mu} = \delta^{\sigma}_{\varrho}; \qquad h_{\mu\varrho}h^{\mu\sigma} = \delta^{\sigma}_{\varrho}; \qquad f_{\mu\varrho}f^{\mu\sigma} = \delta^{\sigma}_{\varrho}, \tag{3}$$

$$\mathrm{d}g = gg^{\mu\nu}\,\mathrm{d}g_{\mu\nu} = -\,gg_{\mu\nu}\,\mathrm{d}g^{\mu\nu}, \tag{4}$$

[3] A. LICHNEROWICZ: *Les théories relativistes de la gravitation et de l'électromagnétisme* (Paris, 1955), p. 288.

[4] M. A. TONNELAT: *Journ. Phys. Rad.*, **16**, 22 (1955), équations (19).

$$\mathrm{d}h = hh^{\mu\nu}\,\mathrm{d}h_{\mu\nu} = -hh_{\mu\nu}\,\mathrm{d}h^{\mu\nu}, \tag{5}$$

$$\mathrm{d}f = ff^{\mu\nu}\,\mathrm{d}f_{\mu\nu} = -ff_{\mu\nu}\,\mathrm{d}f^{\mu\nu}. \tag{6}$$

D'autre part, rappelons les relations suivantes:

1°) Entre les composantes d'un tenseur *symétrique* du second rang:

$$h\varepsilon_{\mu\nu\varrho\sigma}h^{\mu\lambda}h^{\nu\pi} = \varepsilon^{\mu\nu\lambda\pi}h_{\mu\varrho}h_{\nu\sigma}, \tag{7}$$

$\varepsilon_{\mu\nu\varrho\sigma}$ $(= \varepsilon^{\mu\nu\varrho\sigma})$ étant l'indicateur de Levi-Civita habituel.

2°) Entre les composantes d'un tenseur *antisymétrique* du second rang:

$$f^{\mu\nu} = \frac{1}{2\sqrt{f}}\,\varepsilon^{\mu\nu\varrho\sigma}f_{\varrho\sigma}, \qquad f_{\mu\nu} = \frac{\sqrt{f}}{2}\,\varepsilon_{\mu\nu\varrho\sigma}f^{\varrho\sigma}, \tag{8}$$

avec

$$\sqrt{f} = \tfrac{1}{8}\varepsilon^{\mu\nu\varrho\sigma}f_{\mu\nu}f_{\varrho\sigma} = f_{12}f_{34} + f_{31}f_{24} + f_{23}f_{14}. \tag{9}$$

3°) Les déterminants g, h et f sont liés par:

$$\frac{1}{g} = \frac{1}{h} + \frac{1}{f} + \frac{1}{2h}\,h_{\mu\varrho}h_{\nu\sigma}f^{\mu\nu}f^{\varrho\sigma}. \tag{10}$$

Un calcul sans difficultés conduit à:

$$\left(\frac{1}{g} - \frac{1}{h} - \frac{1}{f}\right)\delta^{\varepsilon}_{\mu} - \frac{1}{f}\,f_{\mu\varrho}f_{\nu\sigma}h^{\varrho\sigma}h^{\nu\varepsilon} = \frac{1}{h}\,h_{\mu\varrho}h_{\lambda\tau}f^{\varrho\lambda}f^{\varepsilon\tau}. \tag{11}$$

En contractant en ε, μ, on a donc, d'après (10)

$$\frac{1}{h}\,h_{\mu\varrho}h_{\nu\sigma}f^{\mu\nu}f^{\varrho\sigma} = \frac{1}{f}\,f_{\mu\varrho}f_{\nu\sigma}h^{\mu\nu}h^{\varrho\sigma} = 2\left(\frac{1}{g} - \frac{1}{h} - \frac{1}{f}\right). \tag{12}$$

Notons enfin les relations suivantes:

$$g^2 = \gamma h = f\varphi. \tag{13}$$

1·2. *Notations utilisées.*

a) *Introduction des grandeurs surlignées.*

(1) Nous désignerons par $A_{ab\ldots,\varrho}$ un tenseur quelconque dont un indice ϱ

est abaissé au moyen du tenseur symétrique $h_{\mu\nu}$ [5]. Nous définirons:

$$
(14)\qquad \left\{\begin{array}{l}
A_{ab\ldots,\varrho} = h_{\varrho\sigma}A^{\sigma}_{ab\ldots}\,,\\
A_{ab\ldots,\bar{\varrho}} = h_{\varrho\sigma}A^{\bar{\sigma}}_{ab\ldots} = h_{\varrho\sigma}f^{\sigma\lambda}A_{ab\ldots,\lambda}\,,\\
A_{ab\ldots,\bar{\bar{\varrho}}} = h_{\varrho\sigma}A^{\bar{\bar{\sigma}}}_{ab\ldots} = h_{\varrho\sigma}f^{\sigma\tau}h_{\tau\lambda}f^{\lambda\mu}A_{ab\ldots,\mu}\,,\\
A_{ab\ldots,\bar{\bar{\bar{\varrho}}}} = h_{\varrho\sigma}A^{\bar{\bar{\bar{\sigma}}}}_{ab\ldots} = h_{\varrho\sigma}f^{\sigma\tau}h_{\tau\lambda}f^{\lambda\mu}h_{\mu\nu}f^{\nu\pi}A_{ab\ldots,\pi}\,,\\
A_{ab\ldots,\bar{\bar{\bar{\bar{\varrho}}}}} = h_{\varrho\sigma}A^{\bar{\bar{\bar{\bar{\sigma}}}}}_{ab\ldots} = h_{\varrho\sigma}f^{\sigma\tau}h_{\tau\lambda}f^{\lambda\mu}h_{\mu\nu}f^{\nu\pi}h_{\pi\delta}f^{\delta\varepsilon}A_{ab\ldots,\varepsilon}\,,
\end{array}\right.
$$

et

$$
(15)\qquad \left\{\begin{array}{l}
A^{\varrho}_{ab\ldots} = h^{\varrho\sigma}A_{ab\ldots,\sigma}\,,\\
A^{\bar{\varrho}}_{ab\ldots} = f^{\varrho\sigma}A_{ab\ldots,\sigma} = f^{\varrho\sigma}h_{\sigma\lambda}A^{\lambda}_{ab\ldots}\,,\\
A^{\bar{\bar{\varrho}}}_{ab\ldots} = f^{\varrho\sigma}A_{ab\ldots,\bar{\sigma}} = f^{\varrho\sigma}h_{\sigma\tau}f^{\tau\lambda}h_{\lambda\mu}A^{\mu}_{ab\ldots}\\
A^{\bar{\bar{\bar{\varrho}}}}_{ab\ldots} = f^{\varrho\sigma}A_{ab\ldots,\bar{\bar{\sigma}}} = f^{\varrho\sigma}h_{\sigma\tau}f^{\tau\lambda}h_{\lambda\mu}f^{\mu\pi}h_{\pi\delta}A^{\delta}_{ab\ldots}\,,\\
A^{\bar{\bar{\bar{\bar{\varrho}}}}}_{ab\ldots} = f^{\varrho\sigma}A_{ab\ldots,\bar{\bar{\bar{\sigma}}}} = f^{\varrho\sigma}h_{\sigma\tau}f^{\tau\lambda}h_{\lambda\mu}f^{\mu\nu}h_{\nu\pi}f^{\pi\delta}h_{\delta\varepsilon}A^{\varepsilon}_{ab\ldots}\,.
\end{array}\right.
$$

Il existe, entre ces grandeurs, l'identité suivante (cf. Appendice I à la fin de cet article):

$$
(16)\qquad A_{ab\ldots,\bar{\bar{\bar{\varrho}}}} = -h\left(\frac{1}{g}-\frac{1}{h}-\frac{1}{f}\right)A_{ab\ldots,\bar{\varrho}} - \frac{h}{f}A_{ab\ldots,\varrho}\,.
$$

Enfin, pour abréger, nous poserons:

$$
(17)\qquad \left\{\begin{array}{l}
\Gamma_{ab\varrho} = \Gamma_{\underset{\vee}{ab},\varrho} + \Gamma_{\underset{\vee}{\varrho a},b} + \Gamma_{\underset{\vee}{b\varrho},a}\,,\\
\bar{\Gamma}_{ab\varrho} = \Gamma_{\underset{\vee}{ab},\bar{\varrho}} + \Gamma_{\underset{\vee}{\varrho a},\bar{b}} + \Gamma_{\underset{\vee}{b\varrho},\bar{a}}\\
\bar{\bar{\Gamma}}_{ab\varrho} = \Gamma_{\underset{\vee}{ab},\bar{\bar{\varrho}}} + \Gamma_{\underset{\vee}{\varrho a},\bar{\bar{b}}} + \Gamma_{\underset{\vee}{b\varrho},\bar{\bar{a}}}\,.
\end{array}\right.
$$

2) En ce qui concerne les champs antisymétriques $f_{\mu\nu}$, pour éviter les confusions avec la convention (3) (une même lettre désignant les composantes covariantes du tenseur, le déterminant formé au moyen de ces composantes et le mineur relatif à chacune d'elles) nous *soulignerons*, pour ces champs $f_{\mu\nu}$,

---

[5] Notons ici que la virgule ($A_{ab\ldots,\varrho}$) sert uniquement à séparer un indice et n'a (dans ce travail) aucun rapport avec la notation dérivée ordinaire.

les indices élevés ou abaissés au moyen des $h_{\mu\nu}$. Nous poserons ainsi:

$$(18)\quad \begin{cases} f_{\underline{\mu\nu}} = h_{\mu\varrho}h_{\nu\sigma}f^{\varrho\sigma}; & f^{\underline{\mu\nu}} = h^{\mu\varrho}h^{\nu\sigma}f_{\varrho\sigma}, \\ f_{\mu\nu\underline{\varrho}} = \partial_{\varrho}f_{\mu\nu} + \partial_{\nu}f_{\varrho\mu} + \partial_{\mu}f_{\nu\varrho}; & f_{\underline{\mu\nu\varrho}} = \partial_{\varrho}f_{\underline{\mu\nu}} + \partial_{\nu}f_{\underline{\varrho\mu}} + \partial_{\mu}f_{\underline{\nu\varrho}}. \end{cases}$$

Avec ces notations, les relations (10), (11), (12) s'écrivent encore:

$$(19)\quad \left(\frac{1}{g}-\frac{1}{h}-\frac{1}{f}\right)\delta^{\nu}_{\mu} = \frac{1}{f}f_{\mu\varrho}f^{\underline{\nu\varrho}} + \frac{1}{h}f_{\underline{\mu\varrho}}f^{\nu\varrho},$$

$$(20)\quad \frac{1}{g}-\frac{1}{h}-\frac{1}{f} = \frac{1}{2h}f_{\underline{\mu\nu}}f^{\mu\nu} = \frac{1}{2f}f_{\mu\nu}f^{\underline{\mu\nu}}.$$

b) Introduction des grandeurs $A^{*}_{[\mu\nu]\varrho\ldots}$. – Soit un tenseur quelconque $A_{[\mu\nu]\varrho\ldots}$ *antisymétrique* en μ, ν. Nous définirons:

$$(21)\quad \begin{cases} A^{*}_{[\mu\nu]\varrho\ldots} = \dfrac{\sqrt{-h}}{2}\varepsilon_{\mu\nu\pi\alpha}h^{\pi\beta}h^{\alpha\gamma}A_{[\beta\gamma]\varrho\ldots}, \\ A^{**}_{[\mu\nu]\varrho\ldots} = \dfrac{\sqrt{-h}}{2}\varepsilon_{\mu\nu\pi\alpha}h^{\pi\beta}h^{\alpha\gamma}A^{*}_{[\beta\gamma]\varrho\ldots}. \end{cases}$$

On peut démontrer l'identité suivante:

$$(22)\quad A^{**}_{[\mu\nu]\varrho\ldots} = -A_{[\mu\nu]\varrho\ldots}.$$

On a, en effet, par définition:

$$A^{**}_{[\mu\nu]\varrho\ldots} = -\frac{h}{4}\varepsilon_{\mu\nu\pi\alpha}h^{\pi\beta}h^{\alpha\gamma}\varepsilon_{\beta\gamma\lambda\tau}h^{\lambda\delta}h^{\tau\varepsilon}A_{[\delta\varepsilon]\varrho\ldots}$$

et d'après (7)

$$A^{**}_{[\mu\nu]\varrho\ldots} = -\tfrac{1}{4}\varepsilon^{\pi\alpha\beta\gamma}\varepsilon_{\beta\gamma\lambda\tau}h_{\pi\mu}h_{\alpha\nu}h^{\lambda\delta}h^{\tau\varepsilon}A_{[\delta\varepsilon]\varrho\ldots} = -A_{[\mu\nu]\varrho\ldots}.$$

2. – Résolution des équations $g^{\underline{+-}\,\mu\nu}_{\ ;\varrho} = 0$.

Les équations $g^{\underline{+-}\,\mu\nu}_{\ ;\varrho} = 0$ s'écrivent de la manière suivante:

$$(\mathrm{II})\quad g^{\underline{+-}\,\mu\nu}_{\ ,\varrho} \equiv \partial_{\varrho}g^{\mu\nu} + \Gamma^{\mu}_{\sigma\varrho}g^{\sigma\nu} + \Gamma^{\nu}_{\varrho\sigma}g^{\mu\sigma} = 0.$$

Pour les résoudre, il faut trouver l'expression des $\Gamma^{\varrho}_{\mu\nu}$ en fonction des champs $g^{\mu\nu}$, $h^{\mu\nu}$, $f^{\mu\nu}$ et de leurs dérivées.

Soient $\Gamma^{\varrho}_{\underline{\mu\nu}}$ et $\Gamma^{\varrho}_{\underset{\vee}{\mu\nu}}$ les parties symétrique et antisymétrique de la connexion affine. On a:

$$\Gamma^{\varrho}_{\mu\nu} = \Gamma^{\varrho}_{\underline{\mu\nu}} + \Gamma^{\varrho}_{\underset{\vee}{\mu\nu}} .$$

Désignons le vecteur de torsion par

$$\Gamma_{\varrho} = \Gamma^{\sigma}_{\underset{\vee}{\varrho\sigma}} . \tag{23}$$

On a toujours les identités suivantes:

$$\tfrac{1}{2}(\mathcal{G}^{+-}{}^{\mu\,\varrho}_{\ ;\varrho} - \mathcal{G}^{+-}{}^{\varrho\,\mu}_{\ ;\varrho}) \equiv \partial_{\varrho}(\sqrt{-g} f^{\mu\varrho}) - \sqrt{-g} h^{\mu\varrho}\Gamma_{\varrho} , \tag{24}$$

avec

$$\mathcal{G}^{\mu\varrho} = \sqrt{-g} g^{\mu\varrho} .$$

Si d'après (II), $\mathcal{G}^{+-}{}^{\mu\,\nu}_{\ ;\varrho} = 0$, on déduit de (24)

$$\Gamma_{\varrho} = \frac{1}{\sqrt{-g}} h_{\varrho\sigma}\partial_{\lambda}(\sqrt{-g} f^{\sigma\lambda}) . \tag{25}$$

2°1. *La connexion affine est fonction des coefficients antisymétriques* $\Gamma^{\varrho}_{\underset{\vee}{\mu\nu}}$. — En scindant en parties symétrique et antisymétrique, (II) s'écrit

$$\partial_{\varrho} h^{\mu\nu} + (\Gamma^{\mu}_{\underline{\sigma\varrho}} h^{\sigma\nu} + \Gamma^{\nu}_{\underline{\sigma\varrho}} h^{\sigma\mu}) + (\Gamma^{\mu}_{\underset{\vee}{\sigma\varrho}} f^{\sigma\nu} + \Gamma^{\nu}_{\underset{\vee}{\sigma\varrho}} f^{\sigma\mu}) = 0 , \tag{26}$$

$$\partial_{\varrho} f^{\mu\nu} + (\Gamma^{\mu}_{\underline{\sigma\varrho}} f^{\sigma\nu} - \Gamma^{\nu}_{\underline{\sigma\varrho}} f^{\sigma\mu}) + (\Gamma^{\mu}_{\underset{\vee}{\sigma\varrho}} h^{\sigma\nu} - \Gamma^{\nu}_{\underset{\vee}{\sigma\varrho}} h^{\sigma\mu}) = 0 . \tag{27}$$

En multipliant par $h_{a\mu}h_{b\nu}$ et en tenant compte de (5), on obtient

$$\partial_{\varrho} h_{ab} - \Gamma_{\underline{b\varrho},a} - \Gamma_{\underline{a\varrho},b} - h_{b\nu} f^{\sigma\nu}\Gamma_{\underset{\vee}{\sigma\varrho},a} - h_{a\mu} f^{\sigma\mu}\Gamma_{\underset{\vee}{\sigma\varrho},b} = 0 , \tag{S_1}$$

$$h_{a\mu}h_{b\nu}\partial_{\varrho} f^{\mu\nu} + (h_{b\nu}\Gamma_{\underline{\sigma\varrho},a} - h_{a\nu}\Gamma_{\underline{\sigma\varrho},b}) f^{\sigma\nu} + \Gamma_{\underset{\vee}{b\varrho},a} + \Gamma_{\underset{\vee}{\varrho a},b} = 0 , \tag{A_1}$$

en posant

$$\Gamma_{\underline{\mu\nu},\varrho} = h_{\varrho\sigma}\Gamma^{\sigma}_{\underline{\mu\nu}} \qquad \Gamma_{\underset{\vee}{\mu\nu},\varrho} = h_{\varrho\sigma}\Gamma^{\sigma}_{\underset{\vee}{\mu\nu}} . \tag{28}$$

En permutant, dans (S_1) et (A_1), ϱ et a puis ϱ et b, on obtient des équations

analogues (S_2) et (A_2), puis (S_3) et (A_3). Formons $(S_2) + (S_3) - (S_1)$ et d'autre part $(A_2) + (A_3) - (A_1)$. Nous avons [6]:

$$(S)\qquad 2[ab, \varrho] - 2\underset{\vee}{\Gamma}_{\underline{ab},\varrho} - (h_{\varrho\nu}\underset{\vee}{\Gamma}_{\sigma\underline{a},b} + h_{b\nu}\underset{\vee}{\Gamma}_{\sigma\underline{a},\varrho})f^{\sigma\nu} - \\ - (h_{a\nu}\underset{\vee}{\Gamma}_{\sigma\underline{b},\varrho} + h_{\varrho\nu}\underset{\vee}{\Gamma}_{\sigma\underline{b},a})f^{\sigma\nu} + (h_{b\nu}\underset{\vee}{\Gamma}_{\sigma\underline{\varrho},a} + h_{a\nu}\underset{\vee}{\Gamma}_{\sigma\underline{\varrho},b})f^{\sigma\nu} = 0\,,$$

$$(A)\qquad 2\underset{\vee}{\Gamma}_{\underline{ab},\varrho} + (h_{\varrho\mu}h_{a\nu}\partial_b f^{\mu\nu} + h_{b\mu}h_{\varrho\nu}\partial_a f^{\mu\nu} - h_{a\mu}h_{b\nu}\partial_\varrho f^{\mu\nu}) - \\ - f^{\tau\nu}[h_{b\nu}(\Gamma_{\underline{\tau a},\varrho} + \Gamma_{\underline{\tau\varrho},a}) - h_{a\nu}(\Gamma_{\underline{\tau b},\varrho} + \Gamma_{\underline{\tau\varrho},b}) + h_{\varrho\nu}(\Gamma_{\underline{\tau b},a} - \Gamma_{\underline{\tau a},b})] = 0\,,$$

en posant

$$(29)\qquad [ab, \varrho] = \tfrac{1}{2}(\partial_a h_{b\varrho} + \partial_b h_{a\varrho} - \partial_\varrho h_{ab}); \qquad \left\{ \begin{matrix} \varrho \\ \mu\nu \end{matrix} \right\} = \tfrac{1}{2} h^{\varrho\sigma}(\partial_\mu h_{\nu\sigma} + \partial_\nu h_{\mu\sigma} - \partial_\sigma h_{\mu\nu})\,.$$

Notons qu'en formant $(S_1) + (S_2) + (S_3)$ et $(A_1) + (A_2) + (A_3)$ on obtient

$$(S')\qquad \partial_a h_{b\varrho} + \partial_b h_{\varrho a} + \partial_\varrho h_{ab} - 2(\Gamma_{\underline{ab},\varrho} + \Gamma_{\underline{\varrho a},b} + \Gamma_{\underline{b\varrho},a}) - \\ - f^{\sigma\nu}[h_{a\nu}(\underset{\vee}{\Gamma}_{\sigma\underline{\varrho},b} + \underset{\vee}{\Gamma}_{\sigma\underline{b},\varrho}) + h_{b\nu}(\underset{\vee}{\Gamma}_{\sigma\underline{\varrho},a} + \underset{\vee}{\Gamma}_{\sigma\underline{a},\varrho}) + h_{\varrho\nu}(\underset{\vee}{\Gamma}_{\sigma\underline{b},a} + \underset{\vee}{\Gamma}_{\sigma\underline{a},b})] = 0\,,$$

$$(A')\qquad 2\Gamma_{ab\varrho} + h_{a\mu}h_{b\nu}\partial_\varrho f^{\mu\nu} + h_{\varrho\mu}h_{a\nu}\partial_b f^{\mu\nu} + h_{b\mu}h_{\varrho\nu}\partial_a f^{\mu\nu} + \\ + f^{\sigma\nu}[h_{a\nu}(\Gamma_{\underline{\sigma b},\varrho} - \Gamma_{\underline{\sigma\varrho},b}) + h_{b\nu}(\Gamma_{\underline{\sigma\varrho},a} - \Gamma_{\underline{\sigma a},\varrho}) + h_{\varrho\nu}(\Gamma_{\underline{\sigma a},b} - \Gamma_{\underline{\sigma b},a})] = 0\,,$$

équations qui sont des conséquences de (S) et de (A).

D'après (S)

$$(30)\qquad 2\underset{\vee}{\Gamma}_{\underline{ab},\varrho} = 2[ab, \varrho] - f^{\sigma\nu}[h_{\varrho\nu}(\underset{\vee}{\Gamma}_{\sigma\underline{a},b} + \underset{\vee}{\Gamma}_{\sigma\underline{b},a}) + h_{b\nu}(\underset{\vee}{\Gamma}_{\sigma\underline{a},\varrho} - \underset{\vee}{\Gamma}_{\sigma\underline{\varrho},a}) + h_{a\nu}(\underset{\vee}{\Gamma}_{\sigma\underline{b},\varrho} - \underset{\vee}{\Gamma}_{\sigma\underline{\varrho},b})]\,.$$

Par conséquent, la connexion affine sera complètement déterminée en fonction des champs $h_{\mu\nu}$ et $f_{\mu\nu}$ si l'on connaît les 24 coefficients antisymétriques $\underset{\vee}{\Gamma}_{\mu\nu,\varrho} = h_{\varrho\sigma}\underset{\vee}{\Gamma}^{\sigma}_{\mu\nu}$.

2·2. *Elimination de la partie symétrique de la connexion affine.* – Si l'on porte dans (A) les valeurs (30) de la partie symétrique de la connexion, on obtiendra 24 équations en $\underset{\vee}{\Gamma}_{\underline{ab},\varrho}$.

---

[6] M. Lenoir (*Compt. Rend.*, 1955) a obtenu ces équations en procédant d'une manière légèrement différente.

Désignons par ∇_ϱ la dérivation covariante effectuée au moyen des symboles (29). Par définition:

$$(31)\qquad \begin{cases} \nabla_\varrho h_{\mu\nu} = 0; \qquad \nabla_\varrho f^{\mu\nu} = \partial_\varrho f^{\mu\nu} + \left\{ \begin{matrix} \mu \\ \sigma\varrho \end{matrix} \right\} f^{\sigma\nu} + \left\{ \begin{matrix} \nu \\ \sigma\varrho \end{matrix} \right\} f^{\mu\sigma}, \\ \nabla_\varrho f_{\underline{ab}} = \nabla_\varrho h_{a\mu} h_{b\nu} f^{\mu\nu} = h_{a\mu} h_{b\nu} \partial_\varrho f^{\mu\nu} + h_{b\nu} f^{\sigma\nu}[\sigma\varrho, a] + h_{a\nu} f^{\nu\sigma}[\sigma\varrho, b], \end{cases}$$

d'après (18).

Eliminons dans (A), au moyen de (30), les coefficients symétriques $\Gamma_{\underline{\tau a, \varrho}}$ etc. On a, en tenant compte de (31):

$$(32)\qquad 2\Gamma_{\underset{\vee}{ab,\varrho}} + \nabla_a f_{\underline{b\varrho}} + \nabla_b f_{\underline{\varrho a}} - \nabla_\varrho f_{\underline{ab}} + 2h_{a\nu} h_{b\lambda} f^{\tau\nu} f^{\sigma\lambda} \Gamma_{\underset{\vee}{\tau\sigma,\varrho}} +$$

$$+ f^{\tau\nu} f^{\sigma\lambda}[h_{a\nu} h_{\varrho\lambda}(\Gamma_{\underset{\vee}{\tau\sigma,b}} + \Gamma_{\underset{\vee}{\tau b,\sigma}}) - h_{b\nu} h_{\varrho\lambda}(\Gamma_{\underset{\vee}{\tau\sigma,a}} + \Gamma_{\underset{\vee}{\tau a,\sigma}}) - h_{\varrho\nu} h_{\tau\lambda}(\Gamma_{\underset{\vee}{\sigma a,b}} + \Gamma_{\underset{\vee}{b\sigma,a}})] = 0 .$$

D'après les définitions (14), (18) et (31), les équations (32) peuvent encore s'écrire:

$$(33)\qquad 2\Gamma_{\underset{\vee}{ab,\varrho}} + f_{ab\varrho} - 2\nabla_\varrho f_{\underline{ab}} + h_{a\nu} h_{b\lambda} \Gamma_{\underset{\vee}{\tau\sigma,\varrho}} (f^{\tau\nu} f^{\sigma\lambda} - f^{\sigma\nu} f^{\tau\lambda} - f^{\tau\sigma} f^{\nu\lambda}) + f_{\underline{ab}} f^{\mu\nu} \Gamma_{\underset{\vee}{\mu\nu,\varrho}} +$$

$$+ (h_{a\nu} h_{\varrho\lambda} \Gamma_{\tau\sigma b} - h_{b\nu} h_{\varrho\lambda} \Gamma_{\tau\sigma a} - h_{\varrho\nu} h_{\tau\lambda} \Gamma_{ab\sigma}) f^{\tau\nu} f^{\sigma\lambda} +$$

$$+ \Gamma_{\underset{\vee}{ab,\bar{\bar{\varrho}}}} + 2h_{a\nu} f^{\tau\nu} \Gamma_{\underset{\vee}{b\tau,\bar{\varrho}}} + 2h_{b\nu} f^{\tau\nu} \Gamma_{\underset{\vee}{\tau a,\bar{\varrho}}} + h_{\varrho\lambda} f^{\sigma\lambda} \Gamma_{\underset{\vee}{\sigma b,\bar{a}}} + h_{\varrho\lambda} f^{\sigma\lambda} \Gamma_{\underset{\vee}{a\sigma,\bar{b}}} = 0 ,$$

car $f_{\underline{ab\varrho}} = \nabla_a f_{\underline{b\varrho}} + \nabla_b f_{\underline{\varrho a}} + \nabla_\varrho f_{\underline{ab}}$.

Mais, d'après (8) et (9)

$$(34)\qquad f^{\tau\nu} f^{\sigma\lambda} - f^{\sigma\nu} f^{\tau\lambda} - f^{\tau\sigma} f^{\nu\lambda} = \frac{1}{\sqrt{f}} \varepsilon^{\tau\nu\sigma\lambda} .$$

Donc

$$(35)\qquad h_{a\nu} h_{b\lambda} \Gamma_{\underset{\vee}{\tau\sigma,\varrho}} (f^{\tau\nu} f^{\sigma\lambda} - f^{\sigma\nu} f^{\tau\lambda} - f^{\tau\sigma} f^{\nu\lambda}) = \frac{2\sqrt{-h}}{\sqrt{f}} \Gamma^*_{\underset{\vee}{ab,\varrho}} ,$$

en utilisant les notations (21).

D'autre part, en tenant compte des définitions (14) et (17)

$$(36)\qquad 2f^{\tau\nu}(h_{a\nu} \Gamma_{\underset{\vee}{b\tau,\bar{\varrho}}} + h_{b\nu} \Gamma_{\underset{\vee}{\tau a,\bar{\varrho}}}) + h_{\varrho\lambda} f^{\sigma\lambda}(\Gamma_{\underset{\vee}{\sigma b,\bar{a}}} + \Gamma_{\underset{\vee}{a\sigma,\bar{b}}}) =$$

$$= 2f^{\sigma\lambda}(h_{a\lambda} \bar{\Gamma}_{b\sigma\varrho} + h_{b\lambda} \bar{\Gamma}_{\sigma a\varrho}) + h_{\varrho\lambda} f^{\sigma\lambda} \bar{\Gamma}_{a\sigma b} - 2\bar{\bar{\Gamma}}_{ab\varrho} + \Gamma_{\underset{\vee}{ab,\bar{\bar{\varrho}}}} - 2f^{\sigma\lambda}(h_{a\lambda} \Gamma_{\underset{\vee}{\sigma\varrho,\bar{b}}} + h_{b\lambda} \Gamma_{\underset{\vee}{\varrho\sigma,\bar{a}}}) .$$

Substituant (35) et (36) dans (33), on a:

$$(37)\qquad 2\Gamma_{\underset{\vee}{ab,\varrho}} + f_{\underline{\underline{ab}}\,\underline{\underline{\varrho}}} - 2\nabla_{\varrho} f_{\underline{\underline{ab}}} + \frac{2\sqrt{-h}}{\sqrt{f}}\,\Gamma^{*}_{\underset{\vee}{ab,\varrho}} + f_{\underline{\underline{ab}}} f^{\mu\nu}\Gamma_{\underset{\vee}{\mu\nu,\varrho}} +$$

$$+ (h_{a\nu}h_{\varrho\lambda}\Gamma_{\tau\sigma b} - h_{b\nu}h_{\varrho\lambda}\Gamma_{\tau\sigma a} - h_{\varrho\nu}h_{\tau\lambda}\Gamma_{ab\sigma}) f^{\tau\nu} f^{\sigma\lambda} + 2\Gamma_{\underset{\vee}{ab,\bar{\bar{\varrho}}}} - 2\overline{\overline{\Gamma}}_{ab,\varrho} +$$

$$+ 2f^{\sigma\lambda}(h_{a\lambda}\overline{\Gamma}_{b\sigma\varrho} + h_{b\lambda}\overline{\Gamma}_{\sigma a\varrho}) + h_{\varrho\lambda} f^{\sigma\lambda}\overline{\Gamma}_{a\sigma b} - 2f^{\sigma\lambda}(h_{a\lambda}\Gamma_{\underset{\vee}{\sigma\varrho,\bar{b}}} + h_{b\lambda}\Gamma_{\underset{\vee}{\varrho\sigma,\bar{a}}}) = 0\,.$$

La résolution de ces 24 équations en $\Gamma_{\underset{\vee}{ab,\varrho}}$ permettra l'expression de la connexion affine en fonction des champs $h_{\mu\nu}$ et $f_{\mu\nu}$. Notons ici l'analogie avec la résolution des équations $g_{\underset{+-}{\mu\nu;\varrho}} = 0$. Mais la comparaison des équations (37) avec les équations (E) [cf. (4), p. 25] montre que la résolution des équations $g^{\underset{+-}{\mu\nu}}_{\;\;;\varrho} = 0$ est un peu plus compliquée. Néanmoins, les méthodes employées sont tout à fait comparables.

2·3. *Obtention d'un groupe d'équations en* $\Gamma_{\underset{\vee}{ab,\varrho}}$, $\Gamma^{*}_{\underset{\vee}{ab,\varrho}}$ *et* $\Gamma_{\underset{\vee}{ab,\bar{\bar{\varrho}}}}$. – Nous allons transformer (37) de manière à obtenir un groupe d'équations dans lequel les inconnues, c'est-à-dire les 24 coefficients de connexion affine, interviennent uniquement sous la forme $\Gamma_{\underset{\vee}{ab,\varrho}}$, $\Gamma^{*}_{\underset{\vee}{ab,\varrho}}$ et $\Gamma_{\underset{\vee}{ab,\bar{\bar{\varrho}}}}$ [cf. les définitions (21) et (14)], a, b et ϱ ayant la même valeur dans une équation déterminée.

Nous calculerons successivement les différents termes figurant dans (37) en procédant par étapes. Nous introduirons aussi les deux intermédiaires de calcul suivants:

$$(38)\qquad M_{\varrho} = \tfrac{1}{2} f^{\underline{\underline{\mu\nu}}}\Gamma_{\underset{\vee}{\mu\nu,\varrho}}\,,$$

$$(39)\qquad N_{\varrho} = \tfrac{1}{2} f^{\mu\nu}\Gamma_{\underset{\vee}{\mu\nu,\varrho}}\,.$$

a) Calcul de $f^{\sigma\lambda}\,(h_{a\lambda}\Gamma_{\underset{\vee}{\sigma\varrho,\bar{b}}} + h_{b\lambda}\Gamma_{\underset{\vee}{\varrho\sigma,\bar{a}}})$. – On trouve (cf. Appendice II)

$$(40)\qquad f^{\sigma\lambda}(h_{a\lambda}\Gamma_{\underset{\vee}{\sigma\varrho,\bar{b}}} + h_{b\lambda}\Gamma_{\underset{\vee}{\varrho\sigma,\bar{a}}}) = \frac{\sqrt{-h}}{\sqrt{f}}\,\Gamma^{*}_{[ab]\varrho} - \frac{\sqrt{-h}}{\sqrt{f}}\,\Gamma^{*}_{\underset{\vee}{ab,\varrho}} + \tfrac{1}{2} f^{\sigma\nu} f_{\underline{\underline{ab}}}\Gamma_{\sigma\nu\varrho} - f_{\underline{\underline{ab}}} N_{\varrho}\,.$$

b) Calcul de $\overline{\Gamma}_{\mu\nu\varrho}$. – Le calcul explicité dans l'Appendice III conduit à:

$$(41)\qquad \overline{\Gamma}_{\mu\nu\varrho} = -\frac{h}{\sqrt{f}}\,\varepsilon_{\mu\nu\varrho\sigma} f^{\underline{\underline{\lambda\sigma}}}\Gamma_{\lambda} + \frac{h}{\sqrt{f}}\,\varepsilon_{\mu\nu\varrho\sigma} h^{\sigma\lambda} M_{\lambda}\,.$$

c) Calcul de $\overline{\Gamma}_{ab\varrho}$. – Le détail du calcul est donné dans l'Appendice IV.

On trouve en définitive l'expression suivante:

$$(42)\quad \overline{\overline{\Gamma}}_{ab\varrho} = \left(1 - \frac{h}{g} + \frac{h}{f}\right)\Gamma_{ab\varrho} + \frac{h}{2\sqrt{f}}\,\varepsilon_{ab\varrho\sigma]}f^{\lambda\sigma}f^{\pi\tau}\Gamma_{\lambda\pi\tau} + \frac{h}{\sqrt{f}}\,\varepsilon_{ab\varrho\sigma}(f^{\lambda\sigma}N_\lambda - f^{\lambda\sigma}M_\lambda)\,.$$

d) Calcul de $(h_{a\nu}h_{\varrho\lambda}\Gamma_{\tau\sigma b} - h_{b\nu}h_{\varrho\lambda}\Gamma_{\tau\sigma a})f^{\tau\nu}f^{\sigma\lambda}$. – Cette expression peut s'écrire:

$$\begin{aligned}(h_{a\nu}h_{\varrho\lambda}\Gamma_{\tau\sigma b} - h_{b\nu}h_{\varrho\lambda}\Gamma_{\tau\sigma a})f^{\tau\nu}f^{\sigma\lambda} &= \tfrac{1}{2}h_{a\nu}h_{\varrho\lambda}(f^{\tau\nu}f^{\sigma\lambda} - f^{\sigma\nu}f^{\tau\lambda} - f^{\tau\sigma}f^{\nu\lambda})\Gamma_{\tau\sigma b} + \\ &+ \tfrac{1}{2}h_{a\nu}h_{\varrho\lambda}f^{\tau\sigma}f^{\nu\lambda}\Gamma_{\tau\sigma b} - \tfrac{1}{2}h_{b\nu}h_{\varrho\lambda}(f^{\tau\nu}f^{\sigma\lambda} - f^{\sigma\nu}f^{\tau\lambda} - f^{\tau\sigma}f^{\nu\lambda})\Gamma_{\tau\sigma a} - \tfrac{1}{2}h_{b\nu}h_{\varrho\lambda}f^{\tau\sigma}f^{\nu\lambda}\Gamma_{\tau\sigma a} = \\ &= \frac{h}{2\sqrt{f}}\,h^{\nu\sigma}h^{\lambda\tau}(\varepsilon_{\nu\lambda a\varrho}\Gamma_{\tau\sigma b} - \varepsilon_{\nu\lambda b\varrho}\Gamma_{\tau\sigma a}) + \tfrac{1}{2}f^{\tau\sigma}(f_{a\varrho}\Gamma_{\tau\sigma b} + f_{\varrho b}\Gamma_{\tau\sigma a})\,,\end{aligned}$$

$$(43)\qquad = \frac{\sqrt{-h}}{\sqrt{f}}\,(\Gamma^*_{[a\varrho]b} + \Gamma^*_{[\varrho b]a}) + \tfrac{1}{2}f^{\tau\sigma}(f_{a\varrho}\Gamma_{\tau\sigma b} + f_{\varrho b}\Gamma_{\tau\sigma a})\,,$$

d'après (34), (7) et en utilisant les notations (21).

En portant ces différentes expressions (40), (41), (42) et (43) dans (37), nous obtenons les équations suivantes:

$$\begin{aligned}(44)\quad & 2\Gamma_{\underset{\vee}{ab},\varrho} + \frac{4\sqrt{-h}}{\sqrt{f}}\,\Gamma^*_{\underset{\vee}{ab},\varrho} + 2\Gamma_{\underset{\vee}{ab},\overline{\overline{\varrho}}} + f_{ab}\,{}_{\varrho} - 2\nabla_\varrho f_{ab} + \frac{\sqrt{-h}}{\sqrt{f}}\,(\Gamma^*_{[a\varrho]b} + \Gamma^*_{[\varrho b]a} + \Gamma^*_{[ba]\varrho}) - \\ & - \frac{\sqrt{-h}}{\sqrt{f}}\,\Gamma^*_{[ab]\varrho} + 4f_{ab}N_\varrho - \frac{2h}{\sqrt{f}}\,\varepsilon_{ab\varrho\sigma}f^{\lambda\sigma}N_\lambda + \\ & + \tfrac{1}{2}f^{\tau\sigma}(f_{a\varrho}\Gamma_{\tau\sigma b} + f_{\varrho b}\Gamma_{\tau\sigma a}) - f_{ab}f^{\tau\sigma}\Gamma_{\tau\sigma\varrho} + f_{\varrho\lambda}f^{\sigma\lambda}\Gamma_{ab\sigma} - 2\left(1 - \frac{h}{g} + \frac{h}{f}\right)\Gamma_{ab\varrho} - \\ & - \frac{h}{\sqrt{f}}\,\varepsilon_{ab\varrho\sigma}f^{\lambda\sigma}f^{\pi\tau}\Gamma_{\lambda\pi\tau} + \frac{2h}{\sqrt{f}}\,\varepsilon_{ab\varrho\sigma}f^{\lambda\sigma}M_\lambda + \\ & + \frac{2h}{\sqrt{f}}\,f^{\sigma\lambda}(h_{a\lambda}\varepsilon_{b\sigma\varrho\tau} + h_{b\lambda}\varepsilon_{\sigma a\varrho\tau} + h_{\varrho\lambda}\varepsilon_{a\sigma b\tau})(h^{\tau\mu}M_\mu + f^{\tau\mu}\Gamma_\mu) - \\ & - \frac{h}{\sqrt{f}}\,f^{\sigma\lambda}h_{\varrho\lambda}\varepsilon_{a\sigma b\tau}(h^{\tau\mu}M_\mu + f^{\mu\tau}\Gamma_\mu) = 0\,.\end{aligned}$$

Ces équations peuvent se simplifier en tenant compte des relations suivantes que l'on peut aisément vérifier, pour $a \neq b \neq \varrho$.

$$(45)\qquad \Gamma^*_{[a\varrho]b} + \Gamma^*_{[\varrho b]a} + \Gamma^*_{[ba]\varrho} \equiv 0\,,$$

$$(46)\qquad \tfrac{1}{2}f^{\tau\sigma}(f_{a\varrho}\Gamma_{\tau\sigma b} + f_{\varrho b}\Gamma_{\tau\sigma a} + f_{ba}\Gamma_{\tau\sigma\varrho}) \equiv -\frac{h}{2\sqrt{f}}\,\varepsilon_{ab\varrho\sigma}f^{\lambda\sigma}f^{\pi\tau}\Gamma_{\pi\tau\lambda}\,,$$

$$(47)\qquad (f^{\mu\nu}f^{\lambda\sigma} + f^{\mu\nu}f^{\lambda\sigma})\Gamma_{\mu\nu\lambda} = \frac{\sqrt{f}}{3}\left(\frac{1}{g} - \frac{1}{h} - \frac{1}{f}\right)\varepsilon^{\mu\nu\lambda\sigma}\Gamma_{\mu\nu\lambda}\,.$$

Il suffit de tenir compte des définitions (21) [pour (45)], des relations (III.1) [pour (46)], et des relations (19) et (20) [pour (47)].

Ces 3 dernières relations, (45), (46) et (47) sont naturellement valables pour tout pseudo-vecteur analogue à $\Gamma_{\mu\nu\lambda}$ (17), c'est-à-dire en particulier pour $f_{\mu\nu\lambda}$, $f_{\underline{\mu\nu\lambda}}$, ... D'autre part, on vérifie aisément que pour $a \neq b \neq \varrho$

$$f^{\sigma\lambda}h^{\tau\mu}M_\mu(h_{a\lambda}\varepsilon_{b\sigma\varrho\tau} + h_{b\lambda}\varepsilon_{\sigma a\varrho\tau} + h_{\varrho\lambda}\varepsilon_{a\sigma b\tau}) = -\varepsilon_{ab\varrho\sigma}f^{\lambda\sigma}M_\lambda\,, \tag{48}$$

$$\frac{2h}{\sqrt{f}}f^{\sigma\lambda}f^{\underline{\tau\mu}}\Gamma_\mu(h_{a\lambda}\varepsilon_{b\sigma\varrho\tau} + h_{b\lambda}\varepsilon_{\sigma a\varrho\tau} + h_{\varrho\lambda}\varepsilon_{a\sigma b\tau}) - \frac{h}{\sqrt{f}}h_{\varrho\lambda}f^{\sigma\lambda}\varepsilon_{a\sigma b\tau}f^{\underline{\tau\mu}}\Gamma_\mu = \tag{49}$$

$$= -\frac{2h}{\sqrt{f}}\varepsilon_{ab\varrho\sigma}h^{\lambda\sigma}\Gamma_\lambda + \frac{h}{\sqrt{f}}h_{\varrho\lambda}f^{\sigma\lambda}\varepsilon_{a\sigma b n}f^{\underline{mn}}\Gamma_m\,,$$

en appliquant (48) au quadrivecteur Γ_μ.

Enfin un calcul dont le détail est indiqué dans l'Appendice V conduit à l'expression suivante:

$$\frac{h}{\sqrt{f}}h_{\varrho\lambda}f^{\sigma\lambda}\varepsilon_{ab\sigma\tau}h^{\mu\tau}M_\mu = \frac{h\sqrt{-h}}{f}\overset{*}{\varepsilon}_{[ab]\varrho n}f^{\underline{mn}}M_m + \frac{h}{f}f_{ab}M_\varrho\,. \tag{50}$$

En définitive, en tenant compte de (45), (46), (47), (48), (49), (50), les équations (44) peuvent se mettre sous la forme suivante:

$$2\Gamma_{\underset{\vee}{ab},\varrho} + \frac{4\sqrt{-h}}{\sqrt{f}}\Gamma^*_{\underset{\vee}{ab},\varrho} + 2\Gamma_{\underset{\vee}{ab},\bar{\bar{\varrho}}} + f_{\underline{ab\varrho}} - 2\nabla_\varrho f_{\underline{ab}} - \tag{51}$$

$$-\frac{2h}{\sqrt{f}}\varepsilon_{ab\varrho\sigma}h^{\sigma\lambda}\Gamma_\lambda + \frac{h}{\sqrt{f}}h_{\varrho\lambda}f^{\sigma\lambda}\varepsilon_{a\sigma bn}f^{\underline{mn}}\Gamma_m -$$

$$-\frac{\sqrt{-h}}{\sqrt{f}}\Gamma^*_{[ab]\varrho} - \Gamma_{ab\bar{\bar{\varrho}}} - \left(1 - \frac{h}{g} + \frac{h}{f}\right)\Gamma_{ab\varrho} + \tfrac{1}{2}f^{\tau\sigma}f_{\underline{b\sigma}}\Gamma_{\tau\sigma\varrho} - \frac{h}{2\sqrt{f}}\varepsilon_{ab\varrho\sigma}f^{\lambda\sigma}f^{\underline{\pi\tau}}\Gamma_{\lambda\pi\tau} +$$

$$+ 4f_{\underline{ab}}N_\varrho - \frac{2h}{\sqrt{f}}\varepsilon_{ab\varrho\sigma}f^{\underline{\lambda\sigma}}N_\lambda + \frac{h}{f}f_{ab}M_\varrho + \frac{h\sqrt{-h}}{f}\overset{*}{\varepsilon}_{[ab]\varrho n}f^{\underline{mn}}M_m = 0\,,$$

$\Gamma_{b\sigma\bar{\bar{\varrho}}}$ étant défini par (14)

$$\Gamma_{ab\bar{\bar{\varrho}}} = h_{\varrho\lambda}f^{\lambda\mu}h_{\mu\nu}f^{\nu\pi}\Gamma_{ab\pi}\,.$$

Nous aurons les équations cherchées si, dans (51), nous exprimons $\Gamma_{ab\varrho}$, M_ϱ et N_ϱ en fonction des quantités connues $h_{\mu\nu}$, $f_{\mu\nu}$ et Γ_μ [connu d'après (25)].

Notons ici la différence essentielle avec la résolution des équations $g_{\underset{+}{\mu\nu};\varrho} = 0$ [2]. Outre des équations en général plus compliquées, les intermédiaires de calcul

$\Gamma_{ab\varrho}$, M_ϱ et N_ϱ ne résultent pas directement de (A'). Leur évaluation est beaucoup moins simple, et ne s'obtient pas de la même manière. Nous allons l'indiquer à présent.

e) Calcul de $\Gamma_{ab\varrho}$, M_ϱ *et* N_ϱ. – Dans les équations (51), effectuons une permutation circulaire sur a, b, ϱ et sommons. Compte tenu des relations (42), (III.1), (48) et (45) nous obtenons:

$$2\Gamma_{ab\varrho} + 4\frac{\sqrt{-h}}{\sqrt{f}}(\Gamma^*_{\underset{\vee}{ab,\varrho}} + \Gamma^*_{\underset{\vee}{\varrho a,b}} + \Gamma^*_{\underset{\vee}{b\varrho,a}}) + f_{\underline{\underline{ab\varrho}}} - \frac{5h}{\sqrt{f}}\varepsilon_{ab\varrho\sigma}h^{\sigma\lambda}\Gamma_\lambda - \tag{52}$$

$$- (\Gamma_{a\bar{b}\varrho} + \Gamma_{\varrho\bar{a}\bar{b}} + \Gamma_{b\varrho\bar{a}}) - \frac{h}{\sqrt{f}}\varepsilon_{ab\varrho\sigma}f^{\lambda\sigma}M_\lambda = 0\,.$$

Or, pour $a \neq b \neq \varrho$, on a

$$\Gamma^*_{\underset{\vee}{ab,\varrho}} + \Gamma^*_{\underset{\vee}{\varrho a,b}} + \Gamma^*_{\underset{\vee}{b\varrho,a}} = -\sqrt{-h}\,\varepsilon_{ab\varrho\sigma}h^{\sigma\lambda}\Gamma_\lambda\,. \tag{53}$$

D'autre part, toujours pour $a \neq b \neq \varrho$

$$-(\Gamma_{ab\bar{\varrho}} + \Gamma_{\varrho a\bar{b}} + \Gamma_{b\varrho\bar{a}}) = -2\left(1 - \frac{h}{g} + \frac{h}{f}\right)\Gamma_{ab\varrho} + \frac{h}{2\sqrt{f}}\varepsilon_{ab\varrho\sigma}f^{\sigma\lambda}f^{\pi\tau}\Gamma_{\lambda\pi\tau}\,. \tag{54}$$

On peut donc écrire (52):

$$2h\left(\frac{1}{g} - \frac{1}{f}\right)\Gamma_{ab\varrho} + \frac{h}{2\sqrt{f}}\varepsilon_{ab\varrho\sigma}f^{\sigma\lambda}f^{\pi\tau}\Gamma_{\lambda\pi\tau} - \frac{h}{\sqrt{f}}\varepsilon_{ab\varrho\sigma}f^{\lambda\sigma}M_\lambda + f_{\underline{\underline{ab\varrho}}} - \frac{h}{\sqrt{f}}\varepsilon_{ab\varrho\sigma}h^{\sigma\lambda}\Gamma_\lambda = 0\,. \tag{55}$$

Multiplions (55) par f^{ab}. D'après (8) il vient

$$2h\left(\frac{1}{g} - \frac{1}{f}\right)f^{ab}\Gamma_{ab\varrho} - \frac{h}{f}f^{\pi\tau}\Gamma_{\varrho\pi\tau} - \frac{2h}{f}M_\varrho + f^{ab}f_{\underline{\underline{ab\varrho}}} - \frac{2h}{f}f_{\varrho\sigma}h^{\sigma\lambda}\Gamma_\lambda = 0 \tag{56}$$

d'où l'on tire la valeur de M_ϱ en fonction des champs et de $\Gamma_{ab\varrho}$

$$\boxed{M_\varrho = f\left(\frac{1}{g} - \frac{1}{f}\right)f^{ab}\Gamma_{ab\varrho} - \tfrac{1}{2}f^{ab}\Gamma_{ab\varrho} + \frac{f}{2h}f^{ab}f_{\underline{\underline{ab\varrho}}} - f_{\varrho\sigma}h^{\sigma\lambda}\Gamma_\lambda\,.} \tag{57}$$

D'autre part, en multipliant (51) par $\frac{1}{4}f^{ab}$ et en utilisant les définitions (14),

(21), (39) et (34), on obtient:

$$M_\varrho + N_\varrho + \tfrac{1}{2}M_{\bar{\varrho}} + \tfrac{1}{4}f^{\underline{ab}}f_{\underline{ab}\varrho} - \tfrac{1}{2}f^{\underline{ab}}\nabla_\varrho f_{\underline{ab}} - \tfrac{1}{2}h_{\varrho a}f^{ab}\Gamma_b - \\ - \tfrac{1}{4}\left(1 - \frac{h}{g} + \frac{h}{f}\right)f^{\underline{ab}}\Gamma_{ab\varrho} - \tfrac{1}{4}f^{ab}\Gamma_{ab\varrho} = 0\,, \tag{58}$$

car

$$f_{\varrho\sigma}\varepsilon^{\mu\nu\lambda\sigma}\Gamma_{\mu\nu\lambda} = 3\sqrt{f}\,f^{ab}\Gamma_{ab\varrho}\,. \tag{59}$$

En multipliant (55) par $\frac{1}{4}f^{\underline{ab}}$, puis en formant (58) $-\frac{1}{4}f^{\underline{ab}}$ (55), nous obtenons la relation très simple:

$$\boxed{M_\varrho + N_\varrho - \tfrac{1}{2}f^{\underline{ab}}\nabla_\varrho f_{\underline{ab}} - \tfrac{1}{2}f^{ab}\Gamma_{ab\varrho} - \tfrac{1}{2}f^{\underline{ab}}\Gamma_{ab\varrho} = 0\,.} \tag{60}$$

Enfin, la multiplication de (51) par $\frac{1}{4}f^{ab}$ nous donne après sommation et réduction:

$$\boxed{h\left(\frac{1}{g} - \frac{1}{f}\right)N_\varrho - \frac{3h}{2f}M_\varrho + \frac{h}{4f}f^{\underline{ab}}\Gamma_{ab\varrho} + \tfrac{1}{2}f^{ab}\nabla_a f_{b\varrho} - \tfrac{1}{4}f^{ab}\nabla_\varrho f_{\underline{ab}} - \\ - \frac{h}{2f}f_{\varrho a}h^{ab}\Gamma_b = 0\,.} \tag{61}$$

Nous avons obtenu ainsi 3 relations: (57), (60) et (61), entre les 3 inconnues M_ϱ, N_ϱ, $\Gamma_{ab\varrho}$ qui s'expriment en fonction des champs connus $h_{\mu\nu}$, $f_{\mu\nu}$.

α) *Détermination de* $\Gamma_{ab\varrho}$. – En portant dans (61) les valeurs de M_ϱ et N_ϱ obtenues dans (57) et (60), on obtient une relation où ne figure plus que $\Gamma_{ab\varrho}$ et des quantités connues:

$$\frac{h}{2}\left(\frac{1}{g} - \frac{1}{f}\right)f_{ab}\nabla_\varrho f^{ab} - \frac{f}{2g}f^{ab}f_{\underline{ab}\varrho} - \tfrac{1}{2}f^{ab}\nabla_\varrho f_{\underline{ab}} + \frac{h}{g}f_{\varrho a}h^{ab}\Gamma_b + \\ + \frac{h}{g}\left(1 - \frac{f}{g}\right)f^{ab}\Gamma_{ab\varrho} + \frac{h}{g}f^{\underline{ab}}\Gamma_{ab\varrho} = 0\,. \tag{62}$$

Mais étant donné la définition (31) de la dérivation covariante ∇_ϱ

$$f_{ab}\nabla_\varrho f^{ab} = -\nabla_\varrho \log f = -\partial_\varrho \log\frac{f}{h}\,, \tag{63}$$

$$-\tfrac{1}{2}f^{ab}\nabla_\varrho f_{\underline{ab}} = -\tfrac{1}{2}\nabla_\varrho h\left(\frac{1}{g} - \frac{1}{h} - \frac{1}{f}\right), \tag{64}$$

d'après (20).

On peut donc écrire (62) sous la forme suivante:

$$(65)\qquad -\frac{f}{2g}f^{ab}\underline{\underline{f}}_{ab\varrho}+\frac{h}{2g}\partial_\varrho\log\frac{g}{f}+\frac{h}{g}f_{\varrho\sigma}h^{ab}\Gamma_b+\frac{h}{g}\left(1-\frac{f}{g}\right)f^{ab}\Gamma_{ab\varrho}+\frac{h}{g}\underline{\underline{f}}^{ab}\Gamma_{ab\varrho}=0\,.$$

En multipliant alors (65) par $f^{\varrho\sigma}$, puis par $\underline{\underline{f}}^{\varrho\sigma}$ on a, d'après (34) et (47), deux relations que nous désignerons respectivement par (64_1) et (64_2). Formons $(1-f/g)\ (64_1)+(64_2)$ et multiplions l'équation ainsi obtenue par $\varepsilon_{\mu\nu\lambda\sigma}$. Nous avons:

$$(66)\qquad \Gamma_{\mu\nu\lambda}=\tfrac{1}{2}\left(\frac{g}{f}-1\right)\underline{\underline{f}}_{\mu\nu\lambda}+\frac{g}{4\sqrt{f}}\varepsilon_{\mu\nu\lambda\sigma}\underline{\underline{f}}^{\varrho\sigma}f^{ab}\underline{\underline{f}}_{ab\varrho}-\frac{gh}{4f\sqrt{f}}\left(1-\frac{f}{g}\right)\varepsilon_{\mu\nu\lambda\sigma}\underline{\underline{f}}^{\varrho\sigma}\partial_\varrho\log\frac{g}{f}-$$
$$-\frac{gh}{4f\sqrt{f}}\varepsilon_{\mu\nu\lambda\sigma}\underline{\underline{f}}^{\varrho\sigma}\partial_\varrho\log\frac{g}{f}+\frac{g}{2\sqrt{f}}\varepsilon_{\mu\nu\lambda\sigma}(h^{\sigma\varrho}+f^{\sigma p}f^{\varrho m}h_{pm})\Gamma_\varrho\,.$$

Cette expression peut se simplifier en tenant compte de la valeur (25) de Γ_ϱ, et l'on obtient finalement (voir détail en Appendice VI) l'expression de $\Gamma_{ab\varrho}$ en fonction des $h_{\mu\nu}$ et $f_{\mu\nu}$.

$$(67)\qquad \boxed{\Gamma_{ab\varrho}=-\frac{g}{2f}f_{ab\varrho}-\frac{g}{2h}\underline{\underline{f}}_{ab\varrho}-\frac{gh}{4f\sqrt{f}}\varepsilon_{ab\varrho\sigma}\underline{\underline{f}}^{\mu\nu}f^{\lambda\sigma}f_{\mu\nu\lambda}-\frac{g}{4\sqrt{f}}\varepsilon_{ab\varrho\sigma}\underline{\underline{f}}^{\mu\nu}f^{\lambda\sigma}\underline{\underline{f}}_{\mu\nu\lambda}\,.}$$

β) *Détermination de* M_ϱ. – D'après (57), en remplaçant $\Gamma_{ab\varrho}$ par sa valeur (67) et Γ_ϱ par sa valeur (25), on trouve aisément

$$(68)\qquad \boxed{M_\varrho=\frac{g}{4f}f^{ab}f_{ab\varrho}-\frac{h}{4f}\left(1-\frac{g}{f}\right)\underline{\underline{f}}^{ab}f_{ab\varrho}+\frac{g}{4h}f^{ab}\underline{\underline{f}}_{ab\varrho}-\tfrac{1}{4}\left(1-\frac{g}{f}\right)\underline{\underline{f}}^{ab}\underline{\underline{f}}_{ab\varrho}+\tfrac{1}{2}\partial_\varrho\log\frac{g}{f}}$$

en tenant compte du fait que, d'après (25) (cf. VI.2)

$$(69)\qquad f_{\varrho\sigma}h^{\sigma\lambda}\Gamma_\lambda=-\tfrac{1}{2}\partial_\varrho\log\frac{g}{f}-\tfrac{1}{2}f^{ab}f_{ab\varrho}\,.$$

γ) *Détermination de* N_ϱ. – En portant dans (60) la valeur (67) de $\Gamma_{ab\varrho}$ et la valeur (68) de M_ϱ, on obtient:

$$(70)\qquad \boxed{N_\varrho=-\frac{g}{4f}f^{ab}f_{ab\varrho}-\frac{gh}{4f^2}\underline{\underline{f}}^{ab}f_{ab\varrho}-\frac{g}{4h}f^{ab}\underline{\underline{f}}_{ab\varrho}-\frac{g}{4f}\underline{\underline{f}}^{ab}\underline{\underline{f}}_{ab\varrho}-\tfrac{1}{2}\partial_\varrho\log\frac{g}{h}\,.}$$

Notons qu'on aurait pu calculer différemment ces 3 quantités $\Gamma_{ab\varrho}$, M_ϱ et N_ϱ en nous basant sur les résultats acquis par M. A. TONNELAT dans la résolution des équations $g_{\underset{+}{\mu}\,\underset{-}{\nu};\varrho} = 0$. Cette méthode directe nous a fourni un mode de vérification en nous permettant d'établir la cohérence de nos résultats. A titre d'exemple, nous indiquons (Appendice VII) la marche du calcul de $\Gamma_{\underset{\vee}{ab},\varrho}$ par cette dernière méthode.

En remplaçant enfin les $\Gamma_{ab\varrho}$, M_ϱ et N_ϱ par leur valeur en fonction des champs dans (51), on obtient l'équation

$$\Gamma_{\underset{\vee}{ab},\varrho} + 2\,\frac{\sqrt{-h}}{\sqrt{f}}\,\Gamma^*_{\underset{\vee}{ab},\varrho} + \Gamma_{\underset{\vee}{ab},\bar{\bar{\varrho}}} = U_{\underset{\vee}{ab},\varrho}, \tag{71}$$

où, après réductions [7], $U_{\underset{\vee}{ab},\varrho}$ a la forme suivante:

$$\begin{aligned}
U_{\underset{\vee}{ab}\,\varrho} = {} & -\tfrac{1}{2} f_{\underline{ab}\underline{\varrho}} + \nabla_\varrho f_{\underline{ab}} + \\
& + \left(\frac{g}{f} f_{\mu\nu\varrho} + \frac{g}{h} f_{\underline{\mu\nu}\underline{\varrho}}\right)\left\{\frac{h}{4f}\,(f_{\underline{ab}} f^{\underline{\mu\nu}} - f_{\underline{ab}} f^{\underline{\mu\nu}}) - \tfrac{1}{4} f_{\underline{ab}} f^{\underline{\mu\nu}} + \frac{h^2}{4fg}\left(1 - \frac{g}{f}\right) f_{\underline{ab}} f^{\underline{\mu\nu}}\right\} - \\
& + f_{\underline{ab}}\partial_\varrho \log\frac{g}{h} - \frac{h}{4f} f_{ab}\partial_\varrho \log\frac{g}{f} - \frac{h}{2\sqrt{f}}\,\varepsilon_{ab\varrho\sigma} f^{\underline{\lambda\sigma}}\partial_\lambda \log\frac{g}{h} - \\
& - \frac{h\sqrt{-h}}{4f}\,\varepsilon^*_{[ab]\varrho\sigma} f^{\underline{\lambda\sigma}}\partial_\lambda \log\frac{g}{f} + \\
& + \frac{h}{\sqrt{f}}\,\varepsilon_{ab\varrho\sigma} h^{\sigma\lambda}\Gamma_\lambda - \frac{h}{2\sqrt{f}}\,h_{\varrho\lambda} f^{\sigma\lambda}\varepsilon_{a\sigma bn} f^{\underline{mn}}\Gamma_m\,.
\end{aligned} \tag{72}$$

Dans (72), tout est fonction des champs h et f, y compris ∇_ϱ (31), et Γ_λ (25). Si l'on suppose (comme il résulte de la théorie d'Einstein basée sur l'emploi du tenseur de Ricci) $\Gamma_\varrho = 0$, la dernière ligne de $U_{\underset{\vee}{ab},\varrho}$ dans (72) disparaît [cf. aussi plus loin (83)].

Il reste à présent à expliciter $\Gamma_{\underset{\vee}{ab},\varrho}$ en fonction de $U_{\underset{\vee}{ab},\varrho}$. C'est la dernière partie de ce travail. Notons que cette réduction est tout à fait analogue à la méthode employée dans le cas des équations $g_{\underset{+}{\mu}\,\underset{-}{\nu};\varrho} = 0$.

---

[7] Indiquons la relation suivante qui nous a servi dans la simplification de $\Gamma_{\underset{\vee}{ab},\varrho}$ et que l'on vérifie facilement pour $a \neq b \neq \varrho$

$$f_{ab\bar{\bar{\varrho}}} = \tfrac{1}{2} f_{\underline{ab}} f^{\mu\nu} f_{\mu\nu\varrho} - \frac{h}{2\sqrt{f}}\,\varepsilon_{ab\varrho n} f^{\underline{mn}} f^{\mu\nu} f_{\mu\nu m} - \frac{h}{2f} f_{ab} f^{\underline{\mu\nu}} f_{\mu\nu\varrho}\,.$$

2·4. *Résolution de l'équation* $\Gamma_{\overset{\vee}{ab},\varrho} + 2(\sqrt{-h}/\sqrt{f})\Gamma^{*}_{\overset{\vee}{ab},\varrho} + \Gamma_{\overset{\vee}{ab},\bar{\varrho}} = U_{\overset{\vee}{ab},\varrho}$. — Utilisant les notations (21) pour la partie antisymétrique $[ab]$, formons $(-2\sqrt{-h}/\sqrt{f})$ (71*)

$$-\frac{2\sqrt{-h}}{\sqrt{f}}\,\Gamma^{*}_{\overset{\vee}{ab},\varrho} - \frac{4h}{f}\,\Gamma_{\overset{\vee}{ab},\varrho} - \frac{2\sqrt{-h}}{\sqrt{f}}\,\Gamma^{*}_{\overset{\vee}{ab},\bar{\varrho}} = -\frac{2\sqrt{-h}}{\sqrt{f}}\,U^{*}_{\overset{\vee}{ab},\varrho}, \tag{73}$$

avec (22). Ecrivons maintenant (71), en utilisant les notations surlignées pour l'indice ϱ. On a, avec (16)

$$\Gamma_{\overset{\vee}{ab},\bar{\varrho}} + \frac{2\sqrt{-h}}{\sqrt{f}}\,\Gamma^{*}_{\overset{\vee}{ab},\bar{\varrho}} - h\left(\frac{1}{g} - \frac{1}{h} - \frac{1}{f}\right)\Gamma_{\overset{\vee}{ab},\varrho} - \frac{h}{f}\,\Gamma_{\overset{\vee}{ab},\varrho} = U_{\overset{\vee}{ab},\bar{\varrho}}. \tag{74}$$

Si l'on forme $(2 - h/g + h/f)\times(71) - (73) - (74)$, on trouve:

$$\left(2 - \frac{h}{g} + \frac{6h}{f}\right)\Gamma_{\overset{\vee}{ab},\varrho} + \frac{2\sqrt{-h}}{\sqrt{f}}\left(3 - \frac{h}{g} + \frac{h}{f}\right)\Gamma^{*}_{\overset{\vee}{ab},\varrho} = \tag{75}$$

$$= \left(2 - \frac{h}{g} + \frac{h}{f}\right)U_{\overset{\vee}{ab},\varrho} - U_{\overset{\vee}{ab},\bar{\varrho}} + \frac{2\sqrt{-h}}{\sqrt{f}}\,U^{*}_{\overset{\vee}{ab},\varrho}.$$

La combinaison:

$$\left(2 - \frac{h}{g} + \frac{6h}{f}\right)\cdot(75) - \frac{2\sqrt{-h}}{\sqrt{f}}\left(3 - \frac{h}{g} + \frac{h}{f}\right)\cdot(75^{*}),$$

conduit alors à l'expression suivante:

$$\begin{aligned}
&\left[\left(2 - \frac{h}{g} + \frac{6h}{f}\right)^{2} - \frac{4h}{f}\left(3 - \frac{h}{g} + \frac{h}{f}\right)^{2}\right]\Gamma_{\overset{\vee}{ab},\varrho} = \\
&= \left[\left(2 - \frac{h}{g} + \frac{h}{f}\right)\left(2 - \frac{h}{g} + \frac{6h}{f}\right) - \frac{4h}{f}\left(3 - \frac{h}{g} + \frac{h}{f}\right)\right]U_{\overset{\vee}{ab},\varrho} + \\
&+ \frac{2\sqrt{-h}}{\sqrt{f}}\left[\left(2 - \frac{h}{g} + \frac{6h}{f}\right) - \left(2 - \frac{h}{g} + \frac{h}{f}\right)\left(3 - \frac{h}{g} + \frac{h}{f}\right)\right]U^{*}_{\overset{\vee}{ab},\varrho} - \\
&\left(2 - \frac{h}{g} + \frac{6h}{f}\right)U_{\overset{\vee}{ab},\bar{\varrho}} + \frac{2\sqrt{-h}}{\sqrt{f}}\left(3 - \frac{h}{g} + \frac{h}{f}\right)U^{*}_{\overset{\vee}{ab},\bar{\varrho}}.
\end{aligned} \tag{76}$$

Pour simplifier l'expression (76), nous pouvons aussi poser:

$$a = 2 - \frac{h}{g} + \frac{6h}{f}, \quad b = \frac{-2\sqrt{-h}}{\sqrt{f}}\left(3 - \frac{h}{g} + \frac{h}{f}\right), \tag{77}$$

et

$$V_{\overset{\vee}{ab,\varrho}} = \left(2 - \frac{h}{g} + \frac{h}{f}\right) U_{\overset{\vee}{ab,\varrho}} + \frac{2\sqrt{-h}}{\sqrt{f}} U^{*}_{\overset{\vee}{ab,\varrho}} - U_{\overset{\vee}{ab,\bar{\varrho}}} . \tag{78}$$

L'expression (76) peut alors s'écrire

$$\boxed{(a^2 + b^2)\Gamma_{\overset{\vee}{ab,\varrho}} = a V_{\overset{\vee}{ab,\varrho}} + b V^{*}_{\overset{\vee}{ab,\varrho}} .} \tag{79}$$

Ainsi, la partie antisymétrique de la connexion affine $\Gamma_{\overset{\vee}{ab,\varrho}} = h_{\varrho\sigma}\Gamma^{\sigma}_{\overset{\vee}{ab}}$ est complètement déterminée en fonction des composantes du tenseur fondamental $h^{\mu\nu}$ et $f^{\mu\nu}$, puisqu'il en est ainsi de $U_{\overset{\vee}{ab,\varrho}}$ d'après (72).

En résumé, l'expression générale et rigoureuse de la connexion affine totale en fonction des $h^{\mu\nu}$ et $f^{\mu\nu}$ est complètement et univoquement déterminée par (30) et (76) ou (79). On a:

$$\Gamma_{ab,\varrho} = h_{\varrho\sigma}\Gamma^{\sigma}_{ab} = [ab, \varrho] - \tfrac{1}{2} f^{\sigma\nu}[h_{\varrho\nu}(\Gamma_{\overset{\vee}{\sigma a,b}} + \Gamma_{\overset{\vee}{\sigma b,a}}) + \tag{80}$$

$$- h_{b\nu}(\Gamma_{\overset{\vee}{\sigma a,\varrho}} - \Gamma_{\overset{\vee}{\sigma\varrho,a}}) - h_{a\nu}(\Gamma_{\overset{\vee}{\sigma b,\varrho}} - \Gamma_{\overset{\vee}{\sigma\varrho,b}})] + \Gamma_{\overset{\vee}{ab,\varrho}} ,$$

les $\Gamma_{\overset{\vee}{ab,\varrho}}$ étant donnés par (76) ou (79).

2·5. *Conditions d'existence.* – On voit aisément quelles sont les conditions d'existence de cette solution. D'après (79), on ne pourra calculer $\Gamma_{\overset{\vee}{ab,\varrho}}$ que si

$$a^2 + b^2 \neq 0 ,$$

et en outre si $g \neq 0$ (car seul $h \neq 0$ a une signification physique acceptable). En définitive, il faut donc que

$$g\left|\left(2 - \frac{h}{g} + \frac{6h}{f}\right)^2 - \frac{4h}{f}\left(3 - \frac{h}{g} + \frac{h}{f}\right)^2\right] \neq 0 . \tag{81}$$

En tenant compte de la relation (13), on voit que cette condition est évidemment la même que celle obtenue dans la résolution des équations $g_{\overset{\vee}{\mu\nu,\varrho}} = 0$ [cf. (4), p. 28, condition (87)].

2·6. *Le cas particulier* $1/f = 0$. – Dans ce travail, nous n'avons *jamais* fait intervenir l'hypothèse $1/f \neq 0$. Les quantités $f_{\mu\nu}$ ou $f^{\mu\nu}$ qui figurent dans $U_{\overset{\vee}{ab,\varrho}}$

(72) s'y trouvent, en fait, toujours sous la forme $(1/\sqrt{\bar{f}})f_{\mu\nu}$ ou $(1/\sqrt{\bar{f}})f^{\mu\nu}$ et, d'après (8) et (7) sont équivalentes à

$$\tfrac{1}{2}\varepsilon_{\mu\nu\varrho\sigma}f^{\varrho\sigma} \quad \text{ou} \quad \frac{1}{2h}\varepsilon^{\mu\nu\varrho\sigma}f_{\varrho\sigma},$$

expressions qui sont toujours finies (ou éventuellement nulles). De même, les termes en $(1/f)f_{ab}\partial_\varrho \log f$ ne sont pas indéterminés car ils représentent, en fait, l'expression suivante:

$$\left(\frac{1}{\sqrt{\bar{f}}}f_{ab}\right)\left(-2\partial_\varrho\frac{1}{\sqrt{\bar{f}}}\right) = (\tfrac{1}{2}\varepsilon_{ab\varrho\sigma}f^{\varrho\sigma})\left(-2\partial_\varrho\frac{1}{\sqrt{\bar{f}}}\right).$$

On voit ainsi que ces termes sont nuls dans le cas $1/f = 0$.

Dans ce cas, la solution générale peut se mettre sous la forme simple suivante [$b = 0$ d'après (77)]:

$$a\Gamma_{\overset{\vee}{ab},\varrho} = V_{\overset{\vee}{ab},\varrho} = aU_{\overset{\vee}{ab},\varrho} - U_{\overset{\vee}{ab},\varrho}, \tag{82}$$

avec

$$U_{\overset{\vee}{ab},\varrho} = -\tfrac{1}{2}f_{ab\varrho} + \nabla_\varrho f_{ab} + \frac{g}{h}f_{\mu\nu\varrho}\left(\tfrac{1}{4}f_{ab}f^{\mu\nu} + \frac{h}{16g}\varepsilon_{abrs}f^{rs}\varepsilon^{\mu\nu\lambda\pi}f_{\lambda\pi}\right) + \tag{83}$$

$$+ f_{ab}\partial_\varrho \log\frac{g}{h} - \tfrac{1}{2}(f_{ab}\partial_\varrho + f_{\varrho a}\partial_b + f_{b\varrho}\partial_a)\log\frac{g}{h} + \tfrac{1}{2}h_{\varrho\lambda}f^{\sigma\lambda}(f_{ab}\Gamma_\sigma + f_{\sigma a}\Gamma_b + f_{b\sigma}\Gamma_a).$$

La condition d'existence de la solution (82) dans le cas $1/f = 0$, si $g \neq 0$, se réduit à

$$\boxed{a = 2 - \frac{h}{g} \neq 0}, \tag{84}$$

avec (77).

Tous les calculs effectués sont rigoureux. Si les équations mises en jeu sont plus compliquées que dans la résolution du système $g_{\overset{\mu\nu}{+-};\varrho} = 0$, par contre la solution obtenue (72) et (79) pour le système $g^{\mu\nu}_{+-;\varrho} = 0$, en fonction des champs $h^{\mu\nu}$ et $f^{\mu\nu}$ est aussi simple.

Il n'y a donc pas de raison de simplicité pour opter a priori en faveur de

la métrique $\gamma_{\mu\nu}$, que choisit habituellement EINSTEIN [8], ou de la métrique $h^{\mu\nu}$, préconisée par LICHNEROWICZ [3].

Sous la réserve des conditions d'existence (81) [ou (87), [4] p. 28], les équations $g^{\mu\nu}_{+-,\varrho} = 0$ ou $g_{\underset{+-}{\mu\nu;\varrho}} = 0$ permettent de donner à la connexion affine une expression univoquement déterminée et complètement explicite en fonction des composantes contravariantes ou covariantes du tenseur fondamental.

La solution générale et rigoureuse (72-76) ou (72-77-78-79) peut être appliquée au cas rigoureux mais particulier d'une symétrie sphérique. On retrouve alors, pour la connexion affine, les resultats obtenues par BONNER. Nous n'insisterons pas sur cette application qui fournit ici un test satisfaisant de la validité de cette solution. Dans le cas $(1/f) = 0$, on retrouve aussi les résultats obtenus par Papapetrou ($f^{14} \neq 0$) et par WYMAN ($f^{23} \neq 0$) [9].

APPENDICE I

Relation entre $A_{ab,\underline{\underline{\varrho}}}$, $A_{ab,\varrho}$ et $A_{ab,\bar{\bar{\varrho}}}$.

D'après les définitions (14) et (18) on a

$$A_{ab,\underline{\underline{\varrho}}} = h_{\varrho\sigma} f^{\sigma\lambda} h_{\lambda\mu} f^{\mu\pi} h_{\pi\delta} f^{\delta\varepsilon} A_{ab,\varepsilon} = - h_{\varrho\sigma} f^{\sigma\lambda} f_{\underline{\lambda\delta}} f^{\varepsilon\delta} A_{ab,\varepsilon} .$$

Or, d'après (19), ceci peut encore se mettre sous la forme suivante:

$$\text{(I.1)} \quad A_{ab,\underline{\underline{\varrho}}} = - h_{\varrho\sigma} f^{\sigma\lambda} \left[h \left(\frac{1}{g} - \frac{1}{h} - \frac{1}{f} \right) \delta^{\varepsilon}_{\lambda} - \frac{h}{f} f_{\lambda\delta} f^{\underline{\varepsilon\delta}} \right] A_{ab,\varepsilon} =$$

$$= - h \left(\frac{1}{g} - \frac{1}{h} - \frac{1}{f} \right) A_{ab,\bar{\varrho}} + \frac{h}{f} h^{\varepsilon\alpha} f_{\varrho\alpha} A_{ab,\varepsilon} .$$

D'où, en tenant compte de (I.1) et des relations (3)

$$A_{ab,\underline{\underline{\varrho}}} = h_{\varrho\sigma} f^{\sigma\lambda} A_{ab,\underline{\underline{\lambda}}} = - h \left(\frac{1}{g} - \frac{1}{h} - \frac{1}{f} \right) A_{ab,\bar{\bar{\varrho}}} - \frac{h}{f} A_{ab,\varrho} .$$

---

[8] A. EINSTEIN: *The Meaning of Relativity* (1953), (Appendice à la 4ème édition).

[9] M. E. TONNELAT: *La théorie du champ unifié d'Einstein et quelques-uns de se développements* (Paris, 1955), pp. 71, 76, 80.

Appendice II

Calcul de $f^{\sigma\lambda}(h_{a\lambda}\underset{\vee}{\Gamma}_{\sigma\varrho,\bar{b}} + h_{b\lambda}\underset{\vee}{\Gamma}_{\varrho\sigma,\bar{a}})$.

D'après les définitions (14), ce terme peut s'écrire:

$$(\text{II.1}) \qquad f^{\sigma\lambda}(h_{a\lambda}h_{b\mu}f^{\mu\nu}\underset{\vee}{\Gamma}_{\sigma\varrho,\nu} - h_{b\lambda}h_{a\mu}f^{\mu\nu}\underset{\vee}{\Gamma}_{\sigma\varrho,\nu}) = h^{\sigma p}h^{\nu s}(f_{\underline{p}\underline{a}}f_{\underline{b}\underline{s}} - f_{\underline{p}\underline{b}}f_{\underline{a}\underline{s}})\underset{\vee}{\Gamma}_{\sigma\varrho,\nu} =$$

$$= \sqrt{\underline{f}}h^{\sigma p}h^{\nu s}\varepsilon_{pabs}\underset{\vee}{\Gamma}_{\sigma\varrho,\nu} + h^{\sigma p}h^{\nu s}f_{\underline{b}\underline{a}}f_{\underline{p}\underline{s}}\underset{\vee}{\Gamma}_{\sigma\varrho,\nu},$$

en tenant compte de (34) et en désignant par $\underline{f}$ le déterminant formé par les $f_{\underline{\mu}\underline{\nu}}$.

(II.1) peut encore s'écrire

$$(\text{II.2}) \qquad -\frac{\sqrt{\underline{f}}}{2}h^{\sigma p}h^{\nu s}\varepsilon_{pabs}\Gamma_{\sigma\varrho\nu} - \frac{\sqrt{\underline{f}}}{2}h^{\sigma p}h^{\nu s}\varepsilon_{pabs}\underset{\vee}{\Gamma}_{\nu\sigma,\varrho} + \tfrac{1}{2}h^{\sigma p}h^{\nu s}f_{\underline{b}\underline{a}}f_{\underline{p}\underline{s}}\Gamma_{\sigma\varrho\nu} - \tfrac{1}{2}h^{\sigma p}h^{\nu s}f_{\underline{b}\underline{a}}f_{\underline{p}\underline{s}}\underset{\vee}{\Gamma}_{\nu\sigma,\varrho},$$

$$(\text{II.3}) \qquad = -\tfrac{1}{2}h^{\sigma p}h^{\nu s}(\sqrt{\underline{f}}\varepsilon_{ba\nu s} - f_{\underline{b}\underline{a}}f_{\underline{p}\underline{s}})\Gamma_{\sigma\varrho\nu} + \frac{\sqrt{\underline{f}}}{\sqrt{-h}}\underset{\vee}{\Gamma}^{*}_{ab,\varrho} - f_{\underline{a}\underline{b}}N_{\varrho}$$

d'après (21) et (39).

Calculons à présent $\sqrt{\underline{f}}$.

D'après les relations (9) valables pour tout déterminant formé avec les composantes covariantes d'un tenseur antisymétrique quelconque

$$\sqrt{\underline{f}} = \frac{1}{8}\varepsilon^{\mu\nu\varrho\sigma}f_{\underline{\mu}\underline{\nu}}f_{\underline{\varrho}\underline{\sigma}} = \frac{1}{8}\varepsilon^{\mu\nu\varrho\sigma}h_{\mu a}h_{\nu b}f^{ab}h_{\varrho c}h_{\sigma d}f^{cd} = \frac{h}{8}\varepsilon_{\mu\nu ab}f^{ab}f^{\mu\nu} = \frac{h}{\sqrt{\underline{f}}},$$

en tenant compte de (8).

Portant dans (II.3) et utilisant les notations (21), on a donc

$$(\text{II.4}) \qquad f^{\sigma\lambda}(h_{a\lambda}\underset{\vee}{\Gamma}_{\sigma\varrho,\bar{b}} + h_{b\lambda}\underset{\vee}{\Gamma}_{\varrho\sigma,\bar{a}}) = -\tfrac{1}{2}h^{\sigma p}h^{\nu s}\left(\frac{h}{\sqrt{\underline{f}}}\varepsilon_{ba\nu s} - f_{\underline{b}\underline{a}}f_{\underline{p}\underline{s}}\right)\Gamma_{\sigma\varrho\nu} -$$

$$-\frac{\sqrt{-h}}{\sqrt{\underline{f}}}\underset{\vee}{\Gamma}^{*}_{ab,\varrho} - f_{\underline{a}\underline{b}}N_{\varrho} = \frac{\sqrt{-h}}{\sqrt{\underline{f}}}\Gamma^{*}_{[ab]\varrho} - \frac{\sqrt{-h}}{\sqrt{\underline{f}}}\underset{\vee}{\Gamma}^{*}_{ab,\varrho} + \tfrac{1}{2}f^{\sigma\nu}f_{\underline{a}\underline{b}}\Gamma_{\sigma\nu\varrho} - f_{\underline{a}\underline{b}}N_{\varrho}.$$

Appendice III

Calcul de $\overline{\Gamma}_{\mu\nu\varrho}$.

D'après la définition (17)

$$\overline{\Gamma}_{\mu\nu\varrho} = \underset{\vee}{\Gamma}_{\mu\nu,\bar{\varrho}} + \underset{\vee}{\Gamma}_{\nu\varrho,\bar{\mu}} + \underset{\vee}{\Gamma}_{\varrho\mu,\bar{\nu}} = f^{\sigma\lambda}(h_{\varrho\sigma}\underset{\vee}{\Gamma}_{\mu\nu,\lambda} + h_{\mu\sigma}\underset{\vee}{\Gamma}_{\nu\varrho,\lambda} + h_{\nu\sigma}\underset{\vee}{\Gamma}_{\varrho\mu,\lambda}).$$

On vérifie facilement que pour $\mu \neq \nu \neq \varrho$

$$\overline{\Gamma}_{\mu\nu\varrho} = -(f_{\underline{\mu\nu}}\Gamma_{\varrho} + f_{\underline{\varrho\mu}}\Gamma_{\nu} + f_{\underline{\nu\varrho}}\Gamma_{\mu}) + \frac{h}{2\sqrt{f}}\,\varepsilon_{\mu\nu\varrho\sigma}h^{\sigma\lambda}f_{\underline{\underline{\mu\nu}}}\Gamma_{\underset{\vee}{\mu\nu},\lambda}\,.$$

En tenant compte de la définition (38) et de la relation

$$f_{\underline{\mu\nu}}A_{\varrho} + f_{\underline{\varrho\mu}}A_{\nu} + f_{\underline{\nu\varrho}}A_{\mu} = \frac{h}{\sqrt{f}}\,\varepsilon_{\mu\nu\varrho\sigma}f^{\underline{\lambda\sigma}}A_{\lambda}\,, \tag{III.1}$$

(valable pour un quadrivecteur A_λ quelconque) on a:

$$\Gamma_{\mu\nu\varrho} = -\frac{h}{\sqrt{f}}\,\varepsilon_{\mu\nu\varrho\sigma}f^{\underline{\lambda\sigma}}\Gamma_{\lambda} + \frac{h}{\sqrt{f}}\,\varepsilon_{\mu\nu\varrho\sigma}h^{\sigma\lambda}M_{\lambda}\,. \tag{III.2}$$

Appendice IV

Calcul de $\overline{\overline{\Gamma}}_{ab\varrho}$.

D'après les définitions (17) et (14)

$$\overline{\Gamma}_{ab\varrho} = \Gamma_{\underset{\vee}{ab,\bar{\varrho}}} + \Gamma_{\underset{\vee}{\varrho a,\bar{b}}} + \Gamma_{\underset{\vee}{b\varrho,\bar{a}}} = f^{\lambda\sigma}(f_{\underline{\varrho\lambda}}\Gamma_{\underset{\vee}{ab},\sigma} + f_{\underline{b\lambda}}\Gamma_{\underset{\vee}{\varrho a},\sigma} + f_{\underline{a\lambda}}\Gamma_{\underset{\vee}{b\varrho},\sigma})\,.$$

On vérifie que pour $a \neq b \neq \varrho$

$$\overline{\overline{\Gamma}}_{ab\varrho} = \left(1 - \frac{h}{g} + \frac{h}{f}\right)\Gamma_{ab\varrho} + \frac{h}{2\sqrt{f}}\,\varepsilon_{ab\varrho\sigma}f^{\lambda\sigma}f_{\underline{\underline{\pi\tau}}}\Gamma_{\lambda\pi\tau} + \frac{h}{2\sqrt{f}}\,\varepsilon_{ab\varrho\sigma}(f^{\underline{\lambda\sigma}}f^{\underline{\mu\nu}}\Gamma_{\underset{\vee}{\mu\nu},\lambda} - f^{\lambda\sigma}f_{\underline{\underline{\mu\nu}}}\Gamma_{\underset{\vee}{\mu\nu},\lambda})\,.$$

et d'après les définitions (38) et (39)

$$\overline{\overline{\Gamma}}_{ab\varrho} = \left(1 - \frac{h}{g} + \frac{h}{f}\right)\Gamma_{ab\varrho} + \frac{h}{2\sqrt{f}}\,\varepsilon_{ab\varrho\sigma}f^{\lambda\sigma}f_{\underline{\underline{\pi\tau}}}\Gamma_{\lambda\pi\tau} + \frac{h}{\sqrt{f}}\,\varepsilon_{ab\varrho\sigma}(f^{\underline{\lambda\sigma}}N_{\lambda} - f^{\lambda\sigma}M_{\lambda})\,.$$

Appendice V

Calcul de $(h/\sqrt{f})h_{\varrho\lambda}f^{\sigma\lambda}\varepsilon_{ab\sigma\tau}h^{\mu\tau}M_{\mu}$.

Cette expression peut encore s'écrire d'après (18)

$$\frac{h}{\sqrt{f}}\,h_{\varrho\lambda}f^{\sigma\lambda}\varepsilon_{ab\sigma\tau}h^{\mu\tau}M_{\mu} = \frac{h}{\sqrt{f}}\,\varepsilon_{ab\sigma n}h^{\sigma\mu}h^{nm}f_{\underline{\mu\varrho}}M_{m} =$$

$$= \frac{h}{2\sqrt{f}}\,\varepsilon_{ab\sigma n}h^{\sigma\mu}h^{nm}(f_{\underline{\mu\varrho}}M_{m} + f_{\underline{\varrho m}}M_{\mu} + f_{\underline{m\mu}}M_{\varrho}) - \frac{h}{2\sqrt{f}}\,\varepsilon_{ab\sigma n}h^{\sigma\mu}h^{nm}f_{\underline{m\mu}}M_{\varrho}\,,$$

et en utilisant (III.1), puis les définitions (21) et (8)

$$\frac{h}{\sqrt{f}}\, h_{\varrho\lambda} f^{\sigma\lambda} \varepsilon_{ab\sigma\tau} h^{\mu\tau} M_\mu = \frac{h\sqrt{-h}}{f}\, \varepsilon^{*}_{[ab]\varrho\lambda} f^{\pi\lambda} M_\pi + \frac{h}{f}\, f_{ab} M_\varrho \,.$$

Appendice VI

D'après (25)

$$\text{(VI.1)} \qquad \Gamma_\varrho = \frac{1}{\sqrt{-g}}\, h_{\varrho m} \partial_n (\sqrt{-g} f^{mn}) = h_{\varrho m} \partial_n f^{mn} + \tfrac{1}{2} h_{\varrho m} f^{mn} \partial_n \log g \,.$$

D'où

$$\text{(VI.2)} \qquad \varepsilon_{ab\varrho\sigma} h^{\sigma\lambda} \Gamma_\lambda = \varepsilon_{ab\varrho\sigma} \partial_\lambda f^{\sigma\lambda} + \tfrac{1}{2} \varepsilon_{ab\varrho\sigma} f^{\sigma\lambda} \partial_\lambda \log g = \tfrac{1}{2} \varepsilon_{ab\varrho\sigma} f^{\sigma\lambda} \partial_\lambda \log \frac{g}{f} - \frac{1}{\sqrt{f}}\, f_{ab\varrho} \,.$$

D'autre part

$$\text{(VI.3)} \qquad \frac{g}{2\sqrt{f}}\, \varepsilon_{ab\varrho\sigma} f^{\sigma\nu} f^{\lambda\mu} h_{\mu\nu} \Gamma_\lambda = \frac{g}{2\sqrt{f}}\, \varepsilon_{ab\varrho\sigma} f^{\sigma\nu} \underline{\underline{f}}_{m\nu} \partial_n f^{mn} - \frac{g}{4\sqrt{f}}\, \varepsilon_{ab\varrho\sigma} f^{\sigma\lambda} \partial_{\bar{\lambda}} \log g \,,$$

avec

$$\text{(VI.4)} \qquad \varepsilon_{ab\varrho\sigma} f^{\sigma\lambda} \partial_{\bar{\lambda}} \log g = \tfrac{1}{2} \varepsilon_{ab\varrho\sigma} h_{\lambda\nu} f^{\nu q} h_{qr} (f^{\lambda\sigma} f^{rs} - f^{\lambda s} f^{r\sigma} - f^{r\lambda} f^{s\sigma}) \partial_s \log g +$$

$$+ \tfrac{1}{2} \varepsilon_{ab\varrho\sigma} h_{\lambda\nu} f^{\nu q} h_{qr} f^{r\lambda} f^{s\sigma} \partial_s \log g = \frac{1}{2\sqrt{f}}\, \varepsilon_{ab\varrho\sigma} \varepsilon^{rs\lambda\sigma} h_{\lambda\nu} f^{\nu q} h_{qr} \partial_s \log g -$$

$$- \tfrac{1}{2} \varepsilon_{ab\varrho\sigma} \underline{\underline{f}}_{r\lambda} f^{r\lambda} f^{s\sigma} \partial_s \log g = \frac{h}{f}\, \varepsilon_{ab\varrho\sigma} \underline{\underline{f}}^{\lambda\sigma} \partial_\lambda \log g - h \left(\frac{1}{g} - \frac{1}{h} - \frac{1}{f} \right) \varepsilon_{ab\varrho\sigma} f^{\lambda\sigma} \partial_\lambda \log g \,,$$

et

$$\text{(VI.5)} \qquad \frac{g}{2\sqrt{}}\, \varepsilon_{ab\varrho\sigma} f^{\sigma\nu} \underline{\underline{f}}_{m\nu} \partial_n f^{mn} = \frac{g}{4\sqrt{f}}\, \varepsilon_{ab\varrho\sigma} f^{\sigma\nu} \underline{\underline{f}}_{m\nu} \partial_n \left(\frac{1}{\sqrt{f}}\, \varepsilon^{mnrs} f_{rs} \right) =$$

$$= \frac{g}{4f}\, \varepsilon_{ab\varrho\sigma} \left[h \left(\frac{1}{g} - \frac{1}{h} - \frac{1}{f} \right) \delta^\sigma_m - \frac{h}{f}\, f_{m\nu} \underline{\underline{f}}^{\sigma\nu} \right] \varepsilon^{mnrs} \partial_n f_{rs} -$$

$$- \frac{g}{8f}\, \varepsilon_{ab\varrho\sigma} \left[h \left(\frac{1}{g} - \frac{1}{h} - \frac{1}{f} \right) \delta^\sigma_m - \frac{h}{f}\, f_{m\nu} \underline{\underline{f}}^{\sigma\nu} \right] \varepsilon^{mnrs} f_{rs} \partial_n \log f =$$

$$= - \frac{gh}{2f} \left(\frac{1}{g} - \frac{1}{h} - \frac{1}{f} \right) f_{ab\varrho} - \frac{gh}{12f^2}\, \varepsilon_{ab\varrho\sigma} f_{\nu m} \underline{\underline{f}}^{\sigma\nu} \varepsilon^{nrsm} f_{nrs} +$$

$$+ \frac{gh}{4\sqrt{f}} \left(\frac{1}{g} - \frac{1}{h} - \frac{1}{f} \right) \varepsilon_{ab\varrho\sigma} f^{\lambda\sigma} \partial_\lambda \log f + \frac{gh}{4f\sqrt{f}}\, \varepsilon_{ab\varrho\sigma} \underline{\underline{f}}^{\sigma\lambda} \partial_\lambda \log f \,,$$

d'après (11), (9) et (34).

En tenant compte de (59) valable pour tout pseudo-vecteur, comme $f_{ab\varrho}$,

$$\text{(VI.6)} \qquad \frac{g}{2\sqrt{f}}\,\varepsilon_{ab\varrho\sigma}f^{\sigma p}\underline{f_{mp}}\,\partial_n f^{mn} = -\frac{gh}{4f\sqrt{f}}\,\varepsilon_{ab\varrho\sigma}f^{\lambda\sigma}\underline{f^{\mu\nu}}f_{\mu\nu\lambda} + \\ + \frac{gh}{4\sqrt{f}}\,\varepsilon_{ab\varrho\sigma}\left[\left(\frac{1}{g}-\frac{1}{h}-\frac{1}{f}\right)f^{\lambda\sigma} + \frac{1}{f}\,\underline{f^{\sigma\lambda}}\right]\partial_\lambda \log f\,,$$

avec (47).

En portant (VI.4) et (VI.6) dans (VI.3), on obtient finalement

$$\text{(VI.7)} \qquad \frac{g}{2\sqrt{f}}\,\varepsilon_{ab\varrho\sigma}f^{\sigma p}f^{\lambda\mu}h_{\mu p}\Gamma_\lambda = -\frac{gh}{4f\sqrt{f}}\,\varepsilon_{ab\varrho\sigma}f^{\lambda\sigma}\underline{f^{\mu\nu}}f_{\mu\nu\lambda} + \\ + \frac{gh}{4\sqrt{f}}\,\varepsilon_{ab\varrho\sigma}\left[\left(\frac{1}{g}-\frac{1}{h}-\frac{1}{f}\right)f^{\lambda\sigma} + \frac{1}{f}\,\underline{f^{\sigma\lambda}}\right]\partial_\lambda \log \frac{f}{g}\,.$$

En portant les expressions (VI.2) et (VI.7) dans (66), on obtient sans difficulté la relation (67) où $\Gamma_{ab\varrho}$ est uniquement fonction des champs $h_{\mu\nu}$ et $f_{\mu\nu}$.

Appendice VII

Autre calcul de $\Gamma_{ab\varrho}$.

Par définition

$$\Gamma_{ab\varrho} = h_{\varrho m}\Gamma^m_{\underset{\vee}{ab}} + h_{am}\Gamma^m_{\underset{\vee}{b\varrho}} + h_{bm}\Gamma^m_{\underset{\vee}{\varrho a}}\,.$$

Or (cf. [4] éqs. 19)

$$h_{\varrho m} = \gamma_{\varrho m} + \varphi_{\varrho p}\varphi_{mq}\gamma^{pq}\,.$$

Donc

$$\Gamma_{ab\varrho} = (\gamma_{\varrho m} + \varphi_{\varrho p}\varphi_{mq}\gamma^{pq})\Gamma^m_{\underset{\vee}{ab}} + \text{perm. circ. } a, b, \varrho = (\Gamma'_{\underset{\vee}{ab,\varrho}} - \Gamma'_{\underset{\vee}{ab,\bar{\varrho}}}) + \text{perm. circ. } a, b, \varrho\,,$$

avec, selon les notations (50) et (51) de M. A. Tonnelat [4]

$$\Gamma'_{\underset{\vee}{ab,\varrho}} = \gamma_{\varrho\lambda}\Gamma^\lambda_{\underset{\vee}{ab}}\,, \qquad \Gamma'_{\underset{\vee}{ab,\bar{\varrho}}} = \varphi_{\varrho p}\gamma^{pq}\varphi_{qm}\Gamma^m_{\underset{\vee}{ab}}\,.$$

Donc

$$\Gamma_{ab\varrho} = \Gamma'_{ab\varrho} - \bar{\bar{\Gamma}}'_{ab\varrho}\,.$$

Or les quantités $\Gamma'_{ab\varrho}$ et $\bar{\bar{\Gamma}}'_{ab\varrho}$ sont connues. D'après leurs expressions (II') et (60)

[cf. (1) p. 25 et 26].

$$\Gamma_{ab\varrho} = -\tfrac{1}{2}\varphi_{ab\varrho} - \tfrac{1}{2}\left(1 - \frac{g}{\gamma} + \frac{\varphi}{\gamma}\right)\varphi_{ab\varrho} - \sqrt{\varphi}\varepsilon_{ab\varrho\sigma}\varphi^{\lambda\sigma}\left[\tfrac{1}{2}\delta_\lambda \log\frac{g}{\gamma} - \tfrac{1}{4}\gamma^{\varkappa\nu}\gamma^{\beta\alpha}\varphi_{\varkappa\beta}\varphi_{\nu\alpha\lambda}\right] -$$

$$-\sqrt{\varphi}\varepsilon_{ab\varrho\sigma}\gamma^{\sigma\varkappa}\gamma^{\lambda\beta}\varphi_{\varkappa\beta}\left[\tfrac{1}{2}\delta_\lambda \log\frac{\varphi}{g} - \tfrac{1}{4}\varphi^{\nu\alpha}\varphi_{\nu\alpha\lambda}\right] + \frac{\sqrt{\varphi}}{4}\varepsilon_{ab\varrho\sigma}\gamma^{\varkappa\lambda}\gamma^{\sigma\tau}\varphi_{\lambda\tau}\varphi^{\beta\delta}\varphi_{\varkappa\beta\delta}\,.$$

En remplaçant les $\varphi_{\varkappa\beta}$ et les $\gamma^{\alpha\beta}$ par leurs valeurs en fonction des $h_{\mu\nu}$ et $f_{\mu\nu}$ [cf. (1) équ. (19), p. 22] et en tenant compte de la relation (13), on trouve par un calcul un peu long mais sans difficulté, la valeur (67) de $\Gamma_{ab\varrho}$ en fonction des champs $h_{\mu\nu}$ et $f_{\mu\nu}$. On pourrait procéder d'une manière analogue pour M_ϱ et N_ϱ, ce qui fournit une vérification satisfaisante des résultats obtenus.

RIASSUNTO (*)

Il calcolo rigoroso della soluzione generale delle equazioni di Einstein $g^{\mu\nu}_{+-;\varrho} = 0$ conduce, per la connessione affine, a una semplice espressione univocamente determinata e completamente esplicitata, in funzione delle componenti controvarianti ($h^{\mu\nu} = g^{\mu\nu}$ e $f^{\mu\nu} = g^{\mu\nu}$) del tensore fondamentale $g^{\mu\nu}$. Si danno altresì in forma esplicita le condizioni di questa soluzione generale.

(*) *Traduzione a cura della Redazione.*

IL NUOVO CIMENTO Vol. II, N. 6 1° Dicembre 1955

Phaseshift Analysis of Proton-Proton Scattering Experiments. I. General Formulation.

E. Clementel and C. Villi

Istituti di Fisica dell'Università di Padova e di Trieste
Istituto Nazionale di Fisica Nucleare - Sezione di Padova

(ricevuto il 30 Agosto 1955)

Summary. — The phaseshift analysis problem of proton-proton scattering experiments is considered. In the approximation of S and P waves, a parametrization method is given by which, using directly the experimental data, the four phaseshifts for the singlet S and the triplet P state can be derived. If the contribution of D waves and the effect of the coupling ${}^3P_2 - {}^3F_2$ is included, it is shown that the problem can still be solved resorting to a polynomial method.

Introduction.

The attempts to account for the observed data in nucleon-nucleon scattering, to ascertain the nature of nuclear forces with an analysis based on assumed interaction between nucleons (1), have been so far unsuccessful in explaining both low and high energy data with a unique choice of the nuclear force parameters. The lack of success of this kind of approach and some striking features of high energy proton-proton scattering, mainly an approximate isotropy (except, of course, at small angles) of the differential cross-section in the center-of-mass system, has suggested to Breit and his Collaborators (2)

(1) For a survey on this and related problems we refer to the following review articles: G. Breit and R. L. Gluckstern: *Annual Review of Nuclear Science* **2** 365 (1953); H. S. W. Massey: *Proceedings of the* 1954 *Glasgow Conference* (London, 1955); p. 1.

(2) R. M. Thaler and J. Bengston: *Phys. Rev.* **94** 679 (1954); R. M. Thaler J. Bengston and G. Breit: *Phys. Rev.* **94**, 683 (1954). See also M. Matsumoto and W. Watari: *Progr. Theor. Phys.*, **12**, 503 (1954).

an analysis of high energy experimental data entirely on the basis of phase-shifts, without recourse to any detailed theory of the scattering in terms of some preconceived potential. Because of the large value of the cross-section, which cannot possibly be explained in terms of a pure S-wave scattering, and because of the polarization observed in p-p scattering, this kind of analysis requires as starting point at least the four phaseshifts corresponding to $^1S_1$, $^3P_0$, $^3P_1$ and $^3P_2$ states. The results obtained along these lines do not seem conflicting with the hypothesis of charge independence.

The method used by these Authors is essentially a graphical one, and strict isotropy of the differential cross-section is explicitely used by equating to zero the coefficient of $P_2(\cos\vartheta)$ in the nuclear part of the cross-section formula. Evaluating the K_0 phaseshift for the $^1S_1$ state by means of a potential well consistent with low energy data, it is possible then to fix the values of certain combinations of the phaseshifts of the triplet P-state. The generalization of the method ([3]) by including the polarization data allows the determination of several possible sets of the four phaseshifts directly from the intersection of the « isotropy-surfaces » with the « polarization-surfaces ». The application of this graphical analysis, based essentially on the possibility to neglect Coulomb and interference terms in the nearly isotropic region ($\vartheta > 30°$) of the experimental cross-section, is limited to high energy scattering experiments.

Because of the importance that the knowledge of the « experimental » phaseshifts might have for a better understanding of the nature of nuclear forces ([4]), we felt desirable to seek for an analytical method, giving with satisfactory definiteness the phaseshifts directly from the observed scattering data, regardless of the energy and without any simplifying assumption on the angular dependence of the differential cross-section. In our analysis the polarization data have not been taken explicitely into account, because, apart from mathematical difficulties, they are so far available only for few energies and with an accuracy lower than that of the scattering data.

This paper is concerned with the general formulation of the method. We shall discuss in detail the results obtained for proton-proton and neutron-proton scattering in two subsequent papers, which are now in preparation. Preliminary results, following from the application of a simplified version of the method, have already been given ([5]).

For completeness sake, in the first part (Section **1**) the main steps of the

---

([3]) A. GARREN: *Phys. Rev.*, **92**, 213 (1953); **96**, 1709 (1954); C. A. KLEIN: *Nuovo Cimento*, **1**, 581 (1955); **2**, 38 (1955).

([4]) R. JOST and W. KOHN: *Phys. Rev.*, **87**, 997 (1952); *Kgl. Danske Videnskab Selsab.*, **27**, n. 9 (1953).

([5]) L. BERETTA, E. CLEMENTEL and C. VILLI: *Nuovo Cimento*, **1**, 739 (1955); *Phys. Rev.*, **98**, 1526 (1955).

derivation of the differential cross-section formula are given in the S and P-wave approximation, and the parametrization method, already used in this approximation, is outlined (Section 2). Using the eigenstates of the scattering matrix, the general expression of the proton-proton triplet cross-section is derived in the parity representation (Section 3), and then specialized considering only the five phaseshifts for $^1S_0$, $^1D_2$, $^3P_{0,1,2}$ states and the contribution to the cross-section due to the $^3P_2$-$^3F_2$ coupling (Section 4). In the last part (Section 5) it is shown how the five phaseshifts and the coupling constant can be evaluated by expanding the angular terms of the interference part of the differential cross-section in Legendre polynomials.

Symbols and notation.

k	wave number of the relative motion at large separation;
$\eta = e^2/\hbar v$	parameter measuring the importance of Coulomb effects (v = relative velocity);
ϑ, φ	polar and azimuthal angles of scattering in the center-of-mass-system;
$\sigma(\vartheta)$	cross-section per unit solid angle in the c.m.s.;
$\sigma_C(\vartheta)$	part of $\sigma(\vartheta)$ due only to the Coulomb interaction;
$\sigma_N(\vartheta)$	part of $\sigma(\vartheta)$ due only to the nuclear interaction;
$\sigma_I(\vartheta)$	part of $\sigma(\vartheta)$ due to interference between the outgoing nuclear and Coulomb waves;
L, $\boldsymbol{L}$	orbital angular momentum, with z-component M_L;
S, $\boldsymbol{S}$	total spin angular momentum, with z-component M_S;
J, $\boldsymbol{J} = \boldsymbol{L} + \boldsymbol{S}$	total angular momentum, with z-component M;
K_L	nuclear phaseshift for singler states;
δ_L, δ_{JL}	nuclear phaseshift for triplet states;
$\sigma_L = \arg \Gamma(L + 1 + i\eta)$	Coulomb phaseshift;
${}^{\sigma}\chi_{M_S}$	spin wave function for a state of multiplicity $\sigma = 2S + 1$;
${}^{\sigma}f_C^{M_S}(\vartheta)$	Coulomb scattering amplitude;

${}^{\sigma}f_{\mathcal{N}}^{M_S}(\vartheta)$ nuclear scattering amplitude;

${}^{\sigma}f^{M_S}(\vartheta) = {}^{\sigma}f_{\mathcal{C}}^{M_S}(\vartheta) + {}^{\sigma}f_{\mathcal{N}}^{M_S}(\vartheta)$ total scattering amplitude;

$\mathcal{Y}_{JL}^{M}(\vartheta, \varphi)$ normalized spin spherical harmonics;

$(j_1 j_2 m_1 m_2 | jm)$ Wigner coefficients for vector addition of angular momenta;

$$Q(\delta) = \exp[i\delta] \sin\delta\,, \qquad \sigma_{LL'} = \sigma_L - \sigma_{L'}\,,$$

$$\boldsymbol{c} = \cos(\vartheta/2)\,, \qquad \boldsymbol{s} = \sin(\vartheta/2),$$

$$\alpha_L = \eta \log \boldsymbol{s}^2 + 2\sum_{n=0}^{L} \mathrm{tg}^{-1}(\eta/n)\,, \qquad \boldsymbol{X}_L = \boldsymbol{s}^{-2}\cos\alpha_L + (-1)^L \boldsymbol{c}^{-2}\cos\beta_L,$$

$$\beta_L = \eta \log \boldsymbol{c}^2 + 2\sum_{n=0}^{L} \mathrm{tg}^{-1}(\eta/n)\,, \qquad \boldsymbol{Y}_L = \boldsymbol{s}^{-2}\sin\alpha_L + (-1)^L \boldsymbol{c}^{-2}\sin\beta_L,$$

$$Y_{lm}(\vartheta, q) \quad (-1)^{\frac{1}{2}(m \quad |m|)} \left| \frac{2l \;-\; 1}{4\pi} \frac{(l \;-\; m\;)!}{(l \;-\; |m|)!} \right|^{\frac{1}{2}} \sin^{|m|}\vartheta \left(\frac{\mathrm{d}}{\mathrm{d}\cos\vartheta} \right)^{|m|} P_l(\cos\vartheta) \exp[imq]\,.$$

$$P_l(\cos\vartheta) = \frac{1}{2^l l!} \left(\frac{\mathrm{d}}{\mathrm{d}\cos\vartheta} \right)^l (\cos^2\vartheta - 1)^l = \left(\frac{4\pi}{2l+1} \right)^{\frac{1}{2}} Y_{l0}(\vartheta)\,.$$

1. – S and P wave approximation.

The p-p system is a triplet state in the isotopic spin space, and therefore the antysymmetry prescription $P_x P_\sigma P_\tau = -1$, required by the exclusion principle, where P_x, P_σ, and P_τ are respectively the space, spin and charge symmetry operators, reduces simply to $P_x P_\sigma = -1$, i.e. space and spin functions have opposite parity. It follows that only the singlet even states ${}^1S$, ${}^1D$, etc., and the triplet odd states ${}^3P$, ${}^3F$, etc., are permitted for the two-proton system.

It is well known ([6]) that the asymptotic behavior of the unsymmetrized Coulomb scattered wave, modified by a central nuclear potential, can be written for the z-component M_S of the total spin as

$$(1) \qquad r\exp[-i(kr - \eta\log 2kr)]\,{}^{\sigma}\psi_{sc}^{M_S}(r,\vartheta) \underset{r\to\infty}{\longrightarrow} {}^{\sigma}f^{M_S}(\vartheta) =$$
$$= {}^{\sigma}f_{\mathcal{C}}^{M_S}(\vartheta) + 1/k \sum_L [4\pi(2L+1)]^{\frac{1}{2}} \exp[2i\sigma_L] Q({}^{\sigma}\sigma_L)\, Y_{L0}(\vartheta)\, {}^{\sigma}\chi_{M_S}\,.$$

where $\sigma = 2S + 1$ is the multiplicity of the spin state, and ${}^{\sigma}f_{\mathcal{C}}^{M_S}(\vartheta)$ is given by

$$(2) \qquad {}^{\sigma}f_{\mathcal{C}}^{M_S}(\vartheta) = -(\eta/2k\boldsymbol{s}^2)\exp[-i\eta\log\boldsymbol{s}^2 - 2i\sigma_0]\,{}^{\sigma}\chi_{M_S}\,.$$

([6]) L. I. SCHIFF: *Quantum Mechanics* (New York, 1949), p. 119.

Because of the parity $(-1)^L$ of the spherical harmonic functions, the antisymmetrized scattering amplitude

$$(3) \qquad {}^{\sigma}f^{M_S}(\vartheta) + (-1)^S\, {}^{\sigma}f^{M_S}(\pi - \vartheta)\,,$$

becomes for singlet states ($S = 0$: only *even* values for L)

$$(4) \qquad {}^1f(\vartheta) = {}^1f_C(\vartheta) + {}^1f_{CN}(\vartheta) =$$
$$= (-\eta/2k)\exp[2i\sigma_0]\{\boldsymbol{s}^{-2}\exp[-i\eta\log \boldsymbol{s}^2] + \boldsymbol{c}^{-2}\exp[-i\eta\log \boldsymbol{c}^2]\} +$$
$$+ (2/k)\sum_L [4\pi(2L+1)]^{\frac{1}{2}}\exp[2i\sigma_L]Q(K_L)\,Y_{L0}(\vartheta)\,,$$

and for triplet states ($S = 1$: only *odd* values for L)

$$(5) \qquad {}^3f^{M_S}(\vartheta) = {}^3f_C^{M_S}(\vartheta) + {}^3f_{CN}^{M_S}(\vartheta)$$
$$= (-\eta/2k)\exp[2i\sigma_0]\{\boldsymbol{s}^{-2}\exp[-i\eta\log \boldsymbol{s}^2] - \boldsymbol{c}^{-2}\exp[-i\eta\log \boldsymbol{c}^2]\}\chi_{M_S} +$$
$$+ (2/k)\sum_L (4\pi(2L+1))^{\frac{1}{2}}\exp[2i\sigma_L]Q(\delta_L)\,Y_{L0}(\vartheta)\chi_{M_S}\,,$$

where, for semplicity, the superscript 3 has been omitted in the spin function. The singlet and triplet state differential cross-sections are given simply by

$$(6) \qquad {}^1\sigma(\vartheta) = |\,{}^1f(\vartheta)\,|^2\,, \qquad {}^3\sigma(\vartheta) = \tfrac{1}{3}\sum_{M_S}|\,{}^3f^{M_S}(\vartheta)\,|\,,$$

and, since for a two-nucleon system S^2 is a constant of motion ([7]), the weighted sum of (6) combine to give the total differential cross-section

$$(7) \qquad \sigma(\vartheta) = (1/4)\,{}^1\sigma(\vartheta) + (3/4)\,{}^3\sigma(\vartheta)\,.$$

It is clear from Eqs. (4) and (5) that in both cases the singlet and triplet cross-sections can be written as a sum of three terms, and consequently also the total differential cross-section $\sigma(\vartheta)$ can be separated into three contributions: nuclear, Coulomb and interference.

The Coulomb term is nothing but the known Mott expression

$$(8) \qquad \sigma_C(\vartheta) = (1/4)[\,|\,{}^1f_C(\vartheta)\,|^2 + \sum_{M_S}|\,{}^3f_C^{M_S}(\vartheta)\,|^2] =$$
$$= (\eta/2k)^2[\boldsymbol{s}^{-4} + \boldsymbol{c}^{-4} - (\boldsymbol{sc})^{-2}\cos(\eta\log(\boldsymbol{sc})^{-2})]\,.$$

([7]) This statement, strictly true for the two-proton system, because of the exclusion principle, holds for the neutron-proton scattering provided the interaction Hamiltonian is symmetric in the spin vectors of the two nucleons. In this case the conservation of S^2 follows from symmetry considerations; see J. M. Blatt and V. F. Weisskopf: *Nuclear Physics* (New York, 1952), p. 97.

For the nuclear part of the singlet state scattering, a general formula can be derived using the technique introduced by BLATT and BIEDENHARN [8] for the elastic scattering of spinless particles by a central force. In fact, defining the quantity

$$(9) \qquad B_\lambda = \sum_{L=0}^{\infty} (2L+1)^2 (LL'00\,|\,\lambda 0)^2 \sin^2 K_L +$$

$$+ 2 \sum_{L=0}^{\infty} \sum_{L'=L+2}^{L+\lambda} (2L+1)(2L'+1)(LL'00\,|\,\lambda 0)^2 \sin K_L \sin K_{L'} \cos (K_L - K_{L'} + 2\sigma_{LL'}),$$

we get from Eq. (4)

$$(10) \qquad {}^1\sigma_{\mathcal{R}}(\vartheta) = |\,{}^1f_{\mathcal{R}}(\vartheta)\,|^2 = (4/k^2) \sum_{\lambda=0}^{\infty} B_\lambda P_\lambda(\cos\vartheta) .$$

Because of the exclusion principle, L and L' can assume only even values, and hence $\lambda =$ even number, due to the fact that the Wigner coefficients $[LL'00\ \lambda 0]$ vanish unless $L + L' + \lambda =$ even number (conservation of parity).

The general expression for the interference term of the singlet scattering is straightforward, and we obtain

$$(11) \qquad {}^1\sigma_{\mathcal{I}}(\vartheta) = 2\ \mathrm{Re}\,|\,{}^1f_{\mathcal{C}}(\vartheta)\,{}^1f^*_{\mathcal{R}}(\vartheta)\,| =$$

$$= (4/k^2) \sum_{L=0}^{\infty} (2L+1)[(-\eta \boldsymbol{X}_1/2) \sin K_L \cos K_L + (\eta \boldsymbol{Y}_1/2) \sin^2 K_L] P_L(\cos\vartheta).$$

For triplet state scattering we can not use the nuclear scattering amplitude given in Eq. (5), which is valid only in the hypothesis of central forces. If the non central part of the Hamiltonian is of the $\boldsymbol{L}\cdot\boldsymbol{S}$ type, although L^2 and S^2 remain constant of motion, M_L and M_S do no longer commute with the Hamiltonian, and one has to perform a transformation from the representation characterized by the four quantum numbers L, S, M_L M_S to the scheme $LSJM$. Furthermore, if the Hamiltonian contains tensor forces, L^2 either is no longer a constant of motion, and in this case only S^2, J^2, M and the parity operator P_x, with eigenvalues $(-1)^L$, do commute with the Hamiltonian. Therefore, a transformation from the scheme LSM_LM_S, so far used, to the scheme $LSJM$ does not in general diagonalize the Hamiltonian and, in order to avoid complex phaseshifts for coupled states, a further transformation to the so-called parity representation $(-1)^L SJM$ is required. But, if we limit ourselves to S and P waves and neglect a possible ${}^3P_2$-${}^3F_2$ coupling due to tensor forces, L^2 is obviously a constant of motion, and we can work in the $LSJM$ scheme. It

[8] J. M. BLATT and L. C. BIEDENHARN: *Rev. Mod. Phys.*, **24**, 258 (1952).

is needless to show that all these considerations do not apply to the singlet states, simply because here $L^2=J^2$, and therefore the conservation of total angular momentum reduces to the conservation of orbital angular momentum.

It is known (9) that the spin angular dependence of a wave function in the $LSJM$ scheme is described by the functions $\mathcal{Y}^M_{JL}(\vartheta,\varphi)$, eigenfunctions of the operators P_r, L^2, S^2, J^2 and M. They are derived from the orthogonal spin-angle functions $Y_{LM_L}(\vartheta,\varphi)\chi_{M_S}$, appropriate for the LSM_LM_S representation, with the aid of the following unitary transformation

$$\mathcal{Y}^M_{JL}=\sum_{M_S}(LSM_LM_S|JM)Y_{LM_L}\chi_{M_S}, \tag{12}$$

where $M_L=M-M_S$. The inverse of the transformation (12) reads

$$Y_{LM_L}\chi_{M_S}=\sum_{J=|L-S|}^{L+S}(LSM_LM_S|JM)\mathcal{Y}^M_{JL}, \tag{13}$$

where, as above, the condition $M=M_L+M_S$ holds. In our case $M_L=0$ ($M_S=M$) and $S=1$; therefore, from Eqs. (5) and (13) we get the following expression for the nuclear scattering amplitude

$$^3f^M_{\mathcal{N}}(\vartheta)=(2/k)\sum_J\sum_{L=|J-1|}^{J+1}[4\pi(2L+1)]^{\frac12}\exp[2i\sigma_L]Q(\delta_{JL})(L10M|JM)\mathcal{Y}^M_{JL}. \tag{14}$$

Denoting the quantity $(2L+1)^{\frac12}(L10M|JM)$ by a^M_J for $L=J-1$, and similarly by b^M_J and c^M_J for $L=J$ and $L=J+1$ (Table I), Eq. (14), written down explicitely, reads

$$\begin{aligned}^3f^M_{\mathcal{N}}(\vartheta)=(2/k)(4\pi)^{\frac12}\sum_J\{&a^J_M\exp[2i\sigma_{J-1}]Q(\delta_{J,J-1})\mathcal{Y}^M_{J,J-1}+\\&+b^M_J\exp[2i\sigma_J]Q(\delta_{J,J})\mathcal{Y}^M_{J,J}+c^M_J\exp[2i\sigma_{J+1}]Q(\delta_{J,J+1})\mathcal{Y}^M_{J,J+1}\},\end{aligned} \tag{15}$$

where, according to Eq. (12), $\mathcal{Y}^M_{JL}$ is given by (see Appendix)

$$\mathcal{Y}^M_{JL}=\sum_{M'=-1}^{1}(L1\,,\,M-M',\,M'|JM)Y_{L,M-M'}\chi_{M'}. \tag{16}$$

TABLE I. – $(2L+1)^{\frac12}(L10M|JM)$.

M	±1	0
$a^M_J(L=J-1)$	$[(J+1)/2]^{\frac12}$	$J^{\frac12}$
$b^M_J(L=J)$	$\mp[(2J+1)/2]^{\frac12}$	0
$c^M_J(L=J+1)$	$(J/2)^{\frac12}$	$-(J+1)^{\frac12}$

(9) J. M. BLATT and V. F. WEISSKOPF: *op. cit.*, p. 99.

Specializing Eqs. (15) and (16) for $L = 1$ ($J = 0, 1, 2$), and taking into account the obvious limitations $J \geqslant 0$ and $|M| \leqslant J$, we obtain for the nuclear and interference part of the triplet state scattering

$$(17) \quad {}^3\sigma_{\mathcal{N}}(\vartheta) = (1/3) \sum_{M=-1}^{1} |{}^3f_{\mathcal{N}}^{M}(\vartheta)|^2 = (4/3k^2)\Big\{ \sum_{J=0}^{2} (2J+1) \sin^2 \delta_J + \\ + [(3/2) \sin^2 \delta_1 + (7/2) \sin^2 \delta_2 + 4 \sin \delta_0 \sin \delta_2 \cos(\delta_0 - \delta_2) + \\ + 9 \sin \delta_1 \sin \delta_2 \cos(\delta_1 - \delta_2)] P_2(\cos \vartheta) \Big\},$$

$$(18) \quad {}^3\sigma_{\mathcal{J}}(\vartheta) = (1/3)2 \operatorname{Re} \sum_{M=-1}^{1} |{}^3f_{\mathcal{C}}^{M}(\vartheta) {}^3f_{\mathcal{N}}^{M\,*}(\vartheta)| = \\ = (4/3k^2) \sum_{J=0}^{2} (2J+1)[(-\eta \boldsymbol{X}_1/2) \sin \delta_J \cos \delta_J + (\eta \boldsymbol{Y}_1/2) \sin^2 \delta_J] P_1(\cos \vartheta),$$

where the index $L = 1$ in the phaseshift symbols has been omitted. Adding the singlet state contributions (10) and (11) for $L = 0$, from Eq. (7) one obtains the total differential cross-section in the S and P wave approximation

$$(19) \quad \sigma(\vartheta) - \sigma_{\mathcal{C}}(\vartheta) \equiv \Delta\sigma(\vartheta) = \sigma_{\mathcal{N}}(\vartheta) + \sigma_{\mathcal{J}}(\vartheta),$$

where

$$(20) \quad k^2 \sigma_{\mathcal{N}}(\vartheta) = \sin^2 K_0 + z_1 + z_3 P_2(\cos \vartheta),$$

$$(21) \quad k^2 \sigma_{\mathcal{J}}(\vartheta) = (-\eta \boldsymbol{X}_0/2) \sin K_0 \cos K_0 + (\eta \boldsymbol{Y}_0/2) \sin^2 K_0 + \\ + [(-\eta \boldsymbol{X}_1/2) z_2 + (\eta \boldsymbol{Y}_1/2) z_1] P_1(\cos \vartheta).$$

In Eqs. (20) and (21) we have introduced the following notation [10]

$$(22) \quad \begin{cases} z_1(\delta_0, \delta_1, \delta_2) = \sum_{J=0}^{2} (2J+1) \sin^2 \delta_J, \\ z_2(\delta_0, \delta_1, \delta_2) = \sum_{J=0}^{2} (2J+1) \sin \delta_J \cos \delta_J, \\ z_3(\delta_0, \delta_1, \delta_2) = \text{coefficient of } P_2(\cos \vartheta) \text{ in Eq. (17)}. \end{cases}$$

[10] In the notes quoted in references [5,11], the quantity denoted here as z_3 appears as z_4.

The singlet D-state ($L = 2$) would give a contribution

$$(23) \quad 5 \sin^2 K_2 + [50/7) \sin^2 K_2 + 10 \sin K_0 \sin K_2 \cos (K_2 - K_0 + 2\sigma_{20})] \cdot \cdot P_2(\cos\vartheta) + (90/7) \sin^2 K_2 P_4(\cos\vartheta)$$

to the nuclear part $k^2\sigma_{\mathcal{N}}(\vartheta)$, and a contribution

$$(24) \quad 5[(-\eta X_2/2) \sin K_2 \cos K_2 + (\eta Y_2/2) \sin^2 K_2] P_2(\cos\vartheta)$$

to the interference term $k^2\sigma_{\mathcal{J}}(\vartheta)$.

2. – The parametrization method.

We shall now outline a parametrization method, which gives directly the phaseshift K_0 and the triplet phaseshift combinations z_1, z_2 and z_3. For $\vartheta = \pi/2$, Eqs. (19) (20) and (21) give

$$(25) \quad \Delta z \equiv z_1 - z_3/2 = k^2 \Delta\sigma(\pi/2) + 2\eta \cos(\eta \log 2) \sin K_0 \cos K_0 - - [1 - 2\eta \sin(\eta \log 2)] \sin^2 K_0 ,$$

which fixes the upper ($K_0 = 0$) and the lower ($K_0 = \pm \pi/2$) limit of the quantity Δz as a function of K_0. Neglecting for the moment the experimental errors, Eq. (25) gives, using the experimental value of the cross-section at $\vartheta = \pi/2$, the functional dependence of the combination Δz of the triplet state ($L = 1$) phaseshifts on the singlet state ($L = 0$) phaseshift K_0. Once the function $\Delta z(K_0)$ is given, we can write Eq. (19) in the form

$$(26) \quad k^2 \Delta\sigma(\vartheta) - [1 + (\eta \mathbf{Y}_0/2)] \sin^2 K_0 + (\eta \mathbf{X}_0/2) \sin K_0 \cos K_0 - 2\Delta z(K_0) P_2(\cos\vartheta) = = [1 + (\eta \mathbf{Y}_1/2) P_1(\cos\vartheta) + 2P_2(\cos\vartheta)] z_1 - (\eta \mathbf{X}_1/2) P_1(\cos\vartheta) z_2 .$$

Since the left-hand side of Eq. (26) depends on K_0 only, choosing two new angles ϑ_1 and ϑ_2, the quantities z_1 and z_2, and therefore z_3, can be determined as functions of K_0. It follows that the differential cross-section becomes dependent on K_0 only. Then, satisfying by means of a third angle ϑ_3 the equation $\Delta\sigma(K_0, \vartheta_3) = \Delta\sigma_{\text{exp}}(\vartheta_3)$, the value of K_0, both for positive and negative sign, can be fixed. The further choice between the two signs of K_0 is provided by the best fit over all angles with the experimental cross-section. At this stage, if polarization data are available, they represent the best criterion both for the selection of the sign of K_0 and one out of the four sets $(\delta_0, \delta_1, \delta_2)$. In fact, it has been shown [11] that a maximum number of four different sets

[11] E. Clementel and C. Villi: *Nuovo Cimento*, **2**, 356 (1955). It is worth to point out that the relation (4) of this reference leads to the following rule, extremely useful for the check of the calculations: for a given energy, the sum of the phaseshifts with the same index J of the four solutions compatible with Eqs. (27) and (28) is independent of J.

of triplet P-state phaseshifts are compatible with given values of z_1, z_2 and z_3. These sets can be obtained by considering the following relations, derived from the definition of the z_i's

$$(27) \qquad \sum_{J=0}^{2}(2J+1)\cos 2\delta_J = 9 - 2z_1 \equiv r_1\,, \qquad \sum_{J=0}^{2}(2J+1)\sin 2\delta_J = 2z_2 \equiv r_2\,,$$

$$(28) \qquad \sum_{J=0}^{2}(J+2)^2\cos 2(\delta_2 - \delta_J) = 13 - 8\Delta z \equiv r_3\,.$$

If we suppose fixed the value of the phase δ_2, Eqs. (27) become

$$(29) \qquad \begin{cases} \sum\limits_{J=0,1}(2J+1)\cos 2\delta_J = r_1 - 5\cos 2\delta_2 \equiv x_1\,, \\ \sum\limits_{J=0,1}(2J+1)\sin 2\delta_J = r_2 - 5\sin 2\delta_2 \equiv y_1\,. \end{cases}$$

Since we shall need later (Section 5) the solution of the same system (29), where the coefficient $2J+1$ of the term in δ_J is substituted by a certain energy dependent quantity $d_J \leqslant 2J+1$, we give here the general solution, which is

$$(30) \qquad \cos 2\delta_0 = (1/d_0)(x_1 - d_1\cos 2\delta_1)\,, \qquad \cos 2\delta_1 = p \pm (p^2 - q)^{\frac{1}{2}}\,,$$

where

$$(31) \qquad p = (x_1/2d_1)[1 - (d_1^2 - d_0^2)/(x_1^2 + y_1^2)]\,, \qquad q = (p/x_1)^2 - y_1^2(x_1^2 + y_1^2)\,.$$

With $d_J = 2J+1$, Eqs. (30) and (31) give the solution of the system (29). For any value of δ_2, two pairs (δ_0, δ_1), compatible with Eq. (27), are given by Eq. (30), but only a maximum number of four sets $(\delta_0, \delta_1, \delta_2)$ satisfy Eq. (28) also. This is more readily seen by means of a graphical translation ([11]) of Eqs. (27) and (28), which has suggested a mechanical analyzer, solving automatically the system and giving the required four sets of phaseshifts.

If the experimental polarization $P(\vartheta, \varphi)$ is known, a further selection among the four sets is possible, since the « good » one has to satisfy both Eq. (28) and equation

$$(32) \qquad P(\vartheta, \varphi) = [\sin 2\vartheta\cos\varphi/k^2\sigma(\vartheta)]\cdot$$
$$\cdot[3\sin\delta_0\sin\delta_2\sin(\delta_0 - \delta_2) + (9/2)\sin\delta_1\sin\delta_2\sin(\delta_1 - \delta_2)]\,,$$

which expresses the polarization in the S and P wave approximation ([12]).

([12]) L. J. B. GOLDFARB and D. FELDMAN: *Phys. Rev.*, **85**, 1099 (1952).

Because of the experimental uncertainties and the arbitrariness in choosing the experimental « points » at the angles ϑ_1, ϑ_2 and ϑ_3, the results of this method, in the energy region where to consider the effect of S and P waves only may realistically be regarded as valid, have to be accepted as a first approximation to the correct solution. An obvious improvement would be to apply the previous procedure not the given experimental data, but to their least square fit.

3. – General expression for the triplet cross-section in the parity representation.

We shall now generalize the previous considerations including the ${}^3P_2$-${}^3F_2$ coupling in the triplet state scattering. The wave function describing the scattering process in the parity representation $(-1)^L SJM$ is the same as in the $LSJM$ scheme for $L = J$, whereas for $L = J-1$ and $L = J+1$ states, which have the same parity, is given by a linear combination ([13,14]) of the wave functions corresponding to the two channels $L = J \pm 1$. Denoting by the index α, β and γ the wave functions and the phaseshifts corresponding, for a given value of J, to the states $L = J-1$, J, $J+1$ respectively, we can write

$$\psi^M_{Jn} = \frac{1}{r}[u_{Jn}(r)\mathcal{Y}^M_{J,J-1} + w_{Jn}(r)\mathcal{Y}^M_{J,J+1}], \qquad (n = \alpha, \gamma), \tag{33}$$

where $(u_{J\alpha}, w_{J\alpha})$, and $(u_{J\gamma}, w_{J\gamma})$ are the two linearly independent solutions, regular at the origin, of the two coupled second-order differential equations for $L = J \pm 1$ of the two-proton system. The asymptotic behavior of the radial functions is given by

$$\begin{cases} u_{Jn} \sim A_{Jn} \sin\left(kr - \eta \log 2kr - \frac{\pi}{2}(J-1) + \sigma_{J-1} + \delta^u_{Jn}\right), \\ w_{Jn} \sim C_{Jn} \sin\left(kr - \eta \log 2kr - \frac{\pi}{2}(J+1) + \sigma_{J+1} + \delta^w_{Jn}\right). \end{cases} \qquad (n = \alpha, \gamma). \tag{34}$$

The asymptotic behavior of the wave function (33) can be written also as

$$\begin{cases} \psi^M_{J\alpha} \sim \frac{1}{r}\sin\left(kr - \eta \log 2kr - \frac{\pi}{2}(J-1) + \sigma_{J-1} + \delta_{J\alpha}\right)(\mathcal{Y}^M_{J,J-1} + g_{J\alpha}\mathcal{Y}^M_{J,J+1}), \\ \psi^M_{J\gamma} \sim \frac{1}{r}\sin\left(kr - \eta \log 2kr - \frac{\pi}{2}(J+1) + \sigma_{J+1} + \delta_{J\gamma}\right)(g_{J\gamma}\mathcal{Y}^M_{J,J-1} + \mathcal{Y}^M_{J,J+1}), \end{cases} \tag{35}$$

([13]) F. Rohrlich and J. Eisenstein: *Phys. Rev.*, **75**, 705 (1949).
([14]) J. M. Blatt and L. C. Biedenharn: *Phys. Rev.*, **86**, 399 (1952).

provided

$$(36)\qquad \begin{cases} \delta^u_{J\alpha} = \delta_{J\alpha}\,, \quad \delta^w_{J\alpha} = \delta_{J\alpha} + \sigma_{J-1,J+1} + \pi\,, \quad g_{J\alpha} = C_{J\alpha}/A_{J\alpha}\,, \\ \delta^w_{J\gamma} = \delta_{J\gamma}\,, \quad \delta^u_{J\gamma} = \delta_{J\gamma} + \sigma_{J+1,J-1} - \pi\,, \quad g_{J\gamma} = A_{J\gamma}/C_{J\gamma}\,. \end{cases}$$

The relations (36) have been obtained by comparing the asymptotic expansion (35) with those following from the substitution of Eqs. (34) into Eq. (33). Because of the orthogonality of the α- and γ-eigenfunctions, the following condition holds ([15])

$$(37)\qquad g_J \equiv g_{J\alpha} = -\,g_{J\gamma}\,.$$

The constant $g_{J\alpha}$ measures the amount of admixture of the state $L = J+1$ to the state $L = J-1$, while the constant $g_{J\gamma}$ gives the amount of admixture of the state $L = J-1$ to the state $L = J+1$.

The asymptotic behavior of the incoming unsymmetrized pure Coulomb wave, expanded as a sum of spherical partial waves ([16]), can be expressed in the $LSJM$ scheme, by using Eq. (13) and the notation of Table I, in the form

$$(38)\qquad {}^3\psi^M_{\vec{e}}(r,\vartheta) \sim \frac{(4\pi)^{\frac{1}{2}}}{kr} \sum_J \Big\{ i^{J-1} a^M_J \exp[i\sigma_{J-1}] \cdot$$

$$\cdot \sin\Big(kr - \eta\log 2kr - \frac{\pi}{2}(J-1) + \sigma_{J-1}\Big)\, \mathcal{Y}^M_{J,J-1} + i^J b^M_J \exp[i\sigma_J] \cdot$$

$$\cdot \sin\Big(kr - \eta\log 2kr - \frac{\pi}{2}J + \sigma_J\Big)\, \mathcal{Y}^M_{J,J} + i^{J+1} c^M_J \exp[i\sigma_{J+1}] \cdot$$

$$\cdot \sin\Big(kr - \eta\log 2kr - \frac{\pi}{2}(J+1) + \sigma_{J+1}\Big)\, \mathcal{Y}^M_{J,J+1} \Big\}\,.$$

The asymptotic form of the total wave function, sum of the incident and the scattered wave, is given, in virtue of Eq. (35), by an expression of the form

$$(39)\qquad {}^3\psi^M_{\mathrm{tot}}(r,\vartheta) \sim \frac{(4\pi)^{\frac{1}{2}}}{kr} \sum_J \Big\{ i^{J-1} \alpha^M_J \exp[i\sigma_{J-1} + i\delta_{J\alpha}] \cdot$$

$$\cdot \sin\Big(kr - \eta\log 2kr - \frac{\pi}{2}(J-1) + \sigma_{J-1} + \delta_{J\alpha}\Big)(\mathcal{Y}^M_{J,J-1} + g_{J\alpha}\,\mathcal{Y}^M_{J,J+1}) +$$

$$+ i^J \beta^M_J \exp[i\sigma_J + i\delta_{J\beta}] \sin\Big(kr - \eta\log 2kr - \frac{\pi}{2}J + \sigma_J + \delta_{J\beta}\Big)\mathcal{Y}^M_{J,J} +$$

$$+ i^{J+1}\gamma^M_J \exp[i\sigma_{J+1} + i\delta_{J\gamma}] \sin\Big(kr - \eta\log 2kr - \frac{\pi}{2}(J+1) +$$

$$+ \sigma_{J+1} + \delta_{J\gamma}\Big)(g_{J\gamma}\,\mathcal{Y}^M_{J,J-1} + \mathcal{Y}^M_{J,J+1}) \Big\}\,,$$

([15]) Our g_J corresponds to $\mathrm{tg}\,\varepsilon_J$ of reference (14).

([16]) L. I. SCHIFF: *op. cit.*, p. 118.

which for vanishing nuclear potential, i.e. for $\delta_{J\alpha}^{u,w}$, $\delta_{J\gamma}^{u,w}$ and $\delta_{J\beta} \to 0$, must be identical with the expansion (38). In the limit, taking into account the relations (36), we obtain therefore an alternative expression of ${}^3\psi_{\mathcal{C}}^M(r, \vartheta)$, which in this form can be subtracted from ${}^3\psi_{\text{tot}}^M(r, \vartheta)$ to give the scattered wave. This expression reads

$$(40) \qquad {}^3\psi_{\mathcal{C}}^M(r, \vartheta) \sim \frac{(4\pi)^{\frac{1}{2}}}{kr} \sum_J \Big\{ i^{J-1}(\alpha_J^M + g_{J\gamma}\gamma_J^M)\exp[i\sigma_{J-1}] \sin(kr - \eta \log 2kr - \\ - \frac{\pi}{2}(J-1) + \sigma_{J-1})\, \mathcal{Y}_{J,J-1}^M + i_J\beta_J^M \exp[i\sigma_J] \sin(kr - \eta \log 2kr - \frac{\pi}{2} J + \sigma_J)\, \mathcal{Y}_{J,J}^M + \\ + i^{J+1}(\gamma_J^M + g_{J\alpha}\alpha_J^M)\exp[i\sigma_{J+1}] \sin(kr - \eta \log 2kr - \frac{\pi}{2}(J+1) + \sigma_{J+1})\, \mathcal{J}_{J,J+1}^M \Big\}.$$

Identifying Eq. (40) with the Coulomb wave (38), we derive

$$(41) \qquad \alpha_J^M = (a_J^M + g_J c_J^M)(1 + g_J^2)^{-1}, \qquad \beta_J^M = b_J^M, \qquad \gamma_J^M = (c_J^M - g_J a_J^M)(1 + g_J^2)^{-1}.$$

With these values for the parameters α_J^M, β_J^M and γ_J^M, the nuclear antisymmetrized scattering amplitude, derived by subtraction of Eq. (40) from Eq. (39) is given by

$$(42) \quad {}^3f_{\mathcal{C}}^M(\vartheta) = \frac{2(4\pi)^{\frac{1}{2}}}{k} \sum_J \{\alpha_J^M(\exp[2i\sigma_{J-1}]Q(\delta_{J\alpha})\, \mathcal{Y}_{J,J-1}^M + \\ + g_J \exp[2i\sigma_{J+1}]Q(\delta_{J\alpha} + \sigma_{J-1,J+1})\, \mathcal{Y}_{J,J+1}^M) + \beta_J^M \exp[2i\sigma_J]Q(\delta_{J\beta})\, \mathcal{Y}_{J,J}^M + \\ + \gamma_J^M (\exp[2i\sigma_{J+1}]Q(\delta_{J\gamma})\, \mathcal{Y}_{J,J+1}^M - g_J \exp(2i\sigma_{J-1})Q(\delta_{J\gamma} + \sigma_{J+1,J-1})\mathcal{Y}_{J,J-1}^M)\},$$

which, in the limit $g_J \to 0$, reduces to the $LSJM$ scheme expression (15).

4. – S, P and D wave approximation with coupling of ${}^3F_2$ to ${}^3P_2$ state.

Eq. (42) gives the complete expression of the scattering amplitude for triplet states in terms of the phaseshifts of the eigenstates α and γ of the scattering matrix, the phaseshift of the state β and the coupling parameter g_J, which is a function of the energy of the incident nucleon. The further obvious step of the approximation of Section 1 is to include the effect of the singlet D state and the coupling of the ${}^3F_2$ to ${}^3P_2$ state. This is a consistent approximation only if the phaseshift $\delta_{2\gamma}$ behaves like a typical F wave phaseshift as far as its energy dependence is concerned ([17]). In this way we obtain

([17]) Due to the coupling, the outgoing beam contains an F wave contribution also if in the incoming beam S and P waves only are effective for the scattering. If the effect of the ${}^3F_2$ state not arising from the coupling to the ${}^3P_2$ state is taken into account, the other waves involving F states ($J = 3, 4$) should also be considered for consistency reasons.

from Eq. (42)

$$
(43)\quad \begin{cases} k\,{}^3f^1_{\mathcal{T}}(\vartheta) = 2(4\pi)^{\frac{1}{2}}\{\exp[2i\sigma_1][\beta^1_1 Q(\delta_{1\beta})\mathcal{Q}^1_{11} + \alpha^1_2 Q(\delta_{2\alpha})\mathcal{J}^1_{21}] + \\ \qquad + \alpha^1_2 g_2 \exp[2i\sigma_3) Q(\delta_{2\alpha} + \sigma_{13})\mathcal{Q}^1_{23}\}, \\ k\,{}^3f^0_{\mathcal{T}}(\vartheta) = 2(4\pi)^{\frac{1}{2}}\{\exp[2i\sigma_1][\gamma^0_0 Q(\delta_{0\gamma})\mathcal{Q}^0_{01} + \alpha^0_2 Q(\delta_{2\alpha})\mathcal{Q}^0_{21}] + \\ \qquad + \alpha^0_2 g_2 \exp[2i\sigma_3] Q(\delta_{2\alpha} + \sigma_{13})\mathcal{Q}^0_{23}\}, \\ k\,{}^3f^{-1}_{\mathcal{T}}(\vartheta) = 2(4\pi)^{\frac{1}{2}}\{\exp[2i\sigma_1][\beta^{-1}_1 Q(\delta_{1\beta})\mathcal{Q}^{-1}_{11} + \alpha^{-1}_2 Q(\delta_{2\alpha})\mathcal{Q}^{-1}_{21}] + \\ \qquad + \alpha^{-1}_2 g_2 \exp[2i\sigma_3] Q(\delta_{2\alpha} + \sigma_{13})\mathcal{Q}^{-1}_{23}\}. \end{cases}
$$

From Eqs. (43) and (5) the nuclear and interference terms of the triplet scattering can be calculated. Here we shall limit ourselves to the final formulas, referring to the Appendix for further details.

Adding the contribution of the singlet S and D states, and setting $\delta_{0\gamma} = \delta_0$, $\delta_{1\beta} = \delta_1$, $\delta_{2\alpha} = \delta_2$, $g_2 = g$ and $h = (1 + g^2)^{-1}$, the nuclear part of the differential cross-section is given by

$$
(44)\qquad k^2\sigma_{\mathcal{T}}(\vartheta) = p_0 P_0(\cos\vartheta) + p_2 P_2(\cos\vartheta) + p_4 P_4(\cos\vartheta),
$$

where

$$
(45)\quad \begin{cases} p_0 = \sin^2 K_0 + 5\sin^2 K_2 + h^2\sin^2\delta_0 + 3\sin^2\delta_1 + \\ \qquad + 5h^2\sin^2\delta_2 + 5h^2 g^2\sin^2(\delta_2 + \sigma_{13}), \\ p_2 = (50/7)\sin^2 K_2 + 10\sin K_0 \sin K_2 \cos(K_2 - K_0 + 2\sigma_{20}) + (3/2)\sin^2\delta_1 + \\ \qquad + (7/2)h^2\sin^2\delta_2 + 4h^2\sin\delta_0\sin\delta_2\cos(\delta_0 - \delta_2) + \\ \qquad + 9h\sin\delta_1\sin\delta_2\cos(\delta_1 - \delta_2) - (5/7)6^{\frac{1}{2}}hg\sin(\delta_0 + \sigma_{13})\cdot \\ \qquad \cdot [2h\sin\delta_0\cos(\delta_0 - \delta_2 + \sigma_{13}) - 3\sin\delta_1\cos(\delta_1 - \delta_2 + \sigma_{13}) + \\ \qquad + h\sin\delta_2\cos\sigma_{13}] + 4h^2 g^2\sin^2(\delta_2 + \sigma_{13}), \\ p_4 = (90/7)\sin^2 K_2. \end{cases}
$$

For the interference term we obtain

$$
(46)\qquad \begin{aligned} k^2\sigma_{\mathcal{J}}(\vartheta) = {} & -(\eta \mathbf{X}_0/2)\sin K_0\cos K_0 + (\eta \mathbf{Y}_0/2)\sin^2 K_0 + \\ & + [(-\eta \mathbf{X}_1/2)(h\sin\delta_0\cos\delta_0 + 3\sin\delta_1\cos\delta_1 + 5h\sin\delta_2\cos\delta_2) + \\ & + (\eta \mathbf{Y}_1/2)[h\sin^2\delta_0 + 3\sin^2\delta_1 + 5h\sin^2\delta_2)]\,P_1(\cos\vartheta) + \\ & + 5[(-\eta \mathbf{X}_2/2)\sin K_2\cos K_2 + (\eta \mathbf{Y}_2/2)\sin^2 K_2]P_2(\cos\vartheta). \end{aligned}
$$

In the limit of no coupling ($g = 0$, $h = 1$) and $K_2 = 0$, Eqs. (44) and (46) reduce to Eqs. (20) and (21) respectively.

5. – The polynomial method.

The advantage of this method, against the parametrization one, lies in its capability to take into account simultaneously all the experimental data. It is particularly powerful in the analysis of neutron-proton scattering experiments, but it has been found very useful also in the analysis of proton-proton scattering, although in this case its application requires the expansion of the interference term (46) in Legendre polynomials.

Let us still call z_1 and z_2 the combinations of $\sin^2 \delta_i$ respectively $\sin \delta_i \cos \delta_i$ appearing in $\sigma_{\mathcal{I}}(\vartheta)$. Using the expansions

$$(47) \qquad (\eta/2)\boldsymbol{X}_j P_j(\cos\vartheta) = \sum_\nu x_{2\nu}^{(j)} P_{2\nu}(\cos\vartheta)\,, \qquad (\eta/2)\boldsymbol{Y}_j P_j(\cos\vartheta) = \sum_\nu y_{2\nu}^{(j)} P_{2\nu}(\cos\vartheta)\,,$$

where, owing to the symmetry of the cross-section about $\vartheta = \pi/2$, even polynomials only appear, the interference term may be written as

$$(48) \qquad k^2\sigma_{\mathcal{I}}(\vartheta) = \sum_\nu q_{2\nu} P_{2\nu}(\cos\vartheta)\,,$$

where

$$(49) \qquad q_n = y_n^{(0)} \sin^2 K_0 - x_n^{(0)} \sin K_0 \cos K_0 + y_n^{(1)} z_1 - x_n^{(1)} z_2 + \\ + 5(y_n^{(2)} \sin^2 K_2 - x_n^{(2)} \sin K_2 \cos K_2)\,.$$

It is clear that the expansions (47) have to be calculated for the angular interval involved in the experiment, and that it can be limited to few (five or six) terms, provided the lower limit of the interval is not too near to $\vartheta = 0°$. If this is not the case, the lowest points have to be excluded from the analysis ([18]). We have solved Eq. (47) by means of the least square method, obviously because the equations are not strictly compatible with each other.

Adding the nuclear term to Eq. (48), the general form of the differential cross-section reads

$$(50) \qquad k^2 \Delta\sigma(\vartheta) = \sum_\nu \alpha_{2\nu} P_{2\nu}(\cos\vartheta)\,,$$

([18]) At high energies, the small angle region should be excluded also because, apart from the large errors of the experimental data, the theoretical formulas are not correct, due to relativistic and anomalous magnetic moment effects. We thank Prof. R. E. MARSHAK for calling our attention to this fact.

where

$$\alpha_n = p_n + q_n \,. \tag{51}$$

A least square fit in terms of even polynomials of the experimental data provides, together with Eq. (50), a system of equations having as unknown the phaseshift combinations appearing in the α_n. We have been able to solve the system up to the approximation of Section 4. The illustration of the procedure needs a practical example, and therefore it is deferred to the following paper. It is readily verified that, in the S and P wave approximation, the equations in α_0, α_4, α_6 and α_8 give directly K_0, in magnitude and sign, and the quantities z_1 and z_2; the quantity z_3 follows then from the equation in α_2, and the problem in solved.

In the more general case, the functional dependence of K_0, z_1 and z_2 on g and K_2 is required. When the analysis is carried out for various energies, continuity conditions are of great help in excluding spurious solutions. Finally, we point out that the considerable amount of computational work required for the determination of the triplet phaseshifts, once z_1 and z_2 are given (see Eq. (30) and (31)), may be entirely avoided by using the mechanical analyzer ([11]), provided the arms of lenght 1 and 5 are reduced by the factor $1/(1+g^2)$.

* * *

This research was started during the stay of the authors at the Birmingham University in 1954 ([19]). We should like to express our thanks to Prof. R. E. PEIERLS for several profitable discussions and also for his kind hospitality. We wish to acknowledge Prof. G. BREIT and Prof. R. E. MARSHAK for critical reading of the manuscript, and express our indebtedness to Dr. L. BERETTA for check calculations and computational assistence.

APPENDIX

We shall list here some relations used in various steps of the previous calculations. First we give the normalized spin spherical harmonics, defined in Eq. (16), up to $J = 2$, $L = 3$

([19]) In the meantime, the papers of G. BREIT and M. H. HULL Jr. [*Phys. Rev.*, **97**, 1051 (1955)] have appeared which cover the some extent, yet for a different purpose and with a different formalism, the same ground as the present paer. In the two quoted papers a thorough discussion of the polarization question is given.

$$\mathcal{Y}^0_{01} = (1/3)^{\frac{1}{2}}(Y_{11}\chi_{-1} - Y_{10}\chi_0 + Y_{1-1}\chi_1),$$
$$\mathcal{Y}^{\pm 1}_{11} = \pm (1/2)^{\frac{1}{2}}(Y_{1\pm 1}\chi_0 - Y_{10}\chi_{\pm 1}),$$
$$\mathcal{Y}^0_{21} = (2/3)^{\frac{1}{2}}Y_{10}\chi_0 + (1/6)^{\frac{1}{2}}(Y_{11}\chi_{-1} + Y_{1-1}\chi_1),$$
$$\mathcal{Y}^{\pm 1}_{21} = (1/2)^{\frac{1}{2}}(Y_{1\pm 1}\chi_0 + Y_{10}\chi_{\pm 1}),$$
$$\mathcal{Y}^1_{23} = (10/21)^{\frac{1}{2}}Y_{32}\chi_{-1} - (8/21)^{\frac{1}{2}}Y_{31}\chi_0 + (1/7)^{\frac{1}{2}}Y_{30}\chi_1,$$
$$\mathcal{Y}^0_{23} = (2/7)^{\frac{1}{2}}Y_{31}\chi_{-1} - (3/7)^{\frac{1}{2}}Y_{30}\chi_0 + (2/7)^{\frac{1}{2}}Y_{3-1}\chi_1,$$
$$\mathcal{Y}^{-1}_{23} = (1/7)^{\frac{1}{2}}Y_{30}\chi_{-1} - (8/21)^{\frac{1}{2}}Y_{3-1}\chi_0 + (10/21)^{\frac{1}{2}}Y_{3-2}\chi_1.$$

Using these expressions in Eqs. (15) or (42), it is easily verified that

$$|{}^3f^1_{\mathcal{Y}}(\vartheta)|^2 = |{}^3f^{-1}_{\mathcal{Y}}(\vartheta)|^2.$$

The product of two spherical harmonics can be expressed as a linear combination of Legendre polynomials by means of the formula

$$Y_{lm}(\vartheta,\varphi)Y^*_{l'm'}(\vartheta,\varphi) =$$
$$= (-1)^{m'}\sum_{L=|l-l'|}^{l+l'}\left[\frac{(2l+1)(2l'+1)}{4\pi(2L+1)}\right]^{\frac{1}{2}}(ll'00\,|\,L0)\,(ll',m,-m'\,|\,LM)\,Y_{LM}(\vartheta,\varphi),$$

specialized for the case $m = m'$ $(M = 0)$. The following Wigner coefficients are needed

$$(1\,1\,00\,|\,00) = -(1/3)^{\frac{1}{2}} \qquad (1\,1\,1\,-1\,|\,00) = (1/3)^{\frac{1}{2}}$$
$$(1\,1\,00\,|\,20) = (2/3)^{\frac{1}{2}} \qquad (1\,1\,1\,-1\,|\,20) = (1/6)^{\frac{1}{2}}$$

$$(2\,2\,00\,|\,00) = (1/5)^{\frac{1}{2}} \qquad (2\,2\,00\,|\,20) = -(2/7)^{\frac{1}{2}} \qquad (2\,2\,00\,|\,40) = (18/35)^{\frac{1}{2}}$$

$$(3\,1\,00\,|\,20) = -(3/7)^{\frac{1}{2}} \qquad (3\,1\,1\,-1\,|\,20) = (2/7)^{\frac{1}{2}}$$
$$(3\,1\,00\,|\,40) = (4/7)^{\frac{1}{2}} \qquad (3\,1\,1\,-1\,|\,40) = (3/2.7)^{\frac{1}{2}}$$

$$(3\,3\,00\,|\,00) = -(1/7)^{\frac{1}{2}} \qquad (3\,3\,1\,-1\,|\,00) = (1/7)^{\frac{1}{2}}$$
$$(3\,3\,00\,|\,20) = 2(1/3.7)^{\frac{1}{2}} \qquad (3\,3\,1\,-1\,|\,20) = -(1/2)(3/7)^{\frac{1}{2}}$$
$$(3\,3\,00\,|\,40) = -3(2/7.11)^{\frac{1}{2}} \qquad (3\,3\,1\,-1\,|\,40) = (1/2)(2/7.11)^{\frac{1}{2}}$$
$$(3\,3\,00\,|\,60) = 10(1/3.7.11)^{\frac{1}{2}} \qquad (3\,3\,1\,-1\,|\,60) = (5/2)(3/7.11)^{\frac{1}{2}}$$

$$(3\,3\,2\,-2\,|\,00) = -(1/7)^{\frac{1}{2}}$$
$$(3\,3\,2\,-2\,|\,20) = 0$$
$$(3\,3\,2\,-2\,|\,40) = (7/2.11)^{\frac{1}{2}}$$
$$(3\,3\,2\,-2\,|\,60) = (3/7.11)^{\frac{1}{2}}$$

RIASSUNTO

Si considera il problema dell'analisi delle fasi nelle esperienze di scattering protone-protone. Nell'ambito dell'approssimazione di sole onde S e P, viene formulato un metodo di parametrizzazione tramite il quale, usando direttamente i dati sperimentali, si ricavano le quattro fasi per lo stato di singoletto S e di tripletto P. Nel caso in cui si tenga conto del contributo dovuto all'onda D e dell'effetto dell'accoppiamento $^3P_2$-$^3F_2$ mostra come il problema possa ancora essere risolto servendosi di un metodo polinomiale.

IL NUOVO CIMENTO Vol. II, N. 6 1° Dicembre 1955

On the Production of Mesons in Hydrogen and Carbon above 10 GeV.

Y. Watase, K. Suga, Y. Tanaka and S. Mitani

Department of Physics, Faculty of Science, Osaka University - Osaka, Japan

(ricevuto il 1° Settembre 1955)

Summary. — Penetrating showers from hydrogen and carbon (average energy about 30 GeV) have been studied by CH_2-C subtraction method with a counter hodoscope at mountain altitude. The cross-section for meson production in hydrogen was found to be 67 ± 25 mb and that for multiple production appears to be at least about 70 percent of this value. No difference in the cross-sections for p-p and n-p collisions was observed. The angular distribution of the charged shower secondaries seems to show a forward peak in the p-p collisions and this tendency may be interpreted by the hypothesis that the incident nucleon is emitted into a rather sharp forward cone in the C.M. system, at least when the multiplicity is small.

1. – Introduction.

In this paper, the preliminary results of an experiment on penetrating showers from hydrogen and carbon which has been carried out at the Mt. Norikura Cosmic-Ray Laboratory (2840 m altitude) from autumn to winter of 1954 will be reported. A counter hodoscope system recorded penetrating showers produced in a thin layer of paraffin and graphite by high-energy cosmic-ray protons and neutrons of average energy about 30 GeV.

It is very important to examine the various nuclear interactions of nucleon-nucleon collision at high energies, say above several GeV. At these energies, the multiple production of mesons may be predominant, and two sorts of mechanisms of meson production, plural production and multiple production, may be separated experimentally. Many comprehensive studies with various

methods and techniques ([1-17]) have been carried out using cosmic-ray nucleons. Although the results have not always been consistent with each other, they have shown that at these energies multiple production of mesons does exist. In recent years, artificially accelerated particles of several GeV have become available, and the experimental results ([18-23]) with these nucleons and pions have confirmed the multiple production of mesons and obtained information about the total cross-sections for nuclear interactions and of meson production, and have clarified some parts of the mechanism of the meson production.

The subtraction technique, using a hydrogenous material, has been used to measure both absorption mean free path ([11,15-17]) and meson production cross-sections. With respect to other techniques, a high pressure hydrogen-filled cloud chamber ([13]) or the combination of liquid hydrogen (or compressed hydrogen gas) and a hodoscope (or cloud chamber) ([10-12]) also has been used

---

([1]) For instance, R. E. MARSHAK: *Meson physics* (1952); B. ROSSI: *High Energy Particles* (1952); J. G. ASKOVITCH and K. SITTE: *Phys. Rev.*, **97**, 159 (1955).

([2]) G. WATAGHIN: *Suppl. Nuovo Cimento*, **6**, 528 (1949).

([3]) G. BERTOLINO, M. CINI, P. COLOMBINO and G. WATAGHIN: *Nuovo Cimento*, **9**, 407 (1952).

([4]) C. B. A. MCCUSKER, N. A. PORTER and B. G. WILSON: *Phys. Rev.* **91**, 384 (1953).

([5]) H. SCHULTZ: *Zeits. f. Naturf.*, **9**, 419 (1954).

([6]) P. COLOMBINO, S. FERRONI and G. WATAGHIN: *Nuovo Cimento*, **11**, 572 (1954).

([7]) P. COLOMBINO, S. FERRONI, G. GHIGO and G. WATAGHIN: *Nuovo Cimento*, **12**, 819 (1954).

([8]) M. CERVASI, G. FIDECARO and L. MEZZETTI: *Nuovo Cimento*, **13**, 300 (1955).

([9]) I. MIURA, T. MATANO, Y. TOYOTA and T. MURAYAMA: *Progr. Theor. Phys.*, **13**, 115 (1955).

([10]) M. L. VIDALE and M. SCHEIN: *Nuovo Cimento*, **8**, 774 (1951); *Phys. Rev.*, **84**, 593 (1951).

([11]) W. D. WALKER, N. M. DULLER and J. D. SORRELS: *Phys. Rev.*, **86**, 865 (1952).

([12]) A. B. WEAVER: *Phys. Rev.*, **90**, 86 (1953).

([13]) O. KUSUMOTO, S. MIYAKE, K. SUGA and Y. WATASE: *Phys, Rev.*, **90**, 998 (1953).

([14]) R. L. S. GUPTA, K. K. ROY and T. ROY: *Ind. Journ. Phys.*, **27** 191 (1953).

([15]) G. L. ROLLOSSON: *Phys. Rev.*, **87**, 71 (1952).

([16]) D. FROMAN, J. KENNY and V. H. REGENER: *Phys. Rev.*, **91**, 707 (1953).

([17]) R. H. REDIKER: *Phys. Rev.*, **95**, 526 (1954).

([18]) W. B. FOWLER, R. P. SHUTT, A. M. THORNDIKE and W. L. WHITTEMORE: *Phys. Rev.*, **95**, 1026 (1954).

([19]) L. M. EISBERG, W. B. FOWLER, R. M. LEA, W. D. SHEPARD, R. P. SHUTT, A. M. THORNDIKE and W. L. WHITTEMORE: *Phys. Rev.*, **97**, 797 (1955).

([20]) J. CRUSSARD, W. D. WALKER and M. KOSHIBA: *Phys. Rev.*, **94**, 736 (1954); W. D. WALKER, J. CRUSSARD and M. KOSHIBA: *Phys. Rev.*, **95**, 852 (1954).

([21]) R. L. COOL, L. MADANSKY and O. PICCIONI: *Phys. Rev.* **93**, 249, 637 (1954).

([22]) D. A. HILL, T. COOR, W. F. HORNYAK, L. W. SMITH and G. SNOW: *Phys. Rev.*, **94**, 791 (1954).

([23]) L. W. SMITH, A. W. MCREYNOLDS and G. SNOW: *Phys. Rev.*, **97**, 1186 (1955).

to advantage in the analysis of individual events. But the results of some of these experiments are inconsistent not only in the cross-section for interaction or meson production but also in the difference between the n-p and the p-p process.

In view of the above, it is highly desirable to obtain more information about nucleon-nucleon interactions at these high energies, say above 10 GeV, with experimental bias, which may possibly explain the inconsistence of previous experimental results, kept small. Experiments with pure isolated hydrogen-filled cloud chambers are certainly most desirable, but the CH_2-C subtraction method allows one to obtain without too great difficulty much higher counting rates. Considering the weak flux of cosmic-ray nucleons, this counting-rate advantage is particularly important, though the method contains peculiar problems which must be considered carefully. An experiment using CH_2-C subtraction method with a counter hodoscope has been undertaken to obtain the cross-sections for nuclear interactions and an attempt has been made to gain some information about some of the characteristic features of meson production.

2. – Experimental Arrangement.

A sketch of the apparatus is shown in Fig. 1. The whole apparatus was set under a thin roof of about 5 g/cm² of copper and wood. There were seven trays of G-M counters called A, S_0, S_1, S_2, B, C and AS respectively. Tray S_1 consisted of 26 counters of 36 cm length and 2 cm diameter. Trays A, S_0, S_2 and B contained 14, 8, 14 and 14 counters of 40 cm length and 4 cm diameter, respectively. Tray C was a group of 19 counters of 50 cm length and 4 cm diameter. Eight counters of 80 cm length and 4 cm diameter were used for tray AS.

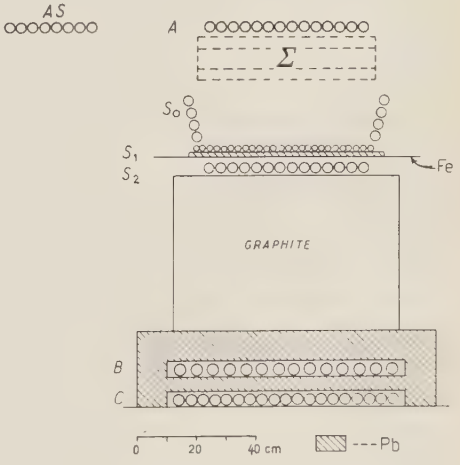

Fig. 1. – A sketch of the experimental arrangement (front view).

Tray A which was set just above the producer Σ was used to distinguish between charged and neutral primaries. S_0 and S_1 are trays for evaluating the number of charged secondaries. Counters of small diameter were used for S_1 in order to resolve particles with small angular spreads. Tray S_0 was used to detect particles emitted at wide angles. Tray S_2 was

separated from S_1 by lead and iron plates whose thicknesses were 1 cm and 0.5 cm respectively. If neutral pions are contained in the secondaries, they cannot discharge the counters of S_1, but can discharge the counters of S_2 through the materialization of the decay γ-rays in this layer. One can therefore obtain some information about neutral pions.

Tray B was separated from tray S_2 by 85 g/cm² graphite and 10 cm of lead. Each counter of this tray was wrapped by a lead sheet of 3 mm in thickness to reduce the effect of knock-on electrons. Tray C was separated from B by a further 5 cm lead. Each side of B and C was shielded by lead blocks. Tray AS_2 was set about 80 cm away from the centre of tray A. All counters of these trays were connected to neon lamps through hodoscope units.

The condition for a master pulse was the discharge of at least two counters of tray S_2 in addition to the discharge of at least three counters in tray B. The coincidence circuit had a resolving time of about 10 μs. The condition ($S \geqslant 2$) instead of ($S_1 \geqslant 2$) avoided bias against neutral pions. Neutral pions may contribute to the triggering with an efficiency about the same as that for charged particles (see section 4·4). Moreover, the condition ($B \geqslant 3$) under thick material (85 g/cm² graphite and 110 g/cm² lead) will prevent the bias which disfavours showers of low multiplicities. Secondary particles will suffer several times of nuclear interactions in the thick layer of about two mean free paths of nuclear interaction before discharging tray B. Neutrons, if contained in the secondary particles, can produce further charged particles and contribute to coincidences. These nucleon cascades average out considerably the fluctuations in the primary interaction. For these considerations the use of a low-Z element rather than a high-Z element was deemed more suitable, since a high-Z element will act as an absorber of energy rather than a generator of further penetrating particles. Low-Z elements are also less apt to cause electromagnetic interactions. The lead layer of 10 cm thickness above tray B acts as an absorber of low-energy particles and especially of the electronic component. This will avoid a bias in favour of events accompanied by cascade showers. The effects of electromagnetic interactions of μ-mesons are also reduced in this layer.

The apparatus was first run with no material in the position of Σ then with 13.25 g/cm² paraffin, and finally with 11.30 g/cm² graphite. The graphite layer was equivalent to the paraffin layer in the amount of carbon, and was placed in position so that its centre plane came up to the same position as the centre of the paraffin layer. The layer Σ changed about every twelve hours. Such repetition of short hour run will increase our confidence in the reliability of the equipment. The hodoscope units and coincidence circuits were checked at the end of every run, and the rates of ($S_2 \geqslant 2$) and of ($B \geqslant 3$) were separately recorded as a check. Barometric pressure was always recorded on a self-recordnig barometer, and the records are used for the later

correction of the rates. The amount of snow on the roof in winter was measured frequently and the absorption of primary particles was found to be completely negligible.

3. – Analysis of the Data.

The events which satisfy the triggering requirements $[(S_2 \geqslant 2) + (B \geqslant 3)]$ consist mainly of local penetrating showers generated in the producer (Σ) or in the surrounding material above S_1-tray, or in the lead or iron sheets between S_1- and S_2-trays. A few extensive showers, cascade showers produced by μ-mesons and chance coincidences contribute to the total number of events satisfying the triggering requirements. The events without struck counters in the AS-tray (i.e., $AS=0$) will be analyzed as local penetrating showers. These cases are divided into two groups. The first group involves events satisfying the condition $(S_1 + S_0 \geqslant 2)$ and is regarded as penetrating showers produced in the material above S_1-tray. These have been used for the analysis of penetrating showers produced in hydrogen and carbon. This analysis will be called the « production-type » analysis. The other group involves events satisfying the conditions ($A=1$, $S_1=1$ and $S_0=0$), and is regarded as penetrating showers produced in the lead or iron sheets by charged primary particles which suffered no interaction in the producer Σ. These have been analyzed for information about the absorption of the charged primary particles, and the analysis will be called the « absorption-type » analysis. Events with struck counters in AS-tray (i.e., $AS \geqslant 1$) satisfying the condition $(S_1 + S_0 \geqslant 2)$ are regarded as being caused by extensive showers and will be used to correct the apparent rates of local penetrating showers. Showers by μ-mesons and chance coincidences will be considered later.

The symbols P, G and B indicate measurements carried out with paraffin, graphite and no producer, respectively. $H = P - G$ and $C = G - B$ will be treated as the contributions of hydrogen and carbon, respectively, though in these subtractions care must be taken as pointed out in section 4·1.

The barometric coefficients (α) for the counting rates in the cases of P, G and B were calculated by means of the method of least squares, assuming the exponential relationship $R = R_0 \exp[-\alpha(p - p_0)]$, where R is the counting rate at the barometric pressure p, and R_0 is that at the standard pressure p_0 (= 53.0 cm Hg). The values obtained were $\alpha(L.P.S.) = 20 \pm 4\%/\text{cm Hg}$ for local penetrating showers and $\alpha(E.S.) = 21 \pm 7\%/\text{cm Hg}$ for extensive showers. These coefficients were used to normalize the observed rates to those at standard pressure. These values are consistent with the values obtained by many authors.

After this correction, the rates obtained from the individual runs were

tested to see whether they obeyed to Poisson distribution or not. All runs were consistent with the Poisson law, and all the data obtained have been included in the following analysis.

An upper limit for the rate of chance coincidence was estimated from the rate of $[(S_2 \geqslant 1) + (B \geqslant 3)]$ obtained in a preliminary experiment. The expected rate was less than 0.01/hr and so is entirely negligible.

3·1. *Production-Type Analysis.* – The total running times with the paraffin, graphite and no producer were 397.1 h, 379.9 h and 319.8 h, respectively. The rates of local penetrating showers produced in the various producers are shown in Table I, together with the rates of hydrogen showers and carbon showers. The first row, labelled $A=0$, shows those events in which no counter was struck in A-tray, and the second row $A=1$ shows those with only one counter struck and so on. The indicated errors, here, and in the rest of this paper, are standard deviations. H/C, in the seventh column, is the ratio of the rate of hydrogen showers to the rate of carbon showers.

TABLE I. – ($AS = 0$, $S_0+S_1 \geqslant 2$, $S_2 \geqslant 2$, $B \geqslant 3$, *rates per hour*).

	P	G	B	H	C	H/C
$A=0$	3.42 ± 0.10	3.03 ± 0.10	2.00 ± 0.09	0.39 ± 0.15	1.03 ± 0.14	0.38 ± 0.17
$A=1$	2.42 ± 0.09	2.14 ± 0.09	1.52 ± 0.08	0.28 ± 0.13	0.62 ± 0.12	0.45 ± 0.26
$A=2$	0.91 ± 0.06	0.88 ± 0.06	0.81 ± 0.06	0.03 ± 0.08	0.07 ± 0.08	—
$A=3$	0.34 ± 0.04	0.52 ± 0.05	0.39 ± 0.05	-0.18 ± 0.06	0.13 ± 0.07	—
$A=4$	0.33 ± 0.04	0.33 ± 0.05	0.34 ± 0.05	0.00 ± 0.06	-0.01 ± 0.06	—

From Table I it is seen that there is a significant rate of hydrogen showers for the cases $A=0$ and $A=1$, but the rates for $A \geqslant 2$ are essentially zero. The showers in the cases $A=0$ and $A=1$ we interpret as being caused mainly by neutral and charged particles (probably neutrons and protons), respectively.

Two corrections must be applied before stating our final value of H/C. First, there is some probability of an extensive shower missing the tray AS. Secondly, counters in A-tray may sometimes be struck by charged secondaries of local penetrating showers.

As shown in Table II, the rate of showers in which one or more counters are struck in AS-tray is increased by the insertion of the carbon producer, but is not further increased by the hydrogen nuclei in the paraffin producer. This may be interpreted as indicating that the efficiency for the detection of extensive showers is increased by the presence of the paraffin or carbon layers.

It is reasonable that there should be no additional contribution from hydrogen, since the radiation length and critical energy of paraffin are very

little different than those of carbon. The carbon showers the rates for which are given in Table I may have involved, therefore, some extensive showers

TABLE II. – ($AS \geqslant 1$, $S_1 + S_0 \geqslant 2$, *rates per hour*).

	P	G	B	H	C
$A = 0$	1.01 ± 0.07	1.05 ± 0.08	0.66 ± 0.07	-0.04 ± 0.11	0.39 ± 0.11
$A = 1$	1.05 ± 0.07	0.99 ± 0.08	0.77 ± 0.07	0.06 ± 0.11	0.22 ± 0.11
$A \geqslant 2$	6.17 ± 0.19	6.25 ± 0.21	6.06 ± 0.21	-0.08 ± 0.28	0.19 ± 0.30

which missed the AS-tray. Using the rates in extensive showers for carbon for each number of struck counters in AS-tray and calculating the probability of missing them, one obtains corrected values as shown in Table III.

TABLE III. – *Corrected values for AS (rates per hour).*

	H	C	H/C
$A = 0$	0.39 ± 0.15	0.86 ± 0.14	0.45 ± 0.17
$A = 1$	0.28 ± 0.13	0.56 ± 0.12	0.50 ± 0.26
$A = 0$ and $A = 1$	0.67 ± 0.19	1.42 ± 0.17	0.47 ± 0.15

From this table, it seems that if there is a difference in the H/C ratios for neutral and charged primaries, it is not large enough to be apparent in this experiment. Therefore, in dealing with these ratios, we shall use the weighted average shown in the third row of Table III.

According to Table I, it will be noticed that events with ($A \geqslant 2$) occurred only in carbon showers. And these events are probably showers with backward-moving charged secondaries. It is reasonable that there should be more backward-moving particles from carbon than from hydrogen. The rate of these showers in the case of carbon is 0.19 ± 0.12/h and must be added to the rate of carbon showers indicated in the third row of Table III. After such correction, one obtains the following final values:

$$H = 0.67 \pm 0.19/\text{h}$$

$$C = 1.61 \pm 0.22/\text{h}$$

$$H/C = 0.42 \pm 0.16 .$$

These values will be used to obtain cross-sections for nucleon-proton collisions in a later section.

The multiplicity distributions in $S_1 + S_0$-trays for the case of local pene-

trating showers are shown in Fig. 2. Since the statistical accuracy is very poor for each multiplicity, detailed information is lacking. But the ratio of the rate of hydrogen showers with at least three struck counters in S_1+S_0-trays divided by the rate with at least two struck counters in the same tray is almost the same for neutral and charged primary showers. The value of this ratio is about 0.7.

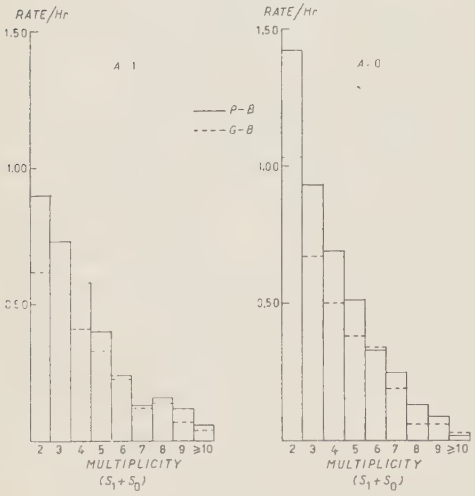

Fig. 2. – Multiplicity Distributions in S_1+S_0-trays in the case of local penetrating showers. The ordinate gives the rate of showers in which n or more counters were struck in S_1+S_0-trays.

3·2. *Absorption-Type Analysis.* – The present experimental procedures were not adequate to obtain an absorption mean free path of primary nucleons in hydrogen and carbon, since an absorber of various thicknesses and a more adequate detector must be used for this purpose. The following analysis has been attempted, however. After correcting for the barometric effect, one obtains the rates $P=1.18\pm0.06$/h, $G=1.35\pm0.07$/h and $B=1.53\pm0.08$/h, for showers satisfying the conditions $A=1$, $S_1=1$ and $S_0=0$.

If λ_H and λ_C represent the absorption mean free paths in hydrogen and carbon, and t_H and t_C the thicknesses of hydrogen in paraffin and carbon in graphite in g/cm², respectively, $P/G=\exp[-t_H/\lambda_H]$ and $G/B=\exp[-t_C/\lambda_C]$. Then, the values $\lambda_H=(15^{+20}_{-6}$ g/cm²), $\lambda_C=(90^{+130}_{-35}$ g/cm²) are obtained.

4. – Results and Discussion.

4·1. *Note on the Subtraction Method* ([8,24]). – The principle of the subtraction method is that the difference of the rates between paraffin and equivalent graphite is regarded as the rate due to hydrogen. But this is only valid in the case of thicknesses which are sufficiently small compared with the interaction mean free path of that material. Otherwise, the difference will not give the correct rate for hydrogen because of the following: (1) in the paraffin layer

---

([24]) Recently, by C. B. A. McCusker (*Zeits. f. Naturf.*, **10**, 238 (1955)) was given the note concerning the increase of multiplicity owing to the secondary interaction in the producer in the case of CH_2-C subtraction method.

a certain fraction of the primary particles are absorbed by hydrogen, and as a result the rate for the carbon in the paraffin is somewhat reduced. This effect acts so as to decrease the apparent rate for hydrogen when the subtraction was made. (2) Moreover, if, as in the present case, the amount of nuclear matter is greater in the paraffin producer than in the carbon producer, secondary interactions will occur with greater probability in the paraffin than in the carbon. Since these secondary interactions increase the multiplicity and the detection probability of the primary event, the apparent rate of H-showers is too large.

These effects will introduce systematic errors in the value of the cross-section and the multiplicity for hydrogen. An estimation of the importance of these effects has been made, with the following assumptions. 1) The interaction mean free paths for carbon and hydrogen are taken as 60 g/cm² and 30 g/cm² respectively for both primary and secondary particles. 2) On the average, four secondary interacting particles are produced in the primary interactions (see Sec. 4'4). 3) The events involving tertiary interactions are negligible.

After a simple calculation one obtains the following probabilities for one incident nucleon to produce various kinds of events. The events in which only a primary interaction occurs and no secondary collision takes place are symbolized by C or H. Events involving secondary interactions are symbolized by two letters. CH, for instance, indicates events in which at least one secondary interaction occurred with hydrogen after a primary interaction with a carbon nucleus.

Paraffin layer		Graphite layer	
C	0.105	C	0.123
H	0.035		
CC	0.053	CC	0.058
CH	0.018		
HC }	0.023		
HH }			

The events actually observed involve the sum of these probabilities each multiplied by certain detection probabilities. Accurate estimation of the detection probabilities is difficult. But a reasonable upper limit for the increase of the detection probability due to secondary production of further charged particles may be made by the following considerations. A primary nucleon of several tens of GeV will produce secondary particles of average several GeV in energy. According to the results of emulsion ([1]) and of Cosmotron experiments ([18-20]), nucleons or pions of these energies are not expected to produce

on the average more than one further charged particle in a secondary interaction. This corresponds to an increase of the number of the charged particles by about 20% for the events involving secondary interactions in the present experiment. Considering that there is a wider spread of angles in the secondary collisions than in the primary interactions it seems reasonable to assume that the increase of detection probability due to secondary interactions is less than 20% of that for primary interactions.

Following these assumptions, one can conclude that the effect of the finite thickness of producers in this experiment may increase the value of H/C by less than 20% and the average multiplicity of H-showers by less than 10%. This deviation does not seem so serious in this experiment comparing with rather large statistical errors.

Therefore, in spite of these effects, the difference (paraffin)-(graphite) may be treated as the rate for hydrogen in the following discussions without explicit corrections for them.

4·2. *Nature and Energy of the Primary Particles.* – It is well known that the primary particles which produce local penetrating showers at mountain altitudes consist mainly of high-energy nucleons. According to COCCONI's result ([25]), one can expect that the electromagnetic interactions of high-energy μ-mesons in the producing layers contribute to recorded events by less than a few percent of the local penetrating showers in this experiment. However, there is a possibility that the knock-on showers from hydrogen cause a similar increase in the rate of showers in paraffin, and it is necessary to confirm that such an effect is really negligible. There is no such contamination in showers of neutral primaries, but a further examination was carried out for the cases of showers having charged primaries. Secondary particles of cascade showers are absorbed much more rapidly than those of the penetrating showers. Therefore, if such an effect is important, it should be indicated by the multiplicity distribution in C-tray. In the multiplicity distribution of C-tray, however, there is no significant difference between the charged-primary showers ($A=1$) and the neutral primary showers ($A=0$) in the case of paraffin and carbon. Moreover, the ratios H/C in showers having charged primaries are, within the experimental errors, the same for both small and high multiplicity in C-tray. The situation is the same whether $B \leqslant C$ or $B > C$. Hence the primary particles of the showers in the present experiment have been taken to be nucleons (protons and neutrons).

It is necessary to estimate the energy of the primary nucleons which triggered the present arrangement. In most cosmic-ray experiments, not only is the incident energy continuous, but also the triggering efficiency varies with

([25]) G. COCCONI: *Phys. Rev.*, **76**, 984 (1949).

energy. Direct determination of the energy is very difficult. But according to the following argument, the energy has been tentatively estimated. For this estimation carbon showers have been used, since the cross-section is well known and the statistical accuracy is better. It would be desirable, of course, to establish that the energies of the hydrogen and carbon showers are not different. In the present results, the average multiplicities measured in B- and C-trays were almost the same for paraffin and carbon showers, and the values of the ratio H/C are equal for both low and high multiplicity as measured by the sum of struck counters in B- and C-trays. This sum gives a scale of the shower size and hence a measure of the energy of shower. So, there may be no difference between the energies of hydrogen and carbon showers.

(i) *Estimation by observed rate.* – The detection probability was approximated by a step function which is zero under the threshold energy E_0 and is equal to a constant value, p, for energies above E_0. A conventional power law spectrum as assumed by various authors has been adopted for the integral flux of protons. After the necessary corrections have been made, one finds the following values for E_0. The cross-section for carbon has been assumed to be 320 millibarns or geometric.

E_0 60 GeV $p = 1$ } $f(\geqslant E) = 4 \cdot 10^{-5}(10/E)^{1.3}$ cm^{-2} sterad^{-1} s^{-1} ([26])
35 GeV $p = \frac{1}{2}$ } E = energy in GeV, at 694 g/cm^2.

20 GeV $p = 1$ } $f(\geqslant E) = 1.1 \cdot 10^{-5}(10/E)^{1.8}$ cm^{-2} sterad^{-1} s^{-1} ([27])
14 GeV $p = \frac{1}{2}$ } E = energy in GeV, at 730 g/cm^2.

The probability p may be considerably smaller than one for the present apparatus, and it is reasonable to assume it to be about $\frac{1}{2}$ from geometrical consideration and the triggering requirements. The probability, p, is, of course, a smooth function in reality.

(ii) *Estimation in comparison with emulsion data.* – The present triggering arrangement demands at least three charged particles of energy greater than 350 MeV. According to the results of the Bristol group ([1]), the primary nucleon energy is greater than 25 GeV under these conditions. The average multiplicity as measured in the trays N_1–N_6 for charged-primary showers from carbon is 5.9 from the present results. This value is a lower limit of true multiplicity,

---

([26]) R. W. Williams: Private Communication to Prof. W. L. Kraushaar.

([27]) J. G. Wilson: *Progress in Cosmic Ray Physics*, I (1952). Value obtained by W. E. Hazen.

and the Bristol emulsion studies [1] imply an energy of about 20 GeV as a probable lower limit.

These estimates of the energy are consistent with an isotropic distribution in center-of-mass system for 30 GeV primary particle. This is discussed forth in Sec. 4·4.

It may be concluded from the above that the primary particles of the showers measured are mostly protons and neutrons and their energies average about 30 GeV but extend from perhaps 10 GeV to several tens of GeV. Our value is consistent with McCUSKER's value [4] deduced for similar experimental arrangement.

4·3. *Cross-Section for Meson Production from Hydrogen and Carbon.* – The ratio H/C and the absorption mean free path introduced in Sec. 3 are intimately connected with the various processes of nuclear interactions in the collisions of nucleons.

The values of H/C for these cases in which $S_1+S_0 \geqslant 2$ can be used to obtain a cross-section for meson production in nucleon-proton interactions by assuming a value for the cross-section for meson production in nucleon-carbon collision. But one must be careful in examining the various corrections. One correction is that arising from secondary interactions in the producting material and this was described in detail in Sec. 4·1. Another correction arises from the following cases. That is, a primary particle makes knock-on electrons at the producer and a shower at the material between S_1- and S_2-trays, so that the appearance of the picture looks as a penetrating shower made at the producer. In a preliminary test, the percentage of knock-on electrons from the paraffin and carbon producers was examined using μ-mesons. The effect on the value of H/C was found to be not too serious, and amounts to less than 10 %. Therefore, considering the rather large statistical errors in the value of H/C, these two corrections do not substantially change the value of the cross-section. Many authors have found the cross-section for penetrating-shower production in nucleon-carbon collisions to be about the geometrical value (about 320 mb $= \pi r_0^2 A^{\frac{2}{3}}$, $r_0 = 1.4 \cdot 10^{-13}$ cm) in the cosmic-ray energy region ([1,26]). Thus, the cross-section for high-energy nucleons to produce penetrating showers with at least two secondaries by nucleon-proton collision is $67 + 25$ mb. One cannot separate experimentally the fraction of the two-prong showers that were caused by elastic scattering. But according to Fermi's theory of meson production, the elastic-scattering contribution to the two-prong showers in p-p collisions should be only about 0.02 % at 30 GeV ([28,29]). Therefore, it

---

([28]) E. FERMI: *Progr. Theor. Phys.*, **5**, 570 (1951); *Phys. Rev.*, **81**, 684 (1951); **92**, 452 (1953).

([29]) Y. P. KWON and Y. KAKUDO: *Progr. Theor. Phys.* (to be published).

may be reasonable to assume that the cross-section mentioned above gives the cross-section for meson production in nucleon-proton collisions. This experimental value of the cross-section may be somewhat too small because particles ejected at wide angles may have missed the apparatus.

In p-p collisions, showers with at least three struck counters indicate the multiple production of at least two mesons. In n-p collisions, on the other hand, three-prong showers can result from the production of just one meson, but this process, according to Fermi's theory, has a relative probability of only 1.5% at 30 GeV ([28,29]). Hence, the showers with $(S_1 + S_0 \geqslant 3)$ may be regarded as cases of multiple meson production. As shown in Sec. 3, the rate for $(S_1+S_0)\geqslant 3)$ divided by the rate for $(S_1+S_0 \geqslant 2)$ is about 0.7 and it may be concluded, considering the fact that some cases of multiple production are included among the 2-prong showers, that the cross-section for multiple meson production is 70% or more of the total cross-section for meson production.

Values of the so-called reaction cross-sections may be obtained from the absorption mean free paths given in Sec. 3. The reaction cross-section presumably has about the same meaning as the production cross-section mentioned above. The statistical accuracy is very poor in the present analysis and several further corrections should be applied. The mean free path, λ_C, is consistent with many previous results ([1]). The cross-section, σ_H, for proton-proton collisions is equal to 108 ± 65 mb, and is not inconsistent with the production cross-section obtained above, considering very large errors.

Hence, it may be concluded that at about 30 GeV meson production and the multiple meson production occur rather frequently in nucleon-proton collisions and the total meson-production cross-section is almost equal to the geometrical value of 60 mb $(= \pi r_0^2,\ r_0 = 1.4 \cdot 10^{-13}$ cm).

4·4. *Character of H- and C- showers.*

a) Multiplicities. – The observed multiplicity distribution has been shown in Sec. 3, Fig. 2. The average multiplicities of secondary charged particles for *H*- and *C*-showers as measured by S_1+S_0 are as follows.

	H	*C*
$A = 0$	4.2 ± 0.8	4.6 ± 0.2
$A = 1$	5.1 ± 0.9	5.9 ± 0.3

The multiplicity for charged-primary showers is perhaps somewhat greater than that for neutral-primary showers. This excess may be reasonably interpreted as being due to the charge of the incident nucleon.

The multiplicity of *C*-showers appears to be slightly higher than that of

H-showers, though the difference does not exceed the limit of errors. This could be a consequence of secondary collisions occurring in the carbon nucleus.

It is interesting to estimate the average multiplicity of all pions (charged and neutral) in H-showers. Assuming that the average number of protons is about 0.5 in the case of neutral-primary showers and is about 1.5 in the case of charged-primary showers, and that neutral-pion to charged-pion production ratio is $\frac{1}{2}$, the average number of pions produced turns out to be about 5.4. This value of the average multiplicity is in general agreement with Fermi's statistical theory ([28]).

There is a tendency for the observed multiplicities to be too small, because some of the charged particles emitted at wide angles are probably missed, and moreover, the finite geometrical resolution may have the effect of decreasing the multiplicity. On the other hand, there are some effects tending to increase the multiplicity. These effects are 1) knock-on electrons accompanying charged secondaries, 2) neutral pions which are materialized inside the producers or in the walls of the counters and 3) the secondary interactions in the producer. However, these effects were found to be negligible using simple estimations based upon the results of a preliminary experiment and the fact mentioned in Sec. 4·1.

b) Neutral pions. – To get some information about the production of neutral pions, the materializing layer of 1 cm lead and 0.5 cm iron between trays S_1 and S_2 was removed for a while in the course of the experiment. The average multiplicities as measured by S_2 with and without the layer between S_1 and S_2 are given below. The difference in the measured multiplicities gives an indication of the contribution of neutral pions.

	H		C	
	$A = 0$	$A = 1$	$A = 0$	$A = 1$
with layer	4.2 ± 0.6	4.9 ± 0.8	4.9 ± 0.2	5.7 ± 0.3
without layer . .	2.1 ± 2.3	3.5 ± 2.5	2.9 ± 0.6	4.6 ± 0.9

Because of the short interval of the experiment without the layer, the large statistical uncertainties do not allow one to draw any quantitative conclusion. However, a considerable amount of neutral-pion contribution is recognized, and the above values are not inconsistent with the value of 0.5 for the ratio of neutral to charged pions.

c) Angular distribution. – It is very difficult to obtain the angular distribution of the secondary particles from the pattern of struck counters in a hodoscope experiment. This difficulty is due to following ambiguities:

i) The shower axis cannot be determined exactly. This ambiguity is more serious in showers having neutral primaries. ii) The angular resolution is insufficient, and particles emitted in wide angles are occasionally missed.

In spite of these difficulties, however, it is interesting and desirable to study angular distribution of secondary particles in H-showers as a characteristic feature of multiple production of mesons at these high energies.

The position of the shower axis is tentatively assumed to be the « centre-of-mass » of the struck counters in the multiplicity trays (S_1 + S_0) in each event. Angles are related to the distances between the struck counters and the position of the axis. The angular distributions so obtained for C- and H-showers are shown in Figs. 3 and 4 respectively. The abscissa shows the number of counters representing the above mentioned distance. The area is normalized so as to give the average multiplicity given in Sec. 4·4*a*.

The distributions for C-showers for neutral and charged primaries are the same well within the statistical errors, and moreover, they are in good agreement with the assumption of 30 GeV energy and an isotropic distribution of secondary particles in the centre-of-mass frame of two nucleons.

On the other hand, there seems to be a difference between the distributions for H-showers for neutral and charged primaries, though the statistical accuracy is much worse in this case than that of C-showers. The distribution for charged primaries has a rather sharp peak near to the axis which is not seen in the distribution for neutral primaries, and the latter shows rather flat distribution near the centre. Moreover, this difference between the angular distribution of H-showers for neutral and charged primaries appears in the two-prong showers, but the existence of such difference in the cases of more

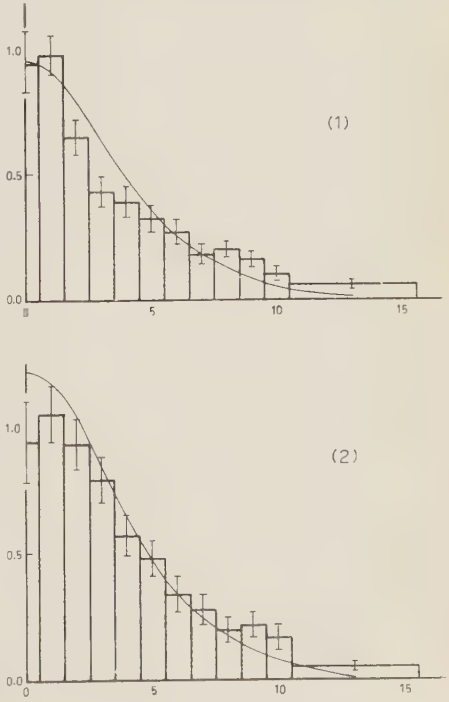

Fig. 3. – Angular Distribution of secondary charged particles of C-showers observed in S_1+S_0-trays, 1) for neutral primary and 2) for charged primary. The ordinates show the number of charged particles per shower, and the abscissae are the distance in terms of the number of counters from the axis of the shower. The solid curves show the distribution expected at 30 GeV energy on the assumption of isotropic distribution of secondary particles in C. M. system of two nucleons, and are normalized to the average multiplicities given in Sec. 4·4*a*.

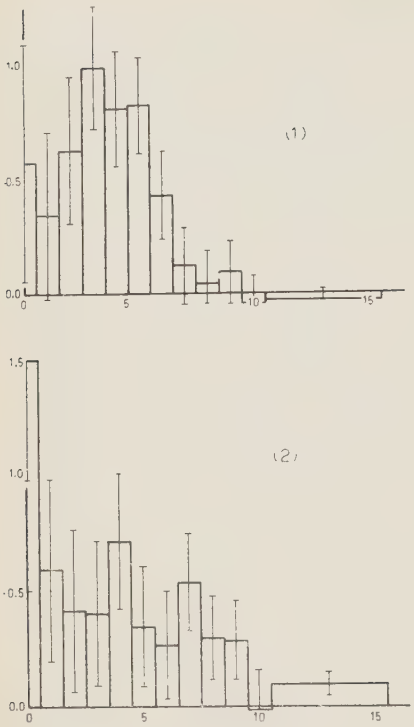

Fig. 4. – Angular Distribution of secondary charged particles of H-showers observed in S_1+S_0-trays, 1) for neutral primary and 2) for charged primary. The ordinates show the number of charged particles per shower, and the abscissae are the distance in terms of the number of counters from the axis of the shower.

than two prongs has remained uncertain because of decreasing statistical accuracy.

The above mentioned difference between the distributions of H-showers for neutral and charged primaries may be interpreted phenomenologically to show that the colliding nucleons in the centre-of-mass system are emitted into forward and backward narrow cones, incident nucleon into the forward cone and target nucleon into backward cone, at least in the case of small multiplicity. Then, in the case of incident protons, a sharp peak near the axis will be observed in the laboratory system. An incident neutron, on the other hand, if it is emitted into a forward cone, and unless charge exchange takes place, consequently causes a deficiency of charged particles near the axis in the laboratory frame ([18-20]).

A difference was noted in the average multiplicity for H-showers produced by neutral and charged primaries in Sec. **4**·4*a*, and this difference appears to be consistent with the above interpretation.

As to the angular distribution of pions, the large statistical uncertainty does not allow any detailed conclusion to be drawn, except that the observed distributions for H-showers are not inconsistent with the assumption of an isotropic distribution of pions in the centre-of-mass system both in n-p and p-p collisions.

d) Ratio of protons to neutrons. – The effective area of counters in tray A was a little less than the area of the producers, hence there is some probability of charged primaries missing tray A. After correcting for the area effect, one obtains for the value of the ratio of protons to neutrons 1.4 ± 0.5 for C-showers at these energies. Moreover, the maximum correction of 20 % for backward-moving shower particles leads to the value of about 1.2. This value, though the statistical accuracy is poor, is consistent with the values of other experiments at these high energies.

4·5. *Comparison with Previous Experiments and Theory.* – Penetrating showers from hydrogen have been investigated by many authors using the subtraction method in production-type experiments. But there is some inconsistency in their results. WALKER *et al.* ([11]), WATAGHIN *et al.* ([2,3,6,7]), MIURA *et al.* ([9]), SCHULTZ ([5]) and CERVASI *et al.* ([8]) have interpreted their results as indicating multiple production of mesons in the cosmic-ray-energy region. On the other hand, the results of MCCUSKER and his co-workers ([14]) have been interpreted as showing infrequent occurrence of multiple production at 30 GeV. Furthermore, WATAGHIN and his collaborators ([6,7]) have shown that there is a large difference in the rate of penetrating showers for n-p and p-p collisions. However, the absence of neutral pions among the possible secondary particles which can trigger the apparatus and the difference, if present, in the angular distribution of the secondary charged particles between n-p and p-p collisions can cause such apparent discrepancies in the shower features and conclusions drawn from them, considering the coincidence requirements and the geometrical resolving power of multiplicity measurement. Therefore, the conclusions of MCCUSKER *et al.* and of. WATAGHIN *et al.* seem to be rather premature even from a purely experimental point of view, and the present results support the conclusions of MIURA *et al.* and the recent results by CERVASI and co-workers. The small differences between their results and ours, for example the nature of the angular distributions and the value of the cross-section, are probably understandable, considering the statistical accuracy and the differences in arrangements and methods of triggering.

The absorption mean free path in hydrogen has been measured at cosmic-ray energies ([15-17]), by comparing the absorption in hydrogenous material to that in non-hydrogenous material. Previous results have shown smaller cross-sections than the value obtained from the present analysis. It is probably possible to interpret these inconsistencies also being due to biases which were introduced by the arrangements and triggering requirements, as mentioned in connection with the production-type analysis.

A tentative comparison of the multiplicity distribution in the present experiment with that given by Fermi's theory ([28]) and assuming charge independence ([29]) shows rather good agreement. But statistical accuracy is poor, and no decisive conclusion can be drawn at the present time.

The theoretical consideration of WILLIAMS ([26]) (*) lead to a value for the total cross-section of nucleon-nucleon collisions at about 30 GeV of $120 \cdot {}^{30}_{20}$ mb. Comparison with the present results must be reserved, until further experiments give the cross-section for elastic part of the nuclear interaction and the missed parts of meson production in present experiment.

(*) We should like to thank to Professor W. L. KRAUSHAAR who has kindly informed us of the private communication from Professor R. W. WILLIAMS.

5. – Conclusions.

The statistical accuracy is rather poor in this experiment, and decisive conclusions are to be reserved in some parts of the present results; the obtained results at 30 GeV are as follows:

1) The cross-section for the production of penetrating showers with at least two charged secondaries is 67 ± 25 mb, and the cross-section for at least three charged secondaries is about 70%. The former, for the most part, may give the total cross-section for meson production and the latter gives a minimum value of the cross-section for multiple meson production. This value of the cross-section is consistent with that obtained from the absorption mean free path of protons. Therefore, the cross-section for nuclear interaction between nucleons is about the geometrical value ($\pi r_0^2 = 60$ mb, $r_0 = 1.4 \cdot 10^{-13}$ cm).

2) There is no substantial difference between n-p and p-p collisions for the cross-sections.

3) The angular distribution of the secondaries in p-p interactions seems to have a sharp forward peak compared to the distribution observed for n-p interactions. This tendency may be interpreted as indicating a mechanism in which the incident nucleon is scattered into a rather sharp forward cone at least in the case of small multiplicity and the produced pions are distributed rather isotropically in the centre-of-mass system.

A similar experiment with a multiplate cloud chamber which contains paraffin, carbon and lead is in preparation, and it is hoped to obtain more quantitative and less ambiguous results.

* * *

The experiment discussed in this paper was performed at Mt. Norikura Inter-University Cosmic-Ray Laboratory. The paraffin, graphite and lead were supplied from the same agency. The authors gratefully acknowledge valuable discussions with members of research group for multiple meson production in Japan. Also, the authors are greatly indebted to Professor W. L. KRAUSHAAR, who has read this article and has given us valuable advices, and to Dr. M. OKAMOTO for his valuable advices for statistical treatment of data. This work was partly financed by the Ministry of Education in Japan under the Fundamental Scientific Research Expenditure, 1954.

RIASSUNTO (*)

Col metodo di sottrazione $CH_2 - C$ si sono studiati in alta montagna per mezzo di un odoscopio di contatori gli sciami penetranti generati in idrogeno e in carbonio. La sezione d'urto per la produzione di mesoni in carbonio è risultata 67 ± 25 mb e quella per produzione multipla appare essere almeno il 70 % di quel valore. Non si è osservata alcuna differenza fra le sezioni d'urto per collisioni p-p e n-p. La distribuzione angolare dei secondari carichi degli sciami sembra mostrare un picco in avanti per le collisioni p-p e tale tendenza si può interpretare supponendo che il nucleone incidente sia emesso in un cono anteriore alquanto serrato nel sistema del baricentro almeno quando la molteplicità è bassa.

(*) *Traduzione a cura della Redazione.*

Disintegrazioni nucleari di alta energia.

M. Baldo-Ceolin e B. Sechi

Istituto di Fisica dell'Università - Padova
Istituto Nazionale di Fisica Nucleare - Sezione di Padova

(ricevuto il 12 Settembre 1955)

Riassunto. — Sono state studiate le distribuzioni e le correlazioni angolari e le distribuzioni energetiche delle particelle cariche emesse in disintegrazioni in cui ci sia stata produzione di mesoni. È stata osservata una diminuzione dell'anisotropia della distribuzione angolare rispetto a stelle di energia più bassa, inoltre si è trovato che le correlazioni a grandi angoli (120°-180°) sono più frequenti di quanto previsto, e che le distribuzioni energetiche presentano una brusca discontinuità per energie dell'ordine di 100 MeV. Si è cercato di interpretare questi effetti come dovuti ad interazioni secondarie dei mesoni con i nucleoni dei nuclei in cui sono stati creati.

L'interazione dei nucleoni con i nuclei si può descrivere, in buon accordo con i fatti sperimentali, usando il modello della cascata nucleonica ([1,2]), fino a quando non si abbia nel nucleo produzione di mesoni, cioè sino a che gli urti tra i nucleoni siano elastici. Quando l'energia del nucleone incidente aumenta, la produzione di mesoni diventa il fenomeno dominante, e si può pensare che le caratteristiche delle stelle di alta energia siano essenzialmente condizionate dai processi cui i mesoni danno luogo. Abbiamo appunto selezionato delle disintegrazioni prodotte dalla radiazione cosmica in lastre nucleari, nelle quali siano stati generati mesoni, e attraverso misure di distribuzioni e correlazioni angolari e distribuzioni energetiche, ci siamo proposti di studiare come e in quali processi in particolare influiscano le interazioni dei mesoni creati nel nucleo.

([1]) M. L. Goldberger: *Phys. Rev.*, **74**, 1269 (1948).
([2]) G. Bernardini, E. T. Booth e S. J. Lindenbaum: *Phys. Rev.*, **88**, 1017 (1952).

1. – Scelta degli eventi e risultati sperimentali.

Per questa ricerca abbiamo usato lastre nucleari Ilford G5 di 600 μm di spessore, esposte alla radiazione cosmica a 27000 m di altitudine, durante uno dei voli effettuati in Sardegna nell'estate del 1952. Su un totale di 2000 stelle di disintegrazione osservate, abbiamo selezionato dapprima 150 stelle, delle quali 90 con primario (P o π) e 60 con primario N, imponendo come sola condizione che ciascuna di esse avesse almeno due rami al minimo di ionizzazione nell'emisfero inferiore, formanti un angolo abbastanza stretto tra di loro ($< 30°$) e vicino a 180° con la direzione del primario, quando questo ci fosse; questo per assicurarci che l'evento fosse di energia sufficientemente alta.

Abbiamo scelto di preferenza stelle situate nel centro dell'emulsione; come al solito, i rami delle stelle sono stati catalogati come neri, quando $I/I_0 > 5.5$; grigi, quando $1.5 \leqslant I/I_0 \leqslant 5.5$ e di sciame quando $I/I_0 < 1.5$.

Di ogni traccia abbiamo misurato la ionizzazione specifica I/I_0, l'angolo con la verticale o con la direzione del primario della proiezione della traccia nel piano dell'emulsione, e l'angolo di inclinazione della traccia rispetto a questo piano, in modo da potere determinare l'angolo vero θ di ogni traccia rispetto al primario o alla verticale.

Per le tracce definite come nere e grigie abbiamo poi determinato la frequenza degli angoli compresi tra ciascuna traccia e la traccia della particella primaria. Gli istogrammi *a*) della fig. 1 e della fig. 2, danno rispettivamente le distribuzioni angolari $P(\theta)$ rispetto al primario, per le tracce nere e grigie. I dati riportati in fig. 1 e 2 sono stati normalizzati per rappresentare il numero di tracce per unità di angolo solido.

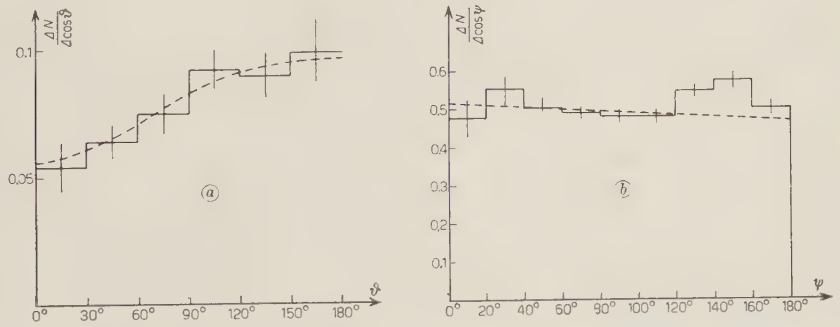

Fig. 1. – L'istogramma *a*) rappresenta le distribuzioni angolari delle tracce nere rispetto al primario, l'istogramma *b*) rappresenta le correlazioni angolari tra tutte le tracce nere. Gli errori segnati danno il solo errore statistico.

Si è quindi cercato di approssimare i detti istogrammi con funzioni del tipo:

$$f(\theta)\,\mathrm{d}\theta = (A + B\cos\theta + C\cos^2\theta)\,\mathrm{d}\theta\,, \tag{1}$$

con i coefficienti A, B e C opportunamente normalizzati (curva tratteggiata negli istogrammi).

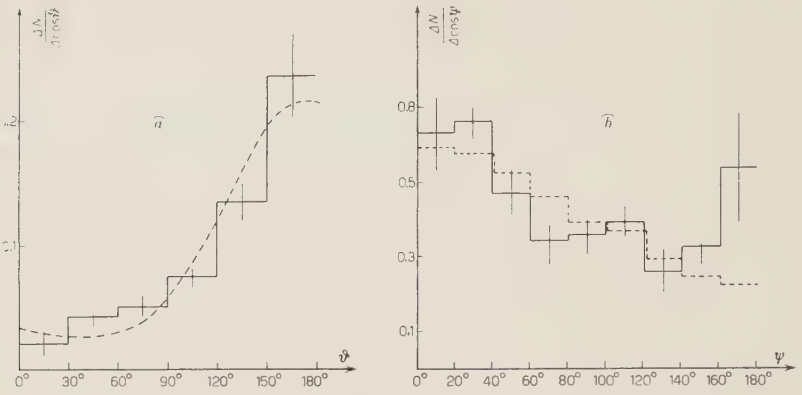

Fig. 2. - L'istogramma *a*) rappresenta le distribuzioni angolari delle tracce grigie rispetto al primario, l'istogramma *b*) rappresenta le correlazioni angolari tra tutte le tracce grigie. Gli errori segnati danno il solo errore statistico.

La probabilità che due tracce di una stella formino tra di loro un angolo compreso da ψ e $\psi+\mathrm{d}\psi$, nell'ipotesi di eventi non correlati intrinsecamente, e tenendo conto dell'anisotropia, $f(\theta)$, presente nelle distribuzioni, è allora data dall'espressione:

$$(2) \qquad P(\psi)\,\mathrm{d}\Omega = \frac{\mathrm{d}\Omega}{4\pi}\int_0^{\pi} \sin\theta f(\theta)\,\mathrm{d}\theta \int_0^{2\pi} f(\cos\theta\cos\psi + \sin\theta\cos\psi'\sin\psi)\,\mathrm{d}\psi\,.$$

Abbiamo quindi paragonato le correlazioni sperimentali (numero di tracce formanti tra loro un angolo dato) per i rami neri e grigi (istogrammi *b*) delle figg. 1 e 2) con quelle prevedibili teoricamente (curve tratteggiate) dalla formula (2).

Abbiamo inoltre calcolato la distribuzione energetica dei rami grigi di 300 stelle, che rispondevano alle caratteristiche imposte, considerando tutte le tracce come dovute a protoni e calcolandone l'energia con misure di ionizzazione. Misure di scattering fatte su 300 tracce grigie indicano che la percentuale di deutoni, tritoni e particelle α è molto bassa (vedi anche [3]). Abbiamo scartato inoltre tutte le tracce inclinate nell'emulsione di più di 30°, il che ci ha permesso di ottenere una maggiore lunghezza per le tracce e quindi un errore minore del 5 % nel conteggio dei grani. Per le basse energie la curva è

---

[3] U. Camerini, P. H. Fowler, W. O. Lock e H. Muirhade: *Phil. Mag.*, **41**, 413 (1952).

stata costruita in base al numero di rami che sono stati definiti come neri. Nella fig. 3 è dato l'istogramma complessivo ottenuto.

Questo presenta un gradino sui 100 MeV, e sembra indicare un massimo tra i 70 e i 100 MeV, effetto già riscontrato da BELLIBONI e VITALE [4] in categorie di stelle analoghe alle nostre. Ora noi pensiamo che, probabilmente, al disotto dei 70 MeV le misure di ionizzazione (il minimo delle nostre lastre è di 14 grani 50 μm) non siano più molto sensibili e vi sia un notevole fattore di perdita, che fa sì che molte tracce che sono grigie vengano contate come nere. Questa ipotesi è confortata del resto da alcune misure fatte su lastre « stripped » (dove l'energia di ogni traccia è quasi sempre esattamente definibile), in stelle analoghe alle nostre, e dove abbiamo ritrovato soltanto la discontinuità nella zona dei 100 MeV e non il minimo sui 60 MeV. D'altronde il tentativo fatto da BELLIBONI e VITALE di spiegare tale minimo, ha dato risultati negativi. Per tale ragione cercheremo in seguito di interpretare l'effetto osservato piuttosto come una rapida variazione nelle distribuzioni energetiche intorno ai 100 MeV, che come un massimo tra i 70 e i 100 MeV, o una lacuna intorno ai 60 MeV.

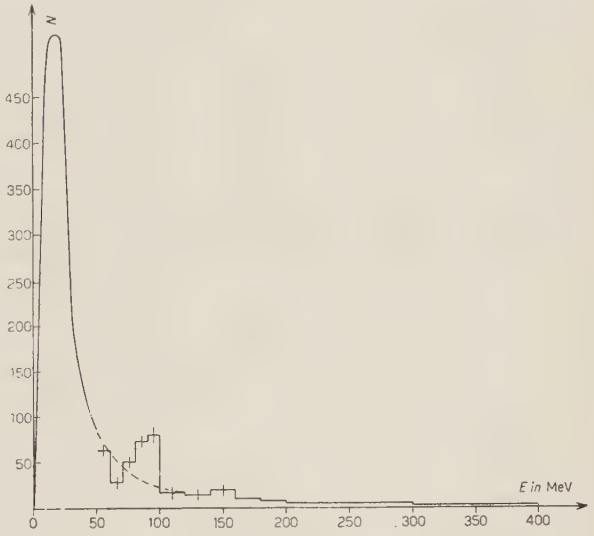

Fig. 3. – Distribuzione energetica delle tracce grigie.

2. – Discussione.

L'analisi dei dati sperimentali riguardanti le distribuzioni e le correlazioni angolari, porta a postulare il riassorbimento nucleare di mesoni lenti, prodotti nell'interazione primaria che dà origine all'evento. Nella fig. 1 infatti si nota nelle distribuzioni che il rapporto avanti-indietro $\simeq 1.32$ è minore di quello che si trova per le stelle il cui primario abbia energia più bassa [2] e [5]. Tale abbassamento dell'anisotropia si può interpretare come dovuto, almeno in

[4] G. BELLIBONI e B. VITALE: *Nuovo Cimento*, **11**, 372 (1954).
[5] G. C. MORRISON, M. MUIRHEAD e W. G. ROSSEN: *Phil. Mag.*, **44**, 1326 (1953).

parte, al fatto che, ai tre noti fenomeni: evaporazione, emissione diretta, ed eventualmente evaporazione locale [6], dei quali il primo porta ad una distribuzione angolare isotropa dei rami delle stelle, mentre gli altri ad una collimazione in avanti, si sovrapponga per le stelle del rango energetico considerato anche un parziale riassorbimento dei mesoni prodotti nell'interazione primaria, che tende ad accentuare l'isotropia della distribuzione angolare: infatti l'assorbimento di ogni mesone dà luogo all'emissione di due nucleoni (o conseguenti cascatelle nucleoniche) opposti l'uno all'altro, ma senza nessun orientamento privilegiato rispetto al primario. Inoltre l'andamento delle correlazioni angolari (fig. 1*b*, 2*b*) che a grandi angoli sono lievemente più frequanti di quanto previsto dalla curva da noi calcolata, si può spiegare con lo stesso effetto, in quanto un mesone riassorbito nel nucleo da una coppia P-N [7] genera due nucleoni di direzione iniziale opposta, e si può pensare che i rami neri derivanti risentano di questa correlazione iniziale.

Nella fig. 2*b* poi, l'eccesso di correlazioni per angoli prossimi a 180° è più notevole, e come già rilevato da Ceccarelli e Zorn [8] si può interpretare nel modo più plausibile attribuendolo a coppie di nucleoni che emergono dal riassorbimento di mesoni.

L'ipotesi del riassorbimento mesonico non è più sufficiente però a spiegare l'andamento delle distribuzioni energetiche. Abbiamo pensato di interpretarlo come dovuto, almeno in parte, allo scattering dei mesoni con i nucleoni del nucleo. Questo ci è suggerito in primo luogo dall'andamento delle sezioni d'urto per scattering dei pioni contro i nucleoni [9], che presenta un massimo per energie cinetiche del mesone incidente dell'ordine di 180 MeV, massimo che è particolarmente accentuato per l'urto $\pi^+ + P$, per il quale la sezione d'urto a 180 MeV diventa circa tripla di quella geometrica. Inoltre le sezioni d'urto differenziali danno in prevalenza diffusione all'indietro, così che una notevole parte dell'energia del pione viene ceduta al nucleone.

Questo ci porta a prevedere che i mesoni creati nel nucleo con energie sui 180 MeV avranno un libero cammino medio di scattering nettamente minore degli altri, e inoltre, per la sezione d'urto prevalentemente all'indietro, cederanno spesso gran parte della loro energia al nucleone colpito (sull'ordine dei 100 MeV).

In base a questa idea abbiamo fatto col metodo di « Monte Carlo » 500 estrazioni per ottenere il probabile andamento, in funzione dell'energia, dei protoni emessi dal nucleo dopo aver subìto un urto $\pi^+ + P \rightarrow \pi^+ + P$, limitandoci a questo solo caso dal quale ci si può attendere l'effetto maggiore.

---

(6) A. Kind: *Nuovo Cimento*, **10**, 176 (1953).
(7) G. Puppi, V. De Sabbata e E. Manaresi: *Nuovo Cimento*, **9**, 726 (1952).
(8) M. Ceccarelli e G. T. Zorn: *Nuovo Cimento*, **10**, 540 (1953).
(9) M. Anderson, E. Fermi, R. Martin e D. Neagle: *Phys. Rev.*, **91**, 155 (1953).

Abbiamo usato per il nucleo il modello statistico a particelle indipendenti con una energia massima per nucleoni di 22 MeV. Assumendo come spettro di produzione dei mesoni nel nucleo una funzione costante per energie comprese tra 100 e 300 MeV, intervallo nel quale la sezione d'urto per lo scattering $\pi^- + P \to \pi^- + P$ ha i valori più alti, abbiamo descritto le loro interazioni con i protoni, nel nucleo, sulla base dei dati sperimentali ora noti [10] e nell'ipotesi che lo scattering dei pioni con nucleoni nella materia nucleare segua le stesse modalità di quello dei pioni contro nucleoni liberi [11,12].

I protoni che dopo questa interazione giungono alla superficie del nucleo hanno una probabilità di uscire che dipende dalla loro energia e dalla loro direzione. Tale probabilità è stata da noi calcolata ammettendo per la buca di potenziale la dipendenza dall'energia data da TAYLOR [13] ed usando il coefficiente di trasmissione classico già usato da KIND e PATERGNANI [14].

L'istogramma della fig. 4 riporta i risultati ottenuti: come si vede si ha nello spettro dei protoni uscenti una notevole variazione nella zona intorno ai 100 MeV. I rapporti delle aree danno infatti 1:2.48:5.2:2.8 rispettivamente per i protoni di energia compresa tra 150 e 200, 100 e 150, 50 e 100, 0 e 50 MeV di energia cinetica; rapporti che verrebbero variati a tutto favore dei pro-

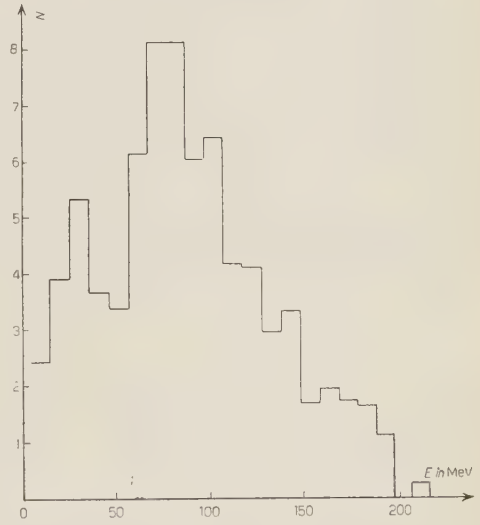

Fig. 4. – Distribuzione energetica, ottenuta col « Monte Carlo », dei protoni emessi dai nuclei dopo avervi subito un urto $\pi^+ + P \to \pi^+ + P$, i rapporti delle aree danno 1:2.48:5.2:2.8 rispettivamente per protoni di energia compresa tra 150 e 200, 100 e 150, 50 e 100, 0 e 50 MeV di energia cinetica.

---

(10) J. ASHKIN, J. P. BLASER, F. FEINER, J. G. CORMAN e M. O. STERN: *Phys. Rev.*, **96**, 1104 (1954); R. A. GRANDEY e A. F. CLARCK: *Phys. Rev.*, **94**, 766 (1954); G. HOMA, G. GOLDHABER e L. M. LEDERMAN: *Phys. Rev.*, **93**, 554 (1954); W. B. FOWLER, R. M. LEA, W. D. SHEPHARD, R. P. SHUTT, A. M. THORNIDIKE e W. L. WHITTEMORE: *Phys. Rev.*, **92**, 832 (1953).

(11) A. MINGUZZI, G. PUPPI e A. RANZI: *Nuovo Cimento*, **11**, 697 (1954).

(12) G. COSTA e G. LANZA: in corso di pubblicazione sul *Nuovo Cimento*.

(13) T. B. TAYLOR: *Phys. Rev.*, **92**, 831 (1953).

(14) A. KIND e G. PATERGNANI: *Nuovo Cimento*, **10**, 1357 (1953).

toni con energia tra 50 e 100 MeV, qualora si usasse uno spettro mesonico plausibile (vedi, per esempio, CINI e WATAGHIN [15]) anzichè ammettere, come abbiamo fatto noi, che il numero dei mesoni sia indipendente dall'energia.

Una trattazione completa richiederebbe che a tali effetti si sovrapponessero pure i contributi dovuti alle reazioni $\pi^+ + N \to \pi^0 + P$ e $\pi^- + P \to \pi^- + P$, naturalmente meno importanti. Pensiamo comunque che l'andamento dell'istogramma di fig. 3 nella zona sui 100 MeV sia almeno in parte, attribuibile all'effetto ora descritto.

Le seguenti considerazioni, di carattere puramente qualitativo, ci portano a convalidare ulteriormente la nostra ipotesi.

a) Notiamo che se confrontiamo lo spettro energerico che si ottiene scegliendo da una parte solo i dati delle stelle con $N_s > 6$, e dall'altra quelli delle stelle con $N_s = 2, 3$, la variazione sui 100 MeV è meno sensibile nel primo caso. Possiamo forse attribuire questo al fatto che le stelle con $N_s > 6$ sono per lo più generate da primari di energia più elevata di quelle con $N_s = 2, 3$, per cui lo spettro dei mesoni in esse prodotti sarà in generale più energico, ed in esso i mesoni della banda di $180 \div 200$ MeV saranno rappresentati con una percentuale meno importante.

b) Inoltre, poichè il libero cammino medio di scattering dei mesoni di 180 MeV è nettamente inferiore a quello di mesoni di altre energie è probabile che nei casi in cui tali mesoni sono prodotti con maggiore frequenza, il numero di scattering sia maggiore e quindi la stella abbia un maggior numero di rami. Selezionando infatti le stelle con molti rami, troviamo che nello spettro energetico dei loro rami neri e grigi, l'anomalia sui 100 MeV è accentuata.

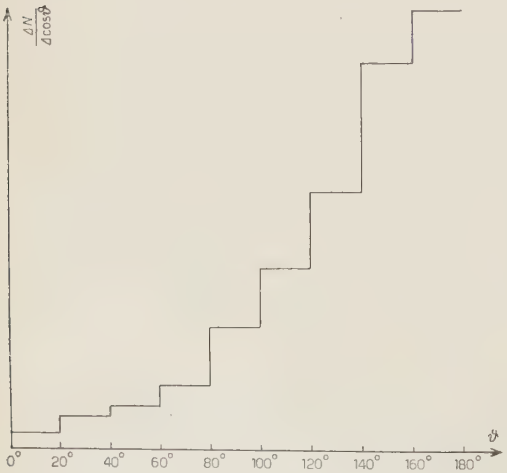

Fig. 5. – Distribuzioni angolari dei protoni emessi dai nuclei dopo un urto $\pi^+ + P \to \pi^+ + P$, quale si ottiene dai « Monte Carlo ».

c) Infine poichè i mesoni prodotti nel sistema del laboratorio sono collimati in avanti ed i loro scattering avvengono prevalentemente all'indietro, è plausibile ammettere che i nucleoni di rinculo di tali scattering siano collimati in avanti e che quindi presentino tra loro correlazioni

[15] M. CINI e G. WATAGHIN: *Nuovo Cimento*, **7**, 135 (1950).

angolari ad angoli piccoli. La fig. 5 mostra la distribuzione angolare dei protoni dopo l'urto $\pi^+ + P \rightarrow \pi^+ + P$, quale si ottiene dal « Monte Carlo » in cui si è supposto che i π^+ siano diretti secondo la verticale). La fig. 6 riporta l'andamento delle correlazioni angolari dei soli rami grigi con energia minore di 100 MeV. Si nota una correlazione per piccoli angoli, che si potrebbe spiegare con il suddetto effetto e che si ritrova anche sull'istogramma di fig. 2

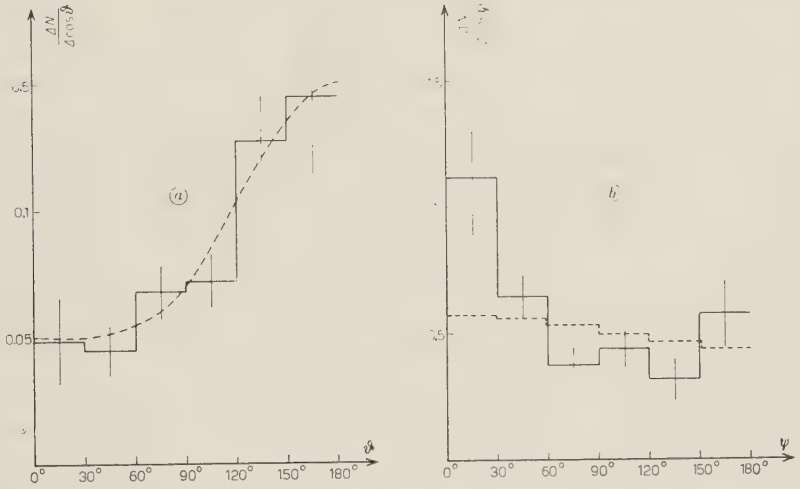

Fig. 6. – Distribuzioni e correlazioni angolari delle tracce grigie con energia compresa tra 50 e 100 MeV.

ottenuto per tutti i rami grigi, dal quale però scompare quando si ricalcolino distribuzioni e correlazioni angolari per i soli rami grigi con energia maggiore di 100 MeV. Nella fig. 6 si nota pure una correlazione per grandi angoli: è probabile che essa si debba alle coppie dei nucleoni derivanti dal riassorbimento dei mesoni.

3. – Conclusione.

I dati precedenti e le interpretazioni di essi hanno, a nostro parere, solo un valore indicativo, che potrebbe venire precisato e confermato da misure più precise e statistiche più abbondanti, e da calcoli più dettagliati e completi. Essi nondimeno lasciano sin d'ora vedere come le particolarità ricavate dalle distribuzioni angolari e dagli spettri energetici dei rami neri e grigi delle stelle si prestino da un lato ad essere interpretati mediante i dati sempre più precisi che si vanno raccogliendo nella fisica dei mesoni, e dall'altro, possano servire da indicatore per scrutare in modo più dettagliato le modalità del complesso fenomeno costituito dalle stelle di alta energia.

* * *

Desideriamo ringraziare vivamente il Prof. N. DALLAPORTA che ci ha suggerito il lavoro e ne ha seguito lo svolgimento, e i professori G. PUPPI e A. KIND per le utili discussioni.

SUMMARY

The scope of this paper is to study nuclear disintegrations produced by high energy primaries ($E_p \gtrsim 5$ GeV), and to show how and in what manner the mesons created in the nucleus can influence the interaction. We have studied disintegrations produced in nuclear emulsions, exposed to the cosmic radiation at an altitude of 27 km. The ionization of the tracks, their energy distribution, their angular distributions and angular correlations, have been analized for 150 stars. Some phenomena such as the anomalous angular distribution of black tracks, i.e. the decrease of angular anisotropy with increasing energy of the nuclear disintegration, and the excess of angles near 180° between black and grey tracks, have been interpreted as due to the reabsorption of π-mesons in the nucleus. The curve for the energy distribution of the grey prongs shows a step for energies below 100 MeV, which can be interpreted as been due to the scattering of π-mesons in nuclear matter. We have been led to this hypothesis by considering that the cross-section for scattering of pions in nuclei, shows a maximum for a kinetic energy of the incident mesons of about 180 MeV, and that the differential cross-section gives a prevalently backward scattering. This leads us to predict that mesons created in the nucleus with energies of about 180 MeV will have much shorter scattering mean free path than other mesons, and that they will more frequently yield a large part of their energy to the recoil nucleon. These views have been checked by 500 « Monte Carlo » extractions to obtain the energy distribution curve of the protons emitted by the nucleus after a collision $\pi^+ + P \rightarrow \pi^+ + P$. The spectrum which is thus obtained shows a marked variation in the region of 100 MeV.

Sulla produzione di mesoni π nei nuclei pesanti ad opera di primari nucleonici energici.

G. Costa e G. Lanza (*)

Istituto di Fisica dell'Università - Padova
Istituto Nazionale di Fisica Nucleare - Sezione di Padova

(ricevuto il 12 Settembre 1955)

Riassunto. — È stata studiata la produzione dei mesoni π in Al, Ag e Pb, assumendo il modello nucleare a particelle indipendenti e trattando le vicende dei mesoni nei nuclei come una successione di urti singoli, dall'atto della loro creazione, in un punto qualunque di un nucleo, fino alla loro fuoruscita od al loro assorbimento. In ciò ci siamo serviti delle sezioni d'urto di scattering, totali e differenziali, ricavate, in parte, direttamente dai risultati delle grandi macchine e, in parte, dedotte mediante il principio dell'indipendenza dalla carica delle forze nucleari e il metodo del bilancio dettagliato; la scarsità di dati precisi sulla sezione d'urto di assorbimento ci ha indotto ad assumere per essa tre curve diverse. Data la complessità dei fenomeni, il problema è stato trattato col metodo di Montecarlo; per ogni tipo di assorbimento assunto, sono state costruite due serie di modelli tridimensionali, rispettivamente per mesoni con energia iniziale di 100 e di 200 MeV (energia all'atto della creazione nell'interno del nucleo). La mancanza di indicazioni precise sullo spettro di produzione dei mesoni π, rende i risultati (che andrebbero mediati su di esso) non direttamente confrontabili con i dati sperimentali, eccetto quelli che si trovano essere abbastanza indipendenti dall'energia iniziale: ciò accade per le sezioni d'urto di produzione dei π in funzione del numero atomico, che hanno tutte un andamento crescente, con tendenza alla saturazione, e per le distribuzioni angolari, che presentano due massimi, uno in avanti ed uno intorno a 100, 120 gradi. Nessuno di questi risultati sembra dipendere sensibilmente dal tipo di assorbimento assunto.

La produzione di mesoni π in diversi elementi pesanti da parte di primari nucleonici della radiazione cosmica a quota di alta montagna è stata speri-

(*) Attualmente presso il Massachusetts Institute of Technology, Cambridge, Mass.

mentalmente studiata da vari autori [1-3] con la tecnica delle lastre nucleari, per quanto riguarda sia la distribuzione angolare dei mesoni prodotti, sia la variazione del coefficiente di produzione in funzione del numero atomico dell'elemento. In queste esperienze, le lastre nucleari venivano in parte esposte sotto determinati spessori di diversi assorbitori e in parte, per confronto, anche libere; i risultati ottenuti, che si possono certamente considerare come indicativi del fenomeno, sono nondimeno difficilmente interpretabili in modo corretto, come rilevano gli stessi autori [3], per le incertezze sul modo di correggere i risultati delle lastre sotto assorbitore dai mesoni di fondo, ottenuti colle lastre libere di confronto. D'altronde, la complessità dei processi prevedibili per i mesoni prodotti in un urto nucleone-nucleone nell'interno di un nucleo pesante, sulla base della fenomenologia di queste particelle, quale ora risulta dalle dirette misure di scattering compiute con le grandi macchine, non lascia facilmente prevedere a priori quali possano essere le caratteristiche dei mesoni emergenti da un nucleo pesante, cosicchè mancano anche gli orientamenti teorici che possano servire da guida nell'interpretazione delle esperienze.

È per tale ragione che non ci è sembrato inutile cercare di prevedere l'andamento da attendersi per gli spettri angolari, energetici ed i numeri relativi dei mesoni prodotti in urti nucleonici, che emergono da un nucleo pesante. A tale scopo, abbiamo cercato di seguire con maggior dettaglio l'idea prospettata in uno dei suddetti lavori [3], consistente nel trattare le vicende dei mesoni nei nuclei come una successione di urti singoli, dall'atto della loro nascita in un urto nucleone-nucleone nell'interno del nucleo, attraverso i possibili scattering e cambiamenti di carica da essi subiti negli urti con gli altri nucleoni, fino alla loro fuoruscita od al loro assorbimento ad opera di una coppia di nucleoni. Un tale trattamento è giustificato dal fatto che, alle energie considerate, la lunghezza d'onda di de Broglie, anche per i mesoni π, è piccola rispetto alle dimensioni del nucleo; esso richiede, per poterlo applicare, anche la conoscenza delle sezioni d'urto di scattering con e senza cambio di carica e di assorbimento dei mesoni π di vario segno. I dati relativi allo scattering si possono in buona parte desumere dai risultati sperimentali diretti, ricavati dalle grandi macchine, e dedurre i rimanenti dall'ipotesi dell'indipendenza dalla carica delle forze nucleari e dal principio del bilancio dettagliato. Indicazioni assai meno precise vi sono invece sull'assorbimento dei mesoni π da coppie di nucleoni e, per tale ragione, ci è sembrato opportuno considerare tale fenomeno come un parametro da far variare entro limiti ragionevoli, in

---

[1] U. Camerini, H. Muirhead, C. F. Powell e D. M. Ritson: *Nature*, **162**, 433 (1948).

[2] N. Dallaporta, M. Merlin, O. Pierucci e A. Rostagni: *Nuovo Cimento*, **9**, 202 (1952).

[3] A. Bonetti, N. Dallaporta, M. Merlin e G. Dascola: *Nuovo Cimento*, **10**, 215 (1953).

modo da vedere come esso influisca sui risultati finali. In quanto al modello nucleare, l'ipotesi più semplice consiste nel rappresenatre i nucleoni nel nucleo come un gas di Fermi contenuto in una opportuna buca di potenziale.

Data la complessità dell'insieme dei fenomeni che si debbono considerare, è ovvio che una trattazione analitica, per essere possibile, richiederebbe tali semplificazioni da rendere assai dubbi i risultati a cui potrebbe condurre. Per tale ragione l'unico metodo adatto ci è sembrato quello di Montecarlo.

I risultati che così si possono ottenere non sono ancora confrontabili, almeno in dettaglio, con i dati sperimentali. Sarebbe infatti necessario, dopo aver eseguito il Montecarlo con mesoni di diversa energia iniziale, pesare tali risultati con un opportuno spettro di produzione dei mesoni stessi. Ora ben poco si sa di preciso su un tale spettro di produzione, specie nel caso dei raggi cosmici, sicchè crediamo inutile tentare di eseguire, allo stato attuale, quest'ultima fase del lavoro, che condurrebbe a risultati alquanto dubbi. Preferiamo, quindi limitarci a studiare l'andamento degli spettri ottenuti con mesoni monoenergetici, che potranno servire, in seguito, a trattare il problema completo, e ci accontentiamo per ora di deduzioni indicative in base ad essi, nei casi in cui i risultati prevedibili non siano dipendenti in modo sensibile dallo spettro ignoto di produzione.

In quanto segue, elencheremo anzitutto i dati essenziali posti alla base del lavoro: 1) le sezioni d'urto di scattering assunte; 2) le diverse ipotesi sulle sezioni d'urto di assorbimento; 3) il modello nucleare; 4) il procedimento del Montecarlo; esporremo quindi: 5) i risultati ottenuti per mesoni π prodotti in un punto generico del nucleo con una data energia, risultati che, combinati con uno spettro di produzione assunto per i mesoni π, dovrebbero permettere di prevedere le distribuzioni dei mesoni π prodotti nei vari nuclei.

1. – Sezioni d'urto di scattering.

I dati sperimentali, che abbiamo usato per le sezioni d'urto totali e differenziali, sono quelli ottenuti con le grandi macchine da vari autori ([4,5]), nelle esperienze di diffusione di mesoni π carichi contro idrogeno.

Ci siamo limitati a studiare il comportamento dei mesoni di energia non

---

([4]) H. L. Anderson, E. Fermi, D. E. Nagle *et al.*: *Phys. Rev.*, **85**, 934 (1952), **86**, 413, 603 (1952); P. J. Isaacs, A. M. Sachs e J. Steinberger: *Phys. Rev.*, **85**, 803 (1952); S. W. Barnes, D. L. Clark, J. P. Perry e C. A. Angell: *Phys. Rev.*, **87**, 669 (1952); J. Ashkin, J. P. Blaser, F. Feiner, J. G. Gornan e M. O. Stern: *Phys. Rev.*, **96**, 1105 (1954).

([5]) H. L. Anderson, E. Fermi, D. E. Nagle, A. Lundby e B. G. Yodh: *Phys. Rev.*, **85**, 935 (1952); P. Isaacs, A. M. Sachs e J. Steinberger: *Phys. Rev.*, **85**, 718

superiore ai 200 MeV. Le sezioni d'urto totali, nell'intervallo energetico compreso tra circa 20 e 200 MeV (energia del mesone nel sistema del laboratorio), per i tre processi:

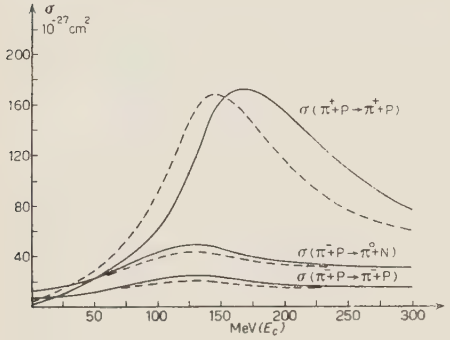

Fig. 1. – Sezioni d'urto totali di scattering relative ai processi (1), (2), (3). Le curve continue si riferiscono alle sezioni d'urto nel sistema del laboratorio, quelle tratteggiate alle sezioni d'urto mediate sulla distribuzione degli impulsi dei nucleoni.

$$(1) \qquad \pi^+ + \mathrm{P} \to \pi^+ + \mathrm{P}$$

$$(2) \qquad \pi^- + \mathrm{P} \to \pi^- + \mathrm{P}$$

$$(3) \qquad \pi^- + \mathrm{P} \to \pi^0 + \mathrm{N}$$

sono ormai ben note (4); il loro andamento, in funzione dell'energia del mesone incidente, è rappresentato nella fig. 1 (curva a tratto continuo).

Per ricavare le sezioni d'urto relative agli altri processi di scattering, che possono aver luogo nel nucleo, abbiamo usato, com'è già stato detto, il principio dell'indipendenza dalla carica delle forze nucleari (6) e il metodo del bilancio dettagliato (7). Riportiamo nella Tab. I i valori assunti per le sezioni d'urto dei vari processi, in funzione di quelle relative ai processi (1), (2), (3) che indichiamo, per semplicità, con σ_1, σ_2, σ_3.

Tabella I.

Processi	Sezioni d'urto
$\pi^- + \mathrm{N} \to \pi^- + \mathrm{N}$	σ_1
$\pi^+ + \mathrm{N} \to \pi^+ + \mathrm{N}$	σ_2
$\pi^+ + \mathrm{N} \to \pi^0 + \mathrm{P}$	σ_3
$\pi^0 + \mathrm{P} \to \pi^+ + \mathrm{N}$	σ_3
$\pi^0 + \mathrm{N} \to \pi^- + \mathrm{P}$	σ_3
$\pi^0 + \mathrm{N} \to \pi^0 + \mathrm{N}$	$2\sigma_3$
$\pi^0 + \mathrm{P} \to \pi^0 + \mathrm{P}$	$2\sigma_3$

(1952); H. L. Anderson, E. Fermi, D. E. Nagle e G. B. Yodh: *Phys. Rev.*, **86**, 793 (1952); J. P. Perry e C. E. Angell: *Phys. Rev.*, **91**, 1289 (1953); H. L. Anderson, E. Fermi, R. Martin e D. E. Nagle: *Phys. Rev.*, **91**, 155 (1953); E. Fermi, M. Glickman, R. Martin, D. E. Nagle: *Phys. Rev.*, **92**, 161 (1953).

(6) J. M. Luttinger: *Phys. Rev.*, **86**, 571 (1952).

(7) J. M. Blatt e V. F. Weisskopf: *Theoretical Nuclear Physics* (New York, 1952), p. 600.

Per quanto riguarda le sezioni d'urto differenziali, la schematizzazione del problema risulta assai meno semplice. Infatti, le misure di queste sezioni d'urto per i tre processi (1), (2), (3), compiute a varie energie ([5]), mostrano come il loro andamento vari con l'energia in modo abbastanza sensibile: la loro pratica utilizzazione per il Montecarlo rende, d'altronde, difficile tener conto di tali variazioni in funzione dell'energia del mesone urtante. Per tale ragione, è stato creduto sufficiente adottare per l'andamento delle sezioni d'urto dei processi (1), (2), (3) (e di conseguenza, degli altri processi, in base alla Tab. I), un certo andamento medio corrispondente approssimativamente ad una energia del mesone urtante di 100 MeV. Esse sono rappresentate nella fig. 2, dove sono riferite al sistema del baricentro.

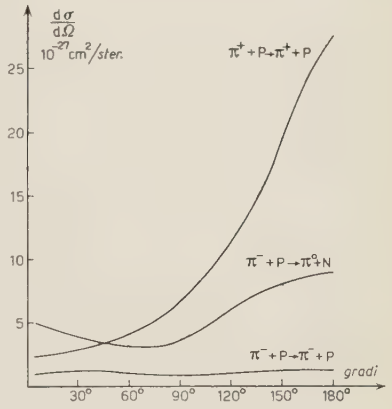

Fig. 2. – Sezioni d'urto differenziali di scattering relative ai processi (1), (2), (3) nel sistema del baricentro.

Per la curva relativa al processo (1), oltre ai risultati di FERMI e collaboratori, abbiamo tenuto conto di dati forniti da PUPPI e da GOLDHABER ([8]), che indicavano una diffusione preponderantemente all'indietro (*).

2. – Sezioni d'urto di assorbimento.

Non vi sono ancora indicazioni precise sull'assorbimento dei mesoni π negli urti con coppie di nucleoni: questo ci ha indotto a compiere vari tentativi, assumendo diversi andamenti per la sezione d'urto di assorbimento, indipendenti dalla carica dei mesoni.

Abbiamo dapprima considerato l'andamento proposto da CHESTON ([9]), secondo il quale l'assorbimento decresce rapidamente all'aumentare dell'energia del mesone; abbiamo normalizzato la curva con due valori diversi, in modo da studiare i due casi di assorbimento relativamente forte e debole: precisa-

([8]) Comunicazioni private.

(*) Dati più recenti (H. BETHE, F. DE HOFFMNAN, N. METROPOLIS, e E. ALEI: *Phys. Rev.*, **95**, 1589 (1954)) indicano che la sezione d'urto differenziale di scattering dei π^+ su protoni risale per piccoli angoli: pensiamo che ciò non porterebbe variazioni apprezzabili nei nostri risultati poichè, a causa del fattore di angolo solido $\sin\vartheta\,d\vartheta$, per cui vanno moltiplicate le sezioni d'urto differenziali, la probabilità di una diffusione in avanti è sempre abbastanza piccola.

([9]) W. B. CHESTON: *Phys. Rev.*, **83**, 1118 (1951).

mente abbiamo assunto per il libero cammino medio di assorbimento a 100 MeV (energia del mesone nel sistema del laboratorio) rispettivamente i valori 10^{-12} cm e $2.8 \cdot 10^{-12}$ cm. Indicheremo nel seguito le due sezioni d'urto di assorbimento per questi due casi con A e B.

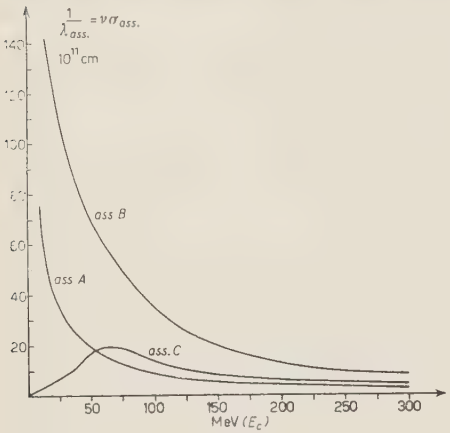

Fig. 3. – Sezioni d'urto di assorbimento.

Indicazioni alquanto diverse si hanno invece dai dati sperimentali riguardanti l'assorbimento dei mesoni π^+ in berillio ([10]), secondo i quali questo aumenterebbe inizialmente con l'energia; tale andamento, che non è in disaccordo con quello della sezione d'urto di assorbimento dei mesoni π^- da parte del deutone ([11]), sembrerebbe indicare, diversamente dal modello da noi usato, un assorbimento da parte di sottostrutture nucleari più complesse; esso è noto inoltre solo per energie inferiori a 50 MeV. Abbiamo voluto tuttavia provare anche tale modello, costruendo una terza curva per la sezione d'urto di assorbimento che indicheremo, nel seguito con C; le tre curve sono riportate nella fig. 3.

3. – Modello nucleare.

Ci siamo basati, per il nostro lavoro, sul modello nucleare a particelle indipendenti, tenendo conto del fatto che la lunghezza d'onda di de Broglie, per un nucleone nel nucleo, ha il valore medio $0.8 \cdot 10^{-13}$ cm, nettamente inferiore al raggio dei nuclei pesanti.

Abbiamo considerato l'interazione nucleone-mesone π come un problema a due corpi di particelle libere; l'azione degli altri nucleoni si esplica, sia sul nucleone urtato, sia sul mesone π, attraverso un potenziale globale. Per il nucleone il nucleo costituisce una buca di potenziale della profondità di circa 30 MeV, e in essa sono disposti, secondo la distribuzione di un gas di Fermi, gli A nucleoni. Anche per i mesoni π il potenziale nucleare è attrattivo, come risulta dalla interferenza coulombiana nello scattering elastico dei π carichi ([12]): i dati sperimentali indicano per esso un valore di circa 20 MeV ([12]), che abbiamo assunto nei nostri calcoli.

([10]) F. H. Tenney e J. Tinlot: *Phys. Rev.*, **93**, 974 (1953).
([11]) R. Durbin, H. Loar e J. Steinberger: *Phys. Rev.*, **84**, 581 (1951).
([12]) H. Byfield, J. Kessler e L. Lederman: *Phys. Rev.*, **86**, 17 (1952).

L'interazione di un mesone π con un nucleo pesante si riduce ad una successione di urti elementari contro i vari nucleoni incontrati lungo la traiettoria, e questa risulta abbastanza ben definita fino a che la lunghezza d'onda λ del mesone si mantiene piccola rispetto alle dimensioni nucleari. Ciò è perfettamente verificato per energie cinetiche dell'ordine di 100 MeV, per le quali λ ha lo stesso valore della lunghezza d'onda dei nucleoni nel nucleo. Per energie più basse, la lunghezza d'onda aumenta, il che implicherebbe anche la possibilità di urti a più corpi; questa, però, viene praticamente annullata dal principio di esclusione: infatti, alle basse energie considerate, è assai improbabile che la poca energia disponibile, divisa tra più di due nucleoni, sia in grado di portarli in livelli situati fuori dalla sfera di Fermi. Per questa ragione, gli urti praticamente possibili anche alle basse energie sono quelli a due corpi e il fatto che anche questi vengano in parte proibiti, ha l'effetto di allungare il libero cammino medio del mesone. Il suo comportamento è quindi analogo a quello che si ha per energie più elevate e il modello da noi usato risulta giustificato.

4. – Svolgimento del Montecarlo.

Le sezioni d'urto precedentemente descritte sono state mediate sulla distribuzione degli impulsi dei nucleoni nel nucleo, poichè quelle date sperimentalmente si riferiscono a nucleoni fermi (fig. 1: curva tratteggiata); la distribuzione assunta è quella di un gas degenere di Fermi, deformata però in modo da tener conto della diversa probabliità, per l'urto del mesone contro un nucleone, a seconda della direzione relativa delle loro velocità.

Per eseguire il Montecarlo, abbiamo diviso in 360 cellette equiprobabili tale distribuzione deformata; analogamente si sono divise in 36 parti equiprobabili le sezioni d'urto differenziali adoperate; mediante estrazioni casuali [13], si stabilivano, caso per caso, il cammino del mesone tra un urto e l'altro, il tipo di processo subìto e l'angolo di scattering. Possiamo illustrare lo svolgimento del Montecarlo, descrivendo brevemente la costruzione di un modello. Un mesone π viene creato con un dato impulso in un certo punto del nucleo da un nucleone della componente primaria, incidente con direzione fissata Z. Da questo punto esso si fa muovere, prima di interagire con un nucleone, per un tratto estratto tra le parti equiprobabili in cui si è diviso il suo percorso; tale tratto dipende dal libero cammino medio del mesone, calcolato in base alle sezioni d'urto totali di tutti i possibili processi ed alla densità dei nucleoni. La natura del nucleone incontrato e il tipo di interazione sono estratti a sorte;

---

[13] M. G. Kendal: *Tables of random sampling numbers* (Cambridge, 1951).

nel caso di uno scattering si estrae pure l'impulso del nucleone; dopo essere passati al sistema del centro di massa ([14]), per mezzo delle sezioni d'urto differenziali, si estrae l'angolo di scattering. Si ritorna quindi al sistema di riferimento iniziale e, a meno che l'urto non risulti proibito dal principio di esclusione (nel qual caso si fa continuare al mesone il suo cammino nella stessa direzione) si ricomincia la stessa serie di operazioni fino a quando il mesone risulti assorbito, oppure raggiunga la superficie del nucleo.

Per trattare il problema in tre dimensioni, la traiettoria di ogni mesone veniva ricostruita mediante un modello meccanico; inoltre per uno stesso mesone si spostava in tutto il nucleo il punto di origine, pesando i risultati ottenuti in ogni punto col fattore $e^{-z/\lambda}$, rappresentante la probabilità che un nucleone della componente primaria di libero cammino medio λ, interagisca con un altro nucleone del nucleo, dopo aver percorso il cammino z nell'interno di esso.

Costruendo in tal modo varie serie di modelli, abbiamo fatto statistiche separate per mesoni π con energia iniziale di 100 e 200 MeV (energia cinetica posseduta all'atto della creazione nell'interno del nucleo), in nuclei di alluminio, argento e piombo; il lavoro è stato ripetuto con ognuno dei tre tipi di assorbimento adottati.

5. – Esposizione e discussione dei risultati ottenuti.

Riportiamo nelle tabelle II e III, per i vari tipi di assorbimento e per i due valori della energia iniziale (100 e 200 MeV), i risultati ottenuti per le sezioni d'urto di produzione dei mesoni π carichi in nuclei di alluminio, argento e piombo (numeri relativi normalizzati a 100); nelle fig. 4 e 5 è rappresentato il loro andamento in funzione del numero atomico.

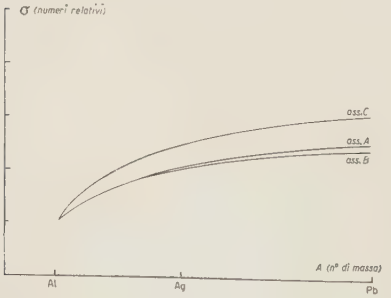

Fig. 4. – Sezioni d'urto di produzione dei π carichi con energia iniziale di 100 MeV.

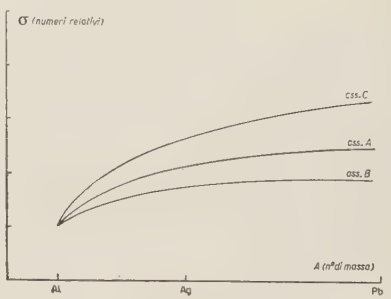

Fig. 5. – Sezioni d'urto di produzione dei π carichi con energia iniziale di 200 MeV.

([14]) A. Gamba e L. A. Radicati: *Nuovo Cimento*, **6**, 374 (1949).

Come si vede, i nostri risultati danno per la sezione d'urto di produzione un andamento abbastanza simile per tutti e tre i tipi di assorbimento, che presenta una tendenza più o meno marcata alla saturazione.

TABELLA II. – *Sezione d'urto di produzione dei π carichi con energia iniziale di* 100 MeV.

Tipo di assorbimento	Elemento		
	Al	Ag	Pb
A	18	37	45
B	18	37	45
C	15	38	47

Nelle fig. 6 e 7 sono riportati gli andamenti degli spettri angolari ed energetici dei mesoni prodotti nei diversi nuclei e con i due valori dell'energia iniziale (100 e 200 MeV).

TABELLA III. – *Sezione d'urto di produzione dei π carichi con energia iniziale di* 200 MeV.

Tipo di assorbimento	Elemento		
	Al	Ag	Pb
A	18	38	44
B	22	38	40
C	13	37	50

Considerando le distribuzioni angolari e tenendo conto delle fluttuazioni statistiche, si vede che esse presentano un andamento abbastanza simile caratterizzato da due massimi principali: uno per angoli molto piccoli ed uno intorno a 100°-120°. Il primo è probabilmente dovuto ai mesoni che escono indeviati dal nucleo, mentre la presenza del secondo si può capire ricordando che le sezioni d'urto differenziali di scattering sono preponderantemente all'indietro. Ora, in generale, è notevole il numero dei π (soprattutto quelli con energia iniziale di 100 MeV) che escono dopo aver subìto un solo scattering e sono appunto questi che hanno maggior probabilità di formare, in media, un angolo con la direzione del primario del valore detto. Tali osservazioni vengono confermate soprattutto dagli spettri angolari dei mesoni di 100 MeV; per quelli

di 200 MeV, si deve pensare che i mesoni uscenti abbiano subìto più scattering e quindi siano orientati in modo più vario: a ciò è dovuta la comparsa, nelle distribuzioni angolari, di altri massimi, accanto ai due principali.

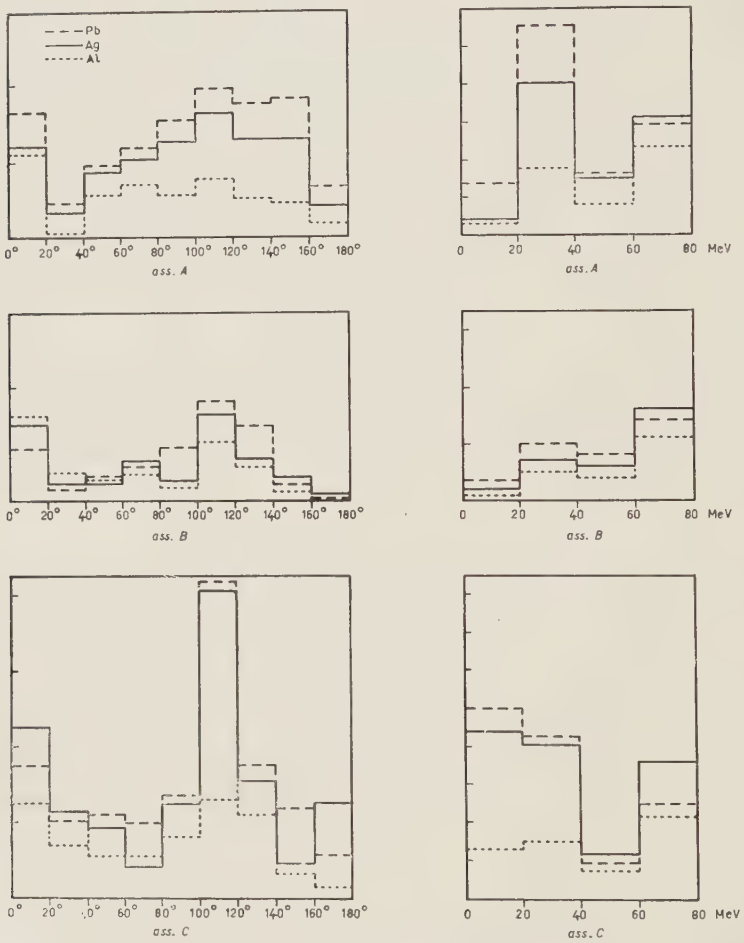

Fig. 6. – Distribuzioni angolari (istogrammi a sinistra) ed energetiche (a destra) dei mesoni π prodotti con energia iniziale di 100 MeV in nuclei di Al, Ag e Pb, per i tre diversi tipi di assorbimento assunti.

Considerando gli spettri energetici relativi ai mesoni con energia iniziale di 100 MeV (80 MeV fuori dal nucleo), si può vedere, nel caso dell'assorbimento *A*, la presenza di un massimo pronunciato a circa 30 MeV e di un altro massimo minore a 80 MeV; essi corrispondono ai due massimi delle distribuzioni angolari: il primo è dovuto a quelli che hanno subìto almeno uno scat-

tering con notevole perdita di energia, avvenendo il più delle volte all'indietro, mentre il secondo si può attribuire ai mesoni che escono indeviati. Per l'assorbimento *B* lo schema interpretativo è lo stesso, salvo che l'importanza dei due massimi s'inverte: dato l'assorbimento notevole per le basse energie, è ora relativamente più importante il numero dei mesoni che escono indeviati. Per

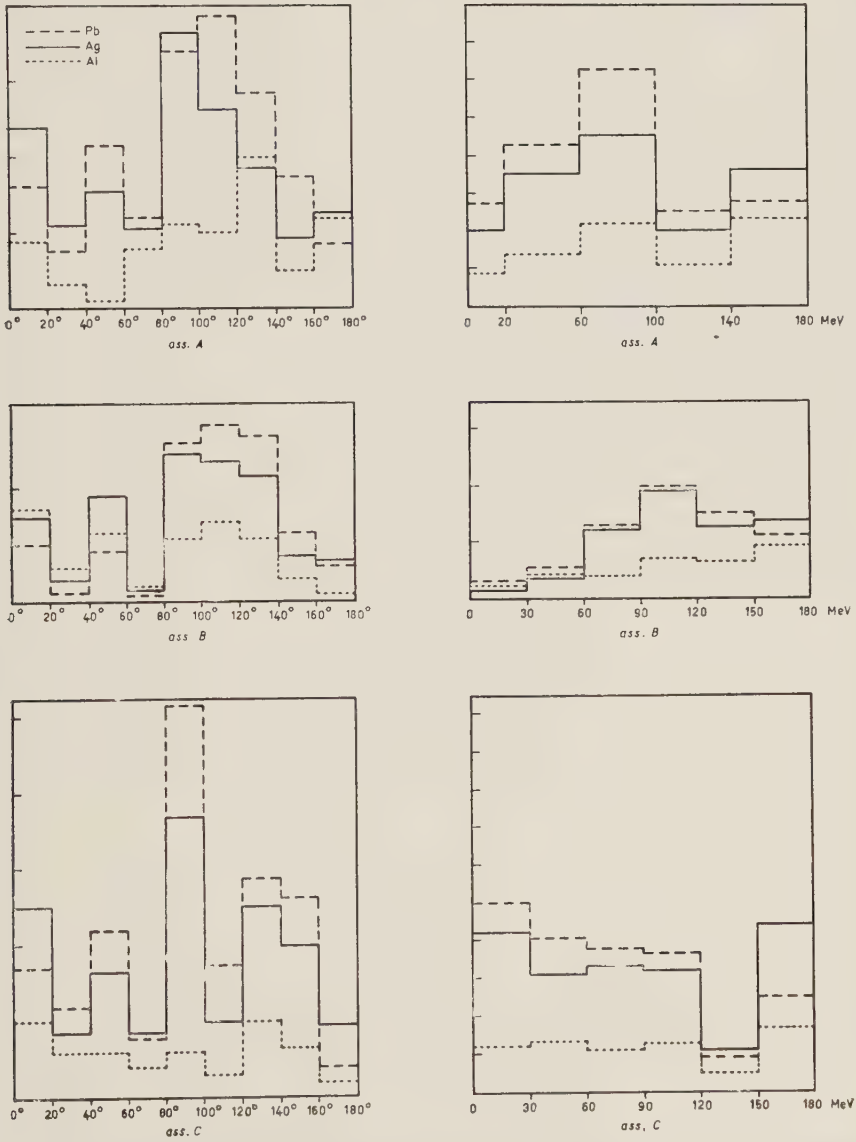

Fig. 7. – Distribuzioni angolari (istogrammi a sinistra) ed energetiche (a destra) dei mesoni π prodotti con energia iniziale di 100 MeV in nuclei di Al, Ag e Pb, per i tre diversi tipi di assorbimento assunti.

l'assorbimento C il primo massimo prevale sul secondo e si estende sino alle energie più basse: ciò dipende dal fatto che al diminuire dell'energia, ad un certo punto, decresce anche l'assorbimento e, quindi, i mesoni poco energici, che hanno subìto più scattering, possono facilmente uscire dal nucleo.

Per i mesoni di 200 MeV (180 MeV fuori dal nucleo), si potrebbero fare considerazioni analoghe, salvo che ora il numero dei mesoni che escono senza subire scattering, rispetto a quelli che ne subiscono, è inferiore al numero corrispondente per i mesoni di 100 MeV.

Come si è già detto all'inizio, dagli spettri così ottenuti non si può direttamente dedurre l'andamento delle curve suscettibili di essere sperimentalmente verificate, se non in quei casi in cui i nostri risultati siano abbastanza indipendenti dall'energia di produzione dei mesoni, in modo che lo spettro di produzione non influisca sensibilmente su di essi. Tale è il caso delle sezioni d'urto di produzione in funzione del numero atomico, per le quali sembra lecito prevedere, in base ai nostri dati, un andamento crescente col numero atomico, che però tende alla saturazione per alti valori di A, ma non è molto sensibile al tipo di assorbimento prescelto. Tale è anche il caso delle distribuzioni angolari, per le quali sembra che si possa prevedere la presenza di un massimo nella direzione in avanti e di un massimo più importante nella zona compresa tra 100 e 120 gradi. Le irregolarità degli spettri energetici dipendono, invece, sensibilmente dall'energia, sicchè sembra probabile che, mediandole con uno spettro di produzione, esse scompaiano e diano luogo ad un andamento in media alquanto regolare. Ora era proprio negli spettri energetici, a differenza di quelli angolari, come ci si può convincere riguardando le fig. 6 e 7, che una certa differenza sembrava manifestarsi in funzione del tipo di assorbimento prescelto. È probabile che il mediare sulle varie energie uniformizzi molto tali andamenti anche sotto tale punto di vista, sicchè, in definitiva, si dovrebbe essere indotti a pensare che nessuno dei fenomeni osservabili, presi qui in considerazione, dovrebbe prestarsi molto come indicatore per distinguere l'andamento della sezione di assorbimento.

* * *

Desideriamo ringraziare vivamente il prof. N. Dallaporta, che ci ha suggerito l'idea del lavoro, per i suoi preziosi consigli e per l'interesse con cui ci ha seguito durante tutto lo svolgimento.

SUMMARY

The production of π-mesons in Al, Ag and Pb has been studied, assuming the independent particles nuclear model, and treating the behavior of the pions in the nuclei, as a succession of single collisions, from their creation, at any point of a nucleus, till their coming out or their absorption. We used, for this, the total and differential scattering cross-sections, partially derived from the big machines data, and partially deduced by the charge independence principle and the detailed balancing method. The scarsity of precise data on the absorption cross-section induced us to assume for it three different curves. Owing to the complexity of the phenomena, we made a Montecarlo calculation, building two series of three-dimensional models, respectively for pions with an initial energy of 100 and of 200 MeV (energy at the creation inside the nucleus). The lack of precise indications on the pion production spectrum, makes our results (which should be averaged over it) not directly comparable with experimental data, except those which are found to be independent enough on the initial energy. This is the case of the total production cross-section of the pions, which increases with the atomic number and shows a tendency to saturation, and of the angular distributions, which indicate a maximum in the foreward direction and another between about 100 and 120 degrees. No one of these results seems to be dependent in a sensible way on the type of assumed absorption.

Urto nucleare elastico di elettroni da 1 MeV in argon.

A. Lovati (*) e C. Succi

Istituto di Scienze Fisiche dell'Università - Milano
Istituto Nazionale di Fisica Nucleare - Sezione di Milano

(ricevuto il 12 Settembre 1955)

Riassunto. — La deflessione nucleare elastica a grande angolo in argon, di elettroni di energia di circa 1 MeV, è stata studiata con una camera a diffusione. Su 11537 tracce di elettroni sono state osservate 739 deflessioni maggiori od uguali a 20°, di cui 56 maggiori di 50°. Nella regione dei grandi angoli, cioè nella regione dove le formule teoriche si differenziano, il valore della sezione totale e la distribuzione angolare delle deflessioni mostrano buon accordo con la formula di Mott.

1. – Introduzione.

1·1. – L'urto nucleare elastico degli elettroni è stato studiato teoricamente per la prima volta da Rutherford [1] dal punto di vista classico e successivamente da Mott [2] dal punto di vista quantistico, facendo uso dell'equazione di Dirac ed assumendo che solo il campo coulombiano del nucleo (considerato puntiforme) interagisca con l'elettrone incidente.

Mott ricavò la probabilità dell'urto elastico sotto forma di una serie di polinomi di Legendre, valida per gli elementi più leggeri; successivamente McKinley e Feshbach [3] svilupparono un metodo che permette di estendere la validità della formula di Mott fino agli elementi con $Z \sim 26$ e di calcolare facilmente le sezioni per l'urto elastico nucleare per deflessioni $> 15°$ con una precisione dell'ordine dell'1 %. La stessa formula è stata recentemente

(*) Attualmente al Gustaf Werner Institute for Nuclear Chemistry, University of Uppsala - Uppsala (Svezia).

(1) E. Rutherford: *Phil, Mag.*, **21**, 669 (1911).

(2) N. F. Mott: *Proc. Roy. Soc.*, A **124**, 425 (1929).

(3) W. A. McKinley jr. e H. Feshbach: *Phys. Rev.*, **74**, 1759 (1948).

ottenuta da DALITZ [4] risolvendo l'equazione di Dirac in seconda approssimazione di Born. Una trattazione teorica dell'argomento è contenuta nel testo di MOTT e MASSEY [5]; gli sviluppi teorici ed i risultati sperimentali più recenti sono raccolti nelle rassegne di BETHE e ASKIN [6] e di CORSON e HANSON [7].

1·2. – La probabilità che un elettrone che si muove con velocità βc in un mezzo di numero atomico Z contenente N nuclei per centimetro cubo, sia deflesso nel percorso di un centimetro, di un angolo compreso tra θ e $\theta + \mathrm{d}\theta$, è espressa dalla formula:

$$P(\theta, \beta)\mathrm{d}\theta = N \cdot f(Z, \beta) \cdot F(\theta, \beta) 2\pi \sin\theta \, \mathrm{d}\theta \, ,$$

con

$$f(Z, \beta) = \left(\frac{Ze^2}{2mc^2}\right)^2 \frac{1-\beta^2}{\beta^4}$$

e

$$F(\theta, \beta) = F_R(\theta) = \mathrm{cosec}^4 \frac{\theta}{2}$$

secondo la formula di Rutherford, e

$$F(\theta, \beta) = F_M(\theta, \beta) = \mathrm{cosec}^4 \frac{\theta}{2} \left[1 - \beta^2 \sin^2 \frac{\theta}{2} + \frac{\pi Z \beta}{137} \sin \frac{\theta}{2} \left(1 - \sin \frac{\theta}{2}\right)\right]$$

secondo la formula di Mott, nell'approssimazione di McKinley e Feshbach (nel seguito la $F_M(\theta, \beta)$ verrà riferita come formula di Mott).

Poichè le sezioni totali secondo RUTHERFORD e secondo MOTT per deflessioni maggiori di 20° non differiscono più di qualche percento è molto difficile, attraverso misure di sezione totale discriminare tra le due formule. L'andamento del rapporto $\mathcal{R} = F_M(\theta, \beta)/F_R(\theta)$ in funzione dell'angolo θ, mostrato in fig. 1 per elettroni da 0.5, 1 ed 1.5 MeV in argon, indica che per decidere tra le due formule è indispensabile sperimen-

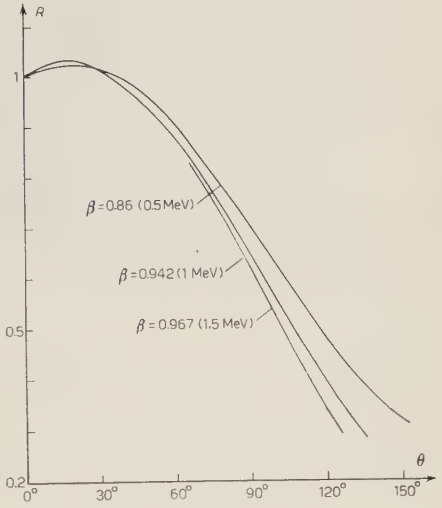

Fig. 1.

(4) R. H. DALITZ: *Proc. Roy. Soc.*, A **206**, 509 (1951).
(5) N. F. MOTT e H. S. W. MASSEY: *The Theory of Atomic Collisions* (Londra, 1949).
(6) H. A. BETHE e J. ASKIN: *Experimental Nuclear Physics*, vol. I (New York, 1953).
(7) D. R. CORSON e A. O. HANSON: *Annual Review of Nuclear Science*, vol. III (Stanford, 1953).

tare ad angoli maggiori di circa 45°. Poichè per deflessioni a grande angolo ed in materiale di basso peso atomico le sezioni d'urto sono estremamente piccole, la sperimentazione risulta particolarmente penosa: i risultati esistenti sono scarsi ed incerti e per conseguenza ci è sembrato interessante effettuare un'ulteriore analisi del problema, utilizzando la tecnica della camera a diffusione che, al pregio di consentire un buon esame dell'evento singolo (comune con la tecnica della camera ad espansione), unisce quello di permettere una rapida raccolta dei fotogrammi.

2. – Misure sperimentali.

2·1. *Il metodo di misura.* – Per poter verificare sperimentalmente la distribuzione $P(\theta, \beta)\mathrm{d}\theta$ con la tecnica della camera a nebbia, si deve determinare:

a) il valore di β per l'elettrone incidente,

b) le deflessioni θ per urto nucleare elastico,

c) la lunghezza totale di traccia.

Per ragioni di rapidità è conveniente evitare la ricostruzione stereoscopica delle tracce ed utilizzare, secondo il metodo suggerito da RANDELS *et al.* [8], il fotogramma ottenuto con la macchina frontale misurando l'angolo Φ, proiezione di θ sul piano della pellicola. O'CEALLAIGH e MAC CARTHAIGH [9] hanno sviluppato un metodo che permette di trasformare la $P(\theta, \beta)$ in una funzione $P(\Phi, \beta)$ dell'angolo proiettato Φ, secondo un'espressione del tipo:

$$P(\Phi, \beta) = N \cdot f(Z, \beta)\psi,$$

dove ψ è una funzione dipendente da $F(\theta, \beta)$, dagli angoli θ e Φ, e dai parametri $\varrho = \lambda_c/2a$ e $k = h/2a$, dove λ_c è la « lunghezza critica » di traccia, $2a$ è l'altezza della zona in cui sono osservate le deflessioni ed h è l'altezza del fascio di elettroni che entrano nella camera nel piano equatoriale della zona di osservazione. Per « lunghezza critica » di traccia si intende la lunghezza minima che la traccia deve possedere prima e dopo la deflessione, perchè la deflessione stessa possa essere presa in considerazione: la convenienza di introdurre una lunghezza critica di traccia è stata discussa da BARKER [10].

2·2. *Le condizioni sperimentali.* – L'esperienza è stata eseguita con una camera a diffusione funzionante a pressione atmosferica posta in campo magne-

---

[8] R. B. RANDELS, K. T. CHAO e H. R. CRANE: *Phys. Rev.*, **68**, 64 (1945).
[9] C. O'CEALLAIGH e M. D. MAC CARTHAIGH: *Proc. Roy. Irish Acad.*, A **50**, 13 (1944).
[10] F. C. BARKER: *Journ. Sci. Instr.*, **25**, 65 (1948).

Fig. 2.

Fig. 3.

tico ([11]). La camera era riempita di argon: la miscela condensante era costituita da alcool metilico e propilico nella proporzione 4 ad 1. Si è valutato che nella zona sensibile il numero di nuclei di idrogeno era circa il 6% del numero totale di nuclei, quelli di carbonio ed ossigeno insieme il 4%.

Gli elettroni provenivano da una sorgente di ^{32}P, di circa 3 microcurie, ed erano immessi nella camera mediante un elettromagnete deflettore, attraverso una finestra chiusa da due sottili fogli di cellophan. L'impulso di comando riduceva la corrente di eccitazione del magnete permettendo agli elettroni di rigidità magnetica $BR \geqslant 3000$ gauss cm di entrare nella camera. Schermi di piombo assicuravano che solo gli elettroni, la cui traiettoria giaceva inizialmente nel piano equatoriale della zona di osservazione, potessero entrare nella camera, realizzando con buona approssimazione la condizione $k = 0$.

Nella zona sensibile della camera il valor medio del campo B era di 300 gauss, con una variazione dal centro ai bordi di circa il 3%.

L'illuminazione era limitata ad una zona di altezza $2a = 3$ cm. Le fotografie erano prese con due macchine fotografiche, una posta frontalmente e l'altra ad un angolo di 25° con l'asse della camera.

In circa 50 ore di funzionamento sono stati raccolti 10000 fotogrammi.

2·3. *L'analisi dei fotogrammi.* – I fotogrammi sono stati analizzati riproiettando le immagini in grandezza naturale: sono state prese in considerazione solo le tracce chiaramente provenienti dalla sorgente e soddisfacenti alle condizioni indicate da RANDELS *et al.* ([8]). Di ogni traccia di lunghezza maggiore di $2\lambda_e = 6$ cm e BR compreso fra 2400 e 7500 gauss cm, veniva misurato il raggio di curvatura e la lunghezza mediante confronto con cerchi di raggio noto e con la circonferenza graduata in centimetri.

Si sono ottenute 11537 tracce, aventi una lunghezza complessiva di 2157 m; una fotografia tipica è mostrata in fig. 2.

La condizione imposta che le tracce deflesse avessero prima e dopo l'urto lunghezza maggiore di 3 cm, richiede che la lunghezza effettiva di ogni traccia sia diminuita di 6 cm. Un'ulteriore riduzione del 10% della lunghezza totale di traccia deve essere applicata per tener conto della presenza del vapore, il cui contributo al numero di deflessioni osservate è praticamente trascurabile.

La lunghezza totale di traccia utilizzabile all'effetto delle misure risulta allora di 1321 m.

Sono state conteggiate 739 deflessioni elastiche con un angolo $\geqslant 20°$, nelle quali la curvatura prima e dopo l'evento, era la stessa (entro il 10% di incertezza) su una lunghezza di almeno 3 cm. Una fotografia che mostra una deflessione con angolo di $\sim 93°$, è riportata in fig. 3.

([11]) A. LOVATI e C. SUCCI: *Nuovo Cimento*, **11**, 163 (1954).

2·4. *Lo spettro degli elettroni analizzati.* – Lo spettro sperimentale degli elettroni presi in considerazione è mostrato in fig. 4. Tale spettro è alterato rispetto a quello vero essenzialmente per due ragioni: 1) la misura di BR è affetta da errore per la disuniformità di B nella zona di osservazione e per l'indeterminazione connessa con il metodo con cui è misurato il raggio di curvatura di ogni singola traccia; 2) la curvatura delle tracce è alterata dalla diffusione multipla coulombiana.

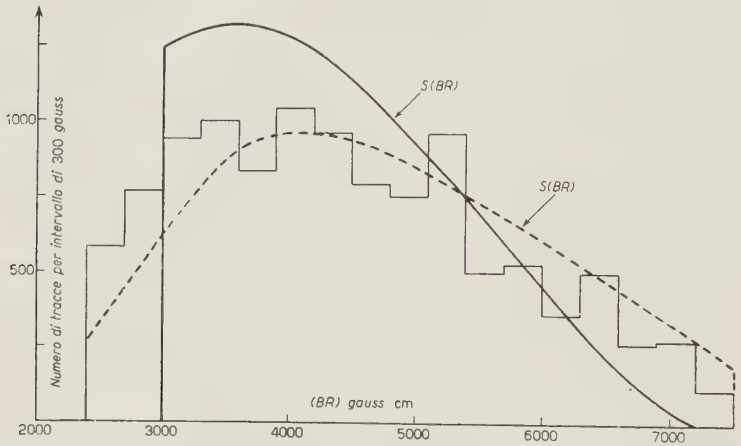

La curva a tratto continuo $S(BR)$ rappresenta lo spettro degli elettroni del ^{32}P. La curva tratteggiata $S(BR)$ rappresenta lo spettro alterato per effetto della diffusione coulombiana.

Fig. 4.

1) I cerchi con cui venivano rilevate le curvature delle tracce sono stati scelti con raggi crescenti di centimetro in centimetro. Nel campo di misura da 2400 a 7500 gauss cm le indeterminazioni per i raggi di curvatura variano dal 12% al 4%. Una maggiore precisione, specie nella regione di bassa energia, sarebbe risultata illusoria a causa della diffusione multipla, che, inoltre, è tale da mascherare completamente le variazioni di curvatura lungo la traccia dovute alla disuniformità del campo magnetico.

2) Per studiare l'effetto della diffusione multipla sullo spettro vero degli elettroni introdotti nella camera, abbiamo calcolato la deformazione che, nelle nostre condizioni sperimentali, viene introdotta nello spettro degli elettroni del radiofosforo ([12]), per $BR \geqslant 3000$ gauss cm.

Secondo Williams ([13]) la diffusione multipla coulombiana altera la traiettoria di un elettrone che si muove con velocità βc in un mezzo di numero

([12]) K. Siegbahn: *Phys. Rev.*, **70**, 127 (1946).
([13]) E. J. Williams: *Phys. Rev.*, **58**, 292 (1940).

atomico Z, contenente N nuclei per centimetro cubo, introducendo una curvatura media apparente $1/\bar{R}_a$. Se $1/R$ è la curvatura dovuta all'effetto di un campo uniforme B, si ha:

$$R_a = A\beta B\bar{R}\,,$$

dove

$$A = t^2 \Big/ \left\{ 2ZeN^{\frac{1}{3}} \left[1.45 + 0.80 \left(7.45 + 2.3 \log_{10} \frac{Z^{\frac{4}{3}}\delta t}{A\beta^2} \right)^{\frac{1}{2}} \right] \right\},$$

essendo δ la densità del mezzo, t la lunghezza della traccia considerata ed A il numero di massa.

La curvatura « vera » $1/\bar{R}$ è allora collegata a quella misurata sperimentalmente dalla relazione:

$$\frac{1}{\bar{R}} = \frac{1}{\bar{R}} \pm \frac{1}{R_a}\,.$$

Nelle condizioni sperimentali realizzate nella presente ricerca e relativamente alla lunghezza media di traccia, risulta $A = 0.012$; essendo β medio uguale a 0.9 e $B = 300$ gauss si ha:

$$\frac{1}{\bar{R}} = \frac{1}{\bar{R}}\,(1 \pm 0.32)\,.$$

Ammettendo che la legge di distribuzione delle curvature sperimentali $1/R$ intorno al valore « vero » $1/\bar{R}$ sia gaussiana, scriviamo:

$$H\left(\frac{1}{R}; \frac{1}{\bar{R}}, \sigma\right) \mathrm{d}\,\frac{1}{R} = \frac{1}{\sqrt{2\pi}\sigma} \exp\left[-\left(\frac{1}{R} - \frac{1}{\bar{R}} \right)^2 \frac{1}{2\sigma^2} \right] \mathrm{d}\,\frac{1}{R}$$

con dispersione

$$\sigma = \sqrt{\frac{\pi}{2}}\,\frac{0.32}{\bar{R}} = \frac{0.40}{\bar{R}} = \frac{s}{\bar{R}}\,.$$

Data una traccia di raggio di curvatura $\bar{R}$, la probabilità che la misura dia un valore compreso fra R e $R+\mathrm{d}R$ è allora espressa da:

$$K(R;\, \bar{R},\, \sigma)\,\mathrm{d}R = -\frac{1}{\sqrt{2\pi}\sigma} \exp\left[-\left(\frac{1}{R} - \frac{1}{\bar{R}} \right)^2 \frac{1}{2\sigma^2} \right] \frac{\mathrm{d}R}{\bar{R}^2} =$$

$$= -\frac{\bar{R}}{\sqrt{2\pi}\,s} \exp\left[-\left(\frac{\bar{R}}{R} - 1 \right)^2 \frac{1}{2s^2} \right] \frac{\mathrm{d}R}{\bar{R}^2}\,.$$

Indicato con $S(B\bar{R})$ lo spettro « vero » degli elettroni, lo spettro alterato

per effetto della diffusione multipla coulombiana risulta:

$$S^*(BR)\,\mathrm{d}(BR) = \mathrm{d}(BR)\int_{\bar{R}_{\min}}^{\bar{R}_{\max}} S(B\bar{R})K(R;\,\bar{R},\,\sigma)\,\mathrm{d}\bar{R}\,.$$

L'integrazione è stata eseguita numericamente nell'intervallo di $\bar{R}$ da 10 a 24 cm, corrispondente all'intervallo di rigidità magnetica da 3000 a 7200 gauss cm; il limite inferiore risulta fissato dalle condizioni sperimentali (vedi 2·2), quello superiore corrisponde al massimo valore $B\bar{R}$ per cui $S \neq 0$.

In fig. 4 è mostrato l'istogramma sperimentale delle 11 537 traccie nell'intervallo da 2400 a 7500 gauss cm (vedi 2·3) e le curve S ed S^* normalizzate allo stesso numero di tracce negli intervalli da 3000 a 7200 e da 2400 a 7500 gauss cm rispettivamente.

L'istogramma e lo spettro S^* si accordano sufficientemente bene e ciò permette di assumere con fiducia nelle considerazioni successive come spettro degli elettroni presi in considerazione quello degli elettroni del radiofosforo aventi rigidità maggiore di 3000 gauss cm.

3. – Risultati sperimentali e confronto con la teoria.

3·1. – Nella Tabella I sono riportati alcuni valori di $\int_{\Phi_1}^{\Phi_2} P(\Phi,\beta)\,\mathrm{d}\Phi$ calcolati per $k = 0$ e $\varrho = 1$, utilizzando le tabelle pubblicate da O'Ceallaigh [14] riferiti a 1000 metri di traccia in argon alla pressione atmosferica, secondo la formula di Rutherford e di Mott.

Il numero di deflessioni per metro di traccia da aspettarsi nell'intervallo angolare $\Phi_2 - \Phi_1$ da un fascio di elettroni il cui spettro sia $S(BR)$, è dato da:

$$\int_{(BR)\min}^{(BR)\max}\int_{\Phi_1}^{\Phi_2} P(\Phi,\beta)\,S(BR)\,\mathrm{d}\Phi\,\mathrm{d}\beta,$$

BR e β essendo legati dalla nota relazione.

L'integrale è stato valutato numericamente per $(BR)_{\min} = 3000$ gauss cm e $(BR)_{\max} = 7200$ gauss cm. I risultati secondo la formula di Rutherford e di

[14] C. O'Ceallaigh: *Proc. Roy. Irish Acad.*, A **53**, 33 (1950).

TABELLA I.

β	$\Phi_2 - \Phi_1$									
	20°-30°	30°-40°	40°-50°	50°-60°	60°-70°	70°-80°	80°-90°	90°-100°	100°-110°	110°-120°
0.850	925	290	119	59.5	33.5	20.7	13.8	10.1	7.55	5.85
	946	**292**	**115**	**55.5**	**29.5**	**16.7**	**10.3**	**7.0**	**4.51**	**2.91**
0.875	694	218	89.3	44.7	25.2	15.5	10.4	7.56	5.58	4.80
	710	**219**	**87.1**	**41.9**	**22.0**	**12.2**	**7.6**	**5.08**	**3.11**	**2.00**
0.900	505	158	65.0	32.4	18.2	11.3	7.52	5.50	4.06	3.21
	516	**158**	**62.4**	**30.0**	**15.9**	**9.0**	**5.31**	**3.61**	**2.12**	**1.41**
0.925	341	107	43.9	22.0	12.4	7.65	5.10	3.72	2.74	2.17
	348	**107**	**42.0**	**20.1**	**11.7**	**5.81**	**3.53**	**2.34**	**1.38**	**0.90**
0.950	209	65.2	27.1	13.0	7.51	4.72	3.12	2.33	1.71	1.31
	214	**65.0**	**25.6**	**11.7**	**6.31**	**3.51**	**2.20**	**1.35**	**0.80**	**0.51**
0.975	94.1	29.4	12.1	6.02	3.41	2.10	1.42	1.03	0.81	0.64
	96.0	**29.2**	**11.5**	**5.41**	**2.81**	**1.54**	**0.83**	**0.67**	**0.41**	**0.24**

Le cifre in carattere tondo si riferiscono ai dati previsti dalla teoria di RUTHERFORD, quelle in neretto a quelli di MOTT.

Mott, normalizzati alla lunghezza di traccia della nostra misura, sono riportati nella Tabella II insieme ai dati sperimentali.

TABELLA II.

	20°-30°	30°-40°	40°-50°	50°-60°	60°-70°	70°-80°	80°-90°	90°-100°	100°-110°	110°-120°
RUTHERFORD	446	139	60.1	28.5	15.6	9.02	5.65	4.06	2.70	1.81
MOTT	455	139	56.2	26.4	13.9	7.65	4.52	3.12	2.05	1.20
Sperimentali	484	143	56	23	17	7	4	2	1	1

3·2. – Nella Tabella III, insieme ai risultati sperimentali della presente ricerca, sono riportati i risultati trovati da altri autori nel campo di energia intorno ad 1 MeV per collisioni in argon ed i valori del rapporto $\mathcal{R}$ tra il numero totale di deflessioni osservate e quello da aspettarsi secondo MOTT (si tenga presente che la sezione totale per $\theta \geqslant 20°$ secondo RUTHERFORD, per elettroni da 1 MeV in argon differisce da quella di MOTT solo di pochi percento).

TABELLA III.

	Energia in MeV	Angoli di deflessione	Lunghezza di traccia in m	Numero di deflessioni	$\mathcal{R}$
ZUBER [15]	1.7-2.4	30°-180°	350	480	0.75
STEPHANOWA [16]	0.2-1.1	20°-150°	103	308	1.0
»	1.5-3	20°-150°	130	84	2.5
BLEULER *et al.* [17]	0.2-3.0	20°-180°	708	153	1.5
RANDELS *et al.* [8]	0.8-3.3	15°- 90°	—	50	1.17
HOWATSON e ATKINSON [18]	0.2-2	20°- 90°	198	70.5	1.02
Presente lavoro, ...	0.5-1.6	20°-120°	1 321	739	1.04
» »	0.5-1.6	50°-120°	1 321	56	0.96

È difficile giustificare la forte dispersione dei valori del rapporto $\mathcal{R}$ in base solo alla diversità delle condizioni sperimentali: ad essa contribuisce probabilmente in maniera sostanziale il fatto di aver dato, in una statistica relativamente povera, ugual peso al numero di deflessioni a grande angolo ed a quello delle deflessioni a piccolo angolo, che, come è facile riconoscere, è affetto da maggiori incertezze. Il considerare, per il confronto fra teoria ed esperimento le piccole deflessioni, che sono estremamente più numerose delle grandi può mascherare completamente anche grandi deviazioni dalla legge teorica nella regione dei grandi angoli.

Nella presente ricerca, sia nell'intervallo 20°-120° che in quello 50°-120° il valore del rapporto $\mathcal{R}$ risulta sensibilmente prossimo all'unità; il rapporto tra il numero di deflessioni trovate e quello da aspettarsi secondo la teoria di Rutherford per angoli maggiori di 50° risulta invece 0.84.

Dopo aver normalizzato i valori da aspettarsi nell'intervallo 20°÷120° al valore sperimentale 739, si è applicato il *criterio del* χ^2 per vedere quale dei due andamenti teorici meglio si accordasse con i valori sperimentali ottenuti. Si è trovato che la probabilità che le deviazioni fra le previsioni teoriche ed i risultati sperimentali siano casuali risulta 55% per la formula di Rutherford e 82% per quella di Mott.

L'esame delle sezioni totali ed il risultato del criterio del χ^2 per le sezioni differenziali portano a concludere che i dati sperimentali trovati si accordano

---

[15] K. ZUBER: *Helv. Phys. Acta*, **11**, 370 (1938).
[16] E. STEPANOWA: *Journ. Phys. USSR*, **1**, 204 (1939).
[17] E. BLEULER, P. SHERRER e W. ZÜNTI: *Phys. Rev.*, **61**, 95 (1942).
[18] A. F. HOWATSON e J. R. ATKINSON: *Phil. Mag.*, **42**, 1136 (1951).

meglio con i valori ottenuti con la formula di Mott che con quelli ottenuti con la formula di Rutherford, benchè essi siano lontani dal permettere di trarre conclusioni circa eventuali piccole divergenze dalla teoria di Mott.

* * *

È nostro gradito dovere ringraziare il Prof. G. POLVANI ed il Prof. P. CALDIROLA per il vivo interesse mostrato alla presente ricerca.

Siamo vivamente grati alla dott. M. CORDONI per il valido aiuto datoci nella lettura dei fotogrammi ed al dott. C. GIORI per la collaborazione prestataci durante l'esecuzione della ricerca. È nostro dovere ringraziare il dott. R. ATTARDO per l'attività prestata in diverse fasi dell'esperienza.

Sentiti ringraziamenti vogliamo rivolgere anche agli Amici dell'Istituto per gli aiuti finanziari accordatici e per la cortese attenzione con cui alcuni hanno personalmente seguito questa ricerca.

Vogliamo pure ringraziare la Società Farmitalia ed il dott. C. POLVANI per i preparati radioattivi gentilmente fornitici.

SUMMARY

The elastic scattering of the electrons of energy about 1 MeV has been analysed by means of a diffusion cloud chamber filled with argon at atmospheric pressure. A total length of 2157 m was measured in about 10000 photographs, collected in 50 hours. The total number of scatterings $\geqslant 20^{\circ}$ is 739, with 56 deflections greater than 50°. The ratio between the experimental and the theoretical total cross-section for angles $\geqslant 50^{\circ}$ is 1.02 according to Mott's prediction and 0.84 according to Rutherford's theory. The analysis of the differential cross-sections showst hat the formula of Mott is in better agreement with the experimental results than the formula of Rutherford.

On the Theory of Superconductivity.

V. L. Ginzburg (*).

P. N. Lebedev Institute of Physics of the Academy of Science of the USSR - Moscow

(ricevuto il 20 Settembre 1955)

Summary. — Macroscopic theory of superconductivity valid for magnetic fields of arbitrary magnitude and the behaviour of superconductors in weak high frequency fields are discussed. The problem of formulating a microscopic theory of superconductivity is also considered.

The theory of superconductivity can be conveniently divided into macroscopic (phenomenological) and microscopic theory. Obviously, quantitative interpretation of the experiments can be made only on the basis of macroscopic theory. Macroscopic relations are, of course, also necessary to verify the results of a microscopic treatment of the motion of electrons in metals. However, in contrast to non superconducting metals in which, in the simplest case, macroscopic theory reduces to almost trivial results such as Ohm's law, the formulation of a macroscopic theory of superconductivity is an independent and important problem. The present paper is mostly devoted to the macroscopic theory of superconductors.

Superconductors in magnetic fields of arbitrary magnitude are considered in § 1 and the behaviour of superconductors in a weak high frequency field is treated in § 2. Numerous investigations devoted to microscopic theory of superconductivity have been carried till now; however, no really satisfactory theory has yet been developed and one may only speak of the various hypotheses and attempts which have been made in this direction. Some remarks concerning microscopic theory of superconductivity are made in § 3.

(*) In the transliteration of Russian names we follow the International System of Transliteration of Cyrillic Characters (2nd Draft Iso Recommendation n°. 6, 1954), published at pag. 388 of the n°. 4 of the *Supplemento* to Vol. 1 (1955) of *Il Nuovo Cimento*.

1. – Macroscopic theory of superconductivity for constant magnetic fields of arbitrary magnitude.

Up to recent times macroscopic theory of superconductivity in a constant magnetic field was based on the following equations [1] relating the superconducting current density $\boldsymbol{j}_s$ and the magnetic field strength $\boldsymbol{H}$:

$$\text{rot } \Lambda \boldsymbol{j}_s = -\frac{1}{c}\boldsymbol{H}, \tag{1}$$

where Λ is a quantity depending only on the temperature (the metal is considered isotropic; the field strength $\boldsymbol{H}$ can be identified with the induction $\boldsymbol{B}$: as the magnetic permeability is practically equal to unity). Equation (1) together with the Maxwell equation:

$$\text{rot } \boldsymbol{H} = \frac{4\pi}{c}\boldsymbol{j}_s, \tag{2}$$

and the conditions $\text{div } \boldsymbol{H} = 0$ and $\text{div } \boldsymbol{j}_s = 0$ leads to the equations:

$$\Delta \boldsymbol{H} - \frac{1}{\delta_0^2}\boldsymbol{H} = 0, \qquad \Delta \boldsymbol{j}_s - \frac{1}{\delta_0^2}\boldsymbol{j}_s = 0, \qquad \delta_0 = \sqrt{\frac{\Lambda c^2}{4\pi}}. \tag{3}$$

It will be shown in § 2 that if a superconductor in a constant magnetic field is described by eq. (1)-(3) its behavior will be equivalent to that of a medium having a complex dielectric constant under the condition that $\omega \to 0$:

$$\left\{ \begin{array}{l} \varepsilon'(\omega) = \varepsilon = -\dfrac{4\pi}{\omega^2 \Lambda} \equiv -\dfrac{c^2}{\delta_0^2 \omega^2} \equiv -\dfrac{4\pi e^2 n_s}{m\omega^2}, \\ \delta_0^2 \equiv \dfrac{\Lambda c^2}{4\pi} \equiv \dfrac{mc^2}{4\pi e^2 n_s} = \dfrac{2.83 \cdot 10^{11}}{n_s} \text{ cm}^2, \end{array} \right. \tag{4}$$

where e^2/m is the ratio between the square of the charge and the mass of a free electron and n_s by definition is the concentration of « superconducting electrons ».

According to (1) and (3) in the case of a plane boundary between the superconductor and vacuum

$$H = H_0 \exp\left[-z/\delta_0\right], \qquad j_s = \frac{c}{4\pi\delta_0} H, \tag{5}$$

where the direction of z-axis is the perpendicular to the boundary and H_0 is the

component of the field strength parallel to this boundary at $z = 0$ (i.e. on the boundary).

It follows from (5) (this can be proved for a superconductor of any form) that the field penetrates the metal only at a depth δ_0; according to experimental data for temperature appreciably lower than the critical T_c temperature, $\delta_0 \sim 5 \cdot 10^{-6}$ cm. This damping of the field within the superconductor and also a number of other conclusions following from eq. (1) indicate that (at least qualitatively) this equation is satisfactory for weak magnetic fields, i.e. for

$$H \ll H_c\,, \tag{6}$$

where H_c is the critical magnetic field strength (i.e. the field strength at which the superconductivity is destroyed).

The question regarding the qualitative correctness of equation (1) under the condition (6) will be considered below. However, we may already note here that in strong fields ($H \sim H_c$) London's theory ([1]), which is based on eq. (1) is certainly in correct ([2,3]). Thus London's theory cannot explain why the superconductivity in samples of any given size is destroyed by a field or current; this theory yields a negative surface energy for the boundary between the superconducting and the normal phases of the metal; it does not account for the dependance of the depth of penetration of the field on its strength etc.

A macroscopic theory of superconductivity valid for arbitrary constant fields and equivalent to London's theory for weak fields was formulated in ([2]) and further developed in ([3-9]). Here it will be only possible for us to discuss briefly the main points of this theory and to consider some of the results it predicts.

In the absence of a magnetic field the transition to the superconducting state at the temperature T_c is a phase transition of the second kind. The general theory of such transition ([10]) involves a parameter η which is zero for $T > T_c$. Thus in ferroelectrics the spontaneous polarization P_s plays the rôle of η while in ferromagnetics the corresponding quantity is μ_s the spontaneous magne-

---

([1]) F. London: *Superfluids*, vol. I (1950).

([2]) V. L. Ginzburg and L. D. Landau: *Žu. Eksper. Teor. Fiz.*, **20**, 1064 (1950).

([3]) V. L. Ginzburg: *Usp. Fiz. Nauk*, **42**, 169, 333 (1950). Translation in *Abhandlungen aus der sowjetischen Physik*, Folge II (Berlin, 1951), p. 135.

([4]) V. L. Ginzburg: *Dokl. Akad. Nauk SSSR*, **83**, 385 (1952).

([5]) V. P. Silin: *Žu. Eksper. Teor. Fiz.*, **21**, 1330 (1951).

([6]) V. L. Ginzburg: *Žu. Eksper. Teor. Fiz.*, **23**, 236 (1952).

([7]) A. A. Abrikosov: *Dokl. Akad. Nauk SSSR*, **86**, 489 (1952).

([8]) A. V. Gurevič: *Žu. Eksper. Teor. Fiz.*, **27**, 195 (1954).

([9]) V. L. Ginzburg: *Žu. Eksper. Teor. Fiz.*, **29**, n. 4 (1955).

([10]) L. D. Landau and E. M. Lifšic: *Statistical Physics* (Moscow, 1951), chap. XIV.

tization (see [11]). It can easily be seen that in superconductors η should be replaced by $\sqrt{n_s}$, where n_s is the concentration of superconducting electrons. In order to generalize for the case when a magnetic field is present it will be necessary to consider that η is complex and hence $\eta\eta^* = |\eta|^2 = n_s$. The quantity η thus becomes similar to a wave function and will be designated below by Ψ (i.e. $n_s = |\Psi|^2$). All observable quantities, of course, should depend on Ψ and Ψ^* in such a way that multiplication of Ψ by a constant of the type $e^{i\alpha}$ does not change their magnitude.

It might be thought that the effective wave function Ψ thus introduced for the superconducting electrons is related to the density matrix of the electrons in the metal $\varrho(\boldsymbol{r}, \boldsymbol{r}')$ by the equation:

$$\Psi^*(\boldsymbol{r})\Psi(\boldsymbol{r}') = \varrho(\boldsymbol{r}, \boldsymbol{r}') = \int \Psi^*(\boldsymbol{r}, \boldsymbol{r}_i')\Psi(\boldsymbol{r}', \boldsymbol{r}_i')\,\mathrm{d}\boldsymbol{r}_i' ,$$

where $\Psi(\boldsymbol{r}, \boldsymbol{r}_i')$, the true wave function of the metal electrons, depends on the coordinates of all the electrons $\boldsymbol{r}_i$ (the $\boldsymbol{r}_i'$ are the coordinates of all the electrons except the one under consideration; for the latter the coordinates are $\boldsymbol{r}$ and at the second point $\boldsymbol{r}'$). However, this relation between Ψ and ϱ has not been proved; in the macroscopic theory [2] Ψ is essentially an auxiliary parameter in terms of which the observable quantities are expressed.

In the superconducting state the free energy density has the form (for details see [2,3,9]):

$$F_{sH} = F_{s0} + \frac{H^2}{8\pi} + \frac{1}{2m}\left| -i\hbar\nabla\Psi - \frac{e}{c}A\Psi \right|^2 , \tag{7}$$

where $\boldsymbol{H} = \mathrm{rot}\,\boldsymbol{A}$ is the magnetic field strength and F_{s0} is the free energy in the absence of the field. Near T_c

$$F_{s0} = F_{n0} + \alpha|\Psi|^2 + \frac{\beta}{2}|\Psi|^4 , \tag{8}$$

where F_{n0} is the free energy density in the normal state.

From the condition of minimum of total free energy $\int F_{sH}\mathrm{d}V$, by varying this expression with respect to Ψ^* and $\boldsymbol{A}$ we obtain the equations defining Ψ and $\boldsymbol{A}$ (it must be assumed that $\mathrm{div}\,\boldsymbol{A} = 0$):

$$\frac{1}{2m}\left(-i\hbar\nabla - \frac{e}{c}\boldsymbol{A}\right)^2\Psi + \frac{\partial F_{s0}}{\partial\Psi^*} = 0 , \tag{9}$$

$$\Delta\boldsymbol{A} = -\frac{4\pi}{c}\boldsymbol{j}_s = \frac{2\pi i e\hbar}{mc}(\Psi^*\nabla\Psi - \Psi\nabla\Psi^*) + \frac{4\pi e^2}{mc^2}|\Psi|^2\boldsymbol{A} . \tag{10}$$

---

[11] V. L. Ginzburg: *Journ. of Phys. USSR*, **10**, 107 (1946); *Žu. Eksper. Teor. Fiz.*, **17**, 883 (1947); **19**, 36 (1949); *Usp. Fiz. Nauk*, **38**, 490 (1949).

As the variation $\delta\Psi^*$ is arbitrary on the surface of the superconductor the following condition should be fulfilled:

$$\boldsymbol{n}\left(-i\hbar\nabla\Psi-\frac{e}{c}\boldsymbol{A}\Psi\right)=0\,, \tag{11}$$

where $\boldsymbol{n}$ is a vector normal to the boundary (*).

In the absence of a magnetic field one may put $\boldsymbol{A}=0$ and thus, in a homogeneous superconductor, $\nabla\Psi=0$, which also agrees with (11). In this case equation (9) obviously signifies the extremum condition for F_{s0}. In the case (8) the condition $\partial F_{s0}/\partial\Psi^*=0$ yields (if $\alpha<0$) a maximum solution $\Psi=0$ and a minimum solution:

$$|\Psi|^2=|\Psi_\infty|^2=-\frac{\alpha}{\beta}=\frac{(\mathrm{d}\alpha/\mathrm{d}T)_c(T_c-T)}{\beta_c}\,,\qquad F_{s0}=F_{n0}-\frac{\alpha^2}{2\beta}\,, \tag{12}$$

where it has been taken into account that near T_s one may put $\beta=\beta(T_c)=\beta_c$ and $\alpha=(\mathrm{d}\alpha/\mathrm{d}T)_c(T-T_c)$. The well known thermodynamical relation ([1,3]) $F_{n0}-F_{s0}=H_{cm}^2/8\pi$, where H_{cm} is the critical field for a massive metal, then yields:

$$H_{cm}^2=\frac{4\pi\alpha^2}{\beta}=\frac{4\pi(\mathrm{d}\alpha/\mathrm{d}T)_c(T_c-T)^2}{\beta_c}\,. \tag{13}$$

It is well known that experiment completely confirms this formula and this may be considered a justification of expansion (8) and of the assumption regarding the form of functions $\alpha(T)$ and $\beta(T)$. For generalization of the theory for arbitrary temperature see ([9,12]). Possible anisotropy of the metal is accounted for in ([6]).

In a weak magnetic field, if the condition (5) is fulfilled, the function Ψ remains practically constant (i.e. the concentration of superconducting electrons $n_s=|\Psi_\infty|^2=\mathrm{const}$) and equation (10) then has the form:

$$\Lambda\boldsymbol{A}=-\frac{4\pi}{c}\boldsymbol{j}_s=\frac{4\pi e^2}{mc^2}|\Psi_\infty|^2\boldsymbol{A}=\frac{4\pi e^2 n_s}{mc^2}\boldsymbol{A}\,. \tag{14}$$

Applying the operation «rot» to (14) and remembering that, according to (4), $\Lambda=m/e^2n_s$, one obtains equation (1).

Thus, in a weak field the theory ([2]) is equivalent to London's theory ([1]).

(*) The condition (11) automatically follows from the variation principle if no auxiliary conditions restricts Ψ on the boundary: that is the case considered here ([2]).

([12]) J. Bardeen: *Phys. Rev.*, **94**, 554 (1954).

In a strong field the function Ψ does not equal Ψ_∞ and, generally speaking, ti depends on the coordinates and strength of the external field. In other words the concentration of superconducting electrons turns out to be dependent on coordinates and field.

In the one-dimensional case the equations (9)-(10) take the form:

$$\frac{\mathrm{d}^2\Psi'}{\mathrm{d}z'^2} = \varkappa^2\{-(1-A'^2)\Psi' + \Psi'^3\}\,, \tag{15}$$

$$\frac{\mathrm{d}^2A'}{\mathrm{d}z'^2} = \Psi'^2A' \tag{16}$$

where the field is assumed to be directed along the y-axis, the current $\boldsymbol{j}$ and the potential $\boldsymbol{A}$ along the x-axis and the function Ψ can be considered real: the following variables have been introduced in (15) and (16):

$$\left\{\begin{array}{l} z' = \dfrac{z}{\delta_0}\,, \qquad \Psi'^2 = \dfrac{\Psi^2}{\Psi_\infty^2}\,, \qquad A' = \dfrac{A}{\sqrt{2}H_{cm}\delta_0}\,, \qquad H' = \dfrac{\mathrm{d}A'}{\mathrm{d}z'} = \dfrac{1}{\sqrt{2}}\dfrac{H}{H_{cm}}\,, \\ \delta_0^2 = \dfrac{mc^2}{4\pi e^2\Psi_\infty^2} = \dfrac{mc^2\beta}{4\pi e^2|\alpha|}\,, \qquad H_{cm}^2 = \dfrac{4\pi\alpha^2}{\beta}\,, \\ \varkappa^2 = \dfrac{1}{2\pi}\left(\dfrac{mc}{e\hbar}\right)^2\,, \qquad \beta = \dfrac{2e^2}{\hbar^2c^2}H_{cm}^2\delta_0^4\,. \end{array}\right. \tag{17}$$

It might seem from (15)-(17) that only two parameters α and β or two directly observable quantities H_{cm} and δ_0 are involved in the theory. This conclusion, however, would be true only if one considers that in (7) and subsequent formulae e is the charge of a free electron: which, however, may not be the case (9). The point here is that in the expression for δ_0 (see (4) and (17)) the quantity e^2/m may be identified with that for free electrons as only δ_0^2 can be measured experimentally and Ψ_∞^2 can be normalized in any suitable manner. However, it does not seem that charge e which we now designate e_{eff} should necessarily equal $e = 4.80\cdot10^{-10}$ e.s.u. although it would seem natural to consider this to be the case. The introduction of an arbitrary constant charge e_{eff} does not invalidate the gauge invariance of the theory. If the charge e_{eff} is not a universal constant it should depend on the coordinates and the gauge invariance will be invalidated. On the other hand in this latter case the theory (2) developed for the one-dimensional case requires a generalization. Thus it is not clear whether one may introduce a charge $e_{\mathrm{eff}} \neq e$. If $e_{\mathrm{eff}} \neq e$ then

$$\varkappa = \frac{\sqrt{2}\,|e_{\mathrm{eff}}|}{\hbar c}H_{cm}\delta_0^2 = 2.16\cdot10^7\left(\frac{e_{\mathrm{eff}}}{e}\right)H_{cm}\delta_0^2\,, \tag{18}$$

and the theory will involve three parameters α, β, and e_{eff} or H_{cm}, δ_0 and $\varkappa$. The

theory can also be verified if $e_{\text{eff}} \neq e$ as the quantity $\varkappa$ determines the magnitude of various physical quantities which can be measured independently (see below). On the boundary between a superconducting half-space and vacuum ($z = 0$) $H = H_0$, $d\Psi/dz = 0$ and inside the superconductor ($z \to \infty$): $H = 0$, $A = 0$, $d\Psi/dz = 0$, $\Psi' = \Psi'_\infty = 1$. With these boundary conditions and for $\varkappa H_0^2 \ll 1$, the system (15)-(16) can easily be solved [2]. Thus, for $z = 0$: $\Psi' - \Psi'_0 = 1 - [(\varkappa H_0'^2)/2(\varkappa + \sqrt{2})]$. The depth of penetration of the field is then

$$\delta = \frac{\int_0^\infty H\,dz}{H_0} = \frac{|A_0|}{H_0} = \delta_0\left\{1 + \frac{\varkappa(\varkappa + 2\sqrt{2})}{B(\varkappa + \sqrt{2})^2}\left(\frac{H_0}{H_{cm}}\right)^2\right\} = \delta_0\left\{1 + f(\varkappa)\left(\frac{H_0}{H_{cm}}\right)^2\right\}. \tag{19}$$

Thus the penetration depth now depends on the field strength. The same will also be true if δ is measured in a weak field H_{10} in the presence of a strong field H_0; in this case

$$\delta_1 = \frac{\int_0^\infty H_1\,dz}{H_{10}} = \delta_0\left\{1 + 3f(\varkappa)\left(\frac{H_0}{H_{cm}}\right)^2\right\}. \tag{20}$$

The phase transition on a boundary between the superconducting and normal phases of the metal will be continuous and the equations (15)-(16) must be solved for the boundary conditions:

$$\begin{cases} z = \infty: \quad \Psi' = \Psi'_\infty = 1, \quad H = 0, \quad A = 0, \quad \dfrac{d\Psi'}{dz'} = 0, \\ z = -\infty: \ \Psi' = 0, \quad \dfrac{d\Psi'}{dz'} = 0, \quad H = H_{cm} \quad \left(\text{i.e. } H' = H'_{cm} = \dfrac{1}{\sqrt{2}}\right). \end{cases} \tag{21}$$

The surface energy is then [2]:

$$\sigma_{ns} = \frac{H_{cm}^2}{2\pi}\,\delta_0 \int_{-\infty}^{+\infty}\left\{\frac{1}{\varkappa^2}\left(\frac{d\Psi'}{dz'}\right)^2 - H'^2 - H'_0 H'\right\} dz'. \tag{22}$$

In the limiting case $\sqrt{\varkappa} \ll 1$:

$$\sigma_{ns} = \frac{A H_{cm}^2}{8\pi}, \qquad A = \frac{8\delta_0}{3\sqrt{2}\varkappa} = \frac{1.89}{\varkappa}\,\delta_0. \tag{23}$$

Practically this formula can be applied only for $\varkappa \lesssim 0.02$; in the general case σ_{ns} must be computed by numerical integration of the system (15)-(16). For

$\varkappa = 0.041$ one obtains $\Delta = 35.6\,\delta_0$; for $\varkappa = 0.165$ $\Delta = 6.1\delta_0$ and for $\varkappa = 0.6$ $\Delta = 0.29\,\delta_0$. For $\varkappa = 1/\sqrt{2}$, $\sigma_{ns} = 0$ and for $\varkappa > 1/\sqrt{2}$, $\sigma_{ns} < 0$. In the range $\varkappa > 1/\sqrt{2}$ the behaviuor of the superconductor should be anomalous ([2]); it might be of interest from the viewpoint of explaining the properties of alloys ([7]). If one puts in ([18]) $e_{\text{eff}} = e = 4.8 \cdot 10^{-10}$, $\varkappa$ may be evaluated from the measured values of H_{cm} and δ_0. Thus for good superconductors one finds $\varkappa \sim 0.1$. $\varkappa$ can be directly determined by measuring σ_{ns} and $\delta(H_0)$. Available data do not yet permit one to determine $\varkappa$ but it is certain that in pure superconductors $\sigma_{ns} \gtrsim \delta_0 > 0$ and apparently there is a dependence of δ on H_0. The old theory ([1]) which led to a negative surface tension and did not account for the dependence of δ on the field strength could not explain these two features.

The solution of the equations for superconducting films ([2,4,8]) and for small cylinders and spheres ([5]) leads to some very interesting results which have been checked by special experiments ([13]). Thus, for thin films for which d/δ_0 is smaller than the critical value (thickness of film $2d$) (*)

$$\frac{d_c}{\delta_0} = \frac{\sqrt{5}}{2} = 1.12\,, \tag{24}$$

the quantity $\Psi = \Psi_0$ in the film decreases with increasing field strength and becomes zero in the critical field

$$\frac{H_c}{H_{cm}} = \sqrt{6}\,\frac{\delta_0}{d}\,. \tag{25}$$

Thus, for $d/\delta_0 < d_c/\delta_0$ the phase transition is a transition of the second kind (superconductivity gradually disappears). For $d/\delta_0 > d_c/\delta_0$ the transition is already one of the first kind and takes place in some field H_c; in this case hysteresis can be and, as a matter of fact, is observed experimentally ([13]). The respective expressions for H_c can be found ([2,4,8]). The magnetic moment of the film depends on the field; for $d/\delta_0 < d_c/\delta_0$ and at $H_0 = H_c$ it equals zero. The destruction of superconductivity in samples of arbitrary size by currents (and not only by field) can also be treated by the theory ([2]).

All the available experimental data (excluding one case, which will be discussed below) are in accord with the theory proposed here; however, owing to large experimental errors only a qualitative comparison can be made (the experiments carried out in ([13]) are a possible exception). The case mentioned

(*) The case $\varkappa \ll 1$ is being considered here; about corrections containing $\varkappa$ see ([8]). For $\varkappa \to 0$ in the film $\Psi = \Psi_0 = \text{const}$, i.e. Ψ is independent of z.

([13]) N. V. Zavarickij: *Dokl. Akad. Nauk SSSR*, **78**, 665 (1951); **85**, 749 (1952).

above in which theory and experiment do not accord refers to the dependence of the penetration depth of the field on the angle θ between the field and the tetragonal axis in tin ([14]). London's theory generalized for cases of anisotropy ([6]) and also the theory developed in ([2]) predict that for $0 \leqslant \theta \leqslant \pi/2$ the dependence $\delta(\theta)$ should be monotonic ([6]) (this can be seen from the fact that in a weak field and in the anisotropic case instead of A the quantity A_{ik} is involved, this being a symmetric tensor of the second order). However in ([14]) a nonmonotonic dependence of δ on θ was found. There are good reasons however to believe that this result may be wrong (see ([15]), p. 161 and ([16])); thus the problem of anisotropy of the depth of penetration (especially in static or low-frequency fields which are considered here) remains an open question. It therefore seems premature to deny the validity of London's theory and in particular of equation (1) for weak fields. It is true, that besides the anisotropy dependence other arguments against the applicability of equation (1) are cited in ([11]), but in our opinion ([9]) they are all unconvincing. At the same time one may mention some facts which strongly speak in favour of the validity of equation (1) in weak fields. Thus, the critical temperature T_c for suitably prepared films possessing half-thicknesses $d \gtrsim 10^{-6}$ cm is the same as for a massive metal ([13]). For films with $d \sim 10^{-6}$ the values of δ_0 are also the same as for thick films. This means that in weak fields the properties of a superconductor and in particular the superconducting current density $\boldsymbol{j}_s(\boldsymbol{r})$ are defined by the field in a region with dimensions $l \ll d_{\min} \sim 10^{-6}$ cm, where $d_{\min}$ is the minimum half-thickness of a film having the same value of T_c and of δ_0 as a massive metal. Within the framework of macroscopic theory, in which distances exceeding $\sim 10^{-7}$ cm are considered, this signifies that the relation between $\boldsymbol{j}_s$ and the field is a differential one and that in the case of a weak field, for which the theory should be linear, we obtain in a natural manner eq. (1) (*).

Thus convincing facts indicate that equation (1) is correct for weak fields and only new experiments will prove if this is really the case or not. Above all it seems desirable to investigate the anisotropy of the penetration depth of static or sufficiently low frequency fields in superconductors. London's theory, on the other hand, is certainly incorrect for strong fields, whereas the theory ([2]) is not only self-consistent in this case but qualitatively agrees with all the experimental facts. Quantitatively the theory ([2]) has been verified

([14]) A. B. Pippard: *Proc. Roy. Soc.*, A. **216**, 547 (1953); *Physica*, **19**, 765 (1953).
([15]) D. Shoenberg: *Superconductivity* (Cambridge, 1952).
([16]) M. S. Hajkin: *Žu. Eksper. Teor. Fiz.*, **28**, 115 (1955).

(*) It is a well known experimental fact that in ideal superconductors the current density $\boldsymbol{j}_s$ is determined by the field $\boldsymbol{H}$. As $\boldsymbol{j}_s$ is a polar vector and $\boldsymbol{H}$ an axial vector, equation (1) is (excluding (2)) the only invariant linear relation between $\boldsymbol{j}_s$ and $\boldsymbol{H}$ which does not contain higher derivatives.

only for thin films and the agreement was found to be very satisfactory. To check the theory ([2]) further it seems desirable to measure the surface energy σ_{ns} and also the dependence of the penetration depth on the magnetic field strength and the mutual orientation of the field and of the cristallographic axes in the metal.

2. Behaviour of superconductors in high frequency fields.

The foregoing exposition referred only to static fields or to fields of sufficiently low frequency. The problem for high frequency fields is generally much more complicated owing to losses and to the anomalous nature of the skin effect in metals at low temperatures. We therefore confine ourselves to weak fields for which the problem is linear.

In a variable field, equation (2) must be substituted by the general equation

$$\text{rot } \boldsymbol{H} = \frac{4\pi}{c}(\boldsymbol{j}_s + \boldsymbol{j}_n) + \frac{\varepsilon_0}{c}\frac{\partial \boldsymbol{E}}{\partial t}, \tag{26}$$

where $\boldsymbol{j}_n$ is the normal current density, ε_0 the dielectric constant in the superconducting state and $\boldsymbol{E}$ the electric field strength. In addition to equation (1) the following equation must be used (for details see ([1,13,17])),

$$\frac{\partial \Lambda \boldsymbol{j}_s}{\partial t} = \boldsymbol{E}. \tag{27}$$

For $T \to 0$ and frequencies

$$\omega < \omega_c \tag{28}$$

the losses in the superconductor are zero (i.e. $\boldsymbol{j}_n = 0$ and for a harmonic process ($H \sim e^{i\omega t}$ etc.) the equations (26) and (27) yield (*)

$$\text{rot } \boldsymbol{H} = i\frac{\omega}{c}\left(\varepsilon_0 - \frac{4\pi}{\Lambda\omega^2}\right)\boldsymbol{E} = i\frac{\omega}{c}\varepsilon'\boldsymbol{E}.$$

Thus according to equation (1) for $T \to 0$ and under the condition (28) the

---

([17]) V. L. Ginzburg: *Žu. Eksper. Teor. Fiz.*, **21**, 979 (1951).

(*) Equation (1) follows from (27) and from the field equation rot $\boldsymbol{E} = -(1/c) \cdot (\delta \boldsymbol{H}/\delta t) = -i(\omega/c)\boldsymbol{H}$ for harmonic processes with $\omega \neq 0$. As ε_0 may possibly depend on the frequency, equation (26) in general has a sense only if all the quantities depend harmonically on time.

superconductor behaves as a substance with a complex dielectric constant

$$\varepsilon' = \varepsilon = \varepsilon_0 - \frac{4\pi}{A\omega^2} \equiv \varepsilon_0 - \frac{c^2}{\delta_0^2\omega^2} \equiv \varepsilon_0 - \frac{4\pi e^2 n_s}{m\omega^2}. \tag{29}$$

For $\omega \to 0$ the equation (29) changes over into (4) as ε_0 is a finite quantity.

For $T \neq 0$ and any frequency $\omega \neq 0$ losses begin to appear; owing to the anomalous character of the skin effect the account of these losses requires a special consideration which is connected with a number of assumptions ([17,18]). It is not possible now to introduce the quantity ε' as the relation between current and field is not differential and therefore the decrease of the field within the metal is no longer exponential but must follow a more complicated law. If we consider only the influence of the superconductor on the field outside the metal (and this is the only type of problem we encounter experimentally) then this circumstance may not be so important as it might seem. The reason of this is (see below) that the influence of the metal on the external field is determined by only one complex quantity – the surface impedance

$$Z(\omega) = R(\omega) + iX(\omega) = \frac{4\pi}{c}\left[\frac{E_x}{H_y}\right]_0 = -\frac{4\pi}{c}\left[\frac{E_y}{H_x}\right]_0, \tag{30}$$

where the symbol « 0 » designates that the fields $E_{y,x}$ and $H_{x,y}$ refer to the surface of the body.

If current and field are related in such a manner that a complex dielectric constant $\varepsilon'(\omega)$ can be introduced, then

$$Z(\omega) = \frac{4\pi}{c\sqrt{\varepsilon'(\omega)}}, \qquad \varepsilon'(\omega) = \varepsilon - i\frac{4\pi\sigma}{\omega} = \frac{16\pi^2}{c^2 Z^2}. \tag{31}$$

Up to terms of the order of $\sim 1/\varepsilon'$ the impedance is independent of the character of the field outside the metal (for radio frequencies and even in the infrared range $\varepsilon' \gg 1$ inside the metal and this approximation therefore is usually sufficient). It can be shown that this latter statement (the universality of impedance) is true even in the case when ε' cannot be introduced but on the condition that the metal remains a good conductor ([9]). Thus, in an isotropic metal impedance measurements do not permit to study how the field decays as it penetrates the metal (i.e. we cannot determine whether the quantity ε' can be applied or not). Thus if additional assumptions are not made preliminarly it does not seem possible to conclude from impedance measu-

([18]) A. A. Abrikosov: *Dokl. Akad. Nauk SSSR*, **86**, 43 (1952).

rements in isotropic samples (*) that the relation between field and current in a superconductor is not differential.

The impedance can always be expressed as follows:

$$(32)\quad Z = \frac{4\pi}{c\sqrt{\varepsilon'_{\text{eff}}(\omega)}}, \qquad \varepsilon'_{\text{eff}} = \varepsilon_{\text{eff}} - i\,\frac{4\pi\sigma_{\text{eff}}}{\omega} = \frac{16\pi^2}{c^2 Z^2} = \frac{16\pi^2}{c^2}\,\frac{(R^2 - X^2) - 2iXR}{(X^2 + R^2)^2},$$

where $\varepsilon'_{\text{eff}}$ is a new quantity playing the role of some effective dielectric constant (for normal skin effect $\varepsilon'_{\text{eff}} = \varepsilon'$; generally $\varepsilon'_{\text{eff}}$ equals ε' of a medium which acts on the field outside the metal in the same way as the metal does). The quantities $Z(\omega)$ and $\varepsilon'_{\text{eff}}$ possess neither poles nor zero's in the lower halfplane of the complex variable ω. It can be shown ([9]) that in particular, the following relation can be obtained

$$(33)\qquad \varepsilon_{\text{eff}} = 1 - \frac{\omega_s^2}{\omega^2} + 8\int_0^\infty \frac{\sigma_{\text{eff}}(\omega')\,d\omega'}{\omega'^2 - \omega^2}, \qquad \sigma_{\text{eff}} = \frac{1}{2\pi^2}\int_0^\infty \frac{\omega'^2\{\varepsilon_{\text{eff}}(\omega') - 1\}\,d\omega'}{\omega'^2 - \omega^2}$$

where we have to take the principal values of the integrals and it is taken into account that for $\omega \to 0$ and within the accuracy of the principal term (+)

$$(34)\qquad \varepsilon'_{\text{eff}} = \varepsilon_{\text{eff}} = -\frac{c^2}{\delta_0^2\omega^2} = -\frac{4\pi e^2 n_s}{m\omega^2} = -\frac{\omega_s^2}{\omega^2}.$$

In the infrared range of the spectrum, at any rate for such metals as Ag, Au, and Cu, there is a frequency range in which:

$$(35)\qquad \varepsilon'_{\text{eff}} \cong \varepsilon \cong -\frac{4\pi e^2 n_0}{m\omega^2} = -\frac{\omega_0^2}{\omega^2},$$

where by definition n_0 is the concentration of the conduction electrons (for details see ([3,17,19])). Although it is quite probable (and it is assumed below) that there is a region in which formula (35) is valid, this point, unfortunately, has not been definitely proved for any superconductor. According to preliminary data which require further refinement, for tin $n_0 \cong 6\cdot 10^{22}$. Comparing (35)

(*) The possibility of characterizing the metal by some tensor ε'_{ik} in the anisotropic case can be checked by measuring the dependence of $Z(\omega)$ on the angle between the crystal axis and the field.

(+) The relation (34) can be obtained from experimental facts even without verifying the validity of equation (1) from which the expression (34) follows directly (see ([4]) and ([29])).

([19]) V. L. Ginzburg and G. P. Motulevič: *Usp. Fiz. Nauk*, **55**, 469 (1955).

with (33) within the limits of the accepted approximation and neglecting unity in the latter equation (which is permissible with the approximation accepted here) one obtains the summation rule:

$$n_0 = n_s + \int_0^\infty n_b(\omega')\,\mathrm{d}\omega', \qquad n_b(\omega') = \frac{2m\sigma_{\mathrm{eff}}(\omega')}{\pi e^2}, \tag{36}$$

where the integration to infinity is quite formal as for the approximation accepted here: the upper limit is smaller than ω_0 or of the same order of magnitude; however the result practically does not depend on this limit. Formulae (33)-(36) are valid for any temperature T. The quantity $n_s = 2.83 \cdot 10^{11}/\delta_0^2$ is then equal to zero for $T = T_c$ and is maximum for $T_c = 0$ and equal to n_{s0}; for tin $\delta_0(T \to 0) \cong 5 \cdot 10^{-6}$ cm and $n_{s0} \cong 1.1 \cdot 10^{22}$. Thus, $n_0 > n_{s0}$ according to available data (which have to be further refined with respect to n_0, a quantity that is practically independent of temperature). If this is true, at $T \to 0$ part of the conduction electrons are in the superconducting state and a part $n_0 - n_{s0}$ change into some bound state. This signifies that for $T \to 0$ (see (33) and (36)):

$$\begin{cases} \varepsilon_{\mathrm{eff}} = 1 + \dfrac{4\pi e^2}{m}\displaystyle\int_0^\infty \frac{n_{b0}(\omega')\,\mathrm{d}\omega'}{\omega'^2 - \omega^2} - \frac{4\pi e^2 n_{s0}}{m\omega^2} = \varepsilon_{00}(\omega) - \frac{4\pi e^2 n_{s0}}{m\omega^2}, \\ n_0 = n_{s0} + \displaystyle\int_0^\infty n_{b0}(\omega')\,\mathrm{d}\omega', \qquad n_{b0} = \frac{2\pi}{\pi e^2}\sigma_{\mathrm{eff}}, \qquad (T = 0), \end{cases} \tag{37}$$

that is, the electrons with the concentration $n_0 - n_{s0}$ behave as bound electrons in the sense of the theory of dispersion. These considerations, which are a generalization of those discussed earlier ([3]), are of a very general nature and do not depend on the concrete form of the superconducting current equation. It follows that if $n_0 > n_{s0}$ in the cases for which formula (35) is valid some of the electrons at $T = 0$ must inevitably be in the bound state and ε_{00} which may have very high values must be taken into account. Indeed, for $\omega \ll \omega_c$ we have

$$\varepsilon_{00} = \frac{4\pi e^2}{m}\int_0^\infty \frac{n_{b0}(\omega')\,\mathrm{d}\omega'}{\omega'^2 - \omega^2} \sim \frac{4\pi e^2(n_0 - n_{s0})}{m\omega_c^2} \sim \frac{4\pi e^2 n_0}{m\omega_c^2} \sim \frac{4\pi e^2 n_0}{m(kT_c/\hbar)^2} \sim 10^7 \div 10^{10}, \tag{38}$$

i.e. the proper frequencies should be of the same order of magnitude as the frequency of the internal photoeffect threshold (i.e. of the quantum absorption threshold) ω_c. In (38) allowance is also made for the fact that even at $T = 0$ the frequency ω_c at which the superconductor begins to absorb electromag-

netic waves is probably of the following order of magnitude (*)

$$\omega_c \sim \frac{kT_c}{\hbar} \sim 10^{11} \div 10^{12}, \qquad \lambda_c = \frac{2\pi c}{\omega_c} \sim 0.1 \div 1 \text{ cm}. \tag{39}$$

At $\omega \sim \omega_c$ the dependence of ε_{00} on ω should be important while for $\omega > \omega_c$ absorption begins to take place, i.e. $\sigma_{\text{eff}} \neq 0$ if $(T \neq 0)$. For $T \neq 0$:

$$\begin{cases} \varepsilon'_{\text{eff}}(\omega, T) = \varepsilon_0(\omega, T) - \dfrac{4\pi e^2 n_s(T)}{m\omega^2} - i\,\dfrac{4\pi\sigma_{\text{eff}}(\omega, T)}{\omega}, \\ \varepsilon_0 = \dfrac{4\pi e^2}{m}\displaystyle\int_0^\infty \frac{n_b(\omega', T)\ \mathrm{d}\omega'}{\omega'^2 - \omega^2}, \qquad n_b(\omega, T) = \dfrac{2m\sigma_{\text{eff}}(\omega, T)}{\pi e^2}, \\ \varepsilon_0(\omega, 0) = \varepsilon_{00}(\omega), \qquad n_s(0) = n_{s0}, \qquad n_b(\omega, 0) = n_{b0}(\omega). \end{cases} \tag{40}$$

« Normal » electrons also contribute to ε_0 and σ_{eff} (for $\omega < \omega_c$ the magnitude of σ_{eff} is completely determined by these electrons; as it was already noted, for $T \to T_c$, $n_s \to 0$ and ε_0 and ε_{eff} approach to the respective values in the normal metal) (+). It seems natural to attempt to evaluate $\varepsilon_0(\omega)$ and $\sigma_{\text{eff}}(\omega)$ (which are related to normal electrons) by applying a method similar to that employed in the theory of the anomalous skin effect in metals in the normal state. It will not be possible to consider here the semi-quantitative results obtained by two different methods ([17,18]) and compared in ([9]).

Thus in a weak high frequency field the behaviour of the superconductor (with respect to measurements conducted outside the metal is determined by a complex quantity $\varepsilon_{\text{eff}}(\omega, T) = 16\pi^2/c^2 Z^2(\omega, T)$. In order to investigate superconductivity it is especially important to determine the frequency ω_c, the quantity $\varepsilon_{00}(\omega) - \varepsilon_0(\omega, 0)$ and the concentration of conduction electrons, without mentioning the concentration of superconducting electrons $n_{s0} = n_s\ (T = 0)$ which can also be found from static experiments (*).

(*) According to ([20]) for tin $\lambda_c < 0.83$ cm; measurements for lower wave lengths and for other metals are not available although the corresponding experiments are quite possible and their importance was emphasized over 10 years ago (see ([21])).

(+) It should be clear from the foregoing that ε_0 designates only one part of the effective dielectric constant, the sign « eff » is omitted in this case for sake of convenience.

([20]) E. Fawcett: *Proc. Phys. Soc.*, A **66**, 1071 (1953).

([21]) V. L. Ginzburg: *Žu. Eksper. Teor. Fiz.*, **14**, 134 (1944).

(*) For $\omega < \omega_c$ and $T \to 0$ as long as $\varepsilon_{\text{eff}} < 0$ the equality $\sigma_{\text{eff}} = 0$ signifies that $R = 0$ and $Z = iX = 4\pi\omega\delta_0(\omega)/c^2 = 4\pi/c\sqrt{\varepsilon_{\text{eff}}}$, where $\delta_0(\omega)$ is by definition the reactive depth of the skin thickness (depth of penetration of the field into the metal). Obviously $\delta_0(\omega) = \delta_0$ is the static depth used in § 1 (for $\omega \to 0$, $\varepsilon_{\text{eff}} = -4\pi e^2 n_s/m\omega^2 = -c^2/\delta_0^2\omega^2$).

Thus it is first of all necessary to measure the quantity $X(\omega, T \to 0)$ for a superconductor and to determine n_0 for the same metal from optical measurement (at any temperature).

3. Some Remarks on the Microscopic Theory of Superconductivity.

The foremost problem of the microscopic theory of superconductivity is the derivation of equation (1) which is assumed to be true for weak fields. Also the cause of superconductivity (which is not observed in metals of the first group) should be elucidated. Furthermore, the temperature dependence of specific heat, of the quantity $\varepsilon_0(\omega, T)$, of the « normal » conductance $\sigma_{\text{eff}}(\omega, T)$ and of some other quantities should also be determined. Finally, leaving aside secondary problems, the theory should explain why superconductivity disappears in fields $H > H_c$ and also throw light on the nature of the isotopic effect. At present sufficient clarity has not been attained in either of these directions but qualitatively some essential points seem to be quite clear. It is our pupose in this section of our paper to make some remarks relating to this question (for details see [22]).

There is quite a large number of investigations (see [22,23]) which are based on the assumption that certain spontaneous currents exist in the superconducting state. However, a number of considerations presented in [22] have led us to the conclusion that this hypothesis is untenable. Thus the diamagnetic hypothesis according to which the superconductor is similar to a gigantic atom seems to be more appealing in all respects. From this viewpoint one not only can understand qualitatively the essence of the problem but also give a quantum-mechanical interpretation [1] of basic equation (1) and this once again speaks in favour of this equation. Indeed, if $\Psi(\boldsymbol{r}_1, ..., \boldsymbol{r}_N)$ is the wave function for a system of N electrons, the current density will be:

$$(41)\quad \boldsymbol{j}(\boldsymbol{r}) = -\sum_{\alpha=1}^{N} \int \left\{ \frac{ieh}{2m} (\Psi^* \nabla_\alpha \Psi - \Psi \nabla_\alpha \Psi^*) - \frac{e^2}{mc} \boldsymbol{A}(\boldsymbol{r}_\alpha) \Psi^* \Psi \right\} \delta(\boldsymbol{r} - \boldsymbol{r}_\alpha)\, \mathrm{d}\boldsymbol{r}_1 \ldots \mathrm{d}\boldsymbol{r}_N ,$$

where in the general case the function Ψ is also a function of the field. In the absence of the field one may put $\boldsymbol{A} = 0$ and in the ground state $\Psi = \Psi_0$, $\boldsymbol{j} = 0$. If now Ψ does not change when the field is turned on, then:

$$(42)\quad \begin{cases} \boldsymbol{j}(\boldsymbol{r}) = -\dfrac{e^2}{mc} \displaystyle\sum_{\alpha=1}^{N} \int \boldsymbol{A}(r_\alpha) \Psi_0^* \Psi \delta(\boldsymbol{r} - \boldsymbol{r}_\alpha)\, \mathrm{d}\boldsymbol{r}_1 \ldots \mathrm{d}\boldsymbol{r}_N = -\dfrac{e^2 n_s(r)}{mc} \boldsymbol{A}(\boldsymbol{r}) , \\ n_s(\boldsymbol{r}) = \displaystyle\sum_{\alpha=1}^{N} \int \Psi^*(\boldsymbol{r}_1, \ldots \boldsymbol{r}_N) \Psi_0(\boldsymbol{r}_1, \ldots \boldsymbol{r}_N) \delta(\boldsymbol{r} - \boldsymbol{r}_\alpha)\, \mathrm{d}\boldsymbol{r}_1 \ldots \mathrm{d}\boldsymbol{r}_N . \end{cases}$$

---

[22] V. L. Ginzburg: *Usp. Fiz. Nauk*, **48**, 25 (1952); Translation in *Fortschritte der Physik* (Berlin), **1**, 101 (1953).

[23] H. Koppe: *Erg. der exakten Naturwiss.*, **23**, 283 (1950).

Assuming further, that $n_s(\boldsymbol{r}) = \text{const}$ and applying the operation « rot » to equation (42) we obtain equation (1) as $\text{rot}\,\boldsymbol{A} = \boldsymbol{H}$ and $\Lambda = m/e^2 n_s$. The same result will be obtained ([1,22]) if Ψ_0 changes in the field in the same way as it changes for a gauge transformation.

Superconductivity thus arises when the wave function is « rigid » (*) and the dependence of the superconductivity electrons concentration on the coordinate is sufficiently weak (as a matter of fact the function $n_s(\boldsymbol{r})$ should weakly vary over distances $\gtrsim \delta_0$). The « rigidity » of the wave function, on the other hand, is connected with the form of the energy spectrum of the system and it in particular arises if there is a gap between the excited and the ground state. This latter point is especially evident in the case of « atoms » of microscopic dimensions or of a charged Bose gas in a vessel ([22]) (this latter case has also been considered recently in ([24])). Thus the general features of the microscopic theory of superconductivity in certain respects seem to be clear and the main unsolved problem is the specification of a more detailed spectrum and the possibility of obtaining this spectrum on the basis of some model of the metal that takes into account the interaction between the electrons and between the lattice and the electrons. The presence of an isotopic effect indicates that this latter interaction is certainly essential and the gap width Δ in the electron spectrum thus depends on the mass of the atoms M (if $\Delta \sim kT_c$, then $\Delta \sim \text{const}/M^{\frac{1}{2}}$). Unfortunately the attempts to take into account the interaction between the electrons and the lattice ([25,26]) have not yielded any definite or convincing result ([22,26,27]) (+). Further progress in microscopic superconductivity theory will probably be possible only by taking into account the dielectric constant ε_0 especially if this constant is large (see § 2). In this case the contribution of thermal radiation to the specific heat is quite appreciable and an excitation of the photon type must necessarily be taken into account ([22]). The introduction of a narrow gap $\Delta \sim kT_c$ leads here to relatively large values of ε_0 and, moreover, permits one to interpret the destruction of superconductivity by the field as the result of Zeeman « closing » of the gap by the magnetic field ([22]). Finally, the introduction of a gap and the account of the influence of ε_0 leads to an exponential dependence of the

---

(*) Of course here we consider weak fields; the function Ψ can vary in strong fields and this is taken into account in § 1.

([24]) M. R. SCHAFROTH: *Phys. Rev.*, **96**, 1149, 1442 (1954).

([25]) H. FRÖHLICH: *Phys. Rev.*, **79**, 845 (1950); *Proc. Phys. Soc.*, A **64**, 129 (1951).

([26]) J. BARDEEN: *Rev. Mod. Phys.*, **23**, 261 (1951).

([27]) M. R. SCHAFROTH: *Helv. Phys. Acta*, **24**, 667 (1951); *Nuovo Cimento*, **9**, 291 (1952).

(+) An exclusion in this respect is the investigation of H. FRÖHLICH: *Proc. Roy. Soc.*, **223**, 296 (1954) in which, however, only the one-dimensional case is considered.

specific heat on temperature, a fact which can be observed experimentally ([28]).

Another trend in the theory of superconductivity which may be called quasimicroscopic, is connected with the treatment of superconductivity as a superfluidity of the metallic electron fluid. The development of such quasimicroscopic theory which would be similar to superfluidity theory ([29]) may turn out to be a fruitful line of advance (for details see ([22])).

([28]) W. S. Corak, B. B. Goodman, G. B. Satterthwaite and A. Wexler: *Phys. Rev.*, **96**, 1442 (1954).

([29]) L. D. Landau: *Journ. of Phys. USSR*, **5**, 71 (1941); **11**, 91 (1947).

RIASSUNTO (*)

Si discute una teoria macroscopica della superconduttività valida per campi magnetici di intensità arbitraria e il comportamento dei superconduttori in campi deboli di alta frequenza. Si considera altresì il problema della formulazione di una teoria microscopica della superconduttività.

(*) *Traduzione a cura della Redazione.*

IL NUOVO CIMENTO Vol. II, N. 6 1° Dicembre 1955

Synchrotron Oscillations in Strong-Focusing Accelerators.

(Linear Theory)

L. L. Goldin and D. G. Koškarev (*)

Academy of Sciences of the USSR - Moscow

(ricevuto il 20 Settembre 1955)

Summary. — Equations describing synchrotron oscillations in strong-focusing accelerators are deduced and solved. In deriving them it was taken into account that the accelerating field frequency is automatically connected with the magnetic field intensity. A general solution for oscillations both in the adiabatic and critical regions has been found, and respective integrals of motion have been obtained. It is shown that motion in the critical region may be simply represented by the « effective frequency » of oscillation. The paper investigates the influence of the fluctuations, ripples and noise of the frequency and amplitude of the accelerating voltage and magnetic field. Computation formulae are given for respective tolerances.

1. – Synchrotron Oscillation Equations.

Accelerated particles gain energy under the action of the h.f. electric field the frequency of which is equal to or is q times that of the particles' revolution within the annular chamber of the accelerator.

As usual, those particles which retain their phase relative to the accelerating field are called equilibrium particles, the other being called non-equilibrium particles. Denoting the maximum energy increase per revolution by eu, and the length of the particle orbit by L, the mean value of field intensity

(*) In the transliteration of Russian names we follow the International System of Transliteration of Cyrillic Characters (2nd Draft Iso Recommendation n°. 6, 1954), published at pag. 388 of the n°. 4 of the *Supplemento* to Vol. 1 (1955) of *Il Nuovo Cimento*.

being u/L, we find that the momentum change of the equilibrium particles is

$$\frac{\mathrm{d}p}{\mathrm{d}t} = \frac{eu \sin \Phi}{L}, \tag{1}$$

where Φ is the acceleration phase of the equilibrium particles with charge e.

Describing the non-equilibrium particles by their momentum Π and phase φ deviations from the momentum and phase of the equilibrium particles, we find (for small deviations):

$$\frac{\mathrm{d}\Pi}{\mathrm{d}t} = \frac{eu}{L}\varphi\cos\Phi + \frac{e}{L}\Delta u \sin\Phi, \tag{2}$$

where the term containing Δu takes account of the error in the accelerating voltage amplitude.

The phase deviations are described by the following equation:

$$\frac{\mathrm{d}\varphi}{\mathrm{d}t} = \Delta\omega_r - q\Delta\omega, \tag{3}$$

where $\Delta\omega_r$ is the r.f. error, and ω is the deviation of the particle revolution frequency from the ideal value.

Denoting by α the coefficient connecting the orbit elongation with the momentum error, we have:

$$\frac{\mathrm{d}L}{L} = \alpha\frac{\mathrm{d}p}{p}. \tag{4}$$

It can be readily seen that

$$\frac{\Delta\omega}{\omega} = \left[\frac{E_0^2}{E^2} - \alpha\right]\frac{\Pi}{p} + \alpha\frac{\Delta H}{H}, \tag{5}$$

where E = total relativistic energy of the particles,
E_0 = rest energy,
H = magnetic field intensity,

and

$$\omega = \frac{2\pi c}{L}\frac{pc}{E}. \tag{6}$$

From (2), (3), (5) and (6) we find

$$\frac{\mathrm{d}}{\mathrm{d}t}\left[\frac{E}{(E_0^2/E^2)-\alpha}\frac{\mathrm{d}\varphi}{\mathrm{d}t}\right] + \frac{2\pi q c^2 eu\cos\Phi}{L^2}\varphi = \frac{\mathrm{d}}{\mathrm{d}t}\left[\frac{E}{(E_0^2/E^2)-\alpha}\Delta\omega_r\right] - \frac{2\pi q c^2 eu\sin\Phi}{L^2}\frac{\Delta u}{u} - \frac{2\pi q\alpha c}{L}\frac{\mathrm{d}}{\mathrm{d}t}\left[\frac{E\sqrt{1-(E_0^2/E^2)}}{(E_0^2/E^2)-\alpha}\frac{\Delta H}{H}\right]. \tag{7}$$

Examining (7) one should bear in mind that $\Delta\dot{\omega}_r$ and ΔH generally are not independent quantities. If the accelerating field frequency follows the magnetic field intensity, the $\Delta\omega_r$ deviations are partly due to drift in the r.f. control system and partly to the magnetic field oscillations. It is natural to consider the latter deviations together with the term which depends on $\Delta H/H$. Assuming that the control system is characterized by the delay time τ, we have instead of the ideal law:

$$\omega_r = \frac{2\pi ceRq}{L} \frac{H}{(E_0^2 + H^2R^2e^2)^{\frac{1}{2}}}, \tag{8}$$

the following law

$$\Delta\omega_r + \tau \frac{\mathrm{d}}{\mathrm{d}t}(\Delta\omega_r) = \frac{2\pi c^2 qpE_0^2}{LE^3} \frac{\Delta H}{H}, \tag{9}$$

where R denotes the curvature radius of the equilibrium particle orbit in the guiding field H.

Of principal significance for practical purposes are the harmonic oscillations $\Delta H = H_w \sin wt$. Hence (9) yields

$$\Delta\omega_r = \frac{2\pi c^2 pE_0^2}{LE^3} q \frac{H_w}{H} \frac{\sin wt - w\tau \cos wt}{1 + w^2\tau^2}. \tag{10}$$

Substituting (10) into (7) and combining it with the term depending on $\Delta H/H$, we retain the notation $\Delta\omega_r$ for the deviations due only to drift in the r.f. control system. Noting further that the magnetic field ripple is due to the coil supply voltage V ripple, and neglecting the active resistance of the coil as compared with its impedance, we obtain

$$\frac{H_w}{H} = \frac{V_w \dot{H}}{V w H} = \frac{eu \sin \Phi}{Lwp} \frac{V_w}{V}. \tag{11}$$

Equation (7) thus acquires the following form:

$$\begin{aligned} \frac{1}{E}\left[\frac{E_0^2}{E^2} - \alpha\right] \frac{\mathrm{d}}{\mathrm{d}t}\left[\frac{E}{(E_0^2/E^2) - \alpha} \frac{\mathrm{d}\varphi}{\mathrm{d}t}\right] + \Omega_t^2 \varphi = \\ = \frac{1}{E}\left[\frac{E_0^2}{E^2} - \alpha\right] \frac{\mathrm{d}}{\mathrm{d}t}\left[\frac{E}{(E_0^2/E^2) - \alpha} \Delta\omega_r\right] - \Omega_t^2 \operatorname{tg} \Phi \frac{\Delta u}{u} + \frac{\Omega_t^2 \operatorname{tg} \Phi}{w(1 + w^2\tau^2)} \frac{\mathrm{d}}{\mathrm{d}t} \cdot \\ \cdot \left[\sin wt - \frac{w\tau}{(E_0^2/E^2) - \alpha} \frac{E_0^2}{E^2}\left(\cos wt + \alpha w\tau \frac{E^2}{E_0^2} \sin wt\right)\right] \frac{V_w}{V}, \end{aligned} \tag{12}$$

where

$$\Omega_t^2 = \frac{2\pi qc^2 eu \cos \Phi}{L^2} \frac{1}{E}\left|\frac{E_0^2}{E^2} - \alpha\right|. \tag{13}$$

Using the independent variable x, determined by

$$x = \frac{pc}{E_0}, \tag{14}$$

instead of time t, and assuming the momentum (and the magnetic field) to increase linearly with time so that the right side of (1) is constant, we obtain from (1):

$$\frac{\mathrm{d}x}{\mathrm{d}t} = \frac{ceu \sin \Phi}{E_0 L}. \tag{15}$$

To simplify calculations we shall use the quantities a and $f(x)$ defined, respectively, by

$$a^2 = \frac{1 - \alpha}{\alpha} \approx \frac{1}{\alpha}, \tag{16}$$

and

$$f(x) = \frac{1 - (x/a)^2}{(1 + x^2)^{\frac{3}{2}}} a^2 \alpha \approx \frac{1 - (x/a)^2}{(1 + x^2)^{\frac{3}{2}}}. \tag{17}$$

The strong-focusing accelerators are characterized by very small values of α, which makes the approximations of (16) and (17) quite accurate.

Equation (12) now takes the following form:

$$f(x) \frac{\mathrm{d}}{\mathrm{d}x}\left[\frac{1}{f(x)} \frac{\mathrm{d}\varphi}{\mathrm{d}x}\right] + \Omega_x^2 \varphi = \Omega_x^2 \operatorname{tg} \Phi \frac{\mathrm{d}}{\mathrm{d}x}\left[\frac{x}{f(x)\sqrt{1 + x^2}} \frac{\Delta\omega_r}{\omega_r}\right] - \Omega_x^2 \operatorname{tg} \Phi \frac{\Delta u}{u} - \tag{18}$$

$$+ \Omega_x^2 \frac{\operatorname{tg} \Phi}{w_x(1 + w^2\tau^2)} \frac{\mathrm{d}}{\mathrm{d}x}\left[\left(\sin wx - \frac{w\tau}{f(x)(1 + x^2)^{\frac{3}{2}}} \cos wx\right) \frac{V_w}{V}\right].$$

In (18) account has been taken of the fact that in cases of practical significance $\alpha\Omega_0^2\tau^2$ is much less than unity. When this is not the case the term $(E^2/E_0^2)\alpha w\tau \sin wx$ should be added to $\cos wx$. The following notations have been adopted in (18):

$$\Omega_x = \Omega_t \frac{\mathrm{d}t}{\mathrm{d}x} = \Omega_0 |f(x)|^{\frac{1}{2}}, \tag{19}$$

$$\Omega_0^2 = \frac{2\pi q E_0 \operatorname{ctg} \Phi}{eu \sin \Phi}, \tag{20}$$

Ω_0 being a dimensionsless quantity numerically equal to the frequency Ω_x at $x = 0$.

The free oscillation equation is derived from (18) by replacing its right

hand side by zero:

$$f(x)\frac{\mathrm{d}}{\mathrm{d}x}\left|\frac{1}{f(x)}\frac{\mathrm{d}\varphi}{\mathrm{d}x}\right| + \Omega_x^2\,\varphi = 0\,. \tag{21}$$

The equations (21) and (18) have regular singularities at $x = a$ when $f(x)$ vanishes. After the singularity, $f(x)$ changes sign; and the motion remains stable only when Ω_x^2, which is proportional to $f(x)$, does not change sign. To prevent change of sign, the acceleration phase must be shifted from Φ to $\pi - \Phi$.

After the critical point, the positive deviation of φ can be defined in two ways. It is natural to define it so that φ is continuous. Momentum Π likewise remains continuous at the critical point. These two conditions determine the transition through the critical point, with $\mathrm{d}\varphi/\mathrm{d}x$ changing sign at this point.

2. – Free Synchrotron Oscillations.

Introducing the new variables v and ψ

$$v = \varphi\Omega_x^{-\frac{1}{2}} \tag{22}$$

and

$$\psi = \int_a^x \Omega_x\,\mathrm{d}x\,, \tag{23}$$

ψ being the oscillation phase, we obtain the following equation instead of (21):

$$\frac{\mathrm{d}^2 v}{\mathrm{d}\psi^2} + \left[1 + \frac{1}{4}\frac{f_x''}{f^2\Omega_0^2} - \frac{7}{16}\frac{(f_x')^2}{|f|^3\Omega_0^2}\right]v = 0\,. \tag{24}$$

In cases of practical interest Ω_0 is very large: $\Omega_0 \gg 1$, so that the terms added to unity in (24) are significant only in the vicinity of $x = a$, where $f(x)$ vanishes. In this region they can be approximated by the first terms of their series expansions. Though this approximation becomes inadequate already at $|x - a| \approx 0.4\,a$, the entire correction is here so small that it is of no consequence.

In the vicinity of a

$$f(x) \approx \frac{2}{a^3}\left|1 - \frac{x}{a}\right|. \tag{25}$$

Equation (23) now takes the form:

$$\frac{\mathrm{d}^2 v}{\mathrm{d}\psi^2} + \left[1 - \frac{7}{36}\frac{1}{\psi^2}\right]v = 0\,. \tag{26}$$

The solution of (26) is

$$v(\psi) = \psi^{\frac{1}{2}}[A_1 J_{-\frac{2}{3}}(\psi) + A_2 J_{\frac{2}{3}}(\psi)], \tag{27}$$

where $J_{\frac{2}{3}}(\psi)$ and $J_{\frac{2}{3}}(\psi)$ are Bessel functions of order $\frac{2}{3}$. Going back to the variable φ, we obtain

$$\varphi = \left(\frac{\Omega}{\Omega_0}\right)^{\frac{1}{2}} \psi^{\frac{1}{2}} [c_1 J_{-\frac{2}{3}}(\psi) + c_2 J_{\frac{2}{3}}(\psi)]. \tag{28}$$

The signs of c_1 and c_2 do not depend on x being smaller or greater than a. This follows from the phase and momentum continuity at the critical point. It will be noted that E. Bodenstedt [1] who investigated the transition through the critical point by means of a mechanical model, because of the inadequacy of his model, came to the wrong conclusion that the sign of c_2 changes (see Fig. 10 in [1]). By large values of ψ (adiabatic region) the asymptotic representation of the Bessel functions can be used:

$$\varphi = \left(\frac{2}{\pi}\right)^{\frac{1}{2}} \left(\frac{\Omega}{\Omega_0}\right)^{\frac{1}{2}} \left[c_1 \cos\left(\psi + \frac{\pi}{12}\right) + c_2 \sin\left(\psi - \frac{\pi}{12}\right)\right]. \tag{29}$$

By small values of ψ, ($|x-a| \ll 0.4a$), φ is a simple function of $\xi = |x-a|$ readily found by means of (19), (20) and (25), ξ being the deviation from the critical point

$$\varphi = \frac{2^{\frac{1}{4}}}{a} \Omega_{\text{eff}}^{\frac{3}{4}} \xi [c_1 J_{-\frac{2}{3}}(\Omega_{\text{eff}}^{\frac{1}{2}} \xi^{\frac{3}{2}}) + c_2 J_{\frac{2}{3}}(\Omega_{\text{eff}}^{\frac{1}{2}} \xi^{\frac{3}{2}})], \tag{30}$$

where

$$\Omega_{\text{eff}} = \frac{2}{3^{\frac{2}{3}}} \Omega_0^{\frac{2}{3}} a^{-\frac{4}{3}} \approx \Omega_0^{\frac{2}{3}} a^{-\frac{4}{3}}. \tag{31}$$

A formula similar to (30) has been obtained for the critical region by Kolomenskij and Sabsovič [2], and by Johnsen [3]. To facilitate the transition from one region to another, the constants in (28), (29) and (30) have been chosen so that c_1 and c_2 retain their values in all equations, and thus are integrals of motion.

We shall now examine in greater detail equation (29) which describes the phase oscillations in the adiabatic region.

[1] E. Bodenstedt: *Ann. der Phys.*, **15**, 35 (1954).

[2] A. A. Kolomenskij and L. L. Sabsovič: *O prohoždenii čerez kritičeskuju energiju v uskoritele s žëstkoj fokusirovkoj* (*On the passage through the critical energy in the strongfocusing accelerator*, unpublished Report, 1953).

[3] K. Johnsen: *Phase Oscillations and Transition Energy Problems* (Lecture presented at the Conference on the Alternating-Gradient Proton Synchrotron, Geneva, 1953).

The present frequency of the synchrotron oscillations is equal to

$$\frac{\mathrm{d}\psi}{\mathrm{d}x} = \Omega_x \,. \tag{32}$$

The oscillation amplitude diminishes when the critical point is approached, and increases after it has been passed, changing as $(\Omega/\Omega_0)^{\frac{1}{2}} = f^{\frac{1}{4}}(x)$. It reaches its maximum value equal to $0.6a^{-\frac{3}{4}}(c_1^2+c_2^2-c_1c_2)$ at $x = (3a^2+2)^{\frac{1}{2}}$. Equations (12) and (18) are derived from (2), (3) and (5) by eliminating the momentum Π. In a similar manner it is possible to eliminate the phase and obtain the momentum oscillation equation. We shall rather derive the momentum value from the solution itself. Replacing t by x in (2) we get

$$\Pi = \frac{E_0}{c}\operatorname{ctg}\Phi\int_{x_a}^{x}\varphi\,\mathrm{d}x + \frac{E_0}{c}\int_{x_0}^{x}\frac{\Delta u}{u}\,\mathrm{d}x \,. \tag{33}$$

From (29) and (33) it follows that the momentum and phase oscillation amplitudes in the adiabatic region are connected by the relation

$$\frac{A_\Pi}{A_\varphi} = \frac{E_0\operatorname{ctg}\Phi}{c\Omega_x} \,, \tag{34}$$

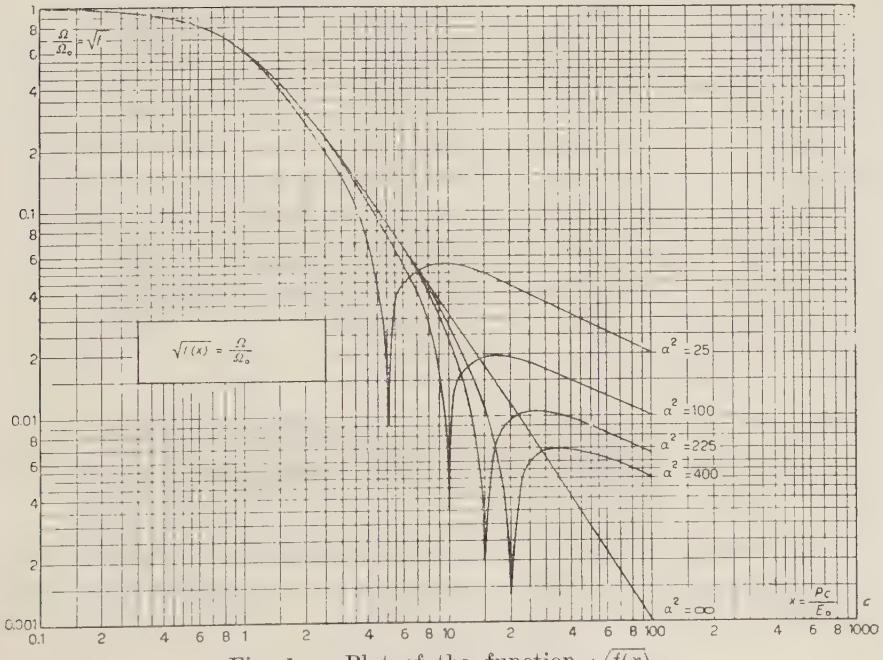

Fig. 1. – Plot of the function $\sqrt{f(x)}$.

so that in this region

$$\Pi(x) = \left(\frac{2}{\pi}\right)^{\frac{1}{2}} \frac{E_0 \operatorname{ctg} \Phi}{c\Omega_0} \left(\frac{\Omega_0}{\Omega}\right)^{\frac{1}{2}} \left| c_1 \sin\left(x - \frac{\pi}{12}\right) - c_2 \cos\left(x - \frac{\pi}{12}\right) \right| . \tag{35}$$

The equations (29) and (35) depend on the function Ω/Ω_0 which is plotted in Fig. 1.

In the critical region we have

$$\Pi(\xi) = \left(\frac{2}{3}\right)^{\frac{1}{3}} \frac{E_0 \operatorname{ctg} \Phi}{c\Omega_0^{\frac{1}{3}}} \xi^{\frac{1}{2}} \left[c_1 J_{\frac{1}{3}}(\Omega_{\text{eff}}^{\frac{3}{2}} \xi^{\frac{3}{2}}) + c_2 J_{-\frac{1}{3}}(\Omega_{\text{eff}}^{\frac{3}{2}} \xi^{\frac{3}{2}}) \right] . \tag{36}$$

It follows from (35) that the amplitude of momentum oscillations increases when the critical point is approached. Further on, up to the point $x = (3a^2 - 2)^{\frac{1}{2}}$, the amplitude drops and then again rises, roughly as $x^{\frac{1}{2}}$. It will be noted that at $x = 0$, according to (36), we have

$$\Pi(a) \approx 0.8 \frac{E_0 \operatorname{ctg} \Phi c_2}{c(\Omega_0 \Omega_{\text{eff}})^{\frac{1}{2}}} . \tag{37}$$

A comparison of (35) and (37) shows that the oscillations in the critical region are described by the «effective frequency» determined by (31). Practically the same value of Ω_{eff} is obtained from (29) and (30).

The effective frequency defines nearly all the tolerances in the critical region. More detailed calculations lead to the following at first sight rather surprising result. Correct solutions for a wide range of problems associated with forced oscillations within the critical region may be obtained by assuming the oscillations to be harmonic with constant amplitude and constant effective frequency.

For a beam of particles it is of interest to compute the mean square phase and momentum deviations which are of particular value for noise problems.

Equation (29) may be written in the following form:

$$\varphi = a_1 \cos \psi + b_1 \sin \psi , \tag{38}$$

where

$$a_1 = \left(\frac{2}{\pi}\right)^{\frac{1}{2}} \left(\frac{\Omega}{\Omega_0}\right)^{\frac{1}{3}} \left| c_1 \cos\frac{\pi}{12} - c_2 \sin\frac{\pi}{12} \right| , \tag{39}$$

$$b_1 = \left(\frac{2}{\pi}\right)^{\frac{1}{2}} \left(\frac{\Omega}{\Omega_0}\right)^{\frac{1}{3}} \left| c_2 \cos\frac{\pi}{12} + c_1 \sin\frac{\pi}{12} \right| . \tag{40}$$

for a beam of particles

$$a_1 = A \cos \chi ; \qquad b_1 = A \sin \chi , \tag{41}$$

where A and χ are arbitrary amplitude and phase. Averaging over A and χ we find

$$\overline{\varphi^2} = \tfrac{1}{2}\overline{A^2} = \tfrac{1}{2}(\overline{a_1^2} + \overline{b_1^2}) = \frac{1}{\pi}\frac{\Omega}{\Omega_0}(\overline{c_1^2} + \overline{c_2^2} - \overline{c_1 c_2}) . \tag{42}$$

From (40) one may readily obtain

$$\overline{c_1^2} = \overline{c_2^2} = \overline{2c_1 c_2} , \tag{43}$$

whence

$$\overline{\varphi^2} = \frac{3}{2\pi}\frac{\Omega}{\Omega_0}\overline{c_2^2} . \tag{44}$$

Comparing the mean square momentum deviations at the critical point and in the adiabatic region, we get

$$\frac{\overline{\Pi_c^2}}{\overline{\Pi_{ad}^2}} = 1.2\,\frac{\Omega_r}{\Omega_{eff}} . \tag{45}$$

3. – Electrical Supply and Radio-Frequency System Tolerances (Non-Resonance Case).

Parameter oscillations of frequency close to that of the synchrotron oscillations are particularly essential because of strict tolerances. They deserve special attention and will be duly taken into account in § 5. More rapid oscillations being quickly averaged are not dangerous and are, therefore, disregarded here.

We shall now consider the rapid changes (jumps) having the form of step functions, and the slow (compared with free oscillation frequency) changes of $\Delta\omega_r$, ΔU, and ΔV.

3·1. *Tolerances Connected with ω_r Jumps.* – To find the oscillation amplitude increase due to the rapid changes of ω_r we shall integrate (18) over the duration of the jump. Assuming the initial values of φ and φ' to be zero, we get

$$\varphi' = \Omega_0^2 \operatorname{tg} \Phi \frac{x}{(1 + x^2)^{\frac{1}{2}}}\frac{\Delta\omega_r}{\omega_r} . \tag{46}$$

Thus the jump $\Delta\omega_r$ occurring in the adiabatic region produces oscillations having an amplitude

$$A_\varphi = \Omega_0^2 \frac{x \operatorname{tg} \Phi}{\Omega_r (1 + x^2)^{\frac{1}{2}}}\frac{\Delta\omega_r}{\omega_r} . \tag{47}$$

The value of x in (47) corresponds to the moment of jump. Further on, this amplitude changes in accordance with the usual formulae, i.e., as $(\Omega/\Omega_0)^{\frac{1}{2}}$.

The influence of the ω_r jumps increases near the critical point. This influence can be readily evaluated in close proximity to the critical point, where the Bessel functions are well approximated by the first term of the series expansion. As can be readily seen, in this case

$$\Delta c_2 \approx 0.6 \frac{a^2 \operatorname{tg} \Phi \Omega^{\frac{3}{2}}}{\Omega_{\text{eff}} \xi} \frac{\Delta\omega_r}{\omega_r}, \tag{48}$$

resulting in very tight tolerances. It should, however, be noted that in this case, only those changes of ω_r should be regarded as jumps which are rapid compared with ξ^{-1} changes. Thus, strict tolerances are imposed only on extremely sharp changes of ω_r, which in practice is not very restrictive. With (34) we obtain the momentum oscillation amplitude due the ω_r jump:

$$A_{\Pi} = \frac{E_0}{c} \frac{\Omega_0^2 x}{\Omega_x^2 (1 + x^2)^{\frac{1}{2}}} \frac{\Delta\omega_r}{\omega_r}. \tag{49}$$

3·2. *Tolerances Due to Slow Changes of $\Delta\omega_r$, ΔU, and ΔV.* – The influence of smooth (compared with free oscillations) oscillations of $\Delta\omega_r$, $\Delta U/U$ and $\Delta V/V$ are readily calculated if one considers the right side of (18) as a constant and finds the shift of the equilibrium point. The maximum deviation is twice as large as the equilibrium point shift. Thus the maximum phase deviation is

$$\varphi = 2 \operatorname{tg} \Phi \frac{\mathrm{d}}{\mathrm{d}x} \left[\frac{x}{(1 + x^2)^{\frac{1}{2}}} \frac{\Omega_0^2}{\Omega_x^2} \frac{\Delta\omega_r}{\omega_r} \right] - 2 \operatorname{tg} \Phi \frac{\Delta u}{u} + \\ + \frac{2 \operatorname{tg} \Phi}{w(1 + w^2\tau^2)} \frac{\mathrm{d}}{\mathrm{d}x} \left[\sin wx - \frac{w\tau \cos wx}{(1 + x^2)^{\frac{3}{2}}} \frac{\Omega_0^2}{\Omega_x^2} \right] \frac{V_w}{V}, \tag{50}$$

and the maximum momentum deviation is

$$\Pi = 2 \frac{E_0}{c} \frac{x}{(1 + x^2)^{\frac{1}{2}}} \frac{\Omega_0^2}{\Omega_x^2} \frac{\Delta\omega_r}{\omega_r} - 2 \frac{E_0}{c} \frac{w}{\Omega_x^2} \frac{u_w}{u} + \\ - 2 \frac{E_0}{c} \frac{1}{(1 + w^2\tau^2)w} \left[\sin wx - \frac{\Omega_0^2}{\Omega_x^2} \frac{w\tau \cos wx}{(1 + x^2)^{\frac{3}{2}}} \right] \frac{V_w}{V}. \tag{51}$$

Formulae (50) and (51) are strictly applicable only to the adiabatic region. But, as mentioned above, in the critical region Ω_x can be simply replaced by Ω_{eff}, which is well confirmed by more rigorous computations. Denoting the allowable phase and momentum deviations in the critical region by $\Delta\varphi$ and $\Delta\Pi$, (50) and (51) yield

$$\frac{\Delta\omega_r}{\omega_r} = \frac{\Delta\Pi}{p} \frac{1}{2} \left| \frac{eu \sin \Phi}{2\pi q E_0 \operatorname{ctg} \Phi} \right|^{\frac{1}{3}} \left(\frac{E_0}{E_{cr}} \right)^{\frac{5}{3}}, \tag{52}$$

and

$$\frac{\Delta\omega_r}{\omega_r} = \frac{\Delta\varphi}{2\ \mathrm{tg}\ \Phi}\left[\frac{eu\ \sin\ \Phi}{2\pi q E_0\ \mathrm{ctg}\ \Phi}\right]^{\frac{1}{3}}\left(\frac{E_0}{E_{cr}}\right)^{\frac{4}{3}}. \tag{53}$$

4. – Transitions Through the Critical Point.

As stated above, the transition through the critical point requires the shift of the acceleration phase from Φ to $\pi - \Phi$. This phase change cannot be accomplished at the precise moment when the equilibrium particle reaches the critical point. The timing error will be denoted by τ_1. For simplicity it is assumed that the acceleration phase change is retarded. Owing to the equations' symmetry with regard to the critical point, this assumption is of no consequence. During the interval between the transition through the critical point and the phase shift of the r.f., Ω_x^2 in (20) is negative, which corresponds to the particle defocusing. In this interval, the particles' motion is described by the following formula:

$$\varphi = \frac{2^{\frac{1}{4}}}{a}\,\Omega_{\mathrm{eff}}^{\frac{1}{2}}\xi\left[c_1 i^{\frac{2}{3}} J_{-\frac{2}{3}}(i\Omega_{\mathrm{eff}}^{\frac{3}{2}}\xi^{\frac{3}{2}}) + c_2 i^{-\frac{2}{3}} J_{\frac{2}{3}}(i\Omega_{\mathrm{eff}}^{\frac{3}{2}}\xi^{\frac{3}{2}})\right], \tag{54}$$

with c_1 and c_2 having the same values they had before the critical point. At the point $\Delta\xi$ the solutions (54) and (30) must be matched, which determines the changes in the values of the constants. Denoting these changes by Δc_1 and Δc_2, and assuming $\Delta\xi$ to be small, we obtain

$$\begin{cases} \dfrac{\Delta c_2}{c_1} \approx 2\,\Omega_{\mathrm{eff}}\,\Delta\xi\,, \\ \dfrac{\Delta c_1}{c_1} \approx -\,0.8\,\Omega_{\mathrm{eff}}^3\,\Delta\xi^3\,. \end{cases} \tag{55}$$

$\Delta c_2/c_1$ and $\Delta c_1/c_1$ should be small, say, equal to 0.1. Then

$$\Delta x = 5\cdot 10^{-2}\,\Omega_{\mathrm{eff}}^{-1}. \tag{56}$$

Thus, the timing error (in seconds) must not exceed

$$\tau_1 = 5\cdot 10^{-2}\left[\frac{eu\ \sin\ \Phi}{2\pi q E_0\ \mathrm{ctg}\ \Phi}\right]^{\frac{1}{3}}\left(\frac{E_{cr}}{E_0}\right)^{\frac{4}{3}}\frac{E_0 L}{ceu\ \sin\ \Phi}. \tag{57}$$

The r.f. phase cannot be changed instantly. This causes an increase in the phase oscillation amplitude. Let us evaluate this effect, assuming that the

r.f. voltage is switched off on a time τ_2, after which it is switched on in the right phase. During τ_2 the particles move without acceleration. It would therefore seem natural to regard x as a constant. However, the computations are simpler when one assumes that x changes according to the old law. Thus the continuing increase of the magnetic field intensity and of the r.f. is properly taken into account. For simplicity it will be assumed that the r.f. voltage is switched off after the transition through the critical point. The equation of motion can be obtained from (18) if we replace $\Delta u/u$ by -1 and exclude $\Omega_x^2\varphi$. Then

$$\frac{\mathrm{d}}{\mathrm{d}x}\left[\frac{1}{f(x)}\frac{\mathrm{d}\varphi}{\mathrm{d}x}\right] = \Omega_0^2 \operatorname{tg}\Phi\,. \tag{58}$$

Integrating (58) and using (25) for $f(x)$ we find

$$\begin{cases} \varphi = \varphi_0 + \tfrac{1}{2}\varphi_0'\dfrac{\xi^2-\xi_0^2}{\xi_0} + \dfrac{2\operatorname{tg}\Phi\Omega_0^2}{a^4}\left[\left(\tfrac{1}{3}\xi - \tfrac{1}{2}\xi_0\right)\xi^2 - \tfrac{1}{6}\xi_0^3\right], \\ \varphi' = \xi\xi_0^{-1}\varphi_0' - \dfrac{2\operatorname{tg}\Phi\Omega_0^2}{a^4}\left[\xi - \xi_0\right]\xi\,, \end{cases} \tag{59}$$

where ξ_0 is the r.f. switch-off moment, and ξ the switch-on moment. At ξ, this solution should be compared with (30) which determines the change of c_1 and c_2. Neglecting the cubic terms we obtain for small $\Delta\xi = \Delta x$

$$\begin{cases} \Delta c_1 = 0\,, \\ \Delta c_2 = \Omega_{\mathrm{eff}}\Delta x c_1 + 1.3\,\dfrac{\Omega_0^2}{a^3}\operatorname{tg}\Phi\Delta x\,. \end{cases} \tag{60}$$

Having determined Δc_1 and Δc_2 it is easy to find the oscillation amplitude increase at the most dangerous point $x = (3a^2-2)^{\frac{1}{2}}$. Since the momentum deviations are most significant in the critical region where the free oscillations reach their maximum, the momentum shift common to all particles should be computed by (60):

$$\Delta x = a\,\frac{\Delta\Pi}{p}\,, \tag{61}$$

$$\tau_2 = \frac{\Delta\Pi}{p}\,\frac{E_{cr}}{E_0}\,\frac{E_0 L}{ceu\sin\Phi}\,. \tag{62}$$

5. – Resonance.

Oscillator frequency, r.f. amplitude, and coil supply voltage may ripple with frequency equal to that of the phase oscillations. In this case resonance occurs and the oscillation amplitude increases.

We shall now examine the resonance harmonics of the forcing terms in (18). Since the various terms are not coherent, each may be considered separately. In the adiabatic approximation, (18) can be written as

$$\varphi'' + \Omega_x^2 \varphi = d \exp[i(wx+\alpha)], \tag{63}$$

where α is the phase of the forcing term.

The free oscillations corresponding to (63) can be represented as follows:

$$\varphi = \varphi_1 e^{\psi i} + \varphi_1^* e^{-i\psi}. \tag{64}$$

Imposing on φ_1 and φ_1^* the additional condition:

$$\varphi_1' e^{i\psi} + \varphi_1^{*\prime} e^{-i\psi} = 0 \tag{65}$$

and using (65) and (64), we can readily solve (63)

$$\varphi_1 = \frac{d}{2i\Omega_x} \int_{x_0}^{x} \exp[i(wx - \psi + \alpha)]\,dx. \tag{66}$$

Expanding the frequency Ω_x at the resonance point, we obtain

$$\Omega_x = w + \Omega'_{\text{res}}(x - x_{\text{res}}) + \dots. \tag{67}$$

Then

$$\varphi_1 = \frac{d \exp[i\beta]}{2\Omega_x i} \int_{x_0 - x_{\text{res}}}^{x - x_{\text{res}}} \exp[-i\Omega'_{\text{res}}(z^2/2)]\,dz. \tag{68}$$

Integration of (68) with $x - x_{\text{res}} = \infty$, $x_0 - x_{\text{res}} = -\infty$ yields:

$$\varphi = 2R_e\varphi_1 \exp[i\psi] = \frac{d}{\Omega_x}\left[\frac{2\pi}{\Omega'_{\text{res}}}\right]^{\frac{1}{2}} \cos(\psi - \gamma'). \tag{69}$$

Averaging over the phase γ we obtain

$$\overline{\varphi^2} = \frac{\pi d^2}{\Omega_{\rm res}^2 \Omega'_{\rm res}} = \frac{2\pi d^2}{\Omega_0^2 \Omega_{\rm res} f'_{\rm res}}. \tag{70}$$

Comparing (63) and (18) and taking into account the change of oscillation amplitude with frequency, we finally get:

$$\begin{cases} \overline{\Delta\varphi^2} = \dfrac{\pi}{2} \operatorname{tg}^2 \Phi \dfrac{\Omega}{f'_{\rm res}} \dfrac{\Omega_0^2 x^2}{1 + x^2} \left(\dfrac{\omega_\Omega}{\omega}\right)^2, \\ \overline{\Delta\varphi^2} = \dfrac{\pi}{2} \operatorname{tg}^2 \Phi \dfrac{\Omega}{f'_{\rm res}} \dfrac{\Omega_{\rm res}^2}{\Omega_0^2} \left(\dfrac{u_\Omega}{u}\right)^2, \\ \overline{\Delta\varphi^2} = \dfrac{\pi}{2} \operatorname{tg}^2 \Phi \dfrac{\Omega}{f'_{\rm res}} \dfrac{\Omega_{\rm res}^2}{\Omega_0^2 (1 + \Omega_{\rm res}^2 \tau^2)} \left[1 + \dfrac{\Omega_0^4 \tau^2}{\Omega_{\rm res}^2 (1 + x^2)^3}\right] \left(\dfrac{V_\Omega}{V}\right)^2, \end{cases} \tag{71}$$

where ω_Ω, u_Ω, and V_Ω are the harmonic components of $\Delta\omega$, Δu and ΔV ($\Delta\omega = \sum_0^\infty \omega_\Omega \cos(\Omega_x + \alpha)$, etc.).

Our results agree with those obtained by BLACHMAN [4]. Formulae (71) yield the mean square values of the oscillation phase change at arbitrary time. In these formulae, Ω_x denotes frequency at x, and $\Omega_{\rm res}$ the resonance frequency under consideration. These formulae have no singularities at the critical point, which is quite understandable, as, when approaching the critical point, the resonances are passed in a shorter time during which no appreciable increase of the synchrotron oscillations occurs. Thus, there is no need for special examination of the critical region. Note that the resonance frequencies are only those that are confined between Ω_0 and $\Omega_{\rm eff}$. At $x = (3a^2+2)^{\frac{1}{2}}$, where the frequency change velocity vanishes, the third term of the expansion (67) should be considered. In this case

$$\begin{cases} \overline{\Delta\varphi^2} = 2.2 \operatorname{tg}^2 \Phi \Omega_0^{\frac{10}{3}} a^{\frac{7}{3}} \left(\dfrac{\omega_\Omega}{\omega}\right)^2, \\ \overline{\Delta\varphi^2} = 0.85 \operatorname{tg}^2 \Phi \Omega_0^{\frac{4}{3}} a^{-\frac{2}{3}} \left(\dfrac{u_\Omega}{u}\right)^2, \\ \overline{\Delta\varphi^2} = 0.85 \operatorname{tg}^2 \Phi \Omega_0^{\frac{4}{3}} a^{-\frac{2}{3}} \left(\dfrac{V_\Omega}{V}\right)^2. \end{cases} \tag{72}$$

Special attention should be given to the momentum oscillations which attain their maximum value at the critical point. Total momentum deviation is expressed by (37) with c_2 substituted from (44) and (71).

[4] N. M. BLACHMAN: *Rev. Sci. Instr.*, **21**, 908 (1950).

6. – Noise.

Investigating the build-up of oscillations due to noise, BLACHMAN [4] solved the problem taking no account of adiabatic damping. He examined (12) using the adiabatic approximation

$$\frac{\mathrm{d}^2 q}{\mathrm{d}t^2} - \Omega_t^2 q = F(t)\,, \tag{73}$$

where $F(t)$ is a noise with spectral intensity Φ per cycle/second and for band width. According to (1) the mean square value of phase deviation is

$$\overline{\varphi^2} = \frac{1}{2}\int_{t_0}^{t} \frac{\Phi}{\Omega_t^2}\,\mathrm{d}t\,. \tag{74}$$

Comparing (12) with (73) and using x instead of t we get

$$\overline{\varphi^2} = 2\pi^2 \frac{E_0 L}{ceu \sin \Phi}\int_{x_0}^{x} \nu\,\mathrm{d}x\,, \tag{75}$$

for noise frequency modulation having the spectral intensity ν in cycle^2/cycle,

$$\overline{\varphi^2} = \tfrac{1}{2}\,\mathrm{tg}^2\,\Phi \frac{ceu \sin \Phi}{E_0 L}\int_{x_0}^{x} \eta \Omega_x^2\,\mathrm{d}x\,, \tag{76}$$

for noise modulation of r.f. voltage $\Delta u/u$ having spectral intensity η in cycle^{-1}, and

$$\overline{\varphi^2} = \tfrac{1}{2}\,\mathrm{tg}^2\,\Phi \frac{ceu \sin \Phi}{E_0 L}\int_{x_0}^{x} \left[\Omega_x^2 + \frac{\Omega_0^4 \tau^2}{(1 + x^2)^3}\right] \frac{\mu\,\mathrm{d}x}{(1 + \Omega^2\tau^2)^2}\,, \tag{77}$$

for coil supply voltage $\Delta V/V$ noise modulation with spectral intensity μ in cycle^{-1}.

We shall now derive an expression for φ^2 with due account of adiabatic changes of oscillation amplitude, which is especially significant for strong-focusing accelerators.

From (29) we obtain

$$\frac{\mathrm{d}\varphi^2}{\mathrm{d}x} = \varphi^2 \frac{f'}{2f}\,. \tag{78}$$

Differentiating (75) we get

$$\frac{\mathrm{d}(\overline{\varphi^2})}{\mathrm{d}x} = 2\pi^2 \frac{E_0 L}{ceu \sin \Phi}\, \nu\,, \tag{79}$$

for the phase build-up due to noise frequency modulation.

The adiabatic damping and noise build-up being independent of each other, (78) and (79) yield

$$f^{\frac{3}{2}}(x) \frac{\mathrm{d}}{\mathrm{d}x} [f^{-\frac{1}{2}}(x) \overline{\varphi^2}] = 2\pi^2 \frac{E_0 L}{ceu \sin \Phi}\, \nu\,. \tag{80}$$

Integrating (80) we obtain

$$\overline{\varphi_\nu^2} = 2\pi^2 \nu \frac{E_0 L}{ceu \sin \Phi} f^{\frac{1}{2}}(x) \int_{x_0}^{x} f^{-\frac{1}{2}}(x)\, \mathrm{d}x\,. \tag{81}$$

Similarly, we get

$$\varphi_\eta^2 = \tfrac{1}{2} \operatorname{tg}^2 \Phi_l \frac{ceu \sin \Phi}{E_0 L} \Omega_0^2 f^{\frac{1}{2}}(x) \int_{x_0}^{x} f^{\frac{1}{2}}(x)\, \mathrm{d}x\,, \tag{82}$$

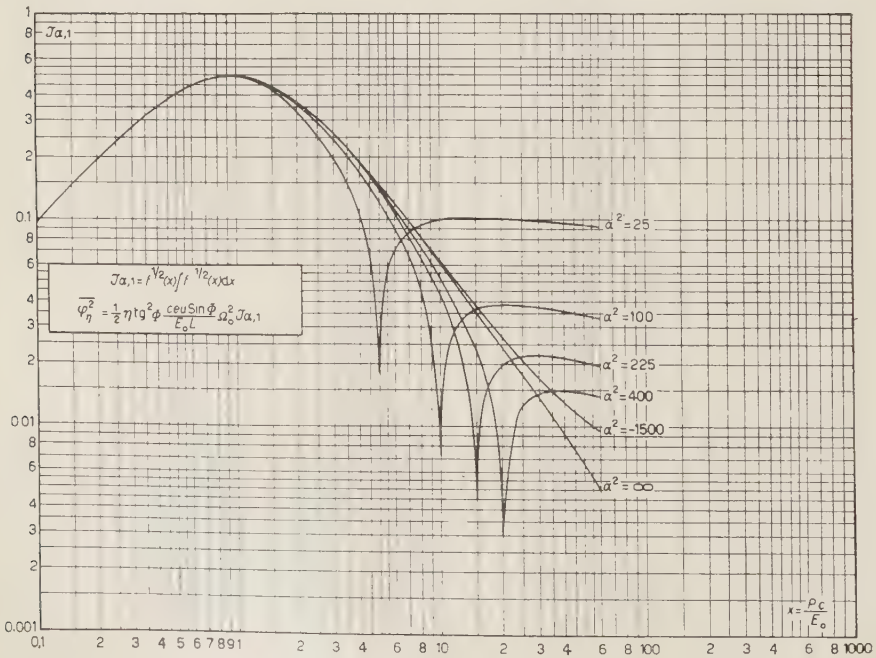

Fig. 2. – Plot of the function $\mathcal{J}_{\alpha,1}$.

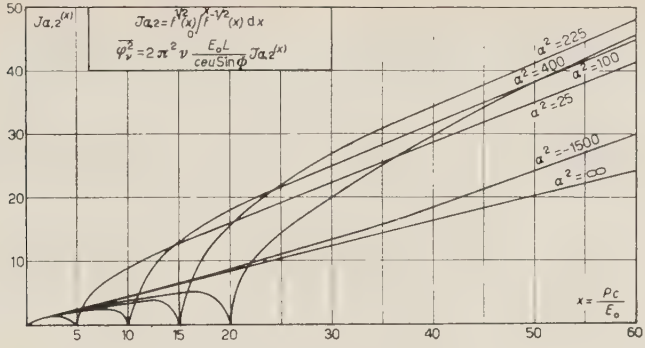

Fig. 3. – Plot of the function $\mathcal{J}_{\alpha,2}$.

for noise modulation of r.f. voltage, and

$$\overline{\varphi_\mu^2} = \tfrac{1}{2}\,\mathrm{tg}^2\,\Phi\mu\,\frac{ceu\,\sin\,\Phi}{E_0L}\,\Omega_0^2 f^{\frac{1}{2}}(x)\int_{x_0}^{x}\left|f^{\frac{1}{2}}(x)+\frac{\Omega_0^2\tau^2}{(1+x^2)^3}f^{\frac{1}{2}}(x)\right|\frac{dx}{(1-\Omega^2\tau^2)^2}\,, \tag{83}$$

for coil supply voltage noise modulation.

In (81), (82) and (83) it was assumed that ν, η and μ do not depend on frequency. These formulae define $\overline{\varphi^2}$ in the adiabatic region.

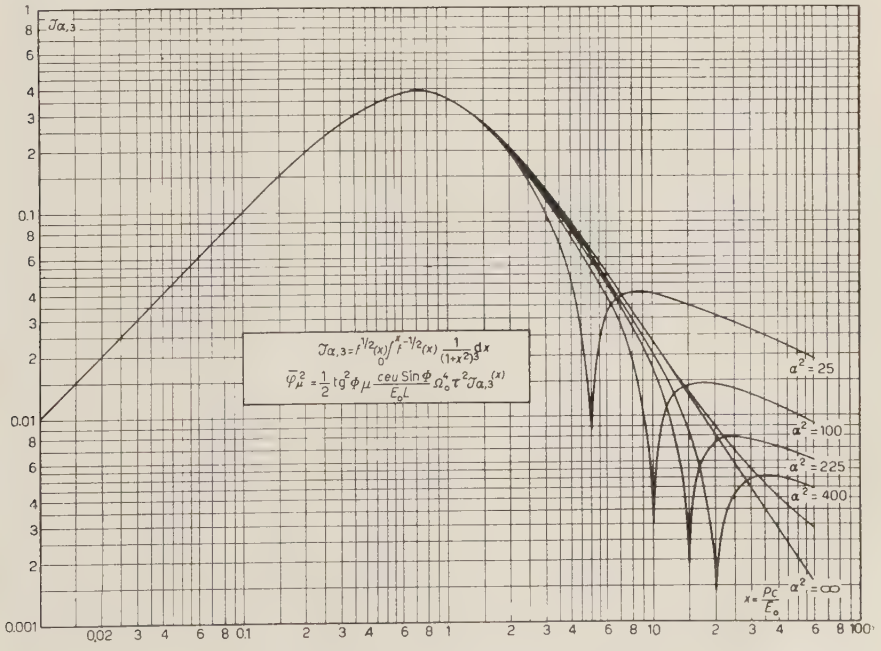

Fig. 4. – Plot of the function $\mathcal{J}_{\alpha,3}$.

Since the influence of noise drops when the critical point is approached, (81), (82) and (83) may be used for the entire acceleration cycle.

Of particular interest is the mean square value of momentum deviation in the critical region.

It may be computed by (37) and (44) substituting $\overline{\varphi^2}$ from (81), (82) and (83).

In conclusion we present in Figs. 2, 3, 4 the plots of the following functions:

$$\mathcal{J}_{\alpha,1} = f^{\frac{1}{2}}(x)\int_0^x f^{\frac{1}{2}}(x)\,\mathrm{d}x; \qquad \mathcal{J}_{\alpha,2} = f^{\frac{1}{2}}(x)\int_0^x f^{\frac{1}{2}}(x)\,\mathrm{d}x; \qquad \mathcal{J}_{\alpha,3} = f^{\frac{1}{2}}(x)\int_0^x \frac{f^{\frac{1}{2}}(x)}{(1-x^2)^3}\,\mathrm{d}x\,.$$

Along with several positive values of a^2 we have computed these functions also for a negative value $a^2 = -1500$, considering the strong-focusing accelerators without critical energy as proposed by VLADIMIRSKIJ and TARASOV (5).

(5) V. V. VLADIMIRSKIJ and K. I. TARASOV: *On the Possibility of eliminating the critical energy in the strong-focusing accelerator* (Paper presented to the International Conference on the Peaceful Uses of Atomic Energy, Geneva, 1955).

RIASSUNTO (*)

Si deducono e risolvono equazioni che descrivono le oscillazioni di sincrotrone negli acceleratori a focalizzazione intensa. Nel ricavarle si è tenuto conto del fatto che la frequenza del campo acceleratore è automaticamente collegata all'intensità del campo magnetico. Si è trovata una soluzione generale sia per le oscillazioni nella regione adiabatica sia per quelle nella regione critica e si sono ottenuti i rispettivi integrali di moto. Si dimostra che nella regione critica il moto può essere semplicemete rappresentato dalla «frequenza effettiva» di oscillazione. Il lavoro esamina l'influenza delle fluttuazioni, ondulazioni e disturbi della frequenza e dell'ampiezza della tensione acceleratrice e del campo magnetico. Si danno formule di calcolo per le rispettive tolleranze.

(*) *Traduzione a cura della Redazione.*

IL NUOVO CIMENTO Vol. II, N. 6 1° Dicembre 1955

The Scattering of Protons with Energies 460-660 MeV on Protons (*).

S. J. Nikitin, J. M. Selector, E. G. Bogomolov and S. M. Zombkovskij
Academy of Sciences of the USSR – Moscow

(ricevuto il 20 Settembre 1955)

Summary (*). — The scattering p-p is studied with protons obtained from the syncrocyclotron of the Institute for Nuclear Problems of the Academy of Sciences of the URSS. The scattering cross-section and the angular distribution have been measured in the interval of energies from 460 up to 660 MeV. The results show that practically up to the proton-energies of 460 MeV the scattering cross-section is isotropic, in the interval 560-660 MeV it is markedly anisotropic. A discussion of the results obtained is given.

(*) *Editor's care.*

1. – Introduction.

In these last years a number of investigations on proton-proton scattering within the energy-intervall 100÷435 MeV was published [1,5]. It was found that in this energy interval the scattering is isotropic in the center of mass

(*) The paper was presented at the All Union Conference on Cosmic-Rays and High-Energy Particles held in Moscow in December 1954.

(**) In the transliteration of Russian names we follow the International System of Transliteration of Cyrillic Characters (2nd Draft Iso Recommendation n°. 6, 1954), published at pag. 388 of the n°. 4 of the *Supplemento* to Vol. 1 (1955) of *Il Nuovo Cimento*.

(1) O. Chamberlain, E. Segrè and C. Wiegand: *Phys. Rev.*, **83**, 923 (1951).

(2) C. Z. Oxley and R. D. Schamberger: *Phys. Rev.*, **95**, 1350 (1954).

(3) D. Fisher and D. Goldhaber: *Phys. Rev.*, **95**, 1350 (1954).

(4) O. Chamberlain, G. Pettengill, E. Segrè and C. Wiegand: *Phys. Rev.*, **95**, 1349 (1954).

(5) O. A. Towler: *Phys. Rev.*, **85**, 1024 (1952).

(c. m.) system, the absolute scattering cross-section being practically independent on the energy and equal to 3.7 mb.

At the energy of the protons near to 430 MeV a certain deviation from the isotropy of the scattering is observed, but the results of the investigations performed with protons of this energy are not in a fair agreement. So in the paper of J. MARSHALL, L. MARSHALL and NEDZEL ([6,7]) it was found that at $E_p = 429$ MeV the scattering cross-section at $\theta = 90°$ equalled 3.42 mb and fell down to 2.86 mb at $\theta = 28°$, at the same time according to the work of MOTT, SUTTON, FOX and KANE ([8]), performed with 435 MeV protons the scattering cross-section equalled 3.39 mb at $\theta = 90°$ and rose up to 4.49 mb at $\theta = 25.2°$. Recently SUTTON, FIELD and collaborators ([9]) published a notice on the (p-p) scattering at $E_p = 437$ MeV. They observed that the differential cross-section slightly increases at small angles ($\sigma(16.6°)/\sigma(90°) = 1.16$) which contradicts the results of MARSHALL *et al.* and is in bad agreement with the result of MOTT, SUTTON, FOX and KANE at the proton-energy $E_p = 435$ MeV.

In the present work the (p-p)-scattering was studied with protons having energies of 460, 560 and 660 MeV. The measurements were performed at the synchro-cyclotron of the Institute for Nuclear Problems of the Academy of Sciences of the USSR.

2. – Method.

The protons obtained from the synchro-cyclotron had energies of 460 and 660 MeV. The protons with energies of 560 MeV were obtained by retarding the 660 MeV protons in carbon-filters.

2·1. *Experimental set-up used with* 460 MeV *protons.* – The experimental set-up used in experiments with 460 MeV protons is shown at Fig. 1.

In the present work paraffin scattering targets were used. The proton-proton scattering effect was obtained as a difference of the entire scattering effect obtained

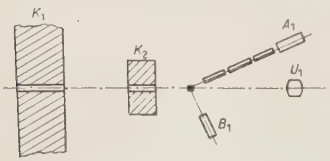

Fig. 1. – Collimator-arrangement used in experiments with 460 MeV protons. K_1: first collimator; K_2: second collimator; A_1; B_1: counter-telescopes; U_1: ionization chamber.

([6]) J. MARSHALL, Z. MARSHALL and V. A. NEDZEL: *Phys. Rev.*, **92**, 884 (1953).
([7]) J. MARSHALL, V. A. NEDZEL and Z. MARSHALL: *Phys. Rev.*, **93**, 927 (1954).
([8]) W. E. MOTT, R. B. SUTTON, J. G. FOX and J. A. KANE: *Phys. Rev.*, **90**, 712 (1953).
([9]) R. B. SUTTON, T. H. FIELDS, J. G. FOX, J. A. KANE, W. E. MOTT and R. A. STALLWOOD: *Bull. Amer. Phys. Soc.*, **29**, 75 (1954).

with paraffin targets and that obtained with carbon targets equivalent in carbon content.

The external beam of protons from the synchro-cyclotron, thoroughly collimated, was directed to the scattering target. The scattered protons were registered by the telescope A_1, containing four proportional counters, the corresponding recoil-protons were registered by the counter B_1 (*). At angles smaller than 45°, where the energy of the recoil-protons was too small for the simultaneous registration of the scattered and the recoil-protons, only the scattered protons were registered by telescope A_1.

The collimator-arrangement used in experiments with 460 MeV protons contained two collimators. The first collimator K_1 was mounted within the 1.5 m concrete shield and consisted of brass-tubes tightly fitting one into the other. At a distance of about 4 m from the first collimator was installed the second collimator K_2, mounted within the 1 m concrete wall. The aperture of the first collimator varied in different experiments from 2 to 3 cm. The aperture of the second collimator was of 5 cm.

The first three counters of the telescope A_1 were 2 cm in diameter and 14.5 cm long and were mounted in a common glass-envelope. The construction of these counters is shown in Fig. 2. The fourth counter of telescope A_1,

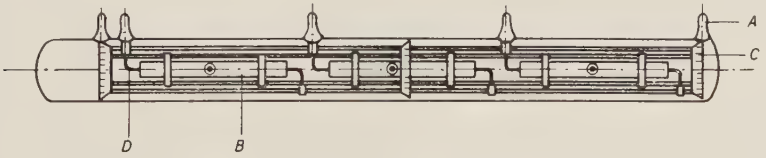

Fig. 2. – Schematic view of the counter-telescope. A: glass-envelope; B: copper-tubes; C: stainless-steel supports; D: copper supports of the inner wires of the counters.

as well as counter B_1 registering the recoil protons, were 4 cm in diameter and 15 cm long. All the counters were filled with spectrally pure argon and methane (100 mm_{Hg} A + 300 mm_{Hg} CH_4).

The counters of the telescope A_1 worked at a potential difference of 200 ÷ 2400 V, the counters of the telescope B_1 at 2500 ÷ 2800 V.

The pulses of the counters were amplified by preamplifiers and were fed to the coincidence-circuits. The gain of each of the channels was of $1.5 \cdot 10^4$. The resolution-time of the coincidence-circuit was of $2 \cdot 10^{-7}$ s. The number of coincidences between the telescopes A_1 and B_1 and the number of coincidences in the telescope A_1 were simultaneously registered.

(*) We denote the high-energy proton as scattered proton, and the less-energetic proton as recoil-proton.

If two protons, taking part in the p-p scattering are to be registered and a fair angular resolution is to be obtained it is necessary that the solid angle subtended by the registering-system should be determined by the longer telescope A_1.

In order to be able to register all the recoil-protons corresponding to the scattered protons registered by the telescope A_1 it is necessary to use in the telescope B_1 counters of considerably large dimensions. In the present experiments, when determining the angular dependence of the scattering cross-section, the counter B_1 was of too small a diameter to be able to register all recoil-protons. This led to the necessity of accounting for the variation of the solid angle subtended by the registering system with the scattering-angle. When measuring the absolute values of the cross-section the telescope B_1 contained a larger counter and all the recoil-protons were registered.

2·2. *Experimental set-up used with* 560 *and* 660 MeV *protons.* – The location of the collimators in experiments with 560 and 660 MeV protons is shown in Fig. 3. The protons from the synchro-cyclotron were deflected by the analyzing magnet M and were collimated by two collimators K_1 and K_2. The collimator K_1 was made out of a steel rod 3,6 m long mounted in the 4 m concrete wall. The aperture of the collimator was of 5 cm. The collimator K_2 was placed at a distance of about 6 m from collimator K_1.

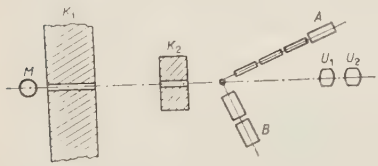

Fig. 3. – Collimator-arrangement used in experiments with 560-660 MeV protons. M: deflecting maguet; K_1: first collimator; K_2: second collimator; A, B: counter-telescopes; U_1, U_2: ionization chambers.

The scattered protons were registered by the telescope A, that was the same used in experiments with 460 MeV protons. The recoil-protons were registered by the telescope B that contained two counters 8 cm in diameter and 14 cm long, and all the recoil-protons corresponding to the scattered protons, passing through the telescope A were registered.

In most cases the distance between the back part of the last counter of the telescope B and the scattering target was of 50 cm. The distance between the scattering target and the end of the third counter of telescope A, which determined the solid angle, was in most cases of 90 cm. The distance between the third and fourth counters of the telescope A was of 7.5 cm. For the purpose of reducing the energy of the protons inside the collimator K_2 carbon-filters could be inserted. After the proton beam had passed through the filters, it was additionally collimated by a brass-tube with the inner diameter 1.9 cm, because the angular divergence of the proton

beam increased considerably, owing to scattering, when it passed through the filters.

2·3. *The measurement of the intensity of the proton beam.* – The relative intensity of the proton beam was measured by means of the ionization chambers In experiments with 460 MeV protons one ionization chamber was placed in the proton beam.

The schematic arrangement of the chamber is shown in Fig. 4. The chamber was filled with pure argon at a pressure of 2 at. The ionization current of the chamber was amplified by a balance electrometric circuit, the output of which was fed to a d.c. amplifier with a recording galvanometer (*).

The balance electrometric circuit and the d.c. amplifier showed a perfect stability, so the zero-drift of the entire device corresponded to the change of the input voltage of the electrometric circuit by 1-2 mV, compared with the change of the input voltage, due to the proton beam, of 200-300 mV.

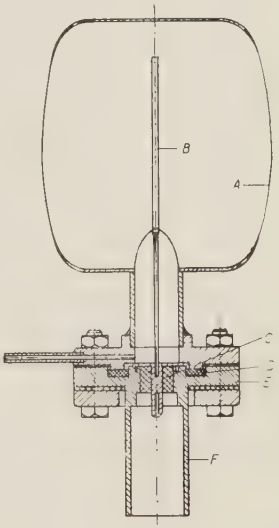

Fig. 4. – Cross-section of the ionization chamber. A: outer electrode of the chamber; B: collecting electrode; C: amber insulator; D: rubber gasket; E, F: shielding tube.

In the experiments with 560 and 660 MeV protons two ionization chambers were placed into the proton beam. The first chamber was used with the same d.c. amplifier as in the experiments with 460 MeV protons. The output of the second chamber was fed to a current integrating device. The absolute calibration of the ionization chambers was performed by comparing the ionization current of the chambers with the charging current of the Faraday cage, specially constructed for this investigation.

2·4. *Scattering targets.* – The paraffin and carbon scattering targets were of cylindrical form and were suspended within a frame, that could be rotated about the vertical axis. During the measurements of the angular dependance of the scattering cross sections the dimensions of the targets were slightly smaller than the beam dimensions. So the targets had diameters equal to $1.5 \div 2$ cm, with the beam diameter $2 \div 3$ cm. During the measurements of the

(*) The d.c. amplifier was constructed by L. L. GOLDIN to whom the authors express their deep thanks.

absolute value of the cross-section the dimensions of the targets exceeded the beam dimensions. The thickness of the paraffin target corresponded to $1.190 \cdot 10^{23}$ hydrogen atoms per cm^2.

The paraffin targets and the corresponding carbon targets contained equal number of carbon atoms per cm^2.

2·5. *Controlling experiments.* – One of the important characteristics of the registering apparatus, showing its correct and stable performance, is the independance of the number of coincidences on the potential of the high voltage supply of the counters (counting plateau). The existence of the counting plateau was verified before each of the series of measurements by simultaneous alteration of the working potential of all counters and by alteration of the working potential of one of the counters with fixed potential on all other counters. A typical curve obtained in the latter case is shown in Fig. 5. As the height of the pulses given by the proportional counters depends on the energy of the protons, the counting plateau curves were obtained for two positions of the telescopes A and B, corresponding to the upper and lower limits of the angular interval investigated. The existence of the counting plateau indicates that the amplified height of the counter pulses considerably exceeds the operation threshold of the circuit and is levelled at the last stages of the amplifier. Thus the number of the coincidences registered does not depend on the variations of the gas amplification of the counters and on the gain of the amplifiers.

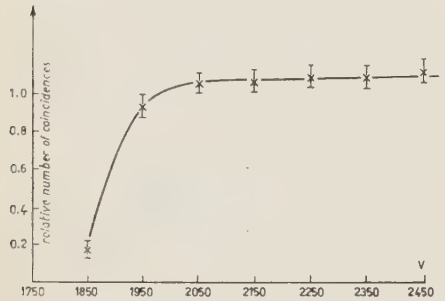

Fig. 5. – The dependence of the coincidences, registered by telescope A on the working potential of one counter, with fixed potential at all other counters.

During the measurements of the angular dependence of the scattering cross-section and of its absolute value serious errors can arise if slow protons are present in the incident proton beam. The absence of a considerable admixture of slow protons in the incident beam was verified in the following manner. As it follows from expression (1) the angle between the directions of the scattered and recoil protons equals 90° for slow protons, and for the protons with $E_p = 450$ MeV it is less than 84° (*). By measuring the dependence of the coincidence-number on the angle between scattered and recoil protons we are able to obtain some data on the number of slow protons

(*) At the scattering angle in c.m. system $\theta = 90°$.

present in the beam. Such measurements were performed with 460 and 660 MeV-protons. The results obtained with 660 MeV-protons are presented in Fig. 6.

The consi'erable width of the curve is due to the large dimensions of counter B. In order to increase the angular resolution, the counter telescope B was moved away from the target to a distance equal to 120 cm. As it can be seen from the figure, the number of coincidences between the telescopes A and B is practically zero when the angle between their axes is of 90°, indicating the absence of slow protons within the incident proton beam.

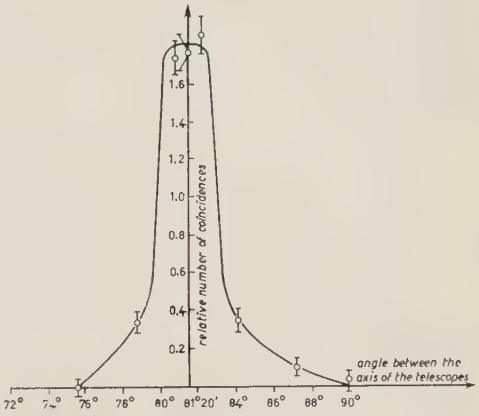

Fig. 6. – The dependence of the number of coincidences on the angle between the axes of the telescopes.

With the 560 MeV protons the diagram as that of Fig. 6 could not be obtained, and only the absence of the coincidences at the angle $\theta = 90°$ between the axes of telescopes A and B was verified.

Proportional counters of a large diameter (up to 8 cm) were used in the experiments. The travelling time of the electrons within the counter from the walls of the counter to the wire may be comparable with the resolving time of the coincidence circuit. In order to show that there are no serious losses in the coincidences registered, the resolving time of the coincidence circuit was varied within the limits $0.2 \div 0.6$ per s.

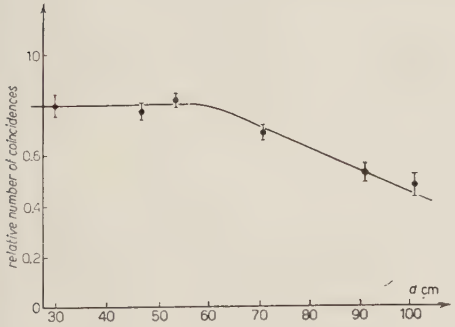

Fig. 7. – The dependence of the number of coincidences between telescopes A and B on the distance from the telescope B to the target.

During this experiment the number of coincidences remained practically constant.

At the proton energy of 560 and 660 MeV all the recoil protons corresponding to the scattered protons registered by telescope A were counted. In order to verify this, the number of coincidences between the telescopes A and B at different distances between telescope B and the target was measured. This control was performed with 660 MeV protons at scattering angles of 30° and 40° in the c.m. system (12° 51′ and 11° 21′ in the la-

boratory coordinate system). The results obtained are shown in Fig. 7. From the curve given it is seen, that at distances between the end of the second counter of telescope B and the target under 70 cm, the number of coincidences between the telescopes A and B does not depend on the distance and thus all recoil protons corresponding to the scattered protons passing through telescope A are registered. In analogous manner it was shown that all recoil protons were registered at a scattering angle equal to 12°56′ (c.m. system). From the curve of the Fig. 7 it also follows, that the multiple scattering of the recoil protons within the target does not affect the number of coincidences registered.

2. – Measurements of the angular dependance of the p-p scattering.

In the present work the relative angular dependence of the scattering cross section was measured first. The absolute value of the cross section was measured for several angles and from these data the whole curve of the angular dependence was normalized. The relative scattering cross section was obtained from the measured values, using the relation:

$$\sigma = A \left(\frac{N_1}{L_1} - \frac{N_2}{L_2} \right) ,$$

where N_1 and N_2 are it the numbers of coincidences measured by the telescopes and B with the paraffin and carbon targets respectively, and L_1 and L_2 the respective integral intensities of the proton beam, expressed in relative units (the number of counts of the integrating ionization chamber, or the area under the curve of the recording galvanometer).

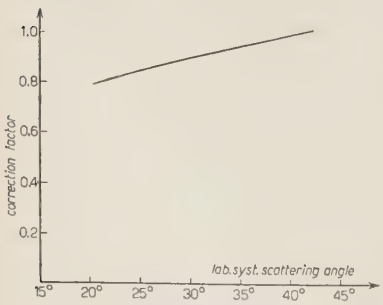

Fig. 8. – The dependence of the correction factor on the laboratory system scattering angle.

The simultaneous registration both of the scattered and recoil protons was performed at 460 MeV within the angle interval 45°÷60°, at 560 MeV within 40÷90° and at 660 MeV within 30°÷90°. (c.m. system).

As at the proton energy 460 MeV the apparatus did not register all the recoil protons, corresponding to the scattered protons registered by telescope A, a correction, that was numerically computed, was introduced. The angular dependence of this correction is shown in Fig. 8. The correctness of the computations of this correction was checked experimentally by measuring the ratio of the

scattering cross-section at 45° and 90° by means of a larger counter B, which registered all the recoil protons.

The data obtained were in accurate agreement with those obtained with the smaller counter, after the correction mentioned above was introduced.

At 460 MeV within the angle interval $30° \div 45°$ only the single scattered protons were registered. In order to exclude the slow protons and π-mesons, generated in reactions $p+p \to \pi+d$ and $p+p \to \pi+p+n$ between the third and fourth counters of telescope A_1 a 125 g/cm² tungsten filter was inserted. The data obtained were normalized with the data obtained by simultaneous registration of the scattered and recoil protons at $\theta = 45°$. In the case when both of the protons taking part in the p-p scattering were registered, the background determined using the carbon target was of about $8 \div 14\%$ at 460 and 660 MeV and did not exceed 25% at 560 MeV. In the case, when only a single proton was registered, the ratio of the number of coincidences obtained with the paraffin target to that of the carbon target was $1.2 \div 1.3$

For each of the proton energy values several series of angular dependance measurements were performed. Usually the results of each of the series were in fair agreement.

3. – The measurements of the absolute differential scattering cross-sections.

The absolute value of the scattering cross-section was measured for 460 MeV protons at 41°49′ and 27°19′, for 560 MeV protons at 26°52′ and for 660 MeV protons at 17°21′ and 26°22′ (laboratory system).

Before each of the absolute cross-section measurements the calibration of the ionization chambers by means of the Faraday cage was performed. The absolute value of the cross-section was obtained from the relation:

$$\sigma_{\text{lab}} = \frac{N_c}{n\Omega N},$$

where n is the number of hydrogen atoms per cm² of the target, Ω the solid angle, N the number of protons crossing the target per second, N_c the number of true p-p coincidences per second.

The largest errors are brought in by the determination of the effective solid angle.

In order to determine the effective solid angle, the number of coincidences, in the telescope A was registered for two different distances between the telescope A and the target. The solid angle Ω was obtained from the relation: $\Omega = s/x^2$, where s is the counter cross-section area, and x is determined from the ratio of the number of coincidences of telescope A in the various posi-

tions $N(x)$ and $N(x+r)$:

$$x = \frac{r}{1 - \sqrt{N(x)/N(x+2)}}$$

both $N(x)$ and $N(x-r)$ being normalized to equal integral intensity of the proton beam.

This method allows to obtaine Ω with an accuracy up to $3.5 \div 4\%$. The determination of the solid angle was performed immediately before each measurement of the absolute cross-section value.

The targets were manufactured out of paraffin of a known chemical content. The error in n did not exceed 0.5%.

The error in the determination of N results from the sum of the errors in the measurement of the relative intensities and from the errors in the calibration of the chambers with the Faraday cage. The errors in the measurements of relative intensity are due to the errors in the intensity readings of the recording galvanometer ($0.5 \div 1\%$), to the errors due to non linearity of the electronic circuit (not more than 0.5%) and to the errors due to zero-drift of the electrometric circuit (not more than $0.6 \div 0.1\%$). The mean value of the error in the relative measurements does not exceed $1.3 \div 1.4\%$. The calibrating errors of the ionization chambers consist from the errors in the capacity determinations of the Faraday cage (less than 0.8%), from the errors due to the corrections accounting for the residual gas pressure within the envelope ($1 \div 1.25\%$) and from the errors due to zero-drift of the electrometric circuit (less than 0.5%). Besides this it is necessary to account for the subjective error due to the observer, which amounts to about 1%. Thus the mean error in the proton intensity determination amounts to about $1.8 \div 2\%$.

4. – Results.

The results of the determination of the absolute cross-section are presented in the Table I.

TABLE I. – *The results of the absolute cross-section measurements.*

E_p (MeV)	ϑ (laborat. syst.)	cm²/sterad $\times 10^{27}$
460	41° 41′	1.10 ± 0.03
460	27° 19′	1.55 ± 0.03
560	26° 52′	1.51 ± 0.13
660	17° 21′	2.32 ± 0.12
660	26° 22′	1.46 ± 0.07

The first measurements of the absolute cross-section values brought us at $E_p = 460$ MeV to the value $\sigma_{c.m.} = 4.2 \cdot 10^{-27}$ cm²/steradian (at $\theta = 90°$). As these measurements were carried out with a relatively low accuracy, additional measurements of the absolute cross-section were performed. In these measurements the 460 MeV proton beam was obtained by retarding the 660 MeV protons in carbon filters, placed at the input part of the collimator (Fig. 3). The scattered protons were registered by means of telescope *A*, containing four proportional counters, and the recoil protons were registered by telescope *B*, containing two proportional counters each 8 cm in diameter and 14 cm long.

All the recoil protons, corresponding to the scattered protons registered by telescope *A*, were counted. By this method were obtained the cross-section values given in Table I (E=460 MeV, $\vartheta = 27°19'$).

The averaged results of the angular dependence measurements were normalized according to the results of the absolute measurement (Table I) and the cross-section data for the c.m. system were obtained using the relation

$$\sigma(\theta) = \frac{[1 + (E/Mc^2)\sin^2\varphi]}{1 + (E/2Mc^2)} \cdot \frac{1}{4\cos\varphi}\,\sigma(\vartheta),$$

where E is the kinetic energy of the primary protons, M the proton rest mass, $\sigma(\theta)$ and $\sigma(\vartheta)$ the cross-sections in the c.m. and laboratory system respectively.

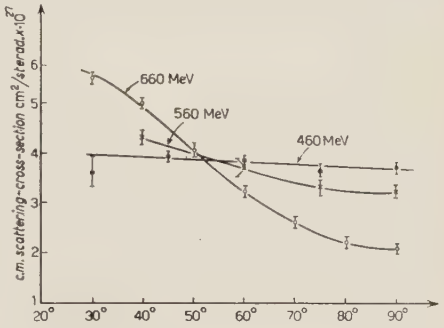

Fig. 9. – The dependence of the scattering cross-section on the angle at 460, 560 and 660 MeV.

The results obtained for the c.m. system are shown in Fig. 9 and are given in Tables II-IV.

At $E_p = 460$ MeV the recoil protons corresponding to the protons scat-

TABLE II. – *Differential cross-section of the* p-p *scattering at* 460 MeV.

Scattering angle (c.m. system)	cm²/sterad $\times 10^{27}$
30°	3.58 ± 0.31
45°	3.89 ± 0.09
60°	3.82 ± 0.09
75°	3.60 ± 0.12
90°	3.68 ± 0.09

TABLE III. – *Differential cross-section of the* p-p *scattering at* 560 MeV.

Scattering angle (c.m. system)	cm²/sterad $\times 10^{27}$
40°	4.32 ± 0.14
60°	3.66 ± 0.19
75°	3.28 ± 0.14
90°	3.22 ± 0.13

TABLE IV. – *Differential scattering cross-section at* 660 MeV.

Scattering angle (c.m. system)	cm²/sterad	Scattering angle (c.m. system)	cm²/sterad
	$\times 10^{27}$		$\times 10^{27}$
30°	5.47 ± 0.12	70°	2.59 ± 0.10
40°	4.97 ± 0.10	80°	2.19 ± 0.11
50°	4.03 ± 0.12	90°	2.06 ± 0.08
60°	3.21 ± 0.12		

tered on 45° (c.m. system) suffered considerable multiple scattering within the target. The data obtained were corrected for this by introducing a numerically computed correction amounting to $\sim 4.5\%$.

5. – Discussion.

The most striking feature of the data obtained is the appearance of a marked anisotropy of the scattering at 560÷660 MeV. As it is well known the scattering remains strictly isotropic (in the c.m. system) up to proton energies of 400 MeV. In the energy-region 415÷435 MeV, data obtained by various authors are in some contradiction. One may assume that at these energies the scattering cross-section slightly rises towards the small angles. Further at $E_p = 460$ MeV, according to the results of the present work, the ratio of the scattering cross-section at 45° and 90° equals 1.06 i.e. there is no considerable anisotropy of scattering. These results are in agreement with the results of SUTTON *et al.* ([9]), who obtained for $\sigma(45°)/\sigma(90°) = 1.16$ at $E_p = 435$ MeV and disagree with the results of MARSHALL *et al.* ([6,7]), who obtained $\sigma(45°)/\sigma(90°) = 0.84$ at $E_p = 429$ MeV and with the results of MOTT. SUTTON *et al.* ([8]) according to which $\sigma(45°)/\sigma(90)° = 1{,}32$ at $E_p = 435$ MeV.

The results of the present experiments show, that practically up to proton-energies of 460 MeV the scattering cross-section does not depend on the scattering angle. The scattering of the 560 MeV protons is markedly anisotropic, the ratio of $\sigma(45°)$ to that of $\sigma(90°)$ being equal to 1.34. Finally the scattering of the 660 MeV protons is roughly anisotropic: $\sigma(45°)/\sigma(90)° = 2.66$.

The appearence of the anisotropy of scattering at proton energies of 560÷660 MeV, is due to the presence of scattered waves with $l > 0$ and is not surprising. A more surprising feature of the scattering process is just the absence of any anisotropy in the 100÷400 MeV region.

From Fig. 9 it follows, that at $\theta = 90°$ the scattering cross-section rapidly falls with energy. At small energies a reverse situation is observed: here the cross-section rapidly rises with energy. At the scattering angles

lying between $50^\circ \div 55^\circ$ the scattering cross-section remains independent from energy in the energy interval $460 \div 660$ MeV and its value is the same than at energies of $260 \div 400$ MeV.

The absolute cross-section value of 460 MeV protons at $\theta = 90^\circ$ (3.68 mb) exceeds considerably the possible maximum-value of the S-scattering. The large value and the practically isotropic character of the scattering may be explained assuming a considerable yield in the scattering cross-section of D and F states.

A comparison of the results obtained was not performed because of lack of any adequate theories of nuclear forces. Due to the same reason no single-valued phase-analysis of the present results can be performed.

An analogous work was performed (scattering of $460 \div 660$ MeV protons) by M. G. MEŠČERJAKOV and others ([10-12]). The data obtained by them agree with the results of the present work within the limits of experimental errors.

* * *

The authors express their thanks to Prof. A. I. ALIHANOV and A. G. MEŠKOVSKIJ for many helpful discussions.

We wish to express our gratitude to M.G. MEŠČERJAKOV who allowed to perform this work at the synchro-cyclotron of the Institute for Nuclear Problems and to the staff of the synchro-cyclotron.

([10]) M. G. MEŠČERJAKOV, N. P. BOGAČEV, B. S. NEGANOV and E. V. PISKAREV: *Dokl. Akad. Nauk SSSR*, **99**, 955 (1954).

([11]) N. P. BOGAČEV and I. K. VZOROV: *Dokl. Akad. Nauk SSSR*, **99**, 931 (1954).

([12]) M. G. MEŠČERJAKOV, B. S. NEGANOV, L. M. SOROKO and I. K. VZOROV: *Dokl. Akad. Nauk SSSR*, **99**, 959 (1954).

RIASSUNTO (*)

Impiegando protoni prodotti dal sincrociclotrone dell'Istituto per Problemi Nucleari dell'Accademia delle Scienze dell'U. R. S. S. la sezione di scattering e la distribuzione angolare sono state misurate nell'intervallo d'energie da 460 a 660 MeV. I risultati dimostrano che, praticamente, per energie dei protoni fino a 460 MeV, la sezione d'urto di scattering è isotropa; nell'intervallo $560 \div 660$ MeV è marcatamente anisotropa. Si discutono i risultati ottenuti.

(*) *A cura della Redazione.*

IL NUOVO CIMENTO Vol. II, N. 6 1° Dicembre 1955

The Self-Stress Problem and the Limits of Validity of Quantized Field Theories.

E. Arnous

Centre National de la Recherche Scientifique - Paris

W. Heitler

Seminar für theoretische Physik - Universität Zürich

(ricevuto il 28 Settembre 1955)

Summary. — The conditions for the vanishing of the self-stress of a particle are investigated in a generale manner. The following types of fields and interactions are considered: electromagnetic field, electrons, scalar or pseudoscalar mesons, nucleons, with the usual interactions including both types of meson-nucleon interaction, and the five types of β-decay interaction. It is shown that the self-stress of any of these particles vanishes if its exact self-energy at rest is a homogeneous function of the theoretical masses of all existing particles. The condition can easily be fulfilled if a suitable invariant cut-off is introduced. From the mass difference of charged and neutral π-mesons the cut-off momentum can be determined and it turns out to be of the order of the nucleon mass. It is conjectured that this has universal significance. It is shown that the changes introduced by such a cut-off in quantum electrodynamics are beyond the reach of present experiments. The implications on meson theory are discussed.

1. – Introduction.

In order that a particle accompanied by any fields with which it interacts, should behave relativistically like a « particle », (i.e. should possess an energy-momentum vector) it is necessary that its self-stress at rest vanishes. If $T_{\mu\nu}$ is the total energy-momentum tensor of all fields, including the field of which the particle itself is a quantum and the fields with which it interacts (directly

or indirectly), the self-stress is defined as

$$S^0 = \int \langle T^0_{xx} \rangle_1 \, d\tau \, .$$

$\langle \ \rangle_1$ indicates the expectation value for the one particle state and the superscript 0 indicates that the particle is at rest. In order that $S^0 = 0$, it is not sufficient that the self-energy of the particle should be represented in an invariant manner and appear as a mere contribution to its mass. As far as the electron with its electromagnetic field is concerned several investigations have been published. VILLARS and ROHRLICH [1] have shown that after formal regularization S^0 vanishes indeed, but regularization has proved to be a purely formal device without physical contents and we shall not use it in the following. PAIS and EPSTEIN [2] have shown that the vanishing of S^0 can be expressed as a further condition on the self-energy W. The condition concerns the dependence of W on the mass m of the particle. Here and in the following, all masses are always the « theoretical masses », not the experimental masses. S^0 vanishes if W^0 (= self energy of the particle at rest) satisfies the condition

$$W^0 = m \frac{\partial W^0}{\partial m} \, , \tag{1}$$

in other words if $W^0 = m \cdot \text{const}$, where the constant is independent of m. The authors have, however, drawn the wrong conclusion from this correct formula. In which sense such a condition can be fulfilled and further explored will be discussed below.

The first purpose of this work is to generalize the condition (1) to apply to all kinds of fields and particles. The self stress must vanish *exactly* even for a particle like a nucleon which interacts directly with π-mesons and the electromagnetic field and hence indirectly with electrons and all other charged particles. The same must be true for an electron, a π-meson etc., when all these direct and indirect interactions are taken into account. Thus we shall consider all such fields and their interactions in a very general manner. Our considerations must be limited though to linear fields because for non-linear fields quantization cannot so far be carried out satisfactorily and the concept of a one-particle state has not a clear meaning. On the other hand no expansions in the sense of perturbation theory are used and the question of the so-called renormalizibility of an interaction does not arise. Let W^0_1 be the *exact* self energy of any one of the particles considered (we call it number 1) and m_1

[1] F. VILLARS: *Phys. Rev.*, **79**, 122 (1950); F. ROHRLICH: *Phys. Rev.*, **77**, 357 (1950).
[2] A. PAIS and S. T. EPSTEIN: *Rev. Mod. Phys.*, **21**, 445 (1949).

the mass, and let m_q be the masses of all existing particles (including m_1), we shall find that the self-stress vanishes if

$$W_1^0 = \sum_q m_q \frac{\partial W_1^0}{\partial m_q} . \tag{2}$$

Evidently, this means that W_1^0 depends on the masses in the following manner

$$W_1^0 = m_1 F\left(\frac{m_1}{m_2}, \frac{m_1}{m_3}, \ldots\right) \tag{3}$$

where F is some function of the mass ratios m_1/m_q. We take here the view that the theoretical masses are parameters on which physical quantities depend, and that, theoretically, these parameters can be varied. This is the case in all present field theories. It may be argued that in the future correct theory the mass ratios should be determined from the theory itself and that there is no sense in varying the masses. This may be so but this paper is concerned with what can be said about the self-stress problem from the present point of view. We shall also take the view that it has a physical meaning to distinguish between the theoretical and the experimental masses and that the difference is, at least in some cases, observable. This view is substantiated by at least one fact, as will be seen below.

Our next task must be to discuss the question whether, in the present field theories, the self energy of each particle has the required form (3). Clearly, as long as we possess only diverging expressions for W, no unambiguous answer can be given. It has always been strongly suspected and recently been demonstrated more forcibly [3] that all field theories, probably including quantum-electrodynamics, require some fundamental changes of an unknown character, which can be expressed by formally imposing some high energy limit to the validity of the theory. As in our case the invariance of W^0 is essential such a « cut-off » must, of course, be carried out in an invariant manner. This can conveniently be done by representing W^0 as an integral over invariant variables. (3) represents then a condition on the upper limit of integration which, as will be seen, is easily fulfilled.

The theory itself gives no further clue as to the value of this cut-off—and does not even indicate whether this is different for different particles or of a more universal character (except that the consistency of charge renormalization yields a—very large—lower limit for the cut-off; see (§ 3). There is, however

[3] T. D. LEE: *Phys. Rev.*, **95**, 1329 (1954); G. KÄLLÉN and W. PAULI: *Dan. Mat. Fys. Medd.*, in the press; W. THIRRING: *Helv. Phys. Acta*, in the press; E. ARNOUS: to be published in *Journ. de Phys.*

one experimental fact which may be used: it is suggestive to assume that the mass difference of the charged and neutral π-meson is due to the electromagnetic self-energy, since, owing to charge symmetry, the interaction with the nucleon field is the same. Making this assumption we can determine the value of the invariant cut-off limit. It is then convenient to go back to the ordinary momentum variables and thus determine the cut-off as an upper limit of the virtual photon momentum K_0 (this applies to a π-meson at rest, for any other Lorentz-system K is unambiguously determined). It turns out that K_0 is close to the nucleon mass M. Although it does not follow from (3) that the cut-off is universal, it is very suggestive to assume that this is the case, because the cut-off must be due to a new unknown fundamental principle of physics and it is likely that this should affect all field theories in the same manner.

The result $K_0 \sim M$ is a very plausible result indeed. In the first place we shall show that this cut-off prescription changes little in the established results of quantum-electrodynamics. For example, it would affect the value of the anomalous magnetic moment of the electron only in the seventh figure whereas the value is known (and calculated) up to 4 figures only.

The situation is different in meson theory. A cut-off of the order $K_0 \sim M$ means that there is hardly any region where the present meson theory can be regarded as quantitatively correct. This is satisfactory because meson theory, although it gives qualitatively correct results, has failed to explain even a single phenomenon quantitatively and in agreement with the experiments.

2. – The Self-stress condition.

We consider the following types of fields and interactions:

(i) electromagnetic field $\boldsymbol{A}_\lambda$;

(ii) spin $\frac{1}{2}$, mass m, charged, interacting directly with electromagnetic field, notation ψ'. No extra magnetic moment considered. (Example electrons or μ-mesons);

(iii) spin $\frac{1}{2}$, charged and neutral. Interacting with electromagnetic field like nucleons. Mass M, notation ψ. Interaction with meson field (iv) and also with electron-neutrino field (β-decay);

(iv) spin 0, charged and neutral (3 components), interacting with electromagnetic field and wtih nucleon field, like pseudoscalar or scalar meson field, both types of interaction (for example γ_5- and grad-coupling). Mass μ, notation φ_i ($i = 1, 2, 3$).

Each field can be replaced by several fields of the same type but with different masses. For example ψ' could stand for electrons *and* μ-mesons, omitting the interaction leading to the decay of the μ-meson. Similarly, heavy pseudoscalar mesons can be included in the φ_i-field. For simplicity's sake we do not express this in the notation. We adopt the charge symmetrical meson-nucleon interaction, although this is not essential.

We assume the following Lagrangian (*) density ($\hbar = c = 1$):

$$-L_0 = \tfrac{1}{2}(\partial_\mu A_\lambda)^2 + \tfrac{1}{2}[(\partial_\mu \varphi_i)^2 + \mu^2 \varphi_i^2] + \bar{\psi}(\gamma_\mu \partial_\mu + M)\psi + \bar{\psi}'(\gamma_\mu \partial_\mu + m)\psi' , \tag{4}$$

$$\begin{aligned} -L_1 = {} & ie\bar{\psi}\gamma_\lambda A_\lambda \tau_P \psi - ie\bar{\psi}'\gamma_\lambda A_\lambda \psi' + e(\varphi_1 \partial_\mu \varphi_2 - \varphi_2 \partial_\mu \varphi_1) A_\mu + \\ & + \frac{e^2}{2}(\varphi_1^2 + \varphi_2^2) A_\lambda^2 + ig\bar{\psi} D \tau_i \psi \varphi_i + \frac{if}{M} \bar{\psi} D_\mu \tau_i \psi (\partial_\mu \varphi_i) - \\ & - \frac{ief}{M} \bar{\psi} D_\mu A_\mu (\tau_1 \varphi_2 - \tau_2 \varphi_1)\psi + \frac{\lambda}{2}\left(\frac{ig}{M}\bar{\psi} D \tau_i \psi\right)^2 + \frac{\lambda'}{2}\left(\frac{if}{M}\bar{\psi} D_\mu \tau_i \psi\right)^2 \end{aligned} \tag{5}$$

$$-L_2 = \sum_{\varrho=1}^{5} \frac{g_\varrho^2}{2M^2} \bar{\psi} \Gamma_\varrho \frac{\tau_1 + i\tau_2}{2} \psi \bar{\psi}' \Gamma_\varrho \chi + \text{compl. conj.} \tag{5'}$$

τ is the isotopic spin operator, $\tau_P = (1+\tau_3)/2$, $(\tau_1 + i\tau_2)/2$ changes a neutron into a proton and is zero when acting on a proton. D and D_μ are operators which need not be specified (for example $D = \gamma_5$, $D_\mu = \gamma_5\gamma_\mu$). $\partial_\mu = \partial/\partial_{x_\mu}$, $\bar{\psi} = \psi^*\gamma_4$. L_2 describes the β-decay of the nucleons. There are five types of interaction ($\varrho = 1 \ldots 5$) and Γ_ϱ are the corresponding operators, χ is the neutrino field. For simplicity the free neutrino field is omitted.

All coupling constants e, g, f, g_ϱ have the dimensions of a charge (hence the factors M in f/M etc.). All field quantities are operators subjected to quantization. We use Born-Heisenberg representation throughout.

For the meson-nucleon interaction we have added the well-known contact terms (as they occur in the Hamiltonian anyhow) but with arbitrary (dimensionless) coefficients λ, λ', to show that such additions do not jeopardize the relation deduced below.

In the following the equations of motion will be used:

$$\begin{cases} \partial_\mu \dfrac{\partial L}{\partial(\partial_\mu A_\lambda)} - \dfrac{\partial L}{\partial A_\lambda} = 0 , \\ \partial_\mu \dfrac{\partial L}{\partial(\partial_\mu \psi)} - \dfrac{\partial L}{\partial \psi} = 0 \quad \text{(here } \bar{\psi} \text{ is kept constant)} \end{cases} \tag{6}$$

(*) This Lagrangian can also be made charge-symmetrical but this changes nothing in our results.

(same for ψ')

$$\partial_\mu \frac{\partial L}{\partial(\partial_\mu \varphi_i)} - \frac{\partial L}{\partial \varphi_i} = 0 \qquad (i = 1, 2, 3).$$

We shall not write down these well known equations explicitly. The canonical momenta are defined by:

$$(7) \qquad \begin{cases} B_\lambda = \dfrac{1}{i} \dfrac{\partial L}{\partial(\partial_4 A_\lambda)} = i\partial_4 A_\lambda \\ \pi_i = \dfrac{1}{i} \dfrac{\partial L}{\partial(\partial_4 \varphi_i)} = i\partial_4 \varphi_i + \dfrac{f}{M} \bar{\psi} D_4 \tau_i \psi - \begin{cases} + ie\varphi_2 A_4 \\ - ie\varphi_1 A_4 \\ 0 \end{cases} \quad (\text{for } i = 1, 2, 3). \\ \Pi' = \dfrac{1}{i} \dfrac{\partial L}{\partial(\partial_4 \psi_i)} = i\bar{\psi}\gamma_4 \Pi'_i = i\bar{\psi}'\gamma_4 . \end{cases}$$

We define the total canonical energy-momentum tensor in the usual way

$$(8) \qquad \Theta_{\mu\nu} = L\delta_{\mu\nu} - \frac{\partial L}{\partial(\partial_\nu A_\lambda)} \partial_\mu A_\lambda - \frac{\partial L}{\partial(\partial_\nu \psi)} \partial_\mu \psi - \frac{\partial L}{\partial(\partial_\nu \psi')} \partial_\mu \psi' - \frac{\partial L}{\partial(\partial_\nu \varphi_i)} \partial_\mu \varphi_i ,$$

with $\partial\Theta_{\mu\nu}/\partial x_\nu = 0$ on account of the equation of motion. This tensor is neither symmetrical nor hermitian or gauge invariant but can be made so by an addition. To achieve gauge invariance of the whole tensor we add

$$(8') \qquad X_{\mu\nu} = \partial_\lambda\{(\partial_\lambda A_\nu - \partial_\nu A_\lambda) A_\mu\} - \partial_\lambda A_\nu \partial_\mu A_\lambda + \tfrac{1}{2}\delta_{\mu\nu} \partial_\lambda A_\varrho \partial_\varrho A_\lambda$$

with $\partial X_{\mu\nu}/\partial x_\nu = 0$. The tensor $\Theta_{\mu\nu} + X_{\mu\nu}$ is now made symmetrical and hermitian (by symmetrization) in the well known manner (cf. ref. 6, app. 7). The tensor thus obtained will be called $T_{\mu\nu}$ and it has the property $\partial T_{\mu\nu}/\partial x_\nu = \partial T_{\mu\nu}/\partial x_\mu = 0$.

We shall require only (i) the spur of $T_{\mu\nu}$ and (ii) the Hamiltonian $H = -T_{44}$. These quantities differ from Sp $\Theta_{\mu\nu}$ and Θ_{44} only by a 4- or 3-dimensional divergence respectively which will disappear below. Thus we could actually operate with the canonical tensor $\Theta_{\mu\nu}$ as well.

It is for the following essential that Sp T and T_{44} are expressed in terms of the canonical variables (7) and not in terms of the space derivatives of the fields, but as Π is practically identical with $\bar{\psi}$ we may leave $\bar{\psi}$ and $\bar{\psi}'$ standing. We use the equations of motion in their explicit form and obtain after some straightforward calculation:

$$(9) \qquad \text{Sp } T \equiv \sum_\mu T_{\mu\mu} = -M\bar{\psi}\psi - m\bar{\psi}'\psi' - \mu^2\varphi_i^2 +$$

$$+ \frac{if}{M} \bar{\psi} D_k \tau_i \psi(\partial_k \varphi_i) + \frac{f}{M} \bar{\psi} D_4 \tau_i \psi \pi_i - \frac{ief}{M} \bar{\psi} D_k A_k (\tau_1 \varphi_2 - \tau_2 \varphi_1)\psi$$

$$- \lambda \left(\frac{ig}{M} \bar{\psi} D \tau_i \psi \right)^2 + \lambda' \left(\frac{if}{M} \bar{\psi} D_k \tau_i \psi \right)^2 + (\lambda' - 1) \left(\frac{if}{M} \bar{\psi} D_4 \tau_i \psi \right)^2 -$$

$$+ \sum_\varrho \frac{g_\varrho^2}{M^2} \bar{\psi} \Gamma_\varrho \frac{\tau_1 + i\tau_2}{2} \psi \bar{\psi}' \Gamma_\varrho \chi + \text{c. c.} + \partial_\mu G_\mu .$$

Here the index k denotes spacial components. The last term $\partial_\mu G_\mu$ is a total 4-divergence of some expression that need not be specified because such terms will vanish below. (Actually, $G_4 = i\pi_i \varphi_i$). Furthermore,

$$(10) \qquad - T_{44} = H = \tfrac{1}{2}(\partial_k A_\lambda)^2 + \tfrac{1}{2} B_\lambda^2 + \bar{\psi}(\gamma_k \partial_k + M)\psi + \bar{\psi}'(\gamma_k \partial_k + m)\psi' +$$

$$+ \tfrac{1}{2}(\partial_k \varphi_i)^2 + \tfrac{1}{2}\pi_i^2 + \tfrac{1}{2}\mu^2 \varphi_i^2 + ie\bar{\psi}\gamma_\mu A_\mu \tau_r \psi - ie\bar{\psi}'\gamma_\mu A_\mu \psi' + ig\bar{\psi}\tau_i \psi \varphi_i +$$

$$+ e(\varphi_1 \partial_k \varphi_2 - \varphi_2 \partial_k \varphi_1) A_k + ie\,(\pi_1 \varphi_2 - \pi_2 \varphi_1) A_4 + \frac{e^2}{2}(\varphi_1^2 + \varphi_2^2) A_k^2 +$$

$$- \frac{if}{M} \bar{\psi} D_k \tau_i \psi (\partial_k \varphi_i) + \frac{f}{M} \bar{\psi} D_4 \tau_i \psi \pi_i - \frac{ief}{M} \bar{\psi} D_k A_k (\tau_1 \varphi_2 - \tau_2 \varphi_1)\psi + \frac{\lambda}{2} \left(\frac{ig}{M} \bar{\psi} D \tau_i \psi \right)^2 +$$

$$\frac{\lambda'}{2} \left(\frac{if}{M} \bar{\psi} D_k \tau_i \psi \right)^2 + \frac{\lambda' - 1}{2} \left(\frac{if}{M} \bar{\psi} D_4 \tau_i \psi \right)^2 + \sum_\varrho \frac{g_\varrho^2}{2M^2} \bar{\psi} \Gamma_\varrho \frac{\tau_1 + i\tau_2}{2} \psi \bar{\psi}' \Gamma_\varrho \chi + \text{c. c.}$$

It is now seen that Sp T has only terms which contain one of the masses explicitly. These terms occur also in H, (with different factors and signs) in addition to numerous terms free of m, μ, M. If we regard the masses as parameters on which Sp T and H depend explicitly, we see that the following relation is true: (anticipating that $\partial_\mu G_\mu$ does not contribute)

$$(11) \qquad \text{Sp } T = - m \frac{\partial H}{\partial m} - \mu \frac{\partial H}{\partial \mu} - M \frac{\partial H}{\partial M} .$$

It is essential for this relation that g, f and g_ϱ, like e, are regarded as independent of the masses, and that we do not, for example, write f' for f/M and regard f' as independent of M. g, f and g_ϱ as defined above (and not f/M) have the dimensions of a charge, and it is the charge-like constants which are independent of M. On the other hand, the relation (11) would remain valid if g and f were, more generally, functions of M/μ. (For example we can equally well write f/μ instead of f/M). We write the relation more generally in the form

$$(12) \qquad \text{Sp } T = - \sum_q m_q \frac{\partial H}{\partial m_q}$$

where q are all the particles considered above.

Consider now the state where only one single of the above particles is present.

Let us call this particle $q = 1$. We have to demand then that the expectation value of the total energy and momentum viz. $\int \langle T_{\mu 4} \rangle_1 \, d\tau$ form a 4-vector, and this must be true for each particle. If the particle in question is at rest (upper index 0) it is obvious for reasons of spacial symmetry that

$$\int \langle T^0_{x4} \rangle_1 \, d\tau = \int \langle T^0_{xy} \rangle_1 \, d\tau = \ldots = 0 \tag{13}$$

and only the diagonal elements are different from zero. In addition

$$\int \langle T^0_{xx} \rangle_1 d\tau = \int \langle T^0_{yy} \rangle_1 d\tau = \ldots = S^0 . \tag{14}$$

This quantity will be called the self stress of particle 1. For a moving particle we then have

$$\begin{cases} \int \langle T_{44} \rangle_1 d\tau = \dfrac{1}{\sqrt{1-\beta^2}} \left\{ \int \langle T^0_{44} \rangle_1 \, d\tau - \beta^2 S^0 \right\} \\ i \int \langle T_{x4} \rangle_1 d\tau = -\dfrac{\beta}{\sqrt{1-\beta^2}} \left\{ \int \langle T^0_{44} \rangle_1 d\tau - S^0 \right\} . \end{cases} \tag{15}$$

In order that these are the correct formulae for energy and momentum of a particle it is necessary (and sufficient) that (see ref. [2] and [6], p. 420)

$$S^0 = 0 . \tag{16}$$

All we have to consider therefore is the self-stress S^0_1 for a particle at rest For this purpose we form the expectation value of the space integral of Sp T. We obviously have, by (14),

$$\int \langle \mathrm{Sp} \, T^0 \rangle_1 d\tau = 3S^0 - \int \langle H^0 \rangle_1 d\tau \qquad (H^0 = -T^0_{44}) . \tag{17}$$

In the integral on the left terms of the form $\partial_\mu G^0_\mu$ vanish. The space components vanish on account of the spacial integral. $G_4 \partial^0_4$ is a time derivative, but the expectation value of any quantity for a single particle at rest cannot depend on time. Hence $\langle \partial_4 G^0_4 \rangle_1 = \partial_4 \langle G^0_4 \rangle_1 = 0$.

The expectation value of the Hamiltonian for the state considered is nothing but the rest mass of the particle m_1 (theoretical mass!) plus the self energy W^0_1 of the particle at rest:

$$\int \langle H^0 \rangle_1 d\tau = m_1 + W^0_1 . \tag{18}$$

The condition that S^0 should vanish can now be formulated, with the help of our relation (12) as a condition for the mass-dependence of the self energy. From (12), (17) and (18) we obtain, for $S^0 = 0$,

$$W_1^0 = \sum m_q \frac{\partial W_1^0}{\partial m_q} . \tag{19}$$

This is our general condition for the correct relativistic behaviour of the particle called particle 1. ((19) must of course hold for each particle). It is a condition concerning the mass dependence of the self energy only and is, of course, a generalization of (1). (19) can be regarded as a partial differential equation determining W_1^0 as a function of the masses m_q. The general solution is

$$W_1^0 = m_1 F\left(\frac{m_1}{m_2}, \frac{m_1}{m_3}, \ldots\right) \tag{20}$$

where F is a function of the mass ratios. Thus the condition for the correct relativistic behaviour of a particle can be expressed by saying that the self-energy of the particle at rest must be a homogeneous function of the masses of all existing particles. It should be pointed out that in (20) W_1^0 is the exact and complete self-energy in all orders of approximation and with all couplings.

In the following section we discuss the question whether and under what circumstances the condition (20) is satisfied.

3. – Limits of validity of present field theories.

If we had a theory where W_1^0 would turn out to be finite, it would be almost trivial that the conditions (20) are fulfilled. W^0 has the dimensions of a mass and there is no other constant with the dimensions of a mass, except the masses of the elementary particles themselves. Thus W^0, for mere dimensional reasons, must have the form (20). Almost, but not quite: one could visualize a situation where, in addition to the masses of the particles a universal length, which means a universal mass, appears (as was once suggested by HEISENBERG) which should be responsible for the failure of the present theories. We can conclude that this cannot be the case unless this universal mass is identical with one of the masses of the existing particles and this is what we believe to be the case. As long as we have only diverging expressions for the self-energies no answer to our question can be given. We have, however, every reason to believe that all present field theories require a drastic change at some fundamental point. This has recently been demonstrated in the case of simplified models [3]and made probable in quantum electrodynamics by

LANDAU and POMERANTSCHUK (4). The consistency of charge renormalization requires an upper limit for the energy of the virtual particles occurring in the self-charge (*). Thus it is certain that a limit has to be imposed on the validity of present field theories. For our problem this must, of course, be done in an invariant manner. For this purpose it is most convenient to represent the self-energies by invariant variables. These are an easy generalization of the Pauli-Rose variables (5,6). As examples we give the expressions of the first order self-energies in the following cases: (*a*) electromagnetic self-energy of the electron; (*b*) electromagnetic self-energy of the charged π-meson; (*c*) mesonic self-energy of the nucleon (for $g = 0$, $\lambda = 0$, $\lambda' = \frac{1}{2}$) (m = electron mass, μ = meson mass, M = nucleon mass). We call the upper limit z_0.

$$W_1^0 = \frac{m}{2\pi 137}\int_1^{z_0} \frac{3z^2-1}{z^3}\,\mathrm{d}z \tag{21a}$$

$$z = \frac{1}{m}\left(\sqrt{m^2+k^2}+k\right) \tag{21b}$$

(electron)

$$W_1^0 = \frac{\mu}{8\pi 137}\int_1^{z_0} \frac{3z^4+6z^2-1}{z^3}\,\mathrm{d}z \tag{22a}$$

$$z = \frac{1}{\mu}\left(\sqrt{\mu^2+k^2}+k\right) \tag{22b}$$

(π-meson)

$$W_1^0 = \frac{Mf^2}{4\pi^2}\frac{\mu^2}{M^2}\int_1^{z_0}\frac{\mathrm{d}z}{z}\frac{(M+\mu)^2}{z^2(M+\mu)^2-M^2}\left[z^4-2\frac{M^2+\mu^2}{(M+\mu)^2}z^2+\left(\frac{M-\mu}{M+\mu}\right)^2\right]^{\frac{1}{2}} \tag{23a}$$

$$z = \frac{1}{M+\mu}\left(\sqrt{M^2+k^2}+\sqrt{\mu^2+k^2}\right). \tag{23b}$$

(nucleon)

The connexion between z and the momentum k of the virtual photon or meson refers to a particle at rest. z is in each case an invariant. If the particle has momentum p, the connexion is (in the electron or meson case)

$$z^2 = \frac{1}{m^2}\left\{\left(\sqrt{m^2+(\boldsymbol{p}-\boldsymbol{k})^2}+k^2\right)-(\boldsymbol{p}-\boldsymbol{k})^2\right\}. \tag{24}$$

(4) L. LANDAU and I. POMERANTSCHUK: *Dan. Mat. Fys. Medd.*, in press.

(*) From such considerations LANDAU and POMERANTSCHUK establish a (very high) upper limit for the required cut-off, and they discuss a possible connection with gravitation. We believe that the actual limit of validity lies very much lower, see below.

(5) W. PAULI and M. E. ROSE: *Phys. Rev.*, **49**, 462 (1936); S. N. GUPTA: *Proc. Phys. Soc.*, **63**, 681 (1950), and an unpublished paper.

(6) W. HEITLER: *Quantum Theory of Radiation* (Oxford, 1954, 3-rd edition).

The integrands in all formulae depend on the mass ratios only and all that is required in order to fulfil the self-stress conditions is that the upper limit z should in each case, also depend on the mass ratios only. There is no reason why z_0 should be the same in all cases.

Further information about the upper limit z_0 can only come from experiment.

In the following we assume that the self energy is physically meaningful and is, in certain cases at least, observable. There is one case where it is very suggestive to assume that this is really observed, namely the mass difference between the charged and neutral π-meson. Owing to charge symmetry the self-energy due to the meson-nucleon interaction must be same and the mass difference is likely to be due to the electromagnetic self-energy. This, for spin zero particles, increases quadratically with z_0 and is therefore comparatively large (~ 10 electron masses) but it is still small compared with the π-meson mass so that the use of perturbation theory is warranted. Using then the expression (22a) and equating W_1^0 with the experimental result (10 m) we obtain

$$z_0 = 8.9 \ (\pi\text{-meson}). \tag{25}$$

To see the significance of this result we go back to the ordinary momentum variables of the virtual photons (*). The corresponding cut-off K_0 is, according to (22b)

$$K_0 = 4.4\mu \sim \tfrac{2}{3}M \, . \tag{26}$$

The fact that the cut-off turns out to be just the nucleon mass (the numerical factor of order unity has no significance) is a very plausible result and deserves further examination.

As far as our considerations up to the present are concerned we cannot conclude that this cut-off value is universal. Yet, if the limitation of k to values smaller than K_0 is due to a new unknown fundamental principle in field theory it is at least very plausible to assume that this cut-off is universal. We discuss the consequences of this assumption a little further. It is to be understood in the following sense: If the particle is at rest the virtual momenta are limited to values $\leqslant K_0$ given by (26). The upper limit z_0 of the invariant variable z depends then on the masses (according to (21)-(23b)) but is clearly a function of the mass ratios only, as required. If the particle is

(*) The variables z and z_0 have no direct physical significance. There are, of course, many ways to choose invariant variables connected with the virtual momentum k.

not at rest, the value of K_0', say, is to be determined from (24) (etc.) so that $z_0 = z_0'$ remains invariant. This clearly is an invariant cut-off prescription.

The first question which presents itself is whether such a limitation on the theory would lead to appreciable changes of established results in quantum electrodynamics. We consider two examples, (*a*) the anomalous magnetic moment of the electron and (*b*) the Compton effect and bremsstrahlung or pair creation.

(*a*) The anomalous magnetic moment of the electron (at rest) in units of the magneton is represented by (see ref. (6), p. 313; we use the same notation)

$$\Delta g = \frac{2i}{\pi^3 137}\int \mathrm{d}^4k \int_0^1 w^2\,\mathrm{d}w\,\frac{m^2(w-1)}{(k^2+m^2w^2-i\sigma)^3}\Big|_{\sigma\to 0} = \tag{27}$$

$$= \frac{1}{\pi 137}\int_0^\infty \mathrm{d}k \left\{\frac{k^2}{m^2}\left(\frac{k}{\sqrt{m^2+k^2}}-1\right)+\frac{k}{\sqrt{m^2+k^2}}\right\} = \frac{1}{2\pi 137}$$

after integration over k_0, the angle of $\boldsymbol{k}$ and w. The value of the last integral is $\frac{1}{2}$. If now the integration is limited to $k \leqslant K_0$, the change of Δg is

$$\Delta g' = \frac{1}{\pi 137}\int_{K_0}^\infty \mathrm{d}k \left\{\frac{k^2}{m^2}\left(\frac{k}{\sqrt{m^2+k^2}}-1\right)+\frac{k}{\sqrt{m^2+k^2}}\right\} = \simeq \frac{1}{2\pi 137}\,\frac{1}{4}\,\frac{m^2}{K_0^2}\,. \tag{28}$$

With the value (26) for K_0 the relative change of the magnetic moment is

$$\frac{\Delta g'}{\Delta g} = \frac{1}{4}\,\frac{m^2}{K_0^2} = 1.8\cdot 10^{-7}\,. \tag{29}$$

The magnetic moment is known both by experiment and calculation (including the fourth order) to an accuracy of 4 figures. We see that the cut-off will make itself felt only in the seventh figure. Thus present results are not affected.

(*b*) The limitation imposed on the validity of the Klein-Nishina formula can be discussed as follows: in the c.m. system the absolute value of the momentum of the electron does not change during the collision and is $\boldsymbol{p} = -\boldsymbol{k}$. When in the previous cases the virtual photon momentum was $\boldsymbol{k}$, the electron also had a recoil momentum $\boldsymbol{p} = -\boldsymbol{k}$ (the particle as a whole was at rest). Thus we expect that in the c.m.-system the same limitation K_0 to the real photon momentum applies:

$$K \leqslant K_0 \cong 600 \text{ MeV}\,. \tag{30}$$

In the Lorentz-system where the electron is at rest, the corresponding K is

$$K = \frac{2K_0^2}{m} \qquad \text{or} \qquad K = 1.4 \cdot 10^6 \text{ MeV}. \tag{31}$$

Thus we do not expect any substantial changes in the cross-section for the Compton effect up to about 10^{12} eV. Similar limitations apply to the two quanta annihilation of positrons, a process rather similar to the Compton effect.

For bremsstrahlung and pair creation the changes due to the cut-off are even less conspicuous. This is best discussed by using the Weizsäcker-Williams method (*). We consider the bremsstrahlung first in the Lorentz system where the nucleus moves fast and the electron is at rest. The field of the nucleus is decomposed into virtual photons k^*, say, covering an energy range up to $k^* \cong E$, where E is the energy of the electron in the Lorentz-system where the nucleus is at rest. The virtual photons suffer then a Compton scattering by the electron and the scattered photon (after transformation to the system where the nucleus is at rest) appears as bremsstrahl-photon. If we keep the energy of the emitted photon k' (Lorentz-system where nucleus is at rest) fixed, then virtual photons k^* contribute to the process whose energy range is

$$\frac{mk'}{2(E - k')} \leqslant k^* \leqslant E \,. \tag{32}$$

The contribution to the cross-section from k^* is $\mathrm{d}k^*/k^{*2}$ (and terms $\mathrm{d}k^*/k^{*3}$ etc.) thus small k^* give the largest contribution. Now when the cut-off is introduced, k^* is limited to

$$k^* \leqslant K \tag{33}$$

and if $E > K$, a certain change in the cross-section takes place. However, this affects only bremsstrahl-photons k' whose energy is very close to E. So long as $K/m \gg k'/(E - k')$ the influence of the upper limit K is negligible. Thus only the emission of such photons is seriously reduced for which $(E - k')/k' \sim K/m \gg 1$, i.e. whose energy is very close to the upper limit E. Such photons are rare anyhow. We conclude that the cut-off has very little influence on the development of an electron-photon cascade no matter how high the initiating energy E is.

(*) See ref. ([6]), pp. 416-17. We use the same notation.

Thus none of the established results of quantum electrodynamics are changed substantially. The electromagnetic self-energy of spin $\frac{1}{2}$ particles is a small fraction of their mass. From (21) we find $W_1^0 = 0.03\, m$ for an electron and $W_1^0 = 0.0025\, M \cong 5\, m$ for a proton, although the latter result is only an indication of the order of magnitude (see below).

The situation is very different in meson theory. For a nucleon at rest the upper limit for the virtual meson momentum $K_0 \sim \frac{2}{3}M$ is not much greater than the meson mass μ. The invariant limit z_0 is, by (23b) $z_0 = 1.6$ whilst the lower limit is 1. For virtual meson processes there is hardly a significant range of integration left. Except, perhaps, for very slow mesons ($k \ll \mu$) we are nowhere far below the cut-off region, where substantial changes will occur. For example, the mesonic self-energy of a nucleon will be a problem that is outside the scope of the present meson theory. The same must be said of the mass difference between proton and neutron which is likely to be due to mixed mesonic-electromagnetic effects occurring in higher orders of the self-energy. It is satisfactory that the purely electromagnetic self-energy (which would make the proton heavier than the neutron) has turned out to be so small so that one can well imagine that these mixed contributions overcompensate the electromagnetic self-energy.

The situation is similar for the magnetic moments of the nucleons. Since the (much too large) contribution from the relativistic nucleon currents is largely responsible for the present sharp disagreement between theory and experiment it is likely that the drastic cut-off advocated above will improve the situation. However, we cannot hope to obtain correct results because the unknown changes of the theory become operative almost throughout the whole range of integration.

On the other hand the cut-off momentum is still larger than μ and $z_0 > 1$. This means that at least some qualitative significance can be attached to many results derived from meson theory. This characterises the present situation in meson theory very well.

Whilst most qualitative and order of magnitude predictions have come true, not a single really quantitative result has been obtained that could be found in agreement with the facts.

From the above discussion it may be concluded that it is indeed a hypothesis that accounts well for all known features in present field theory, if we assume that some fundamental changes have to be introduced in the theory which becomes effective at a length of the order of the Compton wave length of the nucleon.

RIASSUNTO (*)

Si esaminano da un punto di vista generale le condizioni per l'annullarsi del self-stress di una particella. Si considerano i seguenti tipi di campi e interazioni: campo elettromagnetico, elettroni, mesoni scalari o pseudoscalari, nucleoni, con le usuali interazioni compresi i due tipi di interazione mesone-nucleone, e i cinque tipi di interazione con decadimento β. Si mostra che il self-stress di ognuna di queste particelle si annulla se la sua self-energy a riposo esatta è una funzione omogenea delle masse teoriche di tutte le particelle esistenti. La condizione può essere agevolmente soddisfatta introducendo un opportuno taglio invariante. Dalla differenza di massa dei mesoni π carichi e neutri si può determinare l'impulso a livello del taglio, che risulta essere dell'ordine della massa del nucleone. Si presume che ciò abbia un significato universale. Si dimostra che le variazioni provocate da questo taglio nell'elettrodinamica quantistica cadono fuori dell'ambito della sperimentazione attuale. Si discutono i riflessi sulla teoria mesonica.

(*) *Traduzionea cura della Redazione.*

IL NUOVO CIMENTO Vol. II, N. 6 1° Dicembre 1955

Unique First Forbidden Beta Spectrum of ^{89}Sr.

A. Bisi, S. Terrani and L. Zappa

Istituto di Fisica Sperimentale del Politecnico - Milano

(ricevuto il 20 Ottobre 1955)

Summary. — The β-ray spectrum of ^{89}Sr was investigated in an intermediate image β-ray spectrometer. The transition energy was found to be: $E_0 = 1.462 \pm 0.005$ MeV. The spectral shape from the end-point down to about 140 keV agrees with what is to be exspected from a unique first forbidden transition ($\Delta I = 2$, yes). No branching at the 0.913 MeV isomeric level of ^{89}Y ($\gamma/\beta < 5 \cdot 10^{-6}$), nor other γ-rays were observed.

1. – Introduction.

The decay of ^{89}Sr ($T_{\frac{1}{2}} = 50.4$ d) is known to occur through a pure β^--transition with a disintegration energy of 1.46 MeV [1]. The shape of the β-spectrum was investigated by Langer and Price [2] and by Slack, Braden and Shull [3]. The β-spectrum was found to deviate distinctly from the allowed shape, which was to be expected from considerations relative to the nuclear shell model that predicts a $d_{\frac{5}{2}} \rightarrow p_{\frac{1}{2}}$ transition. Consequently the «unique» shape factor for the first degree of forbiddennes ($\Delta I = 2$, yes) should rectify the conventional Fermi plot. The results of the above investigators support these predictions as far as concerns the energy range between the upper limit and 0.5 MeV. For lower energies no conclusion can be drawn owing to the fact that the employed source was a mixture of ^{89}Sr and ^{90}Sr ($E_0 = 0.53$ MeV, $T_{\frac{1}{2}} = 19.9$ y), in equilibrium with its daughter ^{90}Y ($E_0 = 2.2$ MeV, $T_{\frac{1}{2}} = 65$ h).

---

(1) A comprehensive account of the data concerning the decay of ^{89}Sr is given by: R. W. King: *Rev. Mod. Phys.*, **26**, 327 (1954). See also: G. Hermann: *Zeits. Elektrochem.*, **58**, 626 (1954); G. Hermann und F. Strassmann: *Zeits. Naturfor.*, **10**a, 146 (1955).

(2) L. M. Langer and H. C. Price: *Phys. Rev.*, **76**, 641 (1949).

(3) L. Slack, C. H. Braden and F. B. Shull: *Phys. Rev.*, **75**, 1965 (1949).

(In the investigation carried out by LANGER and PRICE the fraction of Y was chemically separated).

The present work was intended to investigate the β-spectrum of ^{89}Sr down to low energies by using samples free from ^{90}Sr. In this way and through an accurate inspection of γ-radiations, we can also establish if a second, very faint, β^- branch exists, which leads to the isomeric level of ^{89}Y (0.913 MeV).

2. – Radiations from the Source.

The samples of ^{89}Sr were obtained by neutron irradiation of $SrCO_3$ in the Harwell pile. The specific activity was about 500 μC/g. The sample was studied when the short-lived activity due to ^{87}Sr had disappeared.

A survey of the γ-spectrum in the region around 0.913 MeV was made with a single crystal scintillation spectrometer. No evidence at all could be found for the existence of a 0.913 MeV γ-ray. By measuring the total intensity of the β-spectrum in a β-ray spectrometer, it could be established that if the 0.913 MeV γ-ray was present, it would have an intensity lower than $5 \cdot 10^{-6}$ relative to the β spectrum.

Actually only the presence of a peak at 0.517 ± 0.004 MeV was distinctly revealed. Within the accuracy of the measurements these γ-rays could be ascribed, at a first glance, to the annihilation of positrons that might be present as impurities in the source. To check this possibility a measurement of γ-γ angular correlation at 180° was carried out. As no coincidences were found we may conclude that the source is free from β^+ emitters.

With a proportional counter spectrometer a peak at 13.3 ± 0.1 keV was detected, which was interpreted as KX-radiations characteristic of Rb.

These last results suggest that no impurity is present in the irradiated sample except ^{85}Sr which decays through orbital electron capture ($T_{\frac{1}{2}} = 65$ d) into the isomeric level at 0.513 MeV of ^{85}Rb.

At last we note that a preliminary inspection of the β spectrum carried out by means of a hollow crystal spectrometer, shows the β-decay to be a simple one.

3. – The β-Ray Spectrum.

The β-ray spectrum was analyzed in a high transmission intermediate image spectrometer. The baffles were adjusted for a resolving power of 4%. The cut-off energy of the Geiger window, a nylon film, was at about 6 keV.

The strontium samples were prepared from strontium iodide through electrodeposition of ^{89}Sr on thin Cu foils (~ 0.5 mg/cm^2 thick). The strontium iodide

was obtained from $SrCO_3$ through reaction with HI and carefully dried. Two grams of strontium iodide were dissolved in 100 cm³ of pyrydyne and electrodeposition from 10 cm³ of solution was carried out with inox steel rotating anode. The density of current was 2 mA/cm². The sample thickness was 0.19 mg/cm². The autoradiograph of the sample showed complete uniformity.

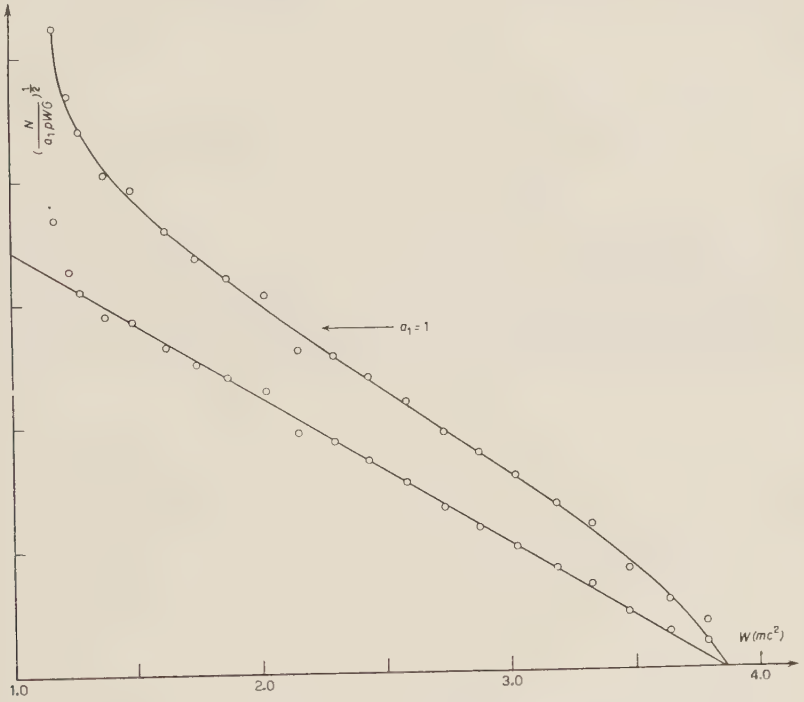

Fig. 1. – Conventional and corrected Fermi plot for the β-ray spectrum of ^{89}Sr.

The conventional Fermi plot of the obtained spectrum is shown in Fig. 1. The upper curve shows the characteristic upward bulge at energies higher than $W_0/2$ as also the upward curvature at lower energies. The lower curve shows the Fermi plot corrected by the shape factor for the « unique » first forbidden transition: $\Delta I = 2$, yes. Neglecting the Coulomb effect on the electron, the shape factor a_1 was simplified as:

$$a_1 = (W^2 - 1) + (W_0 - W)^2 .$$

For low Z this is a good approximation. The corrected plot results to be a straight line from the end point down to about 140 keV. The excess of electrons at lower energies can be reasonably attributed to the finite source thickness and its backing material.

The energy of the transition $^{89}Sr \rightarrow {}^{89}Y$ obtained in the conventional manner was $E_0 = 1.462 \pm 0.005$ MeV, in very good agreement with the value given by LANGER and PRICE [2] ($E_0 = 1.463 \pm 0.005$ MeV).

* * *

Our thanks are due to Prof. G. BOLLA for his kind interest.

RIASSUNTO

Lo spettro β dello ^{89}Sr è stato studiato con uno spettrometro ad immagine intermedia. L'energia massima della transizione risulta: $E_0 = 1.462 \pm 0.005$ MeV. La forma dello spettro dall'estremo superiore fino a circa 140 keV coincide con quella prevista per una transizione proibita, $\Delta I = 2$, si. Non si osservano radiazioni γ e in particolare non v'è traccia di una diramazione al livello isomerico dell'^{89}Y ($\gamma/\beta < 5 \cdot 10^{-6}$).

Masse dei nuclei con $Z \geqslant 40$.

G. Bussetti

Istituto di Fisica dell'Università - Torino
Istituto Nazionale di Fisica Nucleare - Sezione di Torino

(ricevuto il 25 Ottobre 1955)

Riassunto. — Si danno le masse dei nuclei stabili, con $Z \geqslant 40$, calcolate con la formola semiempirica del modello a goccia. Due coefficienti della formola sono stati ricalcolati col metodo dei minimi quadrati.

Nella tabella in fondo al presente lavoro, si danno le masse teoriche dei nuclei stabili, e di alcuni instabili a vita lunghissima, fra ${}^{90}_{40}\mathrm{Zr}$ e ${}^{238}_{92}\mathrm{U}$.

I valori riportati sono stati calcolati con la formola semiempirica di von Weizsäcker, che abbiamo usato nella seguente forma:

$$(1) \qquad {}^{A}_{Z}M = ZM_p + (A-Z)M_n - c_1 A + c_2 \frac{(N-Z)^2}{A} + c_3 \frac{Z(Z-1)}{A^{\frac{1}{3}}} + c_4 A^{\frac{2}{3}} + c_5 \frac{0.036}{A^{\frac{3}{4}}},$$

ove: $c_1 = 0.01483828$

$c_2 = 0.01943875$

$c_3 = 0.00062700$

$c_4 = 0.01273309$

e
$$c_5 = \begin{cases} 0 & \text{per i nuclei con } A \text{ dispari} \\ -1 & \text{per i nuclei con } Z \text{ pari} - N \text{ pari} \\ +1 & \text{per i nuclei con } Z \text{ dispari} - N \text{ dispari.} \end{cases}$$

---

(1) J. W. R. Du Mond e E. R. Cohen: *Rev. Mod. Phys.*, **25**, 691 (1953).

(2) E. Feenberg: *Rev. Mod. Phys.*, **19**, 239 (1947). [Vedi pure alla lett. *d* nella tabella II dell'articolo di A. E. S. Green e N. A. Engler: *Phys. Rev.*, **91**, 42 (1953)].

Per M_n e M_p, masse del neutrone e del protone, si è posto $M_n = 1.0089899$ e $M_p = 1.00759714$, valori ottenuti dai dati di J. MATTAUCH e R. BIERI (*Zeits. Naturforsch.*, 9-A, 303 (1954)). Il valore di M_p è stato ottenuto dalla massa dell'atomo di idrogeno, $M_H = 1.0081459$, togliendo la massa dell'elettrone, $M_e = 0.00054876$ [1].

I valori di c_2 e c_3, qui usati sono quelli riportati da J. M. BLATT e V. F. WEISSKOPF: *Theor. Nuclear Physics* (New York, 1952), p. 229 [2].

I valori di c_1 e c_4, sono stati da noi calcolati col metodo dei minimi quadrati, utilizzando le masse sperimentali dei seguenti 33 nuclei (Z A) con A pari fra $^{84}_{36}$Kr e $^{208}_{82}$Pb:

(36.84) – (36.86) – (38.86) – (38.88) – (40.90) – (42.94) – (42.98)
(46.106) – (46.108) – (48.106) – (48.108) – (48.114) – (50.114) – (50.120)
(50.124) – (52.124) – (52.130) – (54.124) – (54.132) – (56.136) – (56.138)
(58.140) – (58.142) – (60.144) – (60.150) – (72.176) – (72.178) – (72.180)
(74.182) – (74.184) – (78.194) – (78.196) – (82.208).

Sulla tabella seguente nella colonna dei valori sperimentali sono riportate le masse dei nuclei ottenute da quelle degli atomi sottraendo $Z \cdot M_e$:

TABELLA DELLE MASSE DEI NUCLEI CON $Z \geqslant 40$.

	Z	A	massa calcolata con la (1)	massa sperimentale
Zr	40	90	89.9123	89.9112 *b*)
		91	90.9130	
		92	91.9116	
		94	93.9122	
		96	95.9141	
Nb	41	93	92.9126	92.9129 *b*)
Mo	42	92	91.9144	
		94	93.9119	93.9113 *c*)
		95	94.9124	
		96	95.9108	
		97	96.9119	
		98	97.9109	97.9131 *d*)
		100	99.9122	

b) T. L. COLLINS, W. H. JOHNSON e A. O. NIER: *Phys. Rev.*, **94**, 399, (1954).
c) H. E. DUCKWORTH, C. L. KEGLEY, J. M. OLSON e G. STANFORD: *Phys. Rev.*, **83**, 1117 (1951).
d) H. E. DUCKWORTH e R. S. PRESTON: *Phys. Rev.*, **82**, 469, (1951).

TABELLA DELLE MASSE DEI NUCLEI CON $Z \geqslant 40$ (*segue*)

	Z	A	massa calcolata con la (1)	massa sperimentale	
Ru	44	96	95.9151		
		98	97.9122		
		99	98.9124		
		100	99.9106		
		101	100.9114		
		102	101.9103		
		104	103.9111		
Rh	45	103	102.9115		
Pd	46	102	101.9131	101.9123	*e*)
		104	103.9111	103.9114	*e*)
		105	104.9116	104.9132	*e*)
		106	105.9103	105.9116	*e*)
		108	107.9106	107.9128	*e*)
		110	109.9120	109.9144	*e*)
Ag	47	107	106.9120	106.9129	*e*)
		109	108.9115	108.9136	*e*)
Cd	48	106	105.9145	105.9135	*e*)
		108	107.9122	107.9123	*e*)
		110	109.9109	109.9123	*e*)
		111	110.9118	109.9135	*e*)
		112	111.9108	111.9125	*e*)
		113	112.9122	112.9143	*e*)
		114	113.9117	113.9137	*e*)
		116	115.9136	115.9157	*e*)
In	49	113	112.9122	112.9135	*e*)
		115	114.9124	114.9135	*e*)
Sn	50	112	111.9138	111.9133	*e*)
		114	113.9122	113.9120	*e*)
		115	114.9128	114.9127	*e*)
		116	115.9117	115.9119	*e*)
		117	116.9128	116.9131	*e*)
		118	117.9121	117.9124	*e*)
		119	118.9137	118.9138	*e*)
		120	119.9136	119.9132	*e*)
		122	121.9159	121.9151	*e*)
		124	123.9192	123.9175	*e*)

e) R. E. HALSTED: *Phys. Rev.*, **88**, 669 (1952).

TABELLA DELLE MASSE DEI NUCLEI CON $Z \geqslant 40$ (*segue*)

	Z	A	massa calcolata con la (1)	massa sperimentale	
Sb	51	121	120.9141	120.9146	*e*)
		123	122.9157	122.9150	*e*)
Te	52	120	119.9131	119.9144	*e*)
		122	121.9132	121.9134	*e*)
		123	122.9146	122.9152	*e*)
		124	123.9142	123.9143	*e*)
		125	124.9160	124.9161	*e*)
		126	125.9161	125.9157	*e*)
		128	127.9189	127.9180	*e*)
		130	129.9224	129.9200	*e*)
I	53	127	126.9164	126.9162	*e*)
Xe	54	124	123.9152	123.9162	*e*)
		126	125.9149	125.9152	*e*)
		128	127.9155	127.9149	*e*)
		129	128.9170	128.9164	*e*)
		130	129.9169	129.9154	*e*)
		131	130.9189	130.9171	*e*)
		132	131.9192	131.9166	*e*)
		134	133.9224	133.9184	*e*)
		136	135.9263	135.9209	*e*)
Cs	55	133	132.9195		
Ba	56	130	129.9172		
		132	131.9174		
		134	133.9184		
		135	134.9202		
		136	135.9203	135.9181	*c*)
		137	136.9225	136.9195	*c*)
		138	137.9230	137.9191	*c*)
La	57	138	137.9211		
		139	138.9231		
Ce	58	136	135.9199		
		138	137.9206		
		140	139.9221	139.9171	*c*)
		142	141.9243	141.9219	*c*)

c) H. E. DUCKWORTH, C. L. KEGLEY, J. M. OLSON e G. STANFORD: *Phys. Rev.*, **83**, 1117 (1951).

e) R. E. HALSTED: *Phys. Rev.*, **88**, 669 (1952).

TABELLA DELLE MASSE DEI NUCLEI CON $Z \geqslant 40$ (*segue*)

	Z	A	massa calcolata con la (1)	massa sperimentale
Pr	59	141	140.9233	140.9190 *c*)
Nd	60	142	141.9234	
		143	142.9247	
		144	143.9244	143.9231 *c*)
		145	144.9261	
		146	145.9263	
		148	147.9289	
		150	149.9322	149.9358 *c*)
Sm	62	144	143.9268	
		147	146.9279	
		148	147.9275	
		149	148.9289	
		150	149.9289	
		152	151.9311	
		154	153.9340	
Eu	63	151	150.9306	
		153	152.9322	
Gd	64	152	151.9311	
		154	153.9322	
		155	154.9308	
		156	155.9340	
		157	156.9360	
		158	157.9365	
		160	159.9397	
Tb	65	159	158.9376	
Dy	66	156	155.9354	
		158	157.9361	
		160	159.9375	
		161	160.9393	
		162	161.9397	
		163	162.9418	
		164	163.9424	
Ho	67	165	164.9435	
Er	68	162	161.9406	
		164	163.9417	

c) H. E. DUCKWORTH, C. L. KEGLEY, J. M. OLSON e G. STANFORD: *Phys. Rev.*, **83**, 1117 (1951).

TABELLA DELLE MASSE DEI NUCLEI CON $Z \geqslant 40$ (*segue*).

	Z	A	massa calcolata con la (1)	massa sperimentale
Er	68	166	165.9434	
		167	166.9453	
		168	167.9459	
		170	169.9489	
Tn	69	169	168.9474	
Yb	70	168	167.9464	
		170	169.9479	
		171	170.9496	
		172	171.9499	
		173	172.9519	
		174	173.9526	
		176	175.9559	
Lu	71	175	174.9540	
		176	175.9547	
Hf	72	174	173.9529	
		176	175.9546	175.9528 *c*)
		177	176.9564	
		178	177.9569	177.9541 *c*)
		179	178.9590	
		180	179.9598	179.9634 *c*)
Ta	73	181	180.9614	180.9730 *c*)
W	74	180	179.9599	
		182	181.9619	181.9627 *c*)
		183	182.9638	182.9653 *c*)
		184	183.9644	183.9646 *c*)
		186	185.9676	
Re	75	185	184.9664	
		187	186.9691	
Os	76	184	183.9658	
		186	185.9674	
		187	186.9692	
		188	187.9697	
		189	188.9717	
		190	189.9725	
		192	191.9758	

c) H. E. DUCKWORTH, C. L. KEGLEY, J. M. OLSON e G. STANFORD: *Phys. Rev.*, **83**, 1117 (1951).

TABELLE DELLE MASSE DEI NUCLEI CON $Z \geqslant 40$ (*segue*).

	Z	A	massa calcolata con la (1)	massa sperimentale
Ir	77	191	190.9745	
		193	192.9774	
Pt	78	192	191.9755	
		194	193.9780	193.9828 *d*)
		195	194.9801	
		196	195.9810	195.9846 *d*)
		198	197.9845	
Au	79	197	196.9830	
Hg	80	196	195.9820	
		198	197.9841	
		199	198.9861	
		200	199.9868	
		201	200.9890	
		202	201.9900	
		204	203.9937	
Tl	81	203	202.9921	
		205	204.9954	
Pb	82	204	203.9932	
		206	205.9961	
		207	206.9984	
		208	207.9995	207.9974 *a*)
Bi	83	209	209.0016	209.0011 *f*)
Th	90	232	232.0419	232.0599 *a*)
U	92	234	234.0458	234.0625 *a*)
		235	235.0482	
		238	238.0536	238.0737 *a*)

a) G. S. STANFORD, H. E. DUCKWORTH, B. G. HOGG e J. S. GEIGER: *Phys. Rev.*, **86**, 617 (1952).
d) H. E. DUCKWORTH e R. S. PRESTON: *Phys. Rev.*, **82**, 469 (1951),
f) P. I. RICHARDS, E. E. HAYS e S. A. GOUDSMITH: *Phys. Rev.*, **85**, 630 (1952).

SUMMARY (*)

The author gives the masses of nuclei with $Z \geqslant 40$ calculated by the semiempirical formula of the drop model. Two coefficients of the formula have been recalculated with the method of least squares.

(*) *Editor's Translation.*

Considerazioni sui decadimenti dei mesoni π e K in fermioni leggeri.

F. Duimio

Istituto di Scienze Fisiche dell'Università - Milano
Istituto Nazionale di Fisica Nucleare - Sezione di Milano

(ricevuto il 25 Ottobre 1955)

Riassunto. — Si cerca di trarre informazioni sulla possibilità di uno schema generale di interazioni tra particelle elementari da un'analisi di tipo qualitativo di alcune peculiarità dei decadimenti dei mesoni π e K in fermioni leggeri. Le conclusioni sembrano potersi accordare con uno schema proposto da Dallaporta e Gell-Mann.

La caratteristica principale dei vari schemi proposti per spiegare le proprietà delle particelle nuove (iperoni, mesoni pesanti) sta nell'introduzione di due tipi fondamentali di interazione, uno forte (cioè con costante d'accelerazione G dell'ordine di grandezza di quella delle ordinarie interazioni π-nucleone) che giustifica le relativamente grandi sezioni di produzione (in coppie) di tali particelle, e uno debole che rende conto del lento decadimento di esse in nucleoni e mesoni π.

Ma, come è noto, vi sono anche particelle nuove che decadono in fermioni leggeri (K_μ, K_e, ...).

Se vogliamo, come sembra logico, identificare queste particelle con quelle sopraccennate, risulta indispensabile inquadrare in uno schema generale di tutte le particelle elementari anche i leptoni e le loro interazioni con le altre particelle.

Ora, la questione diventa estremamente complicata, soprattutto per i seguenti motivi:

1) Già per le interazioni leptoni-nucleoni-π (ossia l'insieme di tutte le particelle « vecchie ») la situazione è tutt'altro che chiara (1).

---

(1) Vedi ad esempio R. E. Marshak: *Meson Physics*, cap. 4 (1952); H. Yukawa: *Rev. Mod. Phys.*, **21**, 474 (1949); L. Michel: *Progr. in Cosmic Ray Phys.*, **1**, 125 (1952).

2) Se le regole di selezione che regolano i fenomeni concernenti le particelle nuove sono legate alla conservazione dello spin isotopico (GELL-MANN e PAIS: *Proc. Glasgow Confer.*, 1954, p. 342) come si dovrà introdurre questa variabile per i leptoni?

3) In uno schema generale di particelle elementari, da quale principio generale scende la legge di conservazione del numero dei barioni?

Prenderemo in considerazione nel seguito tre schemi tra i più semplici.

A) Riattaccandoci allo schema originale di Yukawa supponiamo l'esistenza di interazioni dirette π-leptoni; la totalità delle interazioni sarebbe quindi (2):

$$(1)\ \text{cost.}\ G\begin{cases}(\mathrm{NN}\pi)\\(\mathrm{YNK})\\(\mathrm{YY}\pi)\end{cases}\qquad(2)\ \text{cost}\,g\begin{cases}(\mathrm{NNK})\\(\mathrm{NY}\pi)\\(\mathrm{YYK})\end{cases}\qquad(3)\ g'?\begin{cases}(\mathrm{ee}\pi)\\(\mathrm{e}\mu\mathrm{K})\\(\mu\mu\pi)\end{cases}\qquad(4)\ G'?\begin{cases}(\mathrm{eeK})\\(\mathrm{e}\mu\pi)\\(\mu\mu\mathrm{K})\end{cases}$$

Questo schema, come è noto, anche quando non si considerino Y e K, reca notevoli difficoltà. Infatti supponiamo di determinare la costante d'accoppiamento G' che rende conto della vita media del decadimento $\pi \to \mu + \nu$ (il tipo di interazione è strettamente determinato dalla richiesta che la branching-ratio tra queste due reazioni sia in accordo con quella sperimentale: ciò si ottiene solo con un accoppiamento pseudovettoriale).

Se ora si vuole calcolare la vita media del decadimento β del neutrone, che qui avviene attraverso le

$$(5)\qquad \mathrm{n} \to \mathrm{p} + \pi^- \to \mathrm{p} + \mathrm{e}^- + \nu\,,$$

con una G che possa rendere conto delle ordinarie forze nucleari, si arriva a un risultato completamente sbagliato (3), (si ottiene una vita media τ dell'ordine di $\sim 10^{10}$ min, contro il τ osservato di ~ 15 min).

Perchè quindi lo schema *A*) possa essere accettato dovrebbe fornire le possibilità di superare questa difficoltà. Allo scopo si potrebbe supporre, per esempio, che $G' \gg g'$ e che il decadimento π-μ tramite le (3) fosse proibito da una qualche regola di selezione (4), che non dovrebbe tuttavia proibire la (5). Da un accurato esame di tutte le possibilità sembra che ciò non sia possibile.

In questo schema la legge di conservazione dei barioni sarebbe ottenibile attribuendo ad essi parità reale e ai leptoni parità immaginaria.

---

(2) Denoteremo genericamente il campo dei nucleoni con N, quello degli iperoni con Y; analogamente useremo μ ed e per i campi descriventi mesoni μ (ed eventualmente μ^0) e gli elettroni (e neutrini). π e K indicheranno i mesoni π e i mesoni pesanti.

(3) E. R. CAIANIELLO: *Phys. Rev.*, **81**, 625 (1951).

(4) Vedi ad esempio T. HAMADA e M. SUGAWARA: *Progr. Theor. Phys.*, 8, 363 (1952).

Anche questa ammissione si presta a forti critiche, sia perchè sembra privo di senso attribuire una parità intrinseca a particelle di massa nulla [5] (neutrini, ν^0), sia poi per la discussa attribuzione ai leptoni di uno spin isotopico [6].

Tale schema è quindi con ogni probabilità da respingere.

B) Al contrario del caso *A*) in cui si cercava di ridurre tutte le interazioni al tipo di interazione diretta fermione-bosone, il tipo di interazione « primitivo » si suppone qui essere un'interazione alla Fermi (*).

Si suppone cioè che i tipi di interazione possibile siano:

a) Un'interazione universale (con costante g_F) tra quattro fermioni qualunque: naturalmente ci dovranno essere opportune limitazioni per evitare l'occorrenza di processi non osservati, quali ad esempio $\mu^{\pm} \to e^{\pm} + e^{+} + e^{-}$ o reazioni che non rispettano la legge di conservazione dei barioni.

b) Le interazioni forti tra mesoni e barioni (con cost G).

In questo modello che sostanzialmente coincide con quello presentato da Gell-Mann al Congresso di Pisa (Giugno 1955) rientrano le recenti considerazioni di Dallaporta [10], in cui si mostra (in modo estremamente approssimato) come esso possa rendere conto della vita media dei decadimenti

$$Y \to N + \pi$$

$$K \to \begin{cases} 2\pi \\ 3\pi \end{cases}$$

supposti avvenire attraverso le seguenti reazioni:

$$(6) \qquad Y \xrightarrow{g_F} \bar{N} + N + N \xrightarrow{G} N + \pi$$

$$(7) \qquad K \xrightarrow{G} \bar{N} + Y \xrightarrow{g_F} \bar{N} + \bar{N} + N + N \xrightarrow{G} \begin{cases} 2\pi \\ 3\pi \end{cases}.$$

---

[5] L. Michel: Tesi.

[6] M. Cini e A. Gamba: *Nuovo Cimento*, **10**, 1040 (1953).

(*) Si potrebbe spingere all'estremo questa posizione in base all'idea avanzata da Fermi e Yang [7] secondo cui il mesone π potrebbe forse considerarsi un sistema fortemente legato nucleone-antinucleone tramite le forze provenienti da un'interazione alla Fermi, estendendola opportunamente in modo da tenere conto degli iperoni e dei mesoni pesanti [8]. Possiamo anche aggiungere che la teoria della fusione di De Broglie [9] potrebbe forse far rientrare anche il campo e.m. in un tale schema.

[7] E. Fermi e C. N. Yang: *Phys. Rev.*, **76**, 1739 (1949).

[8] M. M. Lévy e R. E. Marshak: *Suppl. Nuovo Cimento*, **12**, 253 (1954).

[9] L. De Broglie: *Théorie générale des particules à spin* (Paris, 1943).

[10] N. Dallaporta: *Nuovo Cimento*, **1**, 962 (1955).

Notiamo subito che per quanto riguarda le particelle vecchie, sussistono le note difficoltà connesse, ad esempio, al calcolo dei decadimenti $\pi^0 \to 2\gamma$ o $\pi \to \mu + \nu$ su cui torneremo in seguito.

Inoltre Y e K, oltre a come indicato in 2) e 3), potrebbero in questo schema decadere nei modi seguenti:

$$\text{(8)} \qquad Y \xrightarrow{g_F} N + 2 \text{ leptoni}$$

$$\text{(9)} \qquad K \xrightarrow{G} N + \bar{N} \xrightarrow{g_F} 2 \text{ leptoni}.$$

Processi del tipo (8), per esempio:

$$\text{(10)} \qquad \begin{cases} \Lambda^0 \to p + \mu^- + \nu \\ \Sigma^\pm \to n + \mu^\pm + \nu \end{cases}$$

avrebbero vite abbastanza lunghe confrontate a quelle della (6) per spiegare la loro mancata evidenza sperimentale.

Come abbiamo visto lo schema *A*) ha il vantaggio di fornire una spiegazione ragionevole del rapporto $w(\pi \to \mu + \nu)/w(\pi \to e + \nu)$, ma cade completamente nell'interpretazione del decadimento β. Lo schema *B*) sembra necessario per la spiegazione del decadimento β. Esso però va incontro a gravi difficoltà per la trattazione dei decadimenti di mesoni in leptoni.

C) Uno schema che comprende i vantaggi dei due schemi *A*) e *B*) è stato proposto da alcuni ricercatori giapponesi [11].

I tipi di accoppiamento postulati sono i seguenti:

1) Interazione universale alla Fermi (costante g_F). Occorrono anche qui naturalmente le solite regole per proibire processi indesiderati.

2) Interazioni forti mesone-barione (costante G).

3) Interazioni deboli, universali, bosone-fermione (costante g). Comprendono le interazioni dirette π-leptoni, K-leptoni e le interazioni deboli mesone-barione.

Esso è cioè essenzialmente la « sovrapposizione » degli schemi *A*) e *B*). I citati autori mostrano poi che tale sovrapposizione non dà luogo a contraddizioni interne.

---

[11] S. Ogawa, H. Okonoji e S. Oneda: *Progr. Theor. Phys.*, **11**, 330 (1954); K. Iwaka, S. Ogawa, H. Okonoji, B. Sakita e S. Oneda: *Progr. Theor. Phys.*, **13**, 19 (1955).

L'argomento fondamentale portato in cit. [11] contro lo schema *B*) e quindi a giustificazione dello schema *C*), più ampio, si fonda sulla asserita inadeguatezza dello schema *B*) riguardo alla spiegazione dei fenomeni di decadimento dei π in leptoni.

Ci proponiamo ora di riesaminare questa questione, parallelamente all'analogo problema del decadimento dei K in leptoni. Cioè ci proponiamo essenzialmente di ricavare alcune conseguenze qualitative derivanti dalla trattazione dei seguenti processi con una interazione diretta (interazione debole universale bosone-fermione di cit. [11]), e con una interazione « indiretta » (tramite una coppia di barioni e un'interazione alla Fermi):

(11) $\pi^{\pm} \to \mu^{\pm} + \nu$ (12) $\pi^{\pm} \to \mu^{\pm} + \nu + \gamma$

(13) $\pi^{\pm} \to e^{\pm} + \nu$ (14) $\pi^{\pm} \to e^{\pm} + \nu + \gamma$

(15) $K^{\pm} \to \mu^{\pm} + \nu$ (16) $K^{\pm} \to \mu^{\pm} + \nu + \gamma$

(17) $K^{\pm} \to \mu^{\pm} + \nu + \pi^0$

(18) $K^{\pm} \to e^{\pm} + \nu$ (19) $K^{\pm} \to e^{\pm} + \nu + \gamma$

(20) $K^{\pm} \to e^{\pm} + \nu + \pi^0$

verrà poi eseguito un confronto con i dati sperimentali oggi disponibili. Elenchiamo i dati che ci saranno utili per tale confronto:

I) $$\frac{w(\pi^{\pm} \to e^{\pm} + \nu)}{w(\pi^{\pm} \to \mu^{\pm} + \nu)} = (0.3 \pm 0.9) \cdot 10^{-4} \quad [12]$$

II) $$\frac{w(\pi^{\pm} \to \mu^{\pm} + \nu + \gamma)}{w(\pi^{\pm} \to \mu^{\pm} + \nu)} = (2.8 \pm 1.2) \cdot 10^{-4} \quad [13].$$

III) Non si ha nessuna indicazione sperimentale riguardo l'esistenza della (14).

IV) $$\frac{w(K^{\pm} \to \mu^{\pm} + \nu + ?^0)}{w(K^{\pm} \to \mu^{\pm} + \nu)} = \sim 0.1$$

V) $$\frac{w(K^{\pm} \to e^{\pm} + \nu + ?^0)}{w(K^{\pm} \to \mu^{\pm} + \nu)} = \sim 0.2$$

VI) Non si ha indicazione sperimentale riguardo l'esistenza della (18).

---

[12] S. Lokanathan e J. Steinberger: *Suppl. Nuovo Cimento*, **1**, 161 (1955).
[13] N. F. Fry: *Phys. Rev.*, **86**, 418 (1952).

Le ultime tre stime, naturalmente molto approssimative, provengono da dati preliminari sul G-Stack [14]. In particolare il dato VI) è dubbio data la difficoltà sperimentale di identificazione di elettroni ad alte energie. Qualche evento classificato come K_{e3} potrebbe infatti appartenere al decadimento (18) (K_{e2}). Tuttavia le considerazioni che seguono mantengono la loro validità anche con l'ipotesi meno restrittiva che la frequenza degli eventi K_{e2} sia inferiore a quella degli eventi K_{e3}.

Noi supporremo che i processi (15)-(20) siano altrettanti modi alternativi di decadimento di una stessa particella, a statistica di Bose e avente massa $\sim 965\ m_e$.

Come è noto [15] i processi (11) e (13) e il rapporto I) possono essere spiegati da un'interazione diretta solo se tale interazione è supposta *A*. In questo schema anche i processi (12) e (14) (decadimenti radiativi) possono essere interpretati in modo soddisfacente, in modo cioè da rendere conto dei dati II) e III) [16].

Nello schema « indiretto » il calcolo delle probabilità di transizione per i processi suddetti incontra gravi difficoltà per le divergenze connesse al « closed-loop » nucleonico. Metodi di cut-off [17] e di regolarizzazione [18] sono stati applicati ai processi (11) e (13) con risultati piuttosto dubbi. È però possibile calcolare in modo soddisfacente il rapporto I) poichè in tal caso le espressioni divergenti si elidono.

I risultati per i valori di detto rapporto sono rappresentati nella tabella I.

TABELLA I.

	Ss	*Sv*	*Vv*	*Vt*	*At*	*Aa*	*Pa*	*Pp*
S	5.7	F	F	F	F	X	X	X
V	F	E	4.4	4.4	X	F	F	F
T	F	E	2.7	2.7	2.4	F	F	F
A	X	F	F	F	F	4.4	$1.3 \cdot 10^{-4}$	$1.3 \cdot 10^{-4}$
P	X	F	F	F	F	X	5.7	5.7

Per le combinazioni contrassegnate con una lettera maiuscola il processo è proibito da:

E = teorema di equivalenza
F = teoremi generalizzati di Furry.
X = elemento di matrice = 0 (almeno all'ordine più basso).

---

[14] Di questa e di altre utili informazioni ringraziamo i membri del gruppo lastre di Milano.

[15] B. D'ESPAGNAT: *Compt. Rend.*, **228**, 774 (1949).

[16] H. PRIMAKOFF: *Phys. Rev.*, **84**, 1255 (1951); T. EGUCHI: *Phys. Rev.*, **85**, 943 (1952); T. NAKANO, J. NISHIJIMA e Y. YAMAGUCHI: *Progr. Theor. Phys.*, **6**, 1028 (1951).

[17] M. RUDERMANN e R. FINKELSTEIN: *Phys. Rev.*, **76**, 1458 (1949); S. NAKAMURA, H. FUKUDA e K. ÔNO: *Progr. Theor. Phys.*, **5**, 740 (1950).

[18] J. STEINBERGER: *Phys. Rev.*, **88**, 1266 (1952).

Le uniche combinazioni che possono dare un accordo coi dati sperimentali sono dunque le Pp o Pa per quanto riguarda il π e l'accoppiamento π-N. L'interazione alla Fermi deve contenere l'accoppiamento A e non il P. Condizioni queste che possono non contraddire le indicazioni derivanti dallo studio del β-decay, purchè l'A sia piccolo [11] e che quindi le altre interazioni possibili (non necessariamente tutte) S, V e T, siano presenti con un peso notevole.

Se quindi, come sembra probabile le interazioni V o T sono importanti, sorge una notevole difficoltà.

Infatti i processi (12) e (14) non sono proibiti per le combinazioni Pa-V, Pa-T e Pp-V, Pp-T (mentre lo sono per le combinazioni di Pa e Pp con S, A e P). Si avrebbe in tal caso una prevalenza del processo (14) sul (12); non solo, ma questi processi dovrebbero avvenire con una probabilità piuttosto elevata; si avrebbe (con calcoli eseguiti con cut-off in cit. [11])

$$\frac{w(\pi^{\pm} \to e^{\pm} + \nu + \gamma)}{w(\pi^{\pm} \to \mu^{\pm} + \nu)} = 10^{-2} \sim 10^{-3} .$$

Tutto ciò dunque sarebbe in contraddizione con i dati II) e III).
Questo argomento è portato, come abbiamo accennato, da Oneda e coll. a favore dell'introduzione della loro interazione universale debole bosone-fermione (schema C).

Osserviamo però che anche accettando questo risultato, fondato su metodi matematici certo non convincenti, ci sarebbe ancora una possibilità per superare queste difficoltà. Supponiamo, ad esempio, che l'interazione di Fermi da noi considerata sia una miscela di interazioni A, V e T, e che, ad esempio, gli elementi di matrice corrispondenti alle transizioni

$$(21) \qquad \begin{aligned} \pi &\to N + N \xrightarrow{g_T} \begin{cases} \mu \\ e \end{cases} - \nu + \gamma \\ \pi &\to \overline{N} + N \xrightarrow{g_V} \begin{cases} \mu \\ e \end{cases} + \nu + \gamma \end{aligned}$$

diano contributi di segno opposto. È chiaro allora che la probabilità totale di transizione potrebbe diminuire di molto fino a rendere inosservabile sia il processo (12) che il (14).

Qualcosa di simile si potrebbe ottenere anche prendendo in considerazione coppie virtuali intermedie iperone-antiiperone (*) con un'interazione alla

(*) Questa idea è stata applicata da Kinoshita: *Phys. Rev.*, **94**, 1331 (1954), al decadimento $\pi^0 \to 2\gamma$.

Fermi del tipo (YY)(μν) e simili, per esempio

$$\pi \to \Sigma^+ + \bar{\Lambda}^0 \to \begin{cases} \mu \\ e \end{cases} + \nu + \gamma \,. \tag{22}$$

Riguardo ai decadimenti anomali è chiaro che la spiegazione data in termini di decadimenti radiativi (cioè dovuti all'irraggiamento del μ o dell'e bruscamente accelerati all'atto della formazione) manterrebbe la sua validità.

Entrando ora nel campo dei mesoni K osserviamo che uno schema ad accoppiamento diretto richiederebbe ancora naturalmente un accoppiamento Δ1, in modo da giustificare il dato VI).

I decadimenti a tre corpi dovrebbero essere interpretati come decadimenti radiativi (16) e (19). Ma anche ammesso in tal modo di soddisfare la condizione IV), non sembra possibile spiegare la presenza della (19) e l'assenza della (18).

Usando invece un accoppiamento indiretto (schema *B*)), dovremo considerare il processo di decadimento del K procedente attraverso una coppia virtuale nucleone-antiiperone (o iperone-antinucleone) e una interazione di Fermi (NY)(eν) o (NY)(μμ⁰) (o eventualmente (NY)(eμ⁰) o (NN)(μν)) con costanti di interazione G e g_F supposte allo stesso ordine di grandezza delle G e g_F delle ordinarie interazioni π-N e di Fermi.

È chiaro che in questo caso, essendo sconosciuta la forma esplicita dell'interazione (NYK), non è detto che i teoremi generalizzati di Furry siano applicabili (nel caso delle attribuzioni di spin isotopico tipico dello schema di Gell-Mann-Pais non lo sono ([20])). La tabella I andrebbe perciò modificata.

Ad ogni modo è ragionevole pensare che i decadimenti « mesici » (17) e (20) prevalgano sui decadimenti radiativi (16) e (19), dato che l'interazione π-N è molto più forte dell'interazione e.m. e che pertanto essi avranno una frequenza notevole rispetto ai decadimenti in due corpi.

COSTA e DALLAPORTA ([21]) hanno tentato una stima approssimativa per i detti processi (17) e (20) ottenendo un rapporto:

$$\frac{w(\varkappa^\pm \to e^\pm + \nu + \pi^0)}{w(\varkappa^\pm \to \mu^\mp + \nu + \pi^0)} = 2 \sim 3 \,,$$

che è in buon accordo col rapporto sperimentale ottenibile dalle condizioni IV) e V).

([19]) H. M. MAHMOUD e E. J. KONOPINSKI: *Phys. Rev.*, **91**, 1232 (1952); J. P. DAVIDSON e P. C. PEASLEE: *Phys. Rev.*, **91**, 1232 (1952).

([20]) K. NISHIJIMA: *Progr. Theor. Phys.*, **13**, 285 (1955).

([21]) G. COSTA e N. DALLAPORTA: *Nuovo Cimento*, **2**, 519 (1955).

Essi tuttavia per i singoli rapporti IV) e V) ottengono valori dell'ordine di 10^{-4}, molto lontani da quelli osservati. Ripetiamo però che essi si servono di metodi estremamente approssimativi di stima di ordine di grandezza, che probabilmente incidono più gravemente sulla valutazione della $w(K^{\pm} \to \mu + \nu)$ (la quale dovrà prevalentemente svolgersi attraverso un solo « channel » del tipo $Pa \cdot A$ o $Pp \cdot A$ per rendere conto del dato VI) che non nelle valutazioni delle w dei decadimenti « mesici ».

Su valutazioni più precise dei suddetti rapporti, in base a ipotesi più specifiche sulla natura e sulle interazioni delle Y e K, in connessione al problema dell'identificazione dei K che decadono in leptoni coi K che decadono in π (τ, θ^0, ecc.), ci proponiamo di tornare in seguito in un successivo studio.

Concludendo questa discussione di tipo necessariamente qualitativo possiamo dire che la difficoltà inerente ai decadimenti radiativi del π in uno schema « indiretto », in cui cioè non sia necessario introdurre una « interazione debole universale bosone-fermione » oltre alle interazioni forti barione-mesone e alle interazioni alla Fermi, può essere superata; non solo, ma anche che i recenti dati sperimentali relativi ai modi di decadimento di mesoni K in leptoni sembra possano essere inquadrati in una teoria « indiretta » piuttosto che in una « diretta ».

* * *

Vivi ringraziamenti sono dovuti al prof. P. Caldirola, per il suo interessamento e il suo consiglio.

SUMMARY

One tries to deduce some informations on the possibility of a general scheme of interactions between the elementary particles with a qualitative analysis of some characteristic features of π and K-decays into light fermions. The conclusions seem to be in agreement with a scheme proposed by Dallaporta and Gell-Mann.

LETTERE ALLA REDAZIONE

(La responsabilità scientifica degli scritti inseriti in questa rubrica è completamente lasciata dalla Direzione del periodico ai singoli autori)

Sul cammino libero medio anelastico dei protoni di 450 MeV in emulsioni nucleari.

V. Benzi, M. Ladu e N. Marongiu

Istituto di Fisica dell'Università - Cagliari

(ricevuto il 20 Ottobre 1955)

Sono stati seguiti 4 079 cm di traccia protonica su lastre Ilford G5 di 600 μm di spessore, esposte a un fascio di protoni di 450 ± 30 MeV del ciclotrone di Chicago.

Le tracce di protoni singoli sono state seguite con un ingrandimento di 1300 diametri circa e l'errore nella misura della lunghezza effettiva della traccia è risultato di circa il 3 %.

Sono stati complessivamente osservati 104 eventi anelastici [1] così suddivisi:

a) 65 stelle con uno o più rami;

b) 36 diffusioni (improvviso cambio di direzione della traccia con angolo polare maggiore di 10°);

c) 3 arresti.

Si ha così un c.l.m. di 39.2 ± 4.9 cm.

Recenti risultati sperimentali [2] hanno mostrato che le sezioni di urto totale per neutroni di energia intorno ai 400 MeV differiscono sensibilmente da quelle previste dalla teoria ottica di Fernbach, Serber e Taylor [3] in cui il nucleo diffondente è trattato come una sfera semitrasparente di densità costante.

Con lo scopo di eliminare queste discrepanze, Nakano [4] ha esteso la teoria ottica al modello proposto da Johnson e Teller [5], secondo il quale la densità della materia nucleare si mantiene praticamente uniforme solo nel caso di nuclei leggeri; i risultati della teoria sono allora in buon accordo con quelli sperimentali.

Confrontando il c.l.m. anelastico sperimentale con quello calcolato applicando la teoria ottica al modello J-T si ottiene un ulteriore conferma dell'attendibilità di quest'ultimo.

---

(1) G. Bernardini, E. T. Booth e S. J. Lindenbaum: *Phys. Rev.* **85**, 826, (1952).
(2) V. A. Nedzel: *Phys. Rev.* **94**, 174, (1954).
(3) S. Fernbach, R. Serber e T. B. Taylor: *Phys. Rev.* **75**, 1352, (1949).
(4) Y. Nakano: *Phys. Rev.* **98**, 842, (1955).
(5) M. H. Johnson e E. Teller: *Phys. Rev.* **93** 357, (1954).

Secondo la teoria F-S-T la sezione d'urto anelastico protone-nucleo è data da

$$\sigma_{an} = \pi R^2\{1 - \big(1 - (1+2KR)\exp[-2KR]\big)/2K^2R^2\}, \tag{1}$$

con

$$K = 3C[Z\sigma_{pp} + N\sigma_{pn}]/4\pi R^3 . \tag{2}$$

Nella (2) R è il raggio del nucleo urtato, σ_{pp} e σ_{pn} indicano le sezioni d'urto protone-protone e protone-neutrone rispettivamente e C è un fattore dell'ordine dell'unità che tiene conto dello stato di legame dei nucleoni nel nucleo.

Nel caso in esame, per calcolare le σ_{an} dei vari elementi dell'emulsione in base alle (1) e (2), si può praticamente porre $C=1$, mentre per σ_{pp} e σ_{pn} si possono utilizzare i valori determinati per via sperimentale con nucleoni di ~ 410 MeV [2], pari a 24 mb e 34 mb rispettivamente.

Per R si è preso il valore di $1.36 \cdot A^{\frac{1}{3}} \cdot 10^{-13}$ cm [4].

Con questi valori dei parametri la teoria F-S-T permette di calcolare, per una composizione standard dell'emulsione, il c.l.m. anelastico, che risulta di 32.7 cm.

Per estendere i metodi del modello ottico al caso di nuclei del tipo J-T si è supposto che nel nucleo possano distinguersi una zona interna di raggio R_i in cui sono contenuti Z protoni e Z neutroni ed una zona esterna di raggio R_e contenente i residui $N - Z$ neutroni.

Secondo una proposta di COURANT [6] detti raggi sono stati scelti in modo che la densità di neutroni sia costante in tutto il volume nucleare, cioè $R_i/R_e = (Z/N)^{\frac{1}{3}} = \gamma$.

Al posto dell'unico coefficiente di assorbimento definito dalla (2) debbono ora considerarsi i due coefficienti

$$K_i = 3(\sigma_{pp}+\sigma_{pn})Z/4\pi(\gamma R_e)^3 , \qquad K_e = 3\sigma_{pn}(N - Z)/4\pi R_e^3(1 - \gamma^3) \tag{3}$$

per la zona interna ed esterna rispettivamente.

L'espressione analitica esatta di σ_{an} fornita dall'applicazione dei metodi del modello ottico, è in questo caso piuttosto complicata; una forma più semplice, valida con buona approssimazione quando $2\gamma \cong 1+\gamma^2$, è la seguente

$$\sigma_{an} = \pi R_e^2(I_e + I_i), \tag{4}$$

con

$$I_e = (1 - \gamma^2)\{1 - \big(1 - (1+2\varepsilon R_e)\exp[-2\varepsilon R_e]\big)/2\varepsilon^2 R_e^2\} \tag{4a}$$

$$I_i = \{2(\eta^2 + \varepsilon^2)/(K_e^2 + 2K_i^2) + \\ + \big((1+2\eta R_e)\exp[-2\eta R_e] - (1+2\varepsilon R_e)\exp[-2\varepsilon R_e]\big)/2R_e^2K_i^2\} \tag{4b}$$

dove

$$\varepsilon = K_e(1 - \gamma^2)^{\frac{1}{2}} , \qquad \eta = K_e + (K_i - K_e)\gamma . \tag{4c}$$

Per $N=Z$ la (4) coincide con la (1).

I valori di σ_{an} calcolati per i vari elementi dell'emulsione in base alle (3) e (4)

---

[6] E. D. COURANT: *Phys. Rev.*, **94**, 1081, (1954).

avendo posto $R = 1.36 \cdot A^{\frac{1}{3}} \cdot 10^{-13}$ cm forniscono per il c.l.m. calcolato il valore di 37.4 cm, in buon accordo quindi con quello sperimentale.

Sembra con ciò che il modello J-T, almeno per l'energia in questione, conduca a risultati che si accordano con quelli sperimentali meglio di quelli deducibili dal modello a densità costante.

* * *

Desideriamo esprimere i nostri ringraziamenti ai proff. P. CALDIROLA e G. FRONGIA per il loro interessamento.

Two-Center Integrals for Iron Using Wawe Functions with Exchange.

M. Suffczyński

Institute of Theoretical Physics, University of Warsaw - Warsaw

(ricevuto il 20 Ottobre 1955)

Fletcher and Wohlfarth [1,2] have calculated the energy integrals appearing in the matrix elements of the tight binding approximation as the two-center integrals between the nearest neighbours in the metallic lattice. They based their calculations for nickel on the atomic functions $3d$ of Cu^+ calculated by Hartree [3] with exchange.

For iron no calculations of the Hartree-Fock functions have been performed. Only very recently J. H. Wood [4] of M.I.T. has computed the atomic wave functions of a normal Fe atom taking the exchange into account by the approximate method proposed by Slater [5]. The configuration adopted by Wood for the $3d$ electrons in Fe is five electrons $3d1$ (α spin) and one electron $3d2$ (β spin). The $3d$ functions computed with the inclusion of exchange effects are much more compact than the old functions given by Manning and Goldberg [6] without exchange.

The $3d1$ function of Wood has been used to compute the energy integrals for the metallic body-centered iron. The method and the approximation of Fletcher [2] have been followed exactly. Every integral was calculated as a difference between an integral over all space and an integral over the atomic sphere centered in the origin. The radius of that sphere was always taken as half the distance between the atom in the origin and the neighbour.

The distance of the nearest neighbours was taken as $d = 2.4772$ kX, that of next nearest neighbours as $a = 2.8604$ kX, after the recent measurements of Basinski, Hume-Rothery and Sutton [7]. For converting the kX units to angstrom units and therefrom to Bohr units the values from the table of Cohen and Du Mond [8] have been adopted.

The numerical values of the normalized function P_N $(3d1; r)$ have been

---

(1) G. C. Fletcher and E. P. Wohlfarth: *Phil. Mag.*, **42**, 106 (1951).

(2) G. C. Fletcher: *Proc. Phys. Soc.*, A **65**, 192 (1952).

(3) D. R. Hartree and W. Hartree: *Proc. Roy. Soc.*, A **157**, 490 (1936).

(4) J. H. Wood: to appear in *Phys. Rev.*

(5) J. C. Slater: *Phys. Rev.*, **81**, 385 (1951).

(6) M. F. Manning and L. Goldberg: *Phys. Rev.*, **53**, 662 (1938).

(7) Z. S. Basinski, W. Hume-Rothery and A. L. Sutton: *Proc. Roy. Soc.*, A **229**, 459 (1955).

(8) E. R. Cohen and J. W. M. Du Mond: *Rev. Mod. Phys.*, **25**, 691 (1953).

approximated by the analytical function

$$(1) \quad P_A(r) = r^3(2.815 \exp[-2.1r] + 81.97 \exp[-5.1r]) .$$

and the potential by the function

$$(2) \quad U(r) = -(1 + 25 \exp[-3r])/r .$$

The expression P_A approximates the values of the Wood $3d1$ function satisfactorily, the discrepancy being less than $6.5 \cdot 10^{-2}$ between $r = 0.1$ and $r = 0.35$ and less than $3.6 \cdot 10^{-2}$ everywhere else. The potential as given by (2) is much less well founded.

The energy integrals have been calculated between $d\sigma$, $d\pi$ and $d\delta$ orbitals since SLATER and KOSTER [9] have given convenient tables for reducing the matrix elements of the tight binding approximation in cubic lattices to the two-center integrals between functions of σ, π, δ-type symmetry. The notation of these tables has been adopted here.

The integrals computed using (1) and (2) turned out to be:

for the nearest neighbours

$$(dd\sigma)_1 = -0.4113 \text{ eV} ,$$
$$(dd\pi)_1 = \quad 0.2210 \text{ eV} ,$$
$$(dd\delta)_1 = -0.0332 \text{ eV} ,$$

for the next nearest neighbours

$$(dd\sigma)_3 = -0.1687 \text{ eV} ,$$
$$(dd\pi)_3 = \quad 0.0745 \text{ eV} ,$$
$$(dd\delta)_3 = -0.0094 \text{ eV} .$$

The figures here have been truncated to four decimal places.

These values are about two times smaller than the corresponding values calculated [10] from atomic functions without exchange. Nevertheless they are perhaps still too great since Callaway in his calculations [11] has found a rather narrow band of $3d$ electrons in metallic iron. Furthermore the work of F. STERN [12] has revealed the great sensitivity of the wave functions and density of $3d$ electrons in Fe atom upon the configuration adopted for $3d$ electrons.

* * *

I will express my deep gratitude to Dr. J. H. WOOD for sending me kindly his unpublished tables of atomic functions of the Fe atom. I am very grateful also to Dr. G. C. FLETCHER for his kind and interesting correspondence concerning the two-center integrals. I thank also Prof. J. CALLAWAY for sending me his unpublished papers and to Prof. J. SLATER for sending his paper on the tight binding method.

My thanks are due to Prof. L. INFELD for providing me with a « Facit » on which the computations were performed.

---

[9] J. C. SLATER and G. F. KOSTER: *Phys. Rev.*, **94**, 1498 (1954).

[10] M. SUFFCZYŃSKI: to appear in *Acta Phys. Pol.*

[11] J. CALLAWAY: *Phys. Rev.*, **97**, 933 (1955); **98**, 1150 (1955).

[12] F. STERN: *Phys. Rev.*, **98**, 1552 (1955)

Proton Polarization in (n, p) Reactions and Nuclear Optical Model.

J. Sawicki

Institute of Theoretical Physics, University of Warsaw - Warsaw

(ricevuto il 22 Ottobre 1955)

The polarization of nucleons produced in different nuclear reactions is a good tool in investigating spin-orbit potentials. Recently many authors investigated the spin-orbit potential of the nuclear optical model for high energy nucleon scattering by estimating the degree of polarization. In the medium energy range the « cloudy crystal ball » potential of Feshbach *et al.* [1] modified by an additional spin-orbit term was successful in the description of the elastic scattering of polarized neutrons [2]. Recently this model was applied to the investigation of the proton polarization in (d, p) reactions, for which stripping mechanism was assumed at the deuteron energies ~ 3 MeV [3].

Austern, Butler and Mc Manus [4] have shown that for most nuclei compound nucleus formation should contribute little to the (n, p) reactions in the medium energy range. Experimental angular distributions were satisfactorily explained with the use of the « impulse approximation » and the assumption of direct mechanism of the reaction. The same mechanism is assumed below (proton, initially in a bound state of orbital angular momentum l_i and projection m_i, is knocked out from the surface of the nucleus by the incoming neutron, which is captured into a state of orbital angular momentum l_f and projection m_f).

Recently Demeur [5] discussed the (n, p) reactions with the same assumption using Born approximation similarly as Bhatia *et al.* and the « zero range » neutron-proton interaction. On introducing similarly as in ref. [4] the Butler stripping radius r_0 (cut-off of the plane waves at r_n, $r_p = r_0$) instead of Bhatias approximation and on using the « zero range » approximation we obtain for our matrix element:

$$(1) \quad M_{\dots} = \text{const} \int \mathrm{d}\sigma_n \, \mathrm{d}\sigma_p \int \mathrm{d}\xi \, \mathrm{d}\boldsymbol{r} \Psi_f^*[\mu_f] \exp[\quad i\boldsymbol{k}_p \boldsymbol{r}] \chi^*_{\mu_p}(\sigma_p) \Psi_i[\mu_i] \exp[i\boldsymbol{k}_n \boldsymbol{r}] \chi_{\mu_n}(\sigma_n) \dots ,$$

[1] H. Feshbach, C. E. Porter and V. S. Weisskopf: *Phys. Rev.*, **96**, 448 (1954).
[2] P. Adair, P. Fields and C. Darden: *Phys. Rev.*, **96**, 503 (1954).
[3] W. B. Cheston: *Phys. Rev.*, **96**, 1590 (1954).
[4] N. Austern, S. T. Butler and H. Mc Manus: *Phys. Rev.*, **92**, 350 (1953).
[5] H. Demeur: *Journ. Phys. Rad.*, **16**, 73 (1955).

where:

$$\Psi_i[\mu_i] = \sum_{m_i \mu_p'} C_{l_i \frac{1}{2}}(j_i \mu_i;\, m_i \mu_p')\psi(l_i m_i)\chi_{\mu_p'}(\sigma_p)\Phi_0(\xi);\quad \Psi_f[\mu_f] =$$

$$= \sum_{m_f \mu_n'} C_{l_f \frac{1}{2}}(j_f \mu_f;\, m_f \mu_n')\psi(l_f m_f)\chi_{\mu_p'}(\sigma_n)\Phi_0(\xi)\,,$$

where $\psi(l, m)$ = single particle orbital, $\Phi(\xi)$ = core wave function. The remaining symbols have their usual meaning. The target nucleus is assumed heavy (L-system).

On assuming that the outgoing proton will scatter in a spin-orbit potential $\exp[i\boldsymbol{k}_p\boldsymbol{r}]\chi_{\mu_p}(\sigma_p)$ in (1) must be replaced by:

$$\Psi_p[\mu_p] = \sum_{L M_L} \sum_{J M_J} a^*(L, M_L) C_{L \frac{1}{2}}(J, M_J;\, M_L, \mu_p)\psi(J, L, M_J) \ldots\,, \tag{2}$$

in the notation of ref. [3]. The Coulomb distortion of the proton wave is neglected [the proton polarization due to Coulomb interactions in (d, p) reactions was shown to be very small by I. P. GRANT [6]].

The neutron wave is assumed to be distorted by a nonspin dependent potential, since we are not interested in the neutron polarization and its influence upon the proton polarization is assumed small (the influence of the neutron scattering on the angular distribution is very small) see ref. [4].

Thus $\exp[i\boldsymbol{k}_n\boldsymbol{r}]\chi_{\mu_n}(\sigma_n)$ is replaced by:

$$\Psi_n[\mu_n] = \sum_{L_n M_n} b^*(L_n M_n)\Phi(L_n M_n)\chi_{\mu_n}(\sigma_n) \ldots\,. \tag{3}$$

The axis of quantization is defined as parallel to the vector of polarization i.e. by the vector $\boldsymbol{k}_n \times \boldsymbol{k}_p$ (perpendicular to the plane of scattering). With the quantization axis chosen the proton knocked out from (i)-nucleus in a definite state of spin orientation will maintain this orientation after scattering in the spin-orbit potential. Hence we may write for the partial matrix element of our transition operator T:

$$\langle \psi(J, L, M_J)\psi(l_f, m_f)\chi_{\mu_n'}(\sigma_n) \,|\, T \,|\, \Phi(L_n, M_n)\chi_{\mu_n}(\sigma_n)\psi(l_i, m_i)\chi_{\mu_p}(\sigma_p)\rangle = \tag{4}$$

$$= C_{L \frac{1}{2}}(J, M_J;\, M_L, \mu_p)\delta_{\mu_p \mu_p'}\delta_{\mu_n \mu_n'}\langle \psi(J, L, M_L)\psi(l_f, m_f) \,|\, T \,|\, \Phi(L_n M_n)\psi(l_i, m_i)\rangle \ldots\,,$$

where:

$$\psi(J, L, M_L) = [j_L(k_p r) - \beta(L, J)h_L^{(1)}(k_p r)]^* Y_{L M_L}(\vartheta, \varphi) \ldots\,, \tag{5a}$$

and

$$\Phi(L_n M_n) \quad = [j_{L_n}(k_n r) - \beta(L_n)h_{L_n}^{(1)}(k_n r)]Y_{L_n M_n}(\vartheta, \varphi) \ldots\,, \tag{5b}$$

$\beta = \frac{1}{2}\eta$ being complex numbers describing the distortion of the waves by the nuclear potentials:

$$\psi(l_i m_i) = \text{const}\; k_{l_i}(t_i r)Y_{l_i m_i}(\vartheta, \varphi) \qquad \text{and} \qquad \psi(l_f m_f) = \text{const}\; k_{l_f}(t_f r)Y_{l_f m_f}(\vartheta, \varphi)\,,$$

---

[6] I. P. GRANT: *Proc. Phys. Soc.*, A **68**, 244 (1955).

where

$$k_l(tr) = h_l^{(1)}(itr) .$$

The reaction matrix element becomes:

$$(6)\quad M(\mu_i, \mu_n \to \mu_f, \mu_p) = \sum_{LM_L} \sum_{L_n M_n} \sum_{J=L-\frac{1}{2}}^{L+\frac{1}{2}} a(L, M_L) b^*(L_n, M_n) C^2_{L\frac{1}{2}}(J, M_L + \mu_p; M_L, \mu_p) \cdot$$
$$\cdot C_{l_f \frac{1}{2}}(j_f, \mu_f; \mu_f - \mu_n, \mu_n) C_{l_i \frac{1}{2}}(j_i, \mu_i; \mu_i - \mu_p, \mu_p) \langle \psi(J, L, M_L) \psi(l_f m_f) \cdot$$
$$\cdot |T| \Phi(L_n, M_n) \psi(l_i, m_i) \rangle \dots ,$$

where

$$b^*(L_n M_n) = 4\pi i^{L_n} Y^*_{L_n M_n}\left(\frac{\pi}{2}, 0\right); \quad a(L, M_L) = 4\pi i^{-L} Y_{LM_L}\left(\frac{\pi}{2}, \theta\right),$$

θ being the scattering angle. Finally the degree of the proton polarization is:

$$(7)\quad P = \frac{\sum_{\mu_i, \mu_n, \mu_f} \{|M(\mu_i, \mu_n \to \mu_f, \mu_p = +\frac{1}{2})|^2 - |M(\mu_i, \mu_n \to \mu_f, \mu_p = -\frac{1}{2})|^2\}}{\sum_{\mu_i, \mu_n, \mu_f} \{|M(\mu_i, \mu_n \to \mu_f, \mu_p = +\frac{1}{2})|^2 + |M(\mu_i, \mu_n \to \mu_f, \mu_p = -\frac{1}{2})|^2\}} \dots .$$

It is easily seen that $P(\theta = 0) = P(\theta = \pi) = 0$.

As an illustration let us consider the $(S_{\frac{1}{2}}, S_{\frac{1}{2}})$ case ($l_i = l_f = 0$). The matrix element is:

$$(8)\quad M_{00}(\mu_p) = \text{const} \sum_{LM_L} \sum_{J=L-\frac{1}{2}}^{L+\frac{1}{2}} a(L, M_L) b^*(L, M_L) C^2_{L\frac{1}{2}}(J, M_L + \mu_p, M_L, \mu_p) R_{LJ} \dots ,$$

where:

$$(9)\quad R_{LJ} = \int_0^\infty \mathrm{d}r r^2 k_0(t_i r) k_0(t_f r) [j_L(k_p r) - \beta(L, J) h_L^{(1)}(k_p r)][j_{L_n}(k_n r) - \beta(L_n) h_{L_n}^{(1)}(k_n r)] \dots .$$

The polarization P_{00} is:

$$(10)\quad P_{00} = \{|M_{00}(+\tfrac{1}{2})|^2 - |M_{00}(-\tfrac{1}{2})|^2\} \Big/ \{|M_{00}(+\tfrac{1}{2})|^2 - |M_{00}(-\tfrac{1}{2})|^2\} ,$$

where:

$$(11a)\quad M_{00}(+\tfrac{1}{2}) = \text{const} \sum_L \sum_{M_L=-L}^{L} Y^*_{LM_L}\left(\frac{\pi}{2}, 0\right) Y_{LM_L}\left(\frac{\pi}{2}, \theta\right) \cdot$$
$$\cdot \left\{\left(\frac{L + 1 + M_L}{2L + 1}\right) R_L^+ + \left(\frac{L - M_L}{2L + 1}\right) R_L^-\right\} \dots ,$$

$$(11b)\quad M_{00}(-\tfrac{1}{2}) = \text{const} \sum_L \sum_{M_L=-L}^{L} Y^*_{LM_L}\left(\frac{\pi}{2}, 0\right) Y_{LM_L}\left(\frac{\pi}{2}, \theta\right) \cdot$$
$$\cdot \left\{\left(\frac{L + 1 - M_L}{2L + 1}\right) R_L^+ + \left(\frac{L + M_L}{2L + 1}\right) R_L^-\right\} \dots .$$

where:

$$R_L^+ = R_{L,J=L+\frac{1}{2}}, \qquad R_L^- = R_{L,J=L-\frac{1}{2}}.$$

If the spin-orbit coupling equals zero, then $R_L^+ = R_L^- = R_L$ and $P_{00} = 0$. $P_{00}(\theta = 0) = P_{00}(\theta = \pi) = 0$.

For the sake of discussion of the angular distribution and numerical computations it is reasonable to deal with the case $\beta(L_n) = 0$ (no neutron scattering). The matrix element is then:

$$(12) \qquad M = M_q + M_{sc} = \text{const} \int \mathrm{d}\sigma_n \, \mathrm{d}\sigma_p \int \mathrm{d}\xi \, \mathrm{d}\boldsymbol{r} \{\exp[i\boldsymbol{qr}] + f_{sc}^*(\boldsymbol{r}) \exp[i\boldsymbol{k}_n\boldsymbol{r}]\} \cdot \Psi_f^*[\mu_f]\chi_{\mu_p}^*(\sigma_p)\Psi_i[\mu_i]\chi_{\mu_n}(\sigma_n) \ldots,$$

where $\boldsymbol{q} = \boldsymbol{k}_n - \boldsymbol{k}_p$. In the $(S_{\frac{1}{2}}, S_{\frac{1}{2}})$ case we obtain:

$$(13) \quad M_{00}(\mu_p) = \text{const} \{I_q - \sum_{LM_L} \sum_{J=L-\frac{1}{2}}^{L+\frac{1}{2}} a(L, M_L) b^*(L, M_L) C^2_{L\frac{1}{2}}(J, M_L + \mu_p, M_L, \mu_p) R^{sc}_{LJ}\},$$

where:

$$(14) \qquad I_q = \int_{r_0}^{\infty} \mathrm{d}\Omega r^2 \, \mathrm{d}r k_0(t_i r) k_0(t_f r) \exp[i\boldsymbol{qr}] \quad \text{and} \quad R^{sc}_{LJ} = \beta(LJ) \cdot \int_0^{\infty} \mathrm{d}r r^2 k_0(t_i r) k_0(t_f r) h_L^{(1)}(k_p r) j_L(k_n r) \ldots.$$

Similarly as for C_l^m in ref. [7] only $\beta(L, J)$ with $L \lesssim k_p r_0$ give significant contributions to M_{00}. Thus only several first $\beta(L, J)$ must be retained.

For the numerical computations we use the potential V_p from ref. [1-3]:

$$V_p \text{ (in MeV)} = -19(1 + 0.05i) - 2\boldsymbol{L}\cdot\boldsymbol{S} \qquad r \leqslant r_0 = 1.45A^{\frac{1}{3}} \cdot 10^{-13} \text{ cm}$$
$$= 0 \qquad r > r_0,$$

$\beta(L, J)$ are computed by the method of ref. [2]. Numerical results and further developments of this treatment are in preparation.

---

[7] J. Horowitz and A. M. L. Messiah: *Journ. Phys. Rad.*, **14**, 695 (1953).

Limite supérieure d'un embranchement α de l'UX_1 (^{234}Th).

S. Deutsch (*)

Laboratoire de Physique Nucléaire - Université Libre de Bruxelles

M. Nikolic (+)

(ricevuto il 28 Ottobre 1955)

Lors de la préparation d'une solution de ^{234}Th de haute pureté radioactive, à partir de nitrate d'uranyle (1), nous avons été amenés à vérifier expérimentalement le rapport de l'activité α totale de la solution d'UX_1 à l'activité β due à l'UX_1.

La valeur de ce rapport a été calculée en attribuant l'activité α:

1) aux isotopes de l'Uranium incomplètement séparés du Thorium;

2) au ^{230}Th (Ionium), inséparable chimiquement de son isotope, le ^{234}Th. Le rapport α_{Io}/β_{UX_1} ne peut être inférieur à $8.2 \cdot 10^{-7}$;

3) au ^{231}Pa;

4) au ^{234}U formé par désintégration de l'UX_1.

Nous avons montré que la contribution la plus importante est celle de l'Ionium (1).

L'existence d'un embranchement α de l'UX_1 donnerait à la détermination expérimentale du rapport α/β total, une valeur supérieure à la valeur calculée. La comparaison de ces deux valeurs permet de déduire une limite supérieure de l'embranchement α de l'UX_1.

D'après des considérations de systématique des noyaux lourds (2) on s'attend à un rapport d'embranchement de l'UX_1 de l'ordre de $2 \cdot 10^{-18}$. L'activité α correspondante serait indétectable par la méthode que nous avons employée, mais il nous a cependant semblé intéressant de donner ici une limite supérieure expérimentale de ce rapport d'embranchement.

L'activité β de la solution de ^{234}Th a été mesurée dans un compteur de Geiger à liquide dont le rendement pour les β de UX_1+UX_2 a été déterminé à l'aide d'une solution de teneur connue en nitrate d'uranyle en équilibre avec UX_1+UX_2.

L'activité α a été mesurée par la méthode photographique.

La technique de la double émulsion

(*) Institut Interuniversitaire des Sciences Nucléaires.

(+) En congé de l'Institut de Recherche sur la Structure de la Matière, Belgrade (Yougoslavie).

(1) S. Deutsch et M. Nikolic: *Bull. Soc. Chim. Belges*, **64**, 264 (1955).

(2) R. A. Glass, S. G. Thompson et G. T. Seaborg: *Journ. Inorg. Nucl. Chem.*, **1**, 3 (1955).

a été utilisée ([3]). Les plaques de 100 μm d'épaisseur ont été développées au révélateur à l'amidol et acide borique selon la méthode à deux températures ([4]) (imprégnation: 1 heure à 5° - développement à sec: 1 heure à 19°). Avec ce développement, le dénombrement des α est encore possible, lorsque la Plaque C_2 a reçu moins de 10^7 β de l'UX_1+UX_2 dans un volume de $6 \cdot 10^{-3}$ cm³ d'émulsion environ.

La composition radioactive de la solution conservée pendant deux mois a été vérifiée en mesurant les longueurs des traces horizontales et rectilignes des α dans les plaques. La fig. 1 donne l'histogramme portant sur 230 traces. Celui-ci montre un pic autour de 19 μm avec una dispersion de 1.7 μm. On voit que ce pic correspond bien à l'α de l'Io dont le parcours est 19 μm dans l'émulsion ([5]). (Nous avons étalonné nos plaques avec une solution d'Io). Le rapport expérimental α/β est $(1.6 \pm 0.3) \cdot 10^{-6}$.

Fig. 1. – Histogramme des α dans l'émulsion C_2 portant sur 230 traces.

Dans nos conditions expérimentales, le rapport α/β calculé d'après la contribution des divers émetteurs α énumérés plus haut (Io, Pa, et les isotopes de U) est compris entre 1.7 et $2.2 \cdot 10^{-6}$. L'incertitude sur ce rapport provient de l'imprécision sur la concentration de l'Uranium qui a été déterminé par fluorimétrie.

En comparant la valeur expérimentale et la valeur calculée, nous pouvons conclure que le rapport d'embranchement α/β éventuel de l'UX_1 (ou de l'UX_2) est inférieur à 10^{-6}. Nous estimons que l'activité correspondant à un rapport 10^{-6} aurait donné un écart entre les valeurs expérimentale et calculée largement supérieur aux erreurs expérimentales.

On détermine ainsi une limite supérieure de la constante de désintégration de l'UX_1 ou de l'UX_2 soit

$$\lambda_\alpha < 3 \cdot 10^{-17} \qquad \text{pour } UX_1$$

$$\lambda_\alpha < 10^{-8} \qquad \text{pour } UX_2 .$$

* * *

Nous remercions vivement le Professeur F. G. Houtermans (Institut de Physique de Berne) et le Dr. E. Picciotto (Laboratoire de Physique Nucléaire, Université Libre de Bruxelles) qui ont dirigé ce travail.

([3]) E. E. Picciotto: *Comp. Rend.*, **228**, 220 (1949).

([4]) C. Dilworth, G. P. S. Occhialini e L. Vermaesen: *Bull. Centre de Phys. Nucl., Univ. Libre de Bruxelles*, n. 13a (1950)

([5]) G. Philbert, J. Genin, L. Vigneron: *Journ. Phys. et Rad.*, **15**, 16 (1954).

Zur Frage der Dämpfung elastischer Schwingungen durch Wirbelströme im Magnetfeld (*).

P. Schiller

Istituto Nazionale di Ultracustica « O. M. Corbino » - Roma

(ricevuto l'8 Novembre 1955)

1. – Die innere Dämpfung der Ferromagnetica ist bedeutend größer als in anderen Materialien mit ähnlichen elastischen und plastischen Eigenschaften. Weiter hängt sie in starkem Masse von der Magnetisierung ab. Diese Abhängigkeit ist keinesfalls einfach. Im allgemeinen steigt mit der Magnetisierung auch die Dämpfung an, bis zu einem Maximum kurz von der Sättigung, das etliche Male größer sein kann als der Dämpfungswert ohne Magnetisierung. Bei Magnetisierung über dieses Maximum hinaus fällt die Dämpfung gegen die Sättigung sehr schnell bis auf Werte des unmagnetischen Materials ab. Fig. 1 zeigt eine typische Kurve für das bei unseren Messungen verwendete Nickel, bei einer Dehnungsschwingung von etwa 40 kHz. Ähnliche Kurven wurden auch von anderen Autoren gefunden zum Beispiel von Auwers (1).

Der Einfluß der Magnetisierung auf die innere Dämpfung hat zwei Gründe: makroskopische und mikroskopische Wirbelströme; dazu kommen magnetomechaniche Hysterese und all die andern Einflüsse, die auch in nichtmagnetischen Materialien vorhanden sind (3).

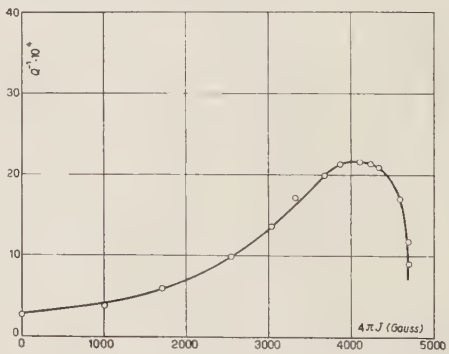

Fig. 1.

Es ist möglich zwischen den verschiedenen Dämpfungseinflüssen auf Grund ihrer Frequenzabhängigkeit zu unterscheiden. Tatsächlich geben die von Kersten (2) und von Becker und Döring (3) ausgeführten Rechnungen folgende Frequenzabhängigkeit der Dämpfung bei Dehnungschwingungen:

(*) Eine ausführliche Arbeit erscheint in Kürze im *Nuovo Cimento*.

(1) O. v. Auwers: *Ann. der Phys.*, **17**, 83 (1933).

(2) M. Kersten: *Zeits. f. Techn. Phys.*, **15**, 463 (1934).

(3) Becker und Döring: *Ferromagnetismus* (Berlin, 1933), p. 374.

Makroskopische Wirbelströme:

$$\delta_1 \sim f \quad \text{für niederes } f$$

oder:

$$\delta_1 \sim \frac{1}{\sqrt{f}} \quad \text{für hohes } f$$

Mikroskopische Wirbelströme:

$$\delta_2 \sim f$$

Magnetomechanische Hysterese:

$$\delta_3 \text{ unabhängig von } f.$$

Insbesondere gilt für makroskopische Wirbelströme bei hohen Frequenzen:

$$(1) \qquad \delta = \frac{4\pi^2 E \eta^2}{\mu} \cdot \frac{1}{R} \cdot \sqrt{\frac{c^2 \varrho}{2\pi\mu} \frac{1}{\omega}} = \pi Q^{-1} .$$

Hier bedeuten: δ das logarithmische Dekrement, E den Elastizitätsmodul, μ die Permeabilität, η den inversen Magnetostriktionskoeffizienten, R den Radius, c die Lichtgeschwindigkeit, ϱ den spezifischen Widerstand, ω die Kreisfrequenz und Q^{-1} den Resonanzfaktor.

2. – Es wurde versucht der durch (1) gegebenen Frequenzabhängigkeit der inneren Dämpfung nachzugehen. Das wurde durch den weiten Frequenzbereich der im Istituto Nazionale di Ultracustica (Roma) entwickelten elektrostatischen Methode zur Messung der elastischen Konstanten im Ultraschallgebiet ermöglicht [4].

Um den Einfluß der Fehler in der Messung der Magnetisierung auszuschalten, erschien es vorteilhaft die Höchstwerte der Dämpfung, der zu Fig. 1 analogen Kurven, bei verschiedenen Frequenzen zu vergleichen. Das erschien auch deshalb zulässig weil keine Abhängigkeit der Lage dieses Maximum von Frequenz und Stabdurchmesser festgestellt werden konnte.

Die experimentellen Ergebnisse sind durch Punkte in Fig. 2 eingetragen.

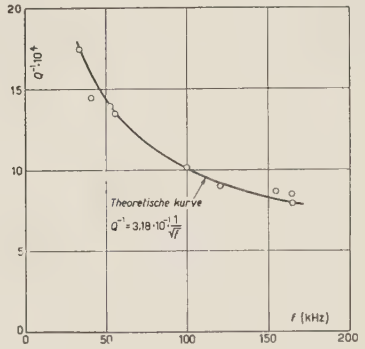

Fig. 2.

Ihr Vergleich mit der theoretischen Kurve $Q^{-1} = a \cdot (1/\sqrt{f})$ zeigt, daß für unser Material das Dämpfungsmaximum fast ganz den makroskopischen Wirbelströmem zuzuschreiben ist. Der Proportionalitätsfaktor kann dadurch bestimmt werden, daß man die theoretische Kurve möglichst gut mit den experimentellen Ergebnissen zur Deckung bringt.

3. – Weiter geht aus (1) hervor, daß sich die Dämpfung auf Grund

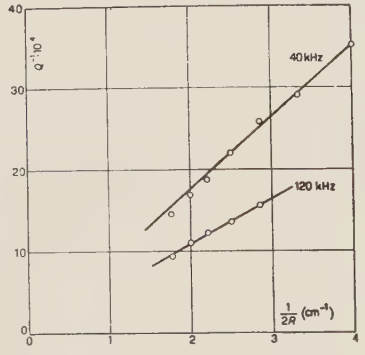

Fig. 3.

[4] P. G. Bordoni: *Nuovo Cimento*, **4**, 177; P. G. Bordoni e M. Nuovo: *Ric. Scient.*, **24**. 560 (1954).

makroskopischer Wirbelströme linear mit dem Reziprokwert des Radius ändern muß. Zur Prüfung dieser Abhängigkeit wurden Messungen an einem Stab durchgeführt, dessen Radius schrittweise verkleinert wurde.

Fig. 3 bestätigt die lineare Abhängigkeit von $1/R$.

* * *

Ich möchte an dieser Stelle dem Direktor des Istituto Nazionale di Ultracustica, Herrn Prof. A. Giacomini, für die Aufnahme in sein Institut danken. Herrn Prof. Bordoni gebührt mein Dank für viele wertvolle Hinweise und Ratschläge.

Classification of the Eisenberg and Similar Events.

R. G. Sachs (*) and S. B. Treiman

Palmer Physical Laboratory, Princeton University - Princeton N. J.

(ricevuto il 12 Novembre 1955)

The existence of a metastable particle or fragment which decays into a negative K-meson seems to be well established by the Eisenberg [1] and Wisconsin [2,3] cosmic-ray events. For reasons of energy conservation, these cannot be interpreted as a manifestation of any of the well-known hyperons without dropping the generally accepted principle of heavy particle conservation. In one attempt [4] to design a suitable classification for these events, it was found that two new particles were needed, one to describe the Eisenberg event and the other, the Wisconsin events. The purpose of this note is to show that, in the framework of a recently proposed classification scheme [4], all three events can be described in terms of a single particle—provided we relax the « odd-even » rule relating the isotopic spin to the attribute of the particle.

The Eisenberg [1] particle is most simply interpreted as an object which decays into a neutron or neutral hyperon plus a K^-. The Q-value is then about 5 MeV. The directly measured mass of the initial particle is about $3200\ m_e$, with a rather large error. The first Wisconsin object [2] has the appearance of a very slow hyper-fragment, although it can be interpreted as a slow particle which collides with a nucleus to produce a small star one of whose prongs is a K^-. The visible kinetic energy in 54 MeV.

We suggest an interpretation in terms of a super K-meson, denoted by K_s, whose isotopic spin is $\frac{1}{2}$, the two isotopic spin states having negative and zero charge. The attribute [4] of K_s is taken to be $a=2$. Then the particle can decay slowly according to the scheme

$$K_s \to K_2 + \pi\,, \tag{1}$$

where K_2 denotes either the negative or neutral K-meson having $a=1$. Because of the choice of isotopic spin, the K_s may form metastable hyperfragments. The reactions

$$K_s + N \to N + K_2 \tag{2}$$

$$K_s + N \to \Xi + K_2 \tag{3}$$

$$K_s + N \to \Lambda + \pi \tag{4}$$

(*) On leave of absence from the University of Wisconsin. This work supported in part by the University of Wisconsin Research Commitee by means of funds provided by the Wisconsin Alumni Research Foundation.

(1) Y. Eisenberg: *Phys. Rev.*, **96**, 541 (1954).

(2) W. F. Fry, J. Schneps and M. S. Swami: *Phys. Rev.*, **97**, 1189 (1955).

(3) W. F. Fry, J. Schneps and M. S. Swami: *Nuovo Cimento*, **2**, 346 (1955).

(4) R. G. Sachs: *Phys. Rev.*, **99**, 1573 (1955).

(5) $\quad K_s + N \to \Sigma + \pi$

all have $|\Delta a| = 1$, hence proceed slowly. On the other hand, the reactions

(6) $\quad K_s + N \to \Lambda + K_2$

(7) $\quad K_s + N \to \Sigma + K_2$

(8) $\quad K_s + N \to \Xi + \pi$

all have $\Delta a = 0$ and would proceed rapidly but for the choice of isotopic spin. All the reactions (6)-(8) involve half-integral change in I, which is forbidden for both the strong and the electromagnetic interactions. Presumably the only interactions leading to such a change in I are the very weak ones responsible for slow processes.

The Eisenberg primary particle is now taken to consist of an excited nuclear fragment containing K_s^- bound to a neutron, the (slow) decay being described by any one of the reactions (2), (3), (6), or (7). If we take for K_2^- the mass value 965 m_e and neglect the binding energy of the K_s^-, the corresponding masses for the K_s^- are respectively: 975, 1710, 1320, or 1480 m_e.

The first Wisconsin event [2], taken by itself, could be due to any one of the above reactions occurring in a hyperfragment or following the capture of a K_s^- in a nucleus. The visible energy release is 54 MeV; if momentum is balanced by one additional neutron the total energy release is ~ 75 MeV. This is to be compared with the energy release of 5 MeV in the Eisenberg event. The two events, taken together, may be given a consistent interpretation if it is assumed that the Eisenberg reaction is described by

(9) $\quad (K_s^- + N^0)_{\text{bound}} \to \Sigma^0 + K_2^- + 5 \text{ MeV}$,

and the Wisconsin reaction by

(10) $\quad K_s^- + N^0 \to \Lambda^0 + K_2^- + \sim 80 \text{ MeV}$.

If this interpretation is correct, the mass of the K_s would be 1480 m_e.

A second Wisconsin event [3] involves the emission of a K^--meson of ~ 40 MeV kinetic energy from a slow, or stopped particle. No other secondary particles are seen. This could be interpreted in the same manner as the first Wisconsin event. On the other hand, it is remarkably consistent with an interpretation in terms of the free decay

(11) $\quad K_s^- \to K_2^- + \pi^0$.

The 40 MeV of kinetic energy carried off by the K_2^- is nicely consistent with a mass of 1480 m_e for the K_s^-.

Since K_s^- or (K_s^0) is a boson, it is expected to have a positive (or neutral) counterpart, also having $I = \frac{1}{2}$, but with attribute $a = -2$. This counterpart (denoted $\overline{K}_s$) is helpful for the production of K_s, since the rule forbidding half-integral ΔI disallows the production of K_s in association with any of the other known particles. The threshold for production of the pair K_s and $\overline{K}_s$ in a pion-nucleon collision (nucleon at rest) would be 2.5 GeV of pion kinetic energy. Nuclear motion of the target nucleon would reduce the threshold to some extent.

The assumption that the Eisenberg particle consists of a K_s bound to a single nucleon implies that the binding potential must be at least comparable with the nuclear potential. This system would then be very similar to the deuteron. In order to obtain a potential with an adequate range, the mechanism

(12) $\quad K_s \to (K_s + \pi)_{\text{virtual}}$

is suggested as one possibility for the source of the interaction. For this to be possible, the spin of the K_s would have to be greater than zero, since the pion has odd parity.

The particle proposed here may bear

some relationship to several other unusual events. One of these is the event recently observed by HARTH and BLOCK [5], in which a positive particle of mass between 1150 and 1650 m_e decays into a light particle. If the decay scheme (1) is assumed, they find that the mass of the unstable particle is $1462 \pm 15\ m_e$; in excellent agreement with the mass value obtained above. The interpreation of the hyper-fragments having high Q-value [6] may also be made in terms of a K_s undergoing processes (4), (5), or (8), although in these cases the Q-values are quite consistent with the notion of a bound K_1-particle.

Excited fragments formed by the addition of K_s to nuclei would be characterized by the fact that they may emit a hyperon or a secondary hyperfragment, as can be seen from Eqs. (4)-(8).

The abandonment of the odd-even rule makes it possible to find other explanations of the events discussed here, although the above assignment appears to be the simplest. For example, one may introduce a K_s^- with $a=1$ and $I=0$. Then the roles of the ΔI and Δa selection rules are interchanged. Again, a hyperon which violates the odd-even rule would have all the properties needed to account for the Eisenberg and Wisconsin events (but not the event of HARTH and BLOCK).

The introduction of a particle or particles having properties contrary to the odd-even rule seems to be the important step suggested by these unusual events. There may very well exist an entirely new family of bosons and hyperons belonging to this class. This family would be tied together by the principle of associated production, just as in the case of the family of the more familiar particles. At the same time, a fast reaction mixing, the two families would have to involve an even number of particles from each family. Note that the existence of hyperons belonging to the new class would alleviate the need for the reaction of Eq. (12), because an interaction between the K_s and a nucleon could be produced via these hyperons.

It should be remarked that the assignment of quantum numbers to the K_s which has been made here is in direct contradiction to the physical interpretation of the attribute concept mabe by GELL-MANN [7] and NISHIJIMA [8], since the odd-even rule is essential to their present considerations [9].

* * *

The authors have had the benefit of several useful comments concerning this proposal by W. G. HOLLADAY and G. SNOW.

[5] E. M. HARTH and G. M. BLOCK: *Bull. Am. Phys. Soc.* **30** 13 (1955).

[6] W. F. FRY, J. SCHNEPS and M. S. SWAMI: *Phys. Rev.*, **99**, 561 (1955).

[7] M. GELL-MANN: *Phys. Rev.*, **92**, 833 (1952).

[8] K. NISHIJIMA: *Prog. Teor. Phys.*, **12**, 107 (1953).

[9] Note, however, that the notions of GELL-MANN and NISHIJIMA may be generalized to include the new family by writing for the charge of the particle

$$Q = e\left(I_3 + \frac{N}{2} - \frac{a}{2} + \frac{b}{2}\right),$$

where N is the heavy particle number, a is the attribute, and b is a new and independent quantum number: $b = 0$ for the family, $|b| = 1$ for the new family.

A Half-Liter « Clean » Bubble Chamber.

P. Bassi, P. Mittner and I. Scotoni

Istituto di Fisica dell'Università - Padova
Istituto Nazionale di Fisica Nucleare - Sezione di Padova

(ricevuto il 15 Novembre 1955)

We wish to briefly report the successful construction and operation of a liquid pentane bubble chamber of the « clean » type, having a useful volume of 450 cm³. A more detailed account will appear shortly as a « technical note » in the *Nuovo Cimento*.

A diagram of the apparatus is given in Fig. 1. The actual chamber consists of a pyrex bottle of square section, approximately $5.5 \times 5.5 \times 20$ cm, manufactured by the Fischer and Porter Company of Pennsylvania. The front and back faces are optically polished; the top has

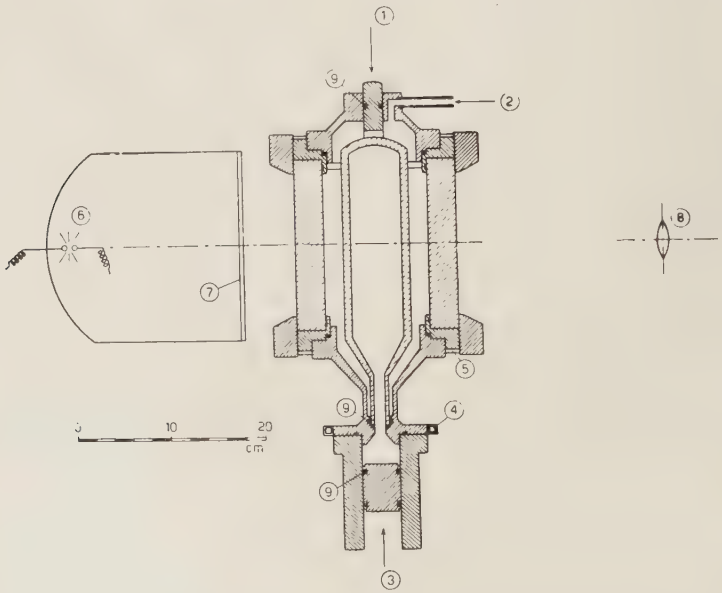

Fig. 1. – 1. Constant force of 60 kg; 2. Vaseline Oil at constant pressure of 12 atmospheres; 3) Control for Chamber pressure; 4. Cooling system; 5. Heaters; 6. Flash; 7. White glass diffuser; 8. O-ring.

Fig. 2.

Fig. 3.

a nearly hemispherical shape, while the bottom ends in the form of a tube through which the variations of pressure are exerted. The bottle is mounted in a pressurized thermostatic bath, consisting of a tank fitted with two glass windows and filled with vaseline oil which is usually at 12 atmospheres pressure and which is heated electrically from outside the tank. A piston working between atmospheric pressure and vacuum is used as a hydraulic lever to provide the necessary large pressure variations. This piston transfers its pressure to a liquid between which and the chamber is a second piston, small and of light weight, which acts as a pressure transducer. All moving and non-moving seals are closed by commercial O-ring.

The mean sensitive time is of the order of 0.1 s, but, so far, it has not been measured accurately. The recycling time depends on the pressure applied, using a pressure of 20 atmospheres it can be as low as 45 s, and we are now trying to determine the fastest recycling time while keeping the pressure within security limits. Bright field illumination is used for the photography; a microsecond flesh (Mullard LSD 2) has been mounted in an automobile headlamp reflector with a white glass diffuser between it and the chamber.

The chamber is expanded at random and the flash is then triggered; mechanical and electronic triggers have both been used successfully. The mechanical method, having an intrinsically long delay, uses a small piston balanced by a spring and acting on a microswitch to detect the variations of pressure within the chamber. Fig. 2 shows a cosmic ray track photographed by this means with a delay of about $5 \cdot 10^{-2}$ s. The flash has also been triggered by a conventional Geiger-telescope. Fig. 3 shows a photograph of a cosmic ray electron shower taken with a delay of 80 μs after the counter pulse. It will be seen from a comparison of Fig.s 2 and 3 that the rate of growth of the bubbles is not constant, which is in agreement with theoretical considerations ([1,2]).

The photographs were taken by the central camera of a stereoscopic group of three used to photograph each event.

In contrast with the greater part of the so-called « dirty » chambers, this instrument is suitable for work both with cosmic rays and with artificially accelerated particles, in fact the photographs which accompany this note are all of cosmic ray tracks. It will be used in the near future for a systematic study of the properties and working conditions of this type of detector (e.g. scattering and ionization problems).

* * *

Dr. M. Annis (*) assisted in the design and in the early stages of the construction of the chamber: we owe a considerable debt for his help and advice.

We are very pleased to be able to thank Prof. Rostagni for his interest in this work.

([1]) M. S. Plesset and S. A. Zwick: *Journ. Appl. Phys.*, **25**, 493 (1954).

([2]) H. K. Forster and N. Zuber: *Journ. Appl. Phys.*, **25**, 474 (1954).

(*) Now at « Allied Research Associates Incorporated » Boston (Mass.).

Average Cross-Sections for the Reactions $^{32}S(n, p)^{32}P$ and $^{31}P(n, p)^{31}Si$ with Fission Neutrons.

B. Grimeland (*)

Institute of Nuclear Science, « Boris Kidrich » - Belgrade

(ricevuto il 16 Novembre 1955)

As is well known there exists a number of (n, p) and (n, α) reactions which are induced by fast neutrons only, and which lead to radioactive end products, Such reactions can be used to determine the flux of fast neutrons in a reactor, if the beta-activity is measured absolutely, and the average cross-sections for the reactions with fission neutrons are known. Values for this average cross-section have been given for a number of such reactions by Hughes [1], and the author has used a few of them to determine the flux of fast neutrons in the reactor at Kjeller, Norway [2]. The absolute beta activity was determined by means of a splitted plastic scintillator and a photomultiplier tube. In the course of these experiments it was found that the value given by Hughes for the reaction $^{32}S(n, p)^{32}P$, did not agree with the values given for the other reactions used, which were: $^{24}Mg\ (n, p)^{24}Na$, $^{27}Al\ (n, p)\ ^{27}Mg$, $^{27}Al\ (n, \alpha)\ ^{24}Na$ and $^{31}P(n, p)^{31}S$. Hughes gives for the sulfur reaction: $\bar{\sigma}_{sulf} = 30$ mb and for the reaction in phosphorus: $\bar{\sigma}_{phos} = 19$ mb which gives for the ratio between the two cross-sections $\bar{\sigma}_{sulf}/\bar{\sigma}_{phos} = 1.58$, whereas the experiments referred to above, gave for this ratio the value 2.37. It has been thought, therefore, to be of some interest to try and calculate $\bar{\sigma}_{sulf}$ and $\bar{\sigma}_{phos}$ from other measurements available, and the results will be given here.

The cross-section for the (n, p) reaction in sulfur has been measured as a function of energy by Klema and Hanson [3] and by Hürlimann and Huber [4]. Kleman and Hanson [3] Huber [4]. Klema and Hanson determined the beta-activity in ^{32}P, whereas Hürlimann and Huber detected the protons in an ionization chamber . The curves are given in Fig. 1. The reaction $^{31}P(n, p)^{31}Si$ has been examined by Metzger, Alder and Huber [5], and

(*) Now at Joint Establishment for Nuclear Energy Research Kjeller per Lillestrom, Norway.

(1) D. J. Hughes: *Pile Neutron Research* (Cambridge, Mass. 1953).

(2) B. Grimeland: *Jener Report* no. 28 (1954).

(3) E. D. Klema and A. D. Hanson: *Phys. Rev.*, **73**, 106 (1948).

(4) T. Hürlimann and P. Huber: *Helv. Phys. Acta*, **28**, 33 (1955).

(5) F. Metzger, F. Alder and P. Huber: *Helv. Phys. Acta*, **21**, 278 (1948).

by LÜSCHER *et al.* [6]. Both groups measured the activity of ^{31}Si, and LÜSCHER and his coworkers have normalized their curve to give the best agreement with the curve obtained by METZGER *et al.* Neither of the measurements

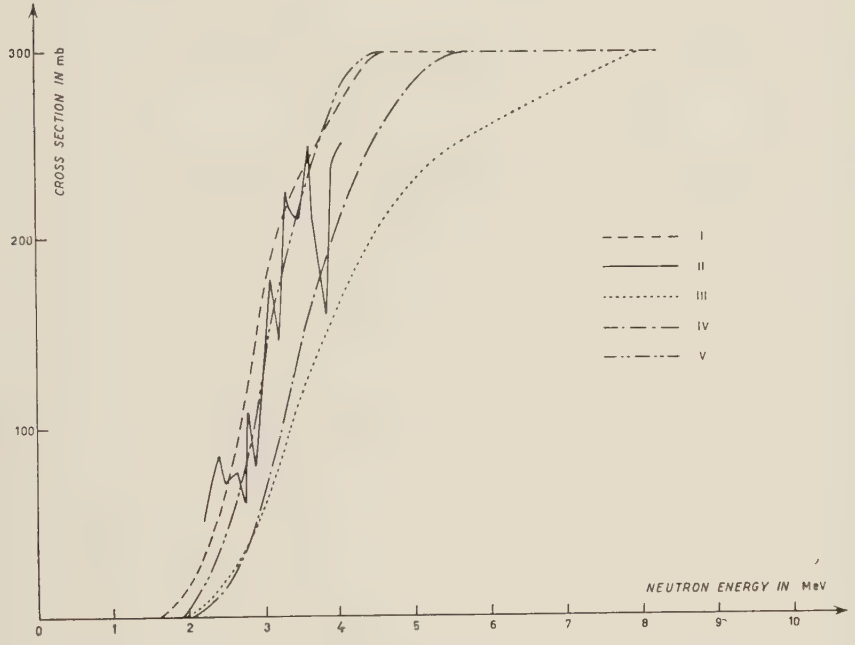

Fig. 1. – Cross-section for the reaction $^{32}S(n, p)^{32}P$. I: Experimental values by KLEMA and HANSON [3]. II: Experimental values by HÜRLIMANN and HUBER [4]. For explanation of curves III, IV and V see text.

cover the complete energy range of fission neutrons, and in order to determine the average cross section for fission neutrons some sort of extrapolation must be made. In this energy range the (n, γ) process is rather improbable, and the neutron will either be reemitted, or there will be emitted a proton or an α-particle. If σ_c is the cross-section for the formation of the compound nucleus and P_n; P_p and P_α are the probabilities for emission of a neutron, a proton and an α-particle respectively, the cross-section for the (n, p) process is

$$(1) \qquad \sigma(n, p) = \sigma_c \frac{P_n + P_p + P_\alpha}{P_p} .$$

In their book *Theoretical Nuclear Physics* BLATT and WEISSKOPF [7] give curves for σ_c; and also tables from which may be computed the cross-sections for the formation of a compound nucleus when the nuclei ^{32}P and ^{31}Si are bombarded with protons, and the nuclei ^{29}Si and ^{28}Al are bombarded with α-particles. If one assumes P_p and P_α to be proportional to the cross-sections computed in this way, and P_n to be proportional to σ_c, it is possible to calculate $\sigma(n, p)$ for the two reactions in question. The

[6] E. LÜSCHER, R. RICAMO, P. SCHERRER and W. ZÜNTI: *Helv. Phys. Acta*, **23**, 561 (1950).

[7] J. M. BLATT and V. F. WEISSKOPF: *Theoretical Nuclear Physics* (New York, 1952) p. 163.

curves obtained in this way, marked III in Figs. 1 and 2, do not, however, agree at all with the experimental curves, as can be seen from the figures. It is necessary, therefore, to try another procedure in order to make the extrapolation,

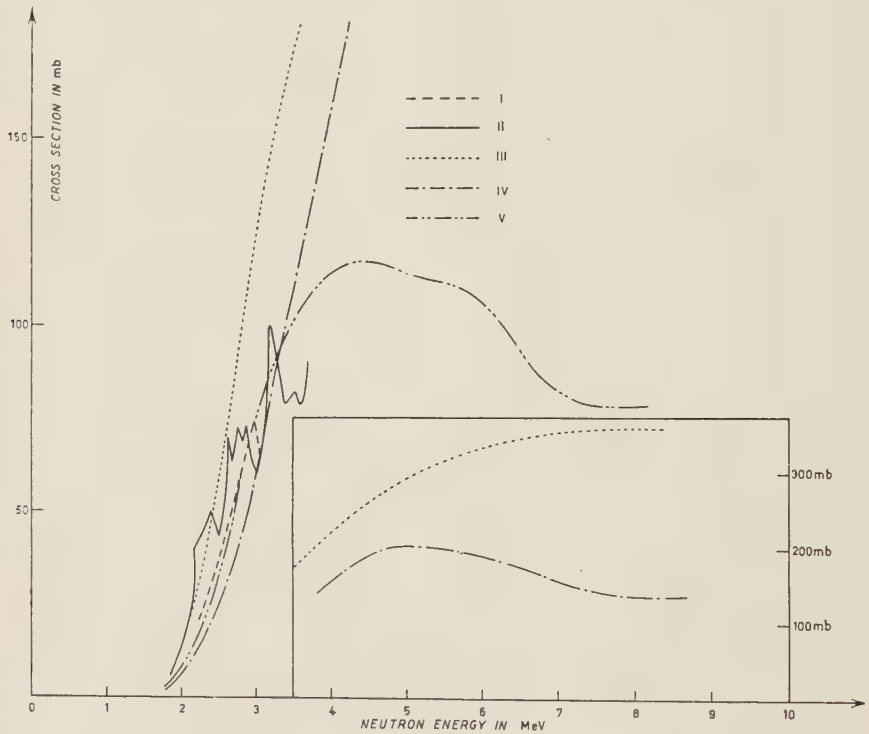

Fig. 2.—Cross-section for the reaction ^{31}P(n, p)^{31}Si. I: Experimental values by METZGER *et al.* ([5]). II: Experimental values by LÜSCHER *et al.* ([6]). For explanation of curves III, IV and V see text.

and the simplest thing to do is to assume σ_c to be constant in the energy range in question, $P_n=1$ and P_p and P_α to be equal to the expression given by BETHE ([8]) for the penetrability of the Coulomb barrier. This expression is:

$$(2) \qquad P = \exp\left[-\frac{4zZe^2}{vh}\right] \cdot [\arccos x^{\frac{1}{2}} - x^{\frac{1}{2}}(1-x)^{\frac{1}{2}}],$$

where v is the velocity of the outgoing particle and $x=E/B$. E is the energy of the particle and $B=zZe^2/R$ is the barrier height. According to BLATT and WEISSKOPF ([7])

$$(3) \qquad R = r_0 A^{\frac{1}{3}} + \varrho$$

where A is the mass number of the rest nucleus. For protons $\varrho = 0$ and for α-particles $\varrho = 1.2 \cdot 10^{-13}$ cm. For r_0 one has chosen in the present work the value $1.5 \cdot 10^{-13}$ cm. Another expression for R is given by MARTIN ([9]). It is:

$$(4) \qquad R = 1.5 \cdot 10^{-13}(A_1^{\frac{1}{3}} + A_2^{\frac{1}{3}}) \quad \text{for} \quad 1 < A < 180 ,$$

Quite different values are obtained for B

([8]) H. A. BETHE: *Rev. Mod. Phys.*, **9**, 69 (1937).

([9]) C. N. MARTIN: *Tables Numériques de Physique Nucléaire* (Paris, 1954).

when the first and the second expression for R is used.

TABLE I. – *Barrier heights in* MeV.

	^{31}P, p	^{29}Si, α	^{31}Si, p	^{28}Al, α
R acc. to eq. (3)	4.54	6.95	4.26	6.50
R acc. to eq. (4)	3.44	5.79	3.25	5.39

This is shown in Table I. Values of the cross-sections for the two (n, p) reactions in question have been computed by means of both the expressions given for R, and the values thus obtained have been normalized to give the best fit to the experimental curves. Curves IV in Fig. 1 and 2 were calculated with R given by eq. (3) and curves V with R given by eq. (4). It is seen that the latter curves give the best agreement with the experimental results. This is expecially clear in the case of the reaction $^{32}S(n, p)^{32}P$ where the experiments cover the longest energy range.

In order to do the calculations described above, the threshold energy for the different reactions must be known. These can be determined from mass spectroscopical data, or from the Q values of the reactions when they are known. The following values were used for the threshold energies. $^{32}S(n, p)^{32}P$: $E_T = 1$ MeV, $^{32}S(n, \alpha)^{28}Si$: $E_T = -1{,}5$ MeV; $^{31}P(n, p)^{31}Si$: $E_T = 0.8$ MeV; $^{31}P(n, \alpha)\ ^{28}Al$: $E_T = 2$ MeV.

According to WATT [10] the energy spectrum of fission neutrons is given by the formula:

$$(5) \qquad \Phi(E) = \text{const} \exp[-E/Q] \cdot \sinh(2Q^{-1}(EE_f m/M)^{\frac{1}{2}}),$$

$Q = 1$ MeV and $E_f m/M = 0.5$ MeV gives the best fit to the experimental results and the formula is then:

$$(6) \qquad \Phi(E) = \text{const} \exp[-E] \sinh 2E^{\frac{1}{2}},$$

$\bar{\sigma}_{sulf}$ and $\bar{\sigma}_{phos}$, may now be calculated from the expression:

$$\bar{\sigma} = \frac{\int_0^\infty \Phi(E)\sigma(E)\,dE}{\int_0^\infty \Phi(E)\,dE}.$$

With the curve of KLEMA and HANSON [3] one obtains

$$\bar{\sigma}_{sulf} = 69.2 \text{ mb}$$

and with curve V, which fits actually better the curve of HÜRLIMANN and HUBER than does the curve of KLEMA and HANSON, one obtains:

$$\bar{\sigma}_{sulf} = 64.2 \text{ mb}.$$

The mean value is: $\bar{\sigma}_{sulf} = 66.7$ mb.

Curve V in Fig. 2 gives for the reaction $^{31}P(n, p)^{31}Si$:

$$\bar{\sigma}_{phos} = 27.1 \text{ mb}$$

and the ratio between the cross-sections is:

$$\bar{\sigma}_{sulf}/\bar{\sigma}_{phos} = 2.50,$$

which agrees quite well with the value of 2.37 found by the author.

It is clear that calculations like those described above can not be expected to give very accurate results, but it seems safe to say that the values given by HUGHES are definitely too low.

[10] B. E. WATT: *Phys. Rev.*, **87**, 1037 (1952).

A Variation of the Rate of Penetrating Expansive Showers with Sidereal Time.

C. B. A. McCusker

Dublin Institute for Advanced Studies

(ricevuto il 18 Novembre 1955)

Some time ago a possible variation of penetrating extensive showers with sidereal time was noted (1). At that time, objections to the reality of the effect were: *a*) the results were the average of a number of comparatively short runs under different thicknesses of lead; *b*) the variation was only marginally established statistically; and *c*) there also seemed to be a possible variation of the same class of event with solar time.

To decide the question, the same apparatus has been run for a year under one thickness of lead (20 cms Pb). The table gives the rates of extensive showers averaged over four hourly periods for the six periods of the sidereal day. The results have been split into two six monthly groups. The totals for the complete time under 20 cm Pb are also given. It will be seen that there is an apparent variation with sidereal time, and that this variation has the same form for both groups.

To test the significance of the variation a X^2 test was applied to the total result, and a straight line drawn through the average value. The value of P obtained was 0.001; that is to say the straight line was a very poor fit. Analysing the same results on solar time, a value of P of 0.20 was obtained thus no variation of the showers with solar time can be considered to be established when results obtained under a single thickness of lead for a whole year are used. It is possible that a solar variation is present (indeed the results suggest a dip just before midday) but if so, it is not large enough to be established with this apparatus in a single year.

One further objection to the reality of the sidereal effect is this; if a solar variation exists and if it shows a variation of amplitude with the seasons, then a spurious sidereal variation may be produced. Such an effect would however also produce a variation with « anti-sidereal » time (2). Accordingly the results have been analyzed with respect to anti-sidereal time. The value of P obtained using a X^2 test of the Null hypothesis was 0.7. The straight line

(1) C. B. A. McCusker, J. G. Dardis and B. G. Wilson: *Proc. Phys. Soc.*, A **68**, 585 (1955).

(2) F. J. M. Farley and J. R. Storey: *Proc. Phys. Soc.*, A **67**, 996 (1955).

was therefore an excellent fit for these points and no variation of this type can be established.

of a sidereal variation is particularly well established for the local penetrating showers. Finally, the absolute size of

TABLE I.

Date of Run	Time (G.S.T.)					
	23-03	03-07	07-11	11-15	15-19	19-23
Up to May 9, 1955	0.289 ± .024	0.380 ± .027	0.336 ± .026	0.322 ± .025	0.372 ± .027	0.380 ± .027
May 9 to Nov. 14, 1955	0.302 ± .021	0.365 ± .023	0.296 ± .021	0.346 ± .022	0.376 ± .023	0.343 ± .022
Total	0.296 ± 0.15	0.372 ± .017	0.315 ± .016	0.335 ± .016	0.374 ± .017	0.360 ± .016

The Table shows the rates per hour averaged over 4 hourly periods of extensive penetrating showers against sidereal time.

During the course of these experiments the apparatus has also recorded 23504 local penetrating showers. For the last 6 months electron showers of very high density ($\sim$ 700 particles per m^2) have been recorded in another experiment. Both of these components show strong variations with solar time ([1,3]), but in neither case has a variation with sidereal time been found. This absence of the variation of the extensive penetrating showers, found by subtracting the maximum and minimum hours is 48 $\pm$ $\pm$ 13 % of the average rate. The implications of these results will be discussed in detail later.

* * *

I am indebted to Dr. B. G. WILSON for his help in running the apparatus and to Prof. C. O'CEALLAIGH for his comments on the manuscript.

([3]) C. B. A. MCCUSKER and B. G. WILSON (in preparation).

Sulle connessioni matematiche fra le teorie classiche dell'elettrone di Feynman e di Rzewuski.

G. M. Prosperi e C. Tosi

Istituto di Scienze Fisiche dell'Università - Milano
Istituto Nazionale di Fisica Nucleare - Sezione di Milano

(ricevuto il 20 Novembre 1955)

Come è noto, l'ordinaria teoria del campo elettromagnetico non può essere presa come punto di partenza per la costruzione di una soddisfacente teoria classica dell'elettrone. Per arrivare a questo scopo sono state proposte parecchie modifiche all'originaria teoria di Maxwell-Lorentz.

Vogliamo qui occuparci delle connessioni matematiche esistenti fra la teoria di Feynman [1] e quella di Rzewuski [2], e applicare le considerazioni svolte allo studio di un fattore di propagazione di Feynman suggerito da una teoria recentemente proposta da Caldirola [3].

Feynman, nella sua teoria, parte senz'altro dal principio di Fokker modificato:

$$\delta\left[\sum_a m_a \int \sqrt{\mathrm{d}\xi_a^\mu \mathrm{d}\xi_{a\mu}} + \frac{1}{2}\sum_{a,b} e_a e_b \int f(s_{ab}^2)\,\mathrm{d}\xi_a^\mu \mathrm{d}\xi_{b\mu}\right] = 0\,, \tag{1}$$

(m_a e_a e ξ_a rappresentano la massa, la carica e le coordinate della particella a), dove $f(s^2)$ è una funzione regolare che si annulla rapidamente quando s^2 diviene maggiore di un parametro λ_0^2 e soddisfa la relazione $\int_{-\infty}^{+\infty} f(s^2)\,\mathrm{d}(s^2) = 1$.

Rzewuski invece parte da una teoria di campo ad interazione non localizzabile e deduce un principio di Fokker ancora della forma (1), ma con

$$f[(x'-x'')^2] = \int F(x'-y')\,\delta[(y'-y'')^2]\,F(y''-x'')\,\mathrm{d}y'\,\mathrm{d}y''\,, \tag{2}$$

dove F è il fattore di forma dell'interazione.

---

[1] R. P. Feynman: *Phys. Rev.*, **74**, 939 (1948). Le unità da noi adottate sono quelle usate in questo lavoro.

[2] J. Rzewuski: *Acta Phys. Pol.*, **9**, 203 (1953).

[3] P. Caldirola: *Nuovo Cimento*, **10**, 1747 (1953); P. Caldirola e D. Duimio: *Nuovo Cimento*, **12**, 699 (1954).

Da un punto di vista matematico la teoria di Rzewuski rientra come caso particolare nella teoria di Feynman.

Mostreremo a quali condizioni deve soddisfare la $f(s^2)$ affinchè la (2), riguardata ora come equazione integrale in F, ammetta soluzioni e quindi la teoria di Feynman si riduca ad una teoria ad interazione non localizzabile.

Benchè ciò non sia in generale verificato (a causa del carattere non definito positivo di $(x'-x'')^2$), ci limiteremo nel seguito al caso fisicamente più significativo in cui la $f[(x'-x'')^2]$ sia sviluppabile in serie quadridimensionale di Fourier e alla ricerca di soluzioni della (2) che godano pur esse di tale proprietà.

Posto allora:

$$f[(x'-x'')^2] = (2\pi)^{-2}\int f(p^2)\exp[ip(x'-x'')]\,\mathrm{d}p\,, \tag{3}$$

$$F(x'-x'') = (2\pi)^{-2}\int F(p^2)\exp[ip(x'-x'')]\,\mathrm{d}p\,, \tag{4}$$

e ricordando che la trasformata di Fourier della $\delta[(y'-y'')^2]$ è $-(1/\pi p^2)$, l'equazione (2) diviene:

$$f(p^2) = -\frac{(2\pi)^4}{\pi}\,\frac{[F(p^2)]^2}{p^2} \tag{5}$$

e, risolvendo rispetto ad F,

$$F(p^2) = \frac{1}{4\pi^{\frac{3}{2}}}\,[-p^2 f(p^2)]^{\frac{1}{2}}\,. \tag{6}$$

Perchè, con una tale scelta della $F(p^2)$, il secondo membro della (4) converga, è necessario che si abbia:

$$\int F(q)\,\mathrm{d}q = \int F(q)q\,\mathrm{d}q = 0\,, \tag{7}$$

dove $q = p^2$. Tali condizioni non sono in generale però sufficienti a garantire che la F sia un'effettiva soluzione della (2), in quanto non bastano ad assicurare la convergenza dell'integrale di essa esteso all'intero spazio-tempo. Bloch [4] ha mostrato che un tale integrale risulta convergente se si suppone che $F(q)$, oltre a soddisfare le (7), sia finita e continua con le sue prime sei derivate e si annulli all'infinito più rapidamente di $1/q^4$.

Poichè, a meno di coefficienti numerici,

$$\frac{\mathrm{d}^n F}{\mathrm{d}q^n} = \sum_{s=0}^{n}\sum_{\substack{l_1 l_2 \ldots \\ t_1 t_2 \ldots \\ \{l_1 t_1 + l_2 t_2 + \ldots = n \\ \{l_1 + l_2 + \ldots = s}} [-qf(q)]^{\frac{1}{2}-s}\left\{\left(\frac{\mathrm{d}^{t_1}[-qf(q)]}{\mathrm{d}q^{t_1}}\right)^{l_1}\cdot\left(\frac{\mathrm{d}^{t_2}[-qf(q)]}{\mathrm{d}q^{t_2}}\right)^{l_2}\cdots\right\} \tag{8}$$

per poter soddisfare queste condizioni occorre che la $f(q)$ sia pure finita e continua almeno con le sue prime sei derivate, che i suoi eventuali poli siano almeno del dodicesimo ordine e che per $q \to \infty$ essa si annulli più rapidamente di $1/q^9$.

---

(4) C. Bloch: *Dan. Mat. Fys. Medd.*, **27** 8 (1952).

Come abbiamo accennato, recentemente è stato proposta da CALDIROLA una equazione classica per l'elettrone, alle differenze finite, che tiene intrinsecamente conto delle forze di reazione. In prima approssimazoine tale equazione coincide con quella che si dedurrebbe dal principio di Fokker-Feynman ponendo

$$f(x'-x'') = \delta[(x'-x'')^2 + \lambda^2], \tag{9}$$

con

$$(x'-x'')^2 = (r'-r'')^2 - c^2(t'-t'')^2$$

(contrariamente a quanto supposto da FEYNMAN, questo propagatore è singolare. tuttavia esso dà luogo a risultati finiti perchè le singolarità non giacciono più sul cono di luce).

La trasformata di Fourier di questa funzione è [5]:

$$f(p^2) = (2\pi)^{-2}\int \delta[x^2+\lambda^2]\exp[-ipx]\,dx = -\frac{\lambda}{2}\,\mathcal{R}\left\{\frac{H_1^{(1)}(i\lambda\sqrt{p^2})}{\sqrt{p^2}}\right\}, \tag{10}$$

dove con $H_1^{(1)}$ abbiamo indicato la funzione di Hankel di prima specie e di ordine uno. Tenendo presente lo sviluppo asintotico [6]:

$$H_\nu^{(1)}(z) = \left(\frac{2}{\pi z}\right)^{\frac{1}{2}}\exp\left[i\left(z-\frac{\nu\pi}{2}-\frac{\pi}{4}\right)\right]\left[\sum_{m=0}^{M-1}\frac{(\nu,m)}{(-2iz)^m}+O(|z|^{-M})\right], \tag{11}$$

vediamo che $f(p^2)$ per $p^2 \to +\infty$ e $p^2 \to -\infty$ si comporta rispettivmaente come

$$\frac{\exp[-\lambda\sqrt{p^2}]}{(p^2)^{\frac{3}{4}}} \qquad \text{e} \qquad \frac{1}{(-p^2)^{\frac{3}{4}}}.$$

Per $p^2 \to -\infty$, $f(p^2)$ si annulla troppo lentamente non solo perchè siano soddisfatte le condizioni di Bloch, ma anche solo perchè possano esserlo le (7). Per $f(x)=\delta(x^2+\lambda^2)$ l'equazione (2) non ammette quindi soluzioni regolari (almeno sviluppabili in serie di Fourier) e la teoria di Caldirola neppure in prima approssimazione sembra possa essere ricondotta ad una teoria di campo ad interazione non localizzabile.

* * *

Desideriamo ringraziare il prof. P. CALDIROLA per il suo gentile interessamento.

[5] Cfr., ad esempio, W. HEITLER: *The Quantum Theory of Radiation*, 3ª ediz., pag. 73-74.

[6] W. MAGNUS e F. OBERHETTINGER: *Formeln und Sätze für die speziellen Funktionen der Mathematischen Physik* (Berlin - Göttingen - Heildelberg, 1948) 2ª ediz., pag. 32.

Anelastic Scattering of π-Mesons on Carbon (*).

M. Della Corte, T. F. Fazzini and A. M. Sona

Istituto di Fisica dell'Università - Arcetri, Firenze

(ricevuto il 30 Giugno 1955)

By scanning a batch of Ilford G5 plates, which had been exposed to $\pi^{\pm}$-meson beams of energy between 60 and 125 MeV, a number of anelastic scatterings has been found, which are accompanied by the emission of low energy particles and are therefore attributable to interactions with light nuclei. When the tracks of the low energy particles end in the emulsion it is possible to set up an energy and momentum balance, thus allowing, in a number of cases, to identify the reaction type.

Here we wish to describe some preliminary results about scatterings with the emission of three low energy particles. This type of event might presumably be due to one of the following reactions:

I) $\pi + {}^{12}_{6}\mathrm{C} = \pi + 3\,{}^{4}_{2}\mathrm{He} - 7.28$ MeV

II) $\pi + {}^{12}_{6}\mathrm{C} = \pi + {}^{6}_{3}\mathrm{Li} + {}^{4}_{2}\mathrm{He} + {}^{2}_{1}\mathrm{H} - 24.61$ MeV

III) $\pi + {}^{12}_{6}\mathrm{C} = \pi + {}^{7}_{3}\mathrm{Li} + {}^{4}_{2}\mathrm{He} + {}^{1}_{1}\mathrm{H} - 26.5$ MeV

IV) $\pi + {}^{14}_{7}\mathrm{N} = \pi + {}^{6}_{3}\mathrm{Li} + 2\,{}^{4}_{2}\mathrm{He} - 16.06$ MeV

which have already been observed (I) in emulsions exposed to γ-rays.

The identification has been made by tentatively ascribing the three tracks to the particles produced in the above reactions and then verifying whether the energy and momentum balance checks or not, namely

$$(1) \qquad \begin{cases} \sum \boldsymbol{p}_i = \Delta \boldsymbol{p}_\pi \\ \sum E_i - Q = \Delta E_\pi \end{cases}$$

where $\Delta \boldsymbol{p}_\pi$ and ΔE_π are the momentum and the energy lost by the meson and Q the characteristic energy of the reaction.

For every single event the approximate value of the meson energy is known being equal to the mean energy of the beam to which the plate has been exposed; to start with, we can therefore assume this value as a datum and evaluate ΔE_π according to the postulated reaction scheme; the momentum of the scattered meson can then be evaluated and $\Delta \boldsymbol{p}_\pi$ follows. If the value thus obtained satisfies 1), the postulated reaction scheme can be considered as consistent with the observed data. Owing to errors of measurement, however, we

(*) This research is part of a program of work supported by I.N.F.N., Sezione di Roma.

cannot expect, generally, that 1) be exactly satisfied; the moduli of the residual momenta $|\Delta \boldsymbol{p}| = |\boldsymbol{p}_i - \Delta \boldsymbol{p}_\pi|$ would rather distribute themselves according to a Maxwellian law, as has been pointed out by GOWARD and WILKINS ([1,2]) in the analogous case of γ-ray stars. For our case the actual distribution is shown in the hystogram of Fig. 1; by inspection of this distribution a reasonable upper limit for $\Delta \boldsymbol{p}$ to be consistent with the postulated scheme can be set at 45 MeV/c.

By following this method 31 events have been identified for certain, of which 25 belong to type I, 4 to type II, 1 to III and 1 to IV.

Scattering of Mesons.

Twelve out of the 25 scatterings on carbon have been found on plates exposed to $70 \simeq 80$ MeV and for these the

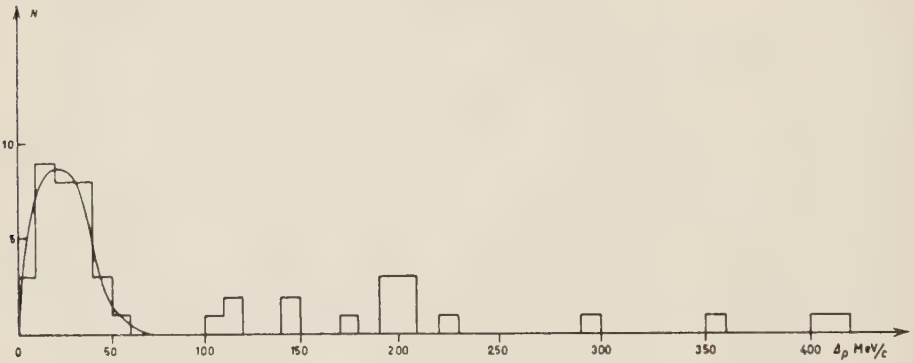

Fig. 1.

Since the meson energy fluctuates around the mean value assumed for the first calculation, it has been found expedient to check the scheme also for values of E_π slightly different from the average. In many cases the energy of the incident meson or of the scattered mesons (or both) could be measured directly by the scattering or ionization method; in every case in which this has been possible and when the accepted scheme of reaction was already found to be correct, these direct measurements have been found to confirm, within the experimental errors, the values obtained by the above indirect procedure.

order of magnitude of the cross-section can be evaluated.

By comparison with the total number of nuclear events (stars + anelastic scatterings) which have been found in the same volume of emulsion and assuming for the total cross-section the value given by BERNARDINI and coll. ([3]) the cross-section for anelastic scattering on carbon with carbon tripartition (reaction I) is found to be about 10% of the geometrical cross-section.

This value is fairly close to that obtained by BYFIELD and coll. ([4]) for the total number of anelastic scatterings in C; we are therefore led to conclude

([1]) GOWARD and WILKINS: *Proc. Phys. Soc.*, A **63**, 663 (1950).

([2]) GOWARD and WILKINS: *Proc. Roy. Soc.*, A **217**, 357 (1953).

([3]) G. BERNARDINI, BOOTH and L. M. LEDERMAN: *Phys. Rev.*, **83**, 1075 (1951).

([4]) H. BYFIELD, J. KESSLER and L. M. LEDERMAN: *Phys. Rev.*, **86**, 17 (1952).

that reaction I is the most probable result of an interaction of this type and that disintegrations with neutron emission are less frequent.

The relative differential cross-section $(1/\sigma)(d\sigma/d\omega)$ which follows from our experimental distribution of the scattering angles is plotted in Fig. 2. We can now compare our results with those obtained by Byfield and coll. in a Wilson Chamber with a number of events which is about the same as ours: a minimum for the cross-section is also found by us for angles between 50° and 90°; however, Byfield and coll. find about equal number of scatterings with angles $> 90°$ and with angles $< 90°$, while from our data a ratio of about 4:1 would follow (22 events against 6).

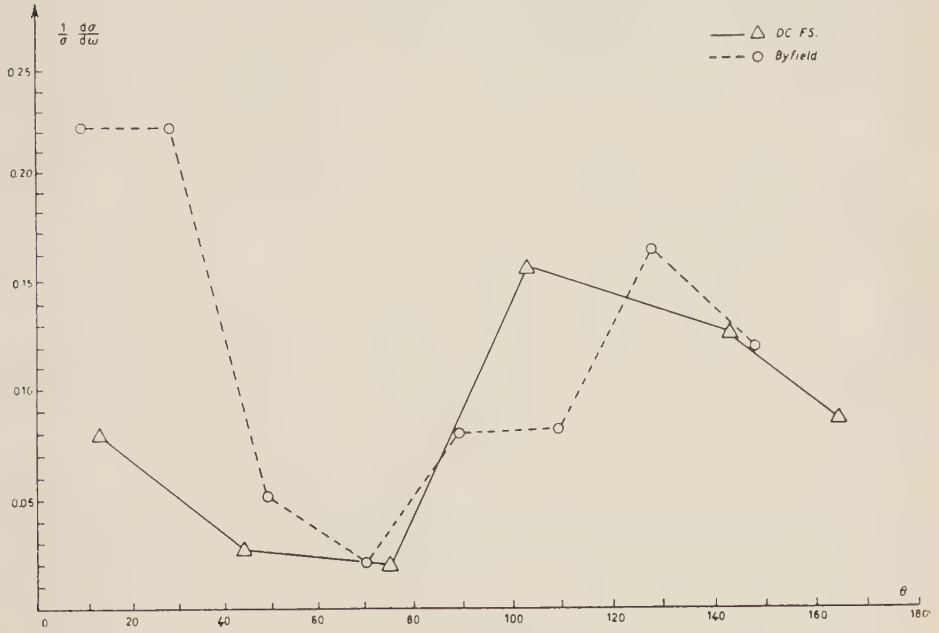

Fig. 2.

Tripartition of ^{12}C.

Goward and Wilkins ([5]) have shown that the tripartition of ^{12}C by γ-rays follows the scheme

$$(Ia) \qquad \begin{cases} \gamma + {}^{12}C \rightarrow {}^{8}Be + {}^{4}He \\ {}^{8}Be \rightarrow {}^{4}He + {}^{4}He \end{cases}$$

and have in fact deduced ^{8}Be levels from the energetic and spatial distribution of the three α-particles. No evidence for a direct tripartition according to scheme I, as suggested by Castel ([6]) has been found by Goward and Wilkins.

In the case of π primary, however there is no a priori reason for the reaction to follow the same scheme I*a*), because π and γ interactions are substantially different.

The two schemes give rise to a different distribution of the energies E_{ij} of the three pairs of α-particles in a star, when evaluated in their center of mass

([5]) Goward and Wilkins: *Proc. Roy. Soc.*, **228**, 376 (1955).

([6]) R. Chastel: *Journ. Phys et Rad.*, **15**, 240 (1954).

system. In fact, if one of the three pairs of a star is due to ^{8}Be decay, the total distribution of E_{ii} should show the characteristic levels of ^{8}Be. By this analysis GOWARD and WILKINS have in fact detected the presence of the 2.95, 4, 10, 15, 16.8 and 17.6 MeV levels and evaluated their relative transition probability.

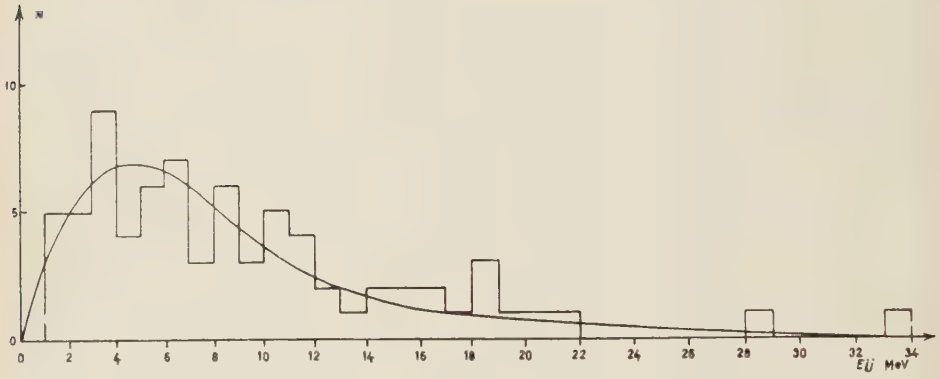

Fig. 3.

In the case of a direct tripartition, instead, the distribution of E_{ij} should follow from a casual distribution of the energy among the three α's. The distribution function of E_{ij} would then be

$$\varphi(E_{ij})\,\mathrm{d}E_{ij} = \frac{8}{\pi}\,\frac{I}{W^2}\sqrt{E_{ij}(W - E_{ij})}\,\mathrm{d}E_{ij}\ ,$$

where W is the total energy of the three α's in their center of mass system.

For every single event we evaluated the value of $\varphi_n(E_{ij})$ and of the function according to

$$\Phi(E_{ij}) = \sum \varphi_n(E_{ij})\ .$$

The comparison with experimental distribution is shown in Fig. 3.

The agreement is satisfactory within the statistical error and there is no evidence for ^{8}Be levels; this result can be assumed as a hint in favour of direct tripartition.

On the other hand a disintegration scheme I*a* could still be possible if, contrary to what happens with γ-rays, the excitation probability should be practically the same for the various levels. In fact, in this hypothesis, the

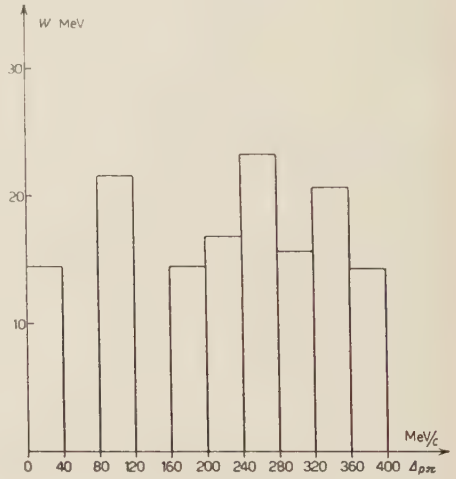

Fig. 4.

levels are numerous enough to show a distribution of E_{ij} which closely resembles a random distribution of energy.

It is interesting to note that the total energy of the three α-particles in their center of mass system does not practically depend on the momentum lost by the π-meson (Fig. 4); this leads one to think either to an interaction of the meson with many nucleons or to a distribution of the energy on the whole nucleus at the moment of the interaction.

* * *

We wish to thank most heartily Prof. M. SCHEIN for the kind exposure of the G5 plates to the Chicago synchrotron. Thanks are also due to Prof. BERNARDINI and Prof. PUPPI for supplying us some material without which the experiment could not have been carried out.

Application of High Magnetic Fields to Nuclear Track Analysis and Solid State Research (*).

H. P. Furth and R. W. Waniek

Cyclotron Laboratory, Harvard University - Cambridge, Massachusetts

(ricevuto il 23 Novembre 1955)

High transient magnetic fields are currently being applied to nuclear track plates at this laboratory. A 3000 V capacitor bank discharges 7800 joules through a variable pulse transformer into a pair of Helmholtz coils, in discharge times of 1 to 10 ms. The magnetic field pattern of a model which has been operating at 160000 gauss, liquid nitrogen temperature, is shown in Fig. 1. The field strength was measured within $\pm 3\%$ by means of a pick-up coil feeding through an RC integrator into an oscilloscope. A slightly smaller magnet, capable of reaching 200000 gauss has also been constructed.

The charge-discharge system, suitable for synchronization with accelerators, was made by adaptation of industrial units [1]. Stability of operation, as monitored by simultaneous display of field and particle intensities along the X and Y axes of an oscilloscope, has been found consistent within 3% of field strength.

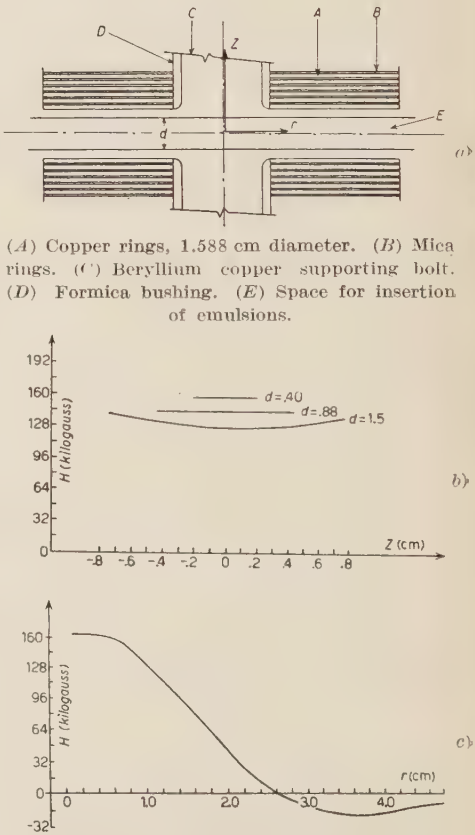

(*A*) Copper rings, 1.588 cm diameter. (*B*) Mica rings. (*C*) Beryllium copper supporting bolt. (*D*) Formica bushing. (*E*) Space for insertion of emulsions.

Fig. 1. – Cross-section of Helmoltz coils and graphs of field strength.

(*) Assisted by the joint program of the Office of Naval Research and the U. S. Atomic Energy Commission.

(1) Weldpower Models 1100 and 8100, Raytheon Manufacturing Co.

The Helmholtz coils are copper-mica double helices, assembled of split rings, like the coils of F. BITTER [2]. Use of a small number of thick (.040″) rings is made compatible with long discharge times by means of the pulse transformer. The assembly is suited for insertion of $1'' \times 3''$ emulsion stacks of variable height. The emulsions may be insulated and maintained at room temperature, but sets of plates exposed to a 95 MeV proton beam at liquid nitrogen temperature have shown normal grain densities and little distortion. The variation of emulsion sensitivity with temperature has been studied at intervals between 4 and 300 °K [3].

The scope of the magnetic method is enlarged by the application of low distortion developing procedures [4] and of a special scheme of track analysis [5]. Use of wire-embedded emulsions [6] and of four times diluted emulsions, having only slightly reduced sensitivity, recommends itself in some work.

Generator-pulsed magnetic fields up to 320 000 gauss were produced in classical experiments by P. KAPITZA [7]. Several authors have described the use of capacitors [8,9] and of low temperature cooling [10,11] in applications involving fields up to 250 000 gauss. The evidence of the present experiments has been that almost arbitrarily high fields can be produced in sufficiently hard and well-insulated (electrically very inefficient) coils, if a correspondingly large and low-inductance source of energy is available. Fields up to 650 000 gauss in volumes of 100 mm³ have already been attained, and further experiments are under way with a 62 500 joule source very kindly made accessible to us by Dr. M. O'DAY of the Cambridge Air Force Research Center.

Very great magnetic intensities are most needed in the sign determination of low energy short-lived particles, such as hyperons from K stars, and in the momentum determination of highly relativistic particles. In the multi-Gev range, where even the best microscopes have difficulty in detecting Coulomb scattering accurately, the presence of, say, 500 000 gauss over 1 cm of track will enhance the mean amplitude of track curvature by a factor of 25. In this range of energy, the nuclear emulsion could in a sense become a high-density, high-field cloud chamber, Pulsed magnetic fields are, of course, inapplicable in cosmic ray studies. In this work, a 34 000 gauss D.C. magnet has been used successfully for charge determination by C. C. DILWORTH *et al.* [12].

A number of projects utilizing high magnetic fields in solid state research are under way both here and in cooperation with other laboratories. The transient field approach lends itself well to such measurements as magneto-resistance, Hall effect, magnetostriction, and magnetothermoelectric effects, where an entire graph can be displayed and photographed instantaneously on the oscilloscope screen, by application of crystal voltages and field strengths along the X and Y axes. Pick-up voltages are detected by the double-valuedness of the

---

[2] F. BITTER: *Rev. Scient. Instr.*, **10**, 373 (1939).

[3] R. W. WANIEK: to be published.

[4] R. FOX and R. W. WANIEK: *Nucleonics*, **13**, 7, 52 (1955); *Phys. Rev.*, **98**, 1153 (1955).

[5] H. P. FURTH: *Rev. Scient. Instr.*, Nov. (1955).

[6] E. SILVER and R. W. WANIEK: *Rev. Scient. Instr.*, **25**, 1119 (1954).

[7] P. KAPITZA: *Proc. Roy. Soc.*, **115**, 658 (1927).

[8] G. RAOULT: *Ann. de Phys.*, **4**, 369 (1949).

[9] K. S. W. CHAMPION: *Proc. Phys. Soc.*, B **63**, 795 (1950).

[10] W. J. DE HAAS and J. B. WESTERDIJK: *Nature*, **158**, 271 (1946).

[11] J. L. OLSEN: *Helv. Phys. Acta*, **26**, 798 (1953).

[12] C. C. DILWORTH, G. P. S. OCCHIALINI and L. VERMAESEN: *Bull. du Centre de Phys. Nucl. de l'Univ. Libre de Bruxelles*, **13** (1950).

resultant oscilloscope trace, and can generally be made negligible by proper disposition of leads. Other extraneous voltages are eliminated by multiple photographic exposure under reversal of current and field. These techniques have been tested in a study of the magneto-resistance of N and P type germanium, 2 Ω cm resistivity, (111) and (100) orientations, which is partly completed. One of the interesting and complicating circumstances discovered in the course of this work is the large « magneto-resistance » of rectifying junctions and contacts at high fields, which tends to alter the pattern of crystal current flow during the magnetic pulse.

The use of transient fields in magnetic resonance work is familiar from low field experiments. Simultaneous display of field strength and radiation absorption on the oscilloscope screen will be suitable. An optically accessible 500 000 gauss magnet for cyclotron resonance work in the far infrared has been constructed.

It is hoped that high fields apparatus embodying the present structural ideas may be found useful in other experiments involving the deflection of charges or the alignment of magnetic dipoles. One thinks particularly of the acceleration of energetic particles in small orbits, and the containment of high temperature, high pressure, ionized gases.

* * *

The authors are indebted to S. Engelsberg for mapping of magnetic fields.

LIBRI RICEVUTI E RECENSIONI

Annual Review of Nuclear Science, vol. 4; G. Berkeley Editor, x+483 pp., Annual Reviews Inc., Stanford Cal., 1954.

Questo quarto volume della ben nota pubblicazione americana contiene diciassette articoli di rassegna tra loro molto diversi per importanza e per mole. Alcuni di essi hanno il carattere di rapida messa a punto bibliografica e trattano il loro argomento limitatamente ai lavori apparsi nell'ultimo periodo. Altri, assai più estesi e di maggiore impegno, tendono a dare un quadro generale, in sè logicamente compiuto, di un capitolo più o meno ampio della ricerca fisica contemporanea.

Crediamo di non sbagliare nell'asserire che, pur essendo gli articoli della prima categoria certamente non inutili, il pregio e l'utilità di un volume di questo tipo è essenzialmente legato a quelli della seconda. Le poche pagine di Blewett sui recenti sviluppi dei proto-sincrotroni possono, ad esempio, essere utilizzate quasi solo dagli specialisti in materia: ma è presumibile che la maggior parte di costoro fosse, già prima della pubblicazione del volume, ben al corrente dei lavori ivi citati.

Viceversa, l'articolo di Perlman e Asaro sulla radioattività alfa, quello di De Benedetti e Corben sul positronio, quello di Kohman e Saito sulle applicazioni della radioattività alla geologia e alla cosmologia, oltre a dare un quadro completo dell'argomento a chi lavora o, si appresta a lavorare in questi campi possono essere letti con utilità e con diletto anche da tutti i fisici che desiderino semplicemente essere informati.

È quindi da augurarsi che gli articoli più estesi e criticamente più elaborati abbiano in futuro una sempre più netta prevalenza sugli altri.

Per ciò che riguarda gli argomenti trattati, cinque articoli sono dedicati alle tecniche. Oltre a quello già citato di Blewett sui protosincrotroni (12 pagine), ve ne sono tre dedicati alla rivelazione di particelle cariche veloci ed uno al metodo di diluizione degli isotopi stabili, come mezzo di analisi (Inghram, 12 pagine).

I primi riguardano: l'elettronica rapida (Bell, 18 pagine), gli scintillatori (Swank, 30 pagine) e i contatori a effetto Čerenkov (Marshall, 16 pagine).

Altri sette articoli sono dedicati alla fisica nucleare classica. Oltre quelli assai già buoni citati, sulla radioattività alfa (34 pagine) e sul positronio (28 pagine), si ha qui una estesa rassegna di Uehling sulla penetrazione di particelle pesanti cariche nella materia (26 pagine), un buon articolo di Levinger sulle teorie delle reazioni fotonucleari (20 pagine), e un altro, relativamente breve, di Pake sulla spettroscopia dei nuclei con microonde e radiofrequenza (18 pagine).

Gli altri due articoli di questo gruppo riguardano: gli standard di radioattività (Manov, 18 pagine) e lo studio radiochimico della scissione alle basse energie (Glendenin e Steinberg, 12 pagine).

Assai belli e ampi i due capitoli dedicati alla fisica delle alte energie. Nel primo Gell-Mann e Watson presentano i risultati fino ad oggi ottenuti sulla

interazione tra mesoni π e nucleoni (52 pagine). L'altro dovuto a DILWORTH, OCCHIALINI e SCARSI, espone criticamente in 44 pagine lo stato presente delle nostre conoscenze sui mesoni pesanti.

Altri due articoli sono di radiobiologia. Il primo di questi, dovuto a DUBOIS e PETERSEN (26 pagine), è una rassegna critica degli scarsi risultati fino ad oggi raggiunti nello studio degli effetti biochimici delle radiazioni. Il secondo, di THOMSON, è dedicato alle azioni letali delle radiazioni sui vertebrati (24 pagine).

Chiude il volume l'ampia rassegna di KOHMAN e SAITO, già citati sulle applicazioni della radioattività alla geologia e cosmologia (52 pagine, corredata da una lista di ben 592 citazioni bibliografiche).

Nel suo complesso, il volume si presenta non meno importante e utile dei precedenti della stessa serie. Esso si apre con una breve, commossa rievocazione di ENRICO FERMI, deceduto mentre si stava per iniziarne la stampa.

MARIO AGENO

P. A. STURROCK – *Static and Dynamic Electron Optics, an Account of Focusing in Lens, Deflector and Accelerator.* Un vol. in-8 di X-240 pagg., della serie « Cambridge Monographs on Mechanics and Applied Mathematics ». Ed. Cambridge University Press, Cambridge (Ingh.), 1955. Prezzo 30 sc.

Fra i trattati di ottica elettronica, ormai abbastanza numerosi, questo è uno di quelli a carattere più nettamente teorico, con scarsi e solo schematici riferimenti alla effettiva realizzazione degli apparecchi. La trattazione è fatta sistematicamente col metodo variazionale, che permette di dedurre in modo elegante e unitario una grande varietà di risultati. Per accrescere l'eleganza delle formule, l'Autore usa speciali unità elettriche e magnetiche, così da far sparire dalle formule tutte le costanti caratteristiche delle particelle (questo particolare da una idea abbastanza chiara della fisionomia dell'opera).

Il volume è diviso in due parti. La prima tratta l'ottica elettronica statica, cioè dei campi costanti nel tempo: in particolare, i sistemi a simmetria di rotazione (di cui vengono studiate anche le aberrazioni e gli effetti delle piccole asimmetrie di costruzione) e quelli a simmetria speculare, come i deflettori e gli spettrometri di massa e beta. La seconda parte, intitolata « Ottica elettronica dinamica », è interamente dedicata agli acceleratori di particelle, che sono qui, per la prima volta, trattati sistematicamente dal punto di vista ottico-elettronico.

L'Autore dichiara, nella prefazione, di aver tenuto presenti anche le esigenze dei lettori che non hanno alcuna preliminare conoscenza dell'ottica elettronica. A noi sembra però che questo tipo di lettori farebbe meglio a cominciare con un altro libro. Coloro invece che hanno già familiari i vari tipi di apparati e le loro proprietà elementari, troveranno in quest'opera un mezzo utilissimo per rivedere le loro cognizioni da un punto di vista più elevato e per apprendere metodi matematici di grande generalità e potenza.

E. PERSICO

G. AUMANN – *Reelle Funktionen*, 1 vol. in-8° di pp. 416 con 22 illustrazioni. Springer-Verlag, Berlin, Göttingen, Heidelberg, 1954.

Come avverte l'A. stesso, quest'opera è necessariamente incompleta, dato che il suo scopo è di offrire una visione panoramica della teoria delle funzioni di variabile reale, differenziandosi dalle trat-

tazioni precedenti non tanto per l'ampiezza, quanto per la modernità dell'inquadramento e della terminologia. L'A. fa infatti uso di un sistema di notazione analogo a quelli introdotti dai logici matematici, in particolare a quello di HILBERT e collaboratori; ciò al fine di realizzare una presentazione concisa, oltre che rigorosa ed omogenea, del materiale antico e recente elaborato dai cultori della teoria in oggetto e di altre collaterali, che oggi non si possono trascurare volendo ottenere una visione organica di essa. Così appare molto utile non solo la raccolta dei contributi forniti alla teoria vera e propria dal 1905 al 1954, ma anche lo sfruttamento delle teorie degli insiemi ordinati e dei reticoli (HAUSDORFF, BIRKHOFF, BOURBAKI), degli anelli di Boole, degli spazi metrici e topologici (ALEKSANDROFF, CARATHÉODORY, STONE, ecc.), come nuovo strumento per l'esposizione sistematica dei risultati riguardanti le funzioni di punto, la teoria della misura e i funzionali positivi lineari.

Una speciale appendice bibliografica fornisce per ogni capitolo l'indicazione degli autori cui risalgono i contributi coordinati in modo uniforme nel corso della trattazione. Quale contributo personale dell'A. vanno segnalate in particolare alcune ricerche sulle funzioni discontinue e sugli anelli di Boole.

C. BÖHM

Proceedings of the 1954 Glasgow Conference on Nuclear and Meson Physics; E. H. BELLAMY and R. G. MOORHOUSE Ed.; IX+352 pp., Pergamon Press, London and New York, 1955.

Sotto gli auspici della Unione Internazionale di Fisica Pura e Applicata si è tenuta a Glasgow nel Luglio del 1954 una conferenza internazionale sulla fisica nucleare e mesonica, i cui atti vengono ora pubblicati in volume.

La conferenza era divisa in due parti, la prima delle quali aveva come tema centrale le forze nucleari e le proprietà dei nuclei atomici, mentre la seconda era dedicata ai mesoni π. Nella seduta di chiusura vennero anche esposti alcuni lavori sui mesoni pesanti e gl'iperoni.

Il volume degli atti contiene le 102 comunicazioni presentate alla Conferenza, suddivise in otto sezioni, le prime quattro delle quali dedicate alla fisica nucleare e le altre alla fisica dei mesoni e delle alte energie.

I titoli delle singole sezioni sono: I) Forze nucleari e scattering nucleonico, II) Costanti e modelli nucleari, III) Fotodisintegrazioni. IV) Transizioni beta e gamma, V) Mesoni π, VI) Teoria dei campi, VII) Tecniche sperimentali delle alte energie, VIII) Mesoni pesanti e iperoni.

Nella prefazione al volume è avvertito che, per ragioni di economia, non tutte le comunicazioni sono riportate per intero; soprattutto il numero delle figure e dei diagrammi è stato drasticamente ridotto. Si è invece, molto opportunamente, riportata alla fine di ogni lavoro, sia pure in forma molto concisa, la discussione avvenuta.

La correzione delle bozze è stata fatta direttamente dagli Editori allo scopo di accelerare la pubblicazione.

Non è evidentemente possibile neppure accennare in questa sede al contenuto dei singoli lavori. Una sufficiente indicazione è del resto costituita dai titoli delle sezioni, sopra riportati, e dalla data in cui la Conferenza è avvenuta. Aggiungeremo soltanto che il volume dà, nel suo complesso, un buon quadro della situazione, teorica e sperimentale, della ricerca a tale data e che esso è uno strumento di consultazione assai utile per chi lavora in questi campi della fisica.

È da augurarsi, a questo proposito, che l'abitudine di pubblicare in volume, il più rapidamente possibile anche a

costo di rinunciare un poco alla perfezione editoriale, gli atti dei congressi internazionali si vada sempre più generalizzando.

MARIO AGENO

A. C. B. LOVELL – *Meteor Astronomy*. Ed. Oxford University Press; G. Cumberlege Publisher, London, 1054; pag. XVI+463; prezzo 60 sh.

Lo studio delle meteore ha subito recentemente una profonda trasformazione ed un importante incremento a causa della introduzione di nuove tecniche fotografiche e delle tecniche dei radio-echi. Questo esteso e chiarissimo volume monografico che fa parte della « International Series of Monographs on Physics » diretta dai Professori N. F. MOTT ed E. C. BULLARD giunge quindi assai opportunamente a colmare una lacuna nella letteratura specializzata.

Nello stendere il progetto dell'opera l'Autore si proponeva di coprire l'intero campo degli studi sulle meteore (non sulle meteoriti) ma data la grande estensione della materia si limitò in questo volume agli argomenti prevalentemente astronomici, proponendosi per il futuro di completare il lavoro con un volume che tratti gli aspetti fisici del problema.

Il libro si apre con tre capitoli sui metodi di osservazione che mettono in particolare rilievo i moderni dispositivi fotografici, come ad esempio l'apparecchio Super Schmidt, e la tecnica del radio-eco con particolare riferimento agli impianti di Jodrell Bank ed ai risultati ivi ottenuti, alcuni dei quali sino ad oggi inediti.

Dopo aver trattato brevemente delle equazioni fondamentali del moto, l'Autore rivolge poi la propria attenzione alla distribuzione delle meteore sporadiche e dedica ben cinque capitoli, ricchi di dati quantitativi, al problema della loro velocità.

La seconda parte tratta dei principali sciami di meteore e si chiude con un capitolo dedicato ai problemi cosmologici. In appendice sono riportate note sui più recenti lavori che aggiornano alla fine del 1953 la bibliografia consultata.

Nel suo insieme quest'opera ci appare assai pregevole per il vasto lavoro di raccolta e di coordinamento dei dati disponibili e come messa a punto sui più moderni metodi di ricerca.

F. A. LEVI

Journal of Inorganic and Nuclear Chemistry, vol. 1, No. 1/2, J. J. KATZ, H. C. LONGUET-HIGGINS, H. A. C. MCKAY Editors; Pergamon Press, London and New York, March 1955.

Il nuovo periodico, di cui questo è il primo fascicolo, trova la sua ragione di essere nel rinnovamento operatosi negli ultimi anni nella chimica inorganica, da un lato con la venuta a maturazione della chimica teorica inorganica, dall'altro con la scoperta e della scissione degli elementi pesanti e dei nuovi elementi transuranici.

Tenuto anche conto della grande importanza assunta dalla chimica in ogni campo della ricerca e della ingegneria nucleare, il programma così implicitamente delineato da WARREN C. JOHNSON e H. J. EMELÉUS nella presentazione è certamente tale da giustificare la pubblicazione di un nuovo periodico. Resta tuttavia il dubbio se questo potrà effettivamente avere una sua fisionomia, sufficientemente caratterizzata.

L'esame del contenuto del primo fascicolo mostra infatti accanto a lavori di vera e propria fisica nucleare (*Nuclear thermodynamics of the heaviest elements*, di GLASS, THOMPSON e SEABORG), altri di radiochimica della scissione (*Fission yields in spontaneous fission of* ^{252}Cf, di GLENDENIN e STEINBERG; *Chemical ef-*

fects in fission products recoil, di WALTON e CROAL, ecc.) e infine altri di carattere strettamente chimico e rivolti a un pubblico di interessi mentali completamente diversi dai precedenti.

A parte questa considerazione, che potrà anche in pratica rivelarsi di importanza assai scarsa, crediamo che un nuovo, vivo periodico di chimica inorganica moderna sarà il benvenuto anche Italia e favorirà senza dubbio tra noi la formazione di quelle nuove leve di chimici specializzati, che ben presto diverranno necessarie per lo sviluppo dei nostri programmi nel campo della ingegneria nucleare.

Il carattere internazionale del periodico è sancito, oltre che dalla direzione anglo-americana, dall'ampio comitato redazionale consultivo, che comprende nomi illustri dei seguenti Paesi: Stati Uniti, Inghilterra e Commonwealth, Austria, Danimarca, Francia, Germania, Olanda, Norvegia, Svezia e Svizzera.

MARIO AGENO

GRIMSEHL – *Lehrbuch der Physik*, Erster Band: *Mechanik, Wärmelehre, Akustik*. Sechzehnte Auflage Ss. X+632 mit 722 Abbildungen, B. G. Teubner, Leipzig 1955.

Della 15ª edizione di questo primo volume del GRIMSEHL è già stata data notizia sul *Nuovo Cimento* del 1° Febbraio 1955. La 16ª edizione, che compare ad un anno di distanza, contiene qualche modifica e aggiunta nelle parti riguardanti la termotecnica, l'effetto Doppler, l'igrometro a diffusione di Greinacher, la misura in decibel, ecc.

Sempre assente il nome di FERMI dal pur aggiornato elenco dei fisici maggiori del secolo XX. Il trattato è stato adottato ufficialmente come testo per le Università e le scuole superiori della Repubblica Democratica tedesca.

V. SOMENZI

F. G. TRICOMI: *Funzioni ipergeometriche confluenti*. Monografie matematiche del Consiglio Nazionale delle Ricerche, N. 1. Edizioni Cremonese, Roma, dicembre 1954.

Questo primo volume della nuova collana di monografie matematiche pubblicate a cura del Consiglio Nazionale delle Ricerche tratta un argomento di eminente interesse non soltanto per i matematici, ma anche per i fisici e i tecnici.

È noto infatti che le funzioni ipergeometriche confluenti comprendono, assieme alle funzioni ellittiche, quasi tutte le funzioni speciali che si incontrano nei problemi di applicazioni.

La trattazione di queste funzioni che si dicono confluenti poichè vengono ottenute dalle ipergeometriche facendo confluire in un solo due dei punti singolari, viene basata, secondo una felice idea originale del TRICOMI, sullo studio dell'equazione differenziale

$$x\frac{\mathrm{d}^2y}{\mathrm{d}x^2} + (c - x)\frac{\mathrm{d}y}{\mathrm{d}x} - ay = 0, \qquad (1)$$

con a, c costanti. Se ne considerano due opportuni integrali $\Phi(a, c; x)$, $\Psi(a, c; x)$, funzione uniforme il primo, non uniforme il secondo, ma comunque più semplici di quelli — entrambi non uniformi — di WHITTAKER, che si usano di solito nelle trattazioni delle funzioni confluenti.

Il contenuto dell'opera si può riassumere come segue.

Nel Cap. I si dimostra come vari tipi di equazioni differenziali possano essere ricondotte o alla «equazione confluente (1) o alla equazione di Bessel. La (1) viene studiata, in un primo tempo, sotto l'ipotesi che c non sia intero, nel qual caso l'integrale generale della (1) può essere determinato mediante la sola funzione $\Phi(a, c; x)$ (funzione di KUMMER), della quale vengono studiate poi varie proprietà.

Il Cap. II culmina in una forma del-

l'integrale generale della (1) valida senza restrizioni sulle costanti a e c, anzi in un elenco di forme fra cui si possono scegliere quelle adatte ad ogni caso. A tale scopo viene introdotta la seconda soluzione Ψ della (1). Inoltre si deducono le relazioni fra Φ e Ψ e quelle esistenti fra tali due funzioni e le funzioni menzionate sopra di Whittaker, nonchè numerose formule concernenti Φ e Ψ.

Il Cap. III è dedicato allo studio di proprietà asintotiche e descrittive delle funzioni confluenti.

Nel Cap. IV, particolarmente utile per le applicazioni, vengono studiati i casi speciali delle funzioni confluenti come la funzione gamma incompleta, la funzione degli errori e le funzioni del cilindro parabolico, arrivando a numerose formule di evidente importanza pratica.

Il Cap. V, di particolare interesse per i fisici, contiene una rassegna di esempi di applicazioni delle funzioni confluenti. Si trattano i seguenti argomenti: Il problema dei due corpi in Meccanica ondulatoria, per il quale la risoluzione della equazione di Schrödinger si riconduce a quella di una equazione confluente; la determinazione della flessione di piastre elastiche lenticolari; lo studio del moto di onde marine investenti una costa a picco; il problema della riflessione di onde elettromagnetiche su di un cilindro parabolico, nonchè un problema tratto dalla statistica ed un altro appartenente alla teoria dei numeri.

Il libro, che contiene molti risultati nuovi del Tricomi, è redatto con la maestria e con la chiarezza che distinguono le opere dell'Autore stesso. Il fatto che le formule più importanti siano messe ben in rilievo ovvero raccolte in espressive tabelle, permetteranno anche ad un lettore meno esperto in questa materia di orientarsi con facilità.

M. J. De Schwarz

IL NUOVO CIMENTO

INDICI

DEL VOLUME II - SERIE X

1955

PRINTED IN ITALY

INDICE SISTEMATICO
PER NUMERI SUCCESSIVI DEL PERIODICO

N. 1, 1° Luglio 1955

Lettere alla Redazione:

N. 2, 1° Agosto 1955

N. 3. 1° Settembre 1955

N. 4, 1° Ottobre 1955

Lettere alla Redazione:

N. 5, 1° Novembre 1955

N. 6, 1° Dicembre 1955

Lettere alla Redazione:

INDICE PER AUTORI

Le sigle L., N.T. e N.d.L., si riferiscono rispettivamente alle *Lettere alla Redazione*, alle *Note Tecniche*, e alle *Note di Laboratorio*.

INDICE ANALITICO PER MATERIE

APPARATI E STRUMENTI

Cosmica (radiazione)

Elettrodinamica e teoria dei campi

Lastre nucleari e Camere di Wilson

LIQUIDI E SOLIDI

MECCANICA

MESONI PESANTI E IPERONI

MESONI (π E μ)

MOLECOLE

NUCLEI (FISICA NUCLEARE)

ONDE ELETTROMAGNETICHE

QUANTISTICA (MECCANICA)

RADIOATTIVITÀ

Relatività generale

Scariche nei gas

Superconduttività

Ultrasuoni

INDICE DELLE RECENSIONI

Fine del Volume II, Serie X, 1955

Direttore responsabile: G. POLVANI

Tipografia Compositori - Bologna

Questo fascicolo è stato licenziato dai torchi il 28-XI-1955